SOIL VARIABILITY-BASED IRRIGATION SYSTEM FOR OIL PALM PLANTATION

By

MOHD SHAHKHIRAT BIN NORIZAN

Thesis Submitted to the School of Graduate Studies, Universiti Putra Malaysia, in Fulfillment of the Requirements for the Degree of Doctor of Philosophy

October 2023

FK 2023 32

DEDICATION

To my invaluable supervisor, whose guidance, expertise, and unwavering support have been instrumental in shaping this work; and to my beloved family, whose boundless love, encouragement, and sacrifices have been the cornerstone of my journey - this dissertation is dedicated with heartfelt gratitude and deep appreciation.

Abstract of thesis presented to the Senate of Universiti Putra Malaysia in fulfilment of the requirement for the degree of Doctor of Philosophy

SOIL VARIABILITY-BASED IRRIGATION SYSTEM FOR OIL PALM PLANTATION

By

MOHD SHAHKHIRAT BIN NORIZAN

October 2023

Chairman : Associate Professor Aimrun Wayayok, PhD
Faculty : Engineering

Irrigation has been treated uniformly in oil palm fields, whereas soil water holding capacity can vary spatially across a field, resulting in either over or under water supply. This study evaluated an irrigation system in an oil palm plantation based on the variability of soil water holding capacity, which served three specific objectives. The first step is to define soil water holding capacity to create an Irrigation Management Zone (IMZ). The low-cost emitter for the micro-sprayer was then defined and used in irrigation planning with the IrriPro software. Finally, each IMZ was verified using oil palm yield, growth, and water usage. A grid system was applied for soil sampling using a 100m x 100m distance within the 20.3 ha study area, consisting of three soil depths up to 90 cm. In the laboratory, soil physical analysis was conducted and Available Water Holding capacity (AWHC) was determined using pressure plate analysis. The AWHC was delineated using Geographic Information System (GIS) software and the Kriging method. Several hydraulic emitter tests were conducted to provide additional data for the IrriPro software. IrriPro software was used to simulate and evaluate water uniformity. The Soil Variability-Based Irrigation (SBI) System, which is equipped with a tensiometer was installed according to IMZ. Meanwhile, soil infiltration rates were measured for each IMZ and analysed using Food and Agriculture Organisation - CROPWAT (FAO-CROPWAT) software. Following that, the FAO-CROPWAT 8.0 software was used to simulate estimated irrigation depth (EID) and total net irrigation (TNI) for 2016 and 2017. Recording plots were established in Zones A and C to measure yield and growth. Finally, water usage and Water Productivity (WP) were calculated for specific zones. The results showed that clay, sand, and organic matter (OM) distribution varied with soil depth. However, no significant correlation was found between these variables and AWHC. IMZ was divided into three zones: A, B, and C, with AWHC range of 79 to 167 mm. The highest uniformity for the SBI system was 85% for Christiansen's Uniformity (UCC), and 66% for Emission Uniformity (EU), and the system was deemed 'Good' by Statistical Uniformity (Us). Soil infiltration rates ranged from 1.01 to 8.23 mm hr^{-1}, with Zone C among the lowest. The low-cost emitter has a flow rate of 39-125 L hour^{-1} and a maximum throwing distance of 1.47-2.74 m. According to estate data, EID for 2016 went below the TNI requirement of 73 to 93 mm. In contrast, EID was nearly 55 to 90 mm above TNI in 2017. Zone A had a significantly higher cumulative yield (75.5 t ha^{-1}), followed by Zone C (69.1 t ha^{-1}), and finally the non-irrigation (NIR) plot (51.4 t ha^{-1}). Palms in Zone A had higher growth rates in height, leaf area, frond production, canopy length, and Petiole Cross-Section (PCS). A linear regression line analysis with PCS revealed that actual dry frond biomass had an R^2 of 0.713. Zone A had a significantly higher Crop Growth Rate (CGR) of 208 kg $palm^{-1}$ $year^{-1}$ and a higher Bunch Index (BI) than Zone C and NIR plots. Zone A used 9.72 m^3 $palm^{-1}$, while Zone C used 13.28 m^3 $palm^{-1}$ during the observation period, with the latter having significantly more irrigation events. Zone A had a higher WP (2.37 kg m^{-3}) than Zone C and NIR. Based on simulation cost analysis, the SBI can provide a payback period of 4.5 years with a 5% Return of Investment (ROI) and a net present value (NPV) of RM 14,419. This study found that the IMZs were satisfactorily classified, indicating that lower AWHC required more water and irrigation events.

Keywords: Oil palm, spatial variability, pressurised irrigation, soil-water holding capacity, irrigation management zone

SDG: Industry, innovation and infrastructure, responsible consumption and production, climate action

Abstrak tesis yang dikemukakan kepada Senat Universiti Putra Malaysia sebagai memenuhi keperluan untuk ijazah Doktor Falsafah

SISTEM PENGAIRAN BERDASARKAN VARIASI TANAH DI LADANG KELAPA SAWIT

Oleh

MOHD SHAHKHIRAT BIN NORIZAN

Oktober 2023

Pengerusi : Profesor Madya Aimrun Wayayok, PhD
Fakulti : Kejuruteraan

Pengairan untuk pokok sawit diberikan secara sekata sedangkan pegangan air tanah adalah berbeza-beza, hal ini akan menyebabkan input air menjadi kurang atau lebih. Kajian ini menguji sistem pengairan berasaskan variasi pegangan air di dalam tanah untuk ladang kelapa sawit berdasarkan tiga objektif. Objektif pertama adalah penentuan Zon Pengurusan Pengairan (IMZ) berdasarkan pegangan air tanah. Objektif seterusnya melibatkan penentuan sifat pemancar air kos rendah dan penggunaan perisian pengairan IrriPro. Objektif ketiga melibatkan penilaian pertumbuhan dan hasil pokok beserta jumlah penggunaan air berdasarkan IMZ. Persampelan tanah menggunakan sistem grid dilakukan pada jarak 100 m x 100 m dengan luas persempadanan 20.3 ha. Sampel diambil pada tiga kedalaman berbeza iaitu pada 0-30 cm, 30-60 cm dan 60-90 cm dari paras permukaan tanah. Sifat fizikal tanah diuji dan Keupayaan Menyimpan Air Boleh Dapat (AWHC) dianalisa menggunakan alat plat tekanan. Penentuan IMZ ditetapkan menggunakan Perisian Geografik Informasi Sistem (GIS) dan teknik Kriging. Sifat hidrologi penyebar yang digunakan dikaji terlebih dahulu dan seterusnya digunakan didalam perisian IrriPro. Sesudah itu, ianya digunapakai ke dalam perisian IrriPro untuk membuat perbandingan antara keseragaman simulasi dengan keadaan sebenar. Sistem pengairan berasaskan variabiliti tanah persis (SBI) dipasang mengikut IMZ dengan menggunakan tensiometer sebagai penderia masa nyata. Kadar resapan tanah juga disukat untuk setiap IMZ untuk digunakan di dalam model perisian Organisasi Makanan dan Pertanian CROPWAT (FAO-CROPWAT) 8.0. Anggaran Ukur Dalam Pengairan (EID) yang dilakukan oleh pihak ladang dikenalpasti dan perbandingan dengan Jumlah Pengairan Bersih (TNI) simulasi dari perisian FAO-CROPWAT untuk tahun 2016 dan 2017 dilakukan. Plot kajian diwujudkan mewakili Zon A dan Zon C untuk mendapatkan data pertumbuhan vegetatif, hasil sawit dan produktiviti air. Keputusan menunjukkan peratusan liat, pasir dan bahan organik (OM) berbeza mengikut kedalaman. Tetapi, semuanya tiada hubungkait yang kuat dengan AWHC. IMZ dapat dibahagikan kepada tiga kategori iaitu Zon A, Zon B dan Zon C dengan julat dari 79 sehingga 167 mm. Nilai keseragaman sebenar tertinggi adalah pada 85% untuk Keseragaman Christiansen

(UCC), 66% untuk Keseragaman Pancaran (EU) dan dikategorikan sebagai sistem yang "Baik" berdasarkan Keseragaman Statistik (Us). Kadar resapan tanah diantara 1.01 - 8.23 mm jam^{-1} dan resapan di Zon C adalah yang paling perlahan. Kadar aliran penyebar kos rendah adalah 39-125 L jam^{-1} manakala jejari lontaran maksimum adalah 1.47-2.74 m. Berdasarkan keputusan, EID untuk 2016 jauh lebih rendah berbanding TNI sebanyak 73 - 93 mm. Sebaliknya, EID untuk tahun 2017 pula melebihi TNI sebanyak 55 - 90 mm. Secara kumulatif, Zon A mempunyai hasil yang lebih tinggi (75.5 t ha^{-1}) secara signifkan diikuti oleh Zon C (69.1 t ha^{-1}) dan akhir sekali kawasan tanpa pengairan (NIR) sebanyak 51.4 t ha^{-1}. Zon A mempunyai tumbesaran yang lebih baik dari segi tinggi, luas daun, pertumbuhan pelepah, panjang kanopi dan keratan rentas tangkai pelepah (PCS). Berat kering pelepah sebenar mempunyai sekaitan yang tinggi dengan PCS pada nilai R^2=0.71. Zon A didapati mempunyai Kadar Pertumbuhan Tanaman (CGR) yang tinggi secara signifikan iaitu pada 208 kg pokok^{-1} tahun^{-1} begitu juga dari aspek Indeks Buah (BI) berbanding Zon C dan tanpa pengairan. Zon C menggunakan jumlah air yang lebih tinggi iaitu 13.28 m^3 pokok^{-1} berbanding di Zon A (9.72 m^3 pokok^{-1}) dan bilangan hari pengairan juga lebih banyak. Produktiviti Air (WP) bagi Zon A adalah lebih tinggi iaitu 2.37 kg m^{-3} dari Zon C dan NIR. Berdasarkan analisa kos, SBI berupaya memberikan tempoh pulang modal selepas 4.5 tahun dengan pulangan modal (ROI) bersamaan 5% dan juga Nilai Semasa Bersih (NPV) pada RM 14,419. Secara jelas, IMZ telah diklasifikasikan dengan baik dan kawasan yang rendah AWHC didapati memerlukan jumlah air dan bilangan hari pengairan yang lebih tinggi.

Kata kunci: Kelapa sawit, kebolehubahan ruang, pengairan bertekanan, kapasiti pegangan air tanah, zon pengurusan pengairan

SDG: Industri, inovasi dan infrastruktur, penggunaan dan pengeluaran bertanggungjawab, tindakan iklim

ACKNOWLEDGEMENTS

In the name of Allah SWT, most Gracious, most Compassionate, My deepest appreciation to my respectful supervisor, Associate Professor Dr. Aimrun Wayayok, for his constructive criticisms, suggestions, encouragement, and valuable advice, as well as his contribution towards the completion of this study. My deep appreciation also goes to my co-supervisors and members of the supervisory committee, Dr. Yahya Abd Karim, Dr. Ahmad Fikri bin Abdullah, and Dr Muhammad Razif bin Mahadi @ Othman, for their guidance, suggestions, and support throughout my study. My heartiest gratitude goes to the Head of Oil Palm Agronomy Division, FGV R&D, for his permission, guidance, invaluable advice, and knowledge of experimental design setup in the field. My sincere thanks to all the Agronomy and FGVAS Serting Hilir staffs for their valuable contributions in providing logistics, significant opinion, and field assistance during the study. Last but not least, my appreciation to my parents, beloved wife Rini Abd Razak, and my sons Muhammad Syafi and Ahmad Hadif for their endless love, sacrifices, patience, emotional support, and physical presence to make this dissertation a reality towards the completion of this study.

This thesis was submitted to the Senate of Universiti Putra Malaysia has been accepted as fulfillment of the requirements for the degree of Doctor of Philosophy. The members of the Supervisory Committee were as follows:

Aimrun Wayayok, PhD
Associate Professor Ts.
Faculty of Engineering
Universiti Putra Malaysia
(Chairman)

Ahmad Fikri bin Abdullah, PhD
Associate Professor
Faculty of Engineering
Universiti Putra Malaysia
(Member)

Muhammad Razif bin Mahadi @ Othman, PhD
Senior Lecturer
Faculty of Engineering
Universiti Putra Malaysia
(Member)

Yahya Abd Karim, PhD
General Manager
Head of Research Management
FGV R&D Sdn Bhd
(Member)

ZALILAH MOHD SHARIFF, PhD
Professor and Dean
School of Graduate Studies
Universiti Putra Malaysia

Date: 16 May 2024

TABLE OF CONTENTS

LIST OF TABLES

LIST OF FIGURES

LIST OF ABBREVIATIONS

A	Area, hectares
ABW	Average Bunch Weight
AC	Alternate Current
AET	Actual Evapotranspiration
ANOVA	Analysis of Variance
AWC	Available Water Capacity
AWD	Allowable Water Deficit
AWHC	Available Water Holding Capacity
BD	Bulk Density
BI	Bunch Index
BN	Bunch Number
c	Initial infiltration rate, mm
CD	Critical depletion
CGR	Crop Growth Rate, tonne ha^{-1} $year^{-1}$
COVID	Coronavirus Disease
CPO	Crude Palm Oil
Csand	Coarse Sand
CV	Coefficient of Variation
CVm	Coefficient of Manufacturer Variation
CVT	Coefficient of Technology Variation
CWR	Crop Water Requirement
d	Number of density ha^{-1}
D	Maximum distance over field
DC	Direct Current

D_c	Distribution Characteristic
d_h	Hydraulic diameter, m
DU	Distribution Uniformity
D_w	Water density, g cm^{-3}
ECa	Apparent Electrical Conductivity
EID	Estimate Irrigation Depth
ENSO	El Niño Southern Oscillation
ER	Effective rainfall, mm
ET	Evapotranspiration
ETc	Crop evapotranspiration
ETo	Reference evapotranspiration
EU	Emission Uniformity
EventsA	Number of irrigation events at Zone A
EventsC	Number of irrigation events at Zone C
EVW	Estimated Volume Water
F	FFB, kg $palm^{-1}$ $year^{-1}$
FAO	Food and Agriculture Organization
FC	Field Capacity
FELDA	Federal Land Development Authority
FFB	Fresh Fruit Bunch
FGVAS	FGV Agri Services Sdn Bhd
Fsand	Fine Sand
g	Acceleration due to gravity (m sec^{-1})
GIS	Geographic Information System
Gk	Emitter constant for radius

GPS	Global Positioning System
GS+ Software	Geostatistics for Environmental Sciences Software
GSM	Global System for Mobile communication
Gx	Emitter exponent for radius
H	Operating pressure, m
h	Distance of reliability
HDPE	High Density Polyethylene
HEX	Hexadecimal
H-Q	Emitter head - discharge
H-T	Emitter head - throwing distance
I	cumulative infiltration rate, mm
ID	Internal Diameter
IFSAR	Interferometric Synthetic Aperture Radar
IMZ	Irrigation Management Zone
IOS	Iphone operating system
IoT	Internet of Things
IR	Irrigation, mm
IRHO	Institut Recherche Huiles Oleagineux
K	Emitter discharge coefficient for flow rate
k	Absolute roughness of pipe, m
Kc	Crop factor
KS	Saturated Hydraulic Conductivity
L	Length of pipe, m
LAD	Localised Application Depth
LCD	Liquid Crystal Display

LDW	Leaf Dry Weight, kg palm^{-1}
MAD	Management Allowable Depletion
MAT	Months After Treatment
MaxT	Maximum Temperature
MCO	Movement Control Order
MinT	Minimum temperature
MMD	Meteorological Malaysia Department
MPOB	Malaysia Palm Oil Board
MS	Malaysia Standard
MYR	Malaysia Ringgit
n	Number of emitter for each tree
NDVI	Normalised difference vegetation index
NIR	Non Irrigation
Np	Number of palm
NPV	Net Present Value
OC	Organic carbon
OD	Outer diameter
OM	Organic matter
P	Number of plots
PAWC50	Practical Available Water-Holding Capacity at 50 cm
PC	Pressure compensated
PCS	Petiole Cross Section
PDF	Portable Document Format
PET	Potential evapotranspiration
PI	Precision Irrigation

PWD	Potential Water Deficit
PWP	Permanent Wilting Point
Q_{25}	Average low quarter of flow rate, L $hour^{-1}$
Q_e	Emitter Flow Rate, L $hour^{-1}$
Q_i	Flow rate of single emitter, L $hour^{-1}$
Q_m	Average flow rate of the emitter, L $hour^{-1}$
Q_{med}	Medium flow rate of the emitter, L $hour^{-1}$
Q_{min}	Minimum flow rate of the emitter, L $hour^{-1}$
Q_{SD}	standard deviation of emitter flow rate
r	Canopy radius, m
RH	Relative Humidity
Rn	Reynold's number
ROI	Return of Investment
RSU-V	Remote Sensing Tensiometer
SBI	Soil Variability-Based Irrigation
SAS	Statistical Analysis Software
SD	Standard Deviation
SE	Standard Error
SH	Sunshine hours
SPAW	Soil-Plant-Air-Water
SSIM	Site-Specific Irrigation Management
SWP	Soil water potential
t	time elapsed, min
T	Palm Age
TDR	Time Domain Reflectometry

TDM	Trunk Dry Matter, kg palm^{-1} year^{-1}
TNB	Tenaga Nasional Berhad
TNI	Total Net Irrigation
TOC	Total Organic Carbon
Tsand	Total Sand
UAV	Unmanned Aerial Vehicle
UCC	Christiansen’s Uniformity Coefficient
UPM	University Putra Malaysia
U_S	Statistical Uniformity Coefficient
USB	Universal Serial Bus
USBR	United State Bureau of Reclamation
USDA	U.S Department of Agriculture
USDA-SCS	U.S Department of Agriculture – Soil Conservation Service
V	Velocity of fluids (ms^{-1})
VDM	Vegetative dry matter, kg palm^{-1} year^{-1}
VWC	Volumetric Water Content, %
VolA	Volume of water use at Zone A, m^{3} zone^{-1} year^{-1}
VolC	Volume of water use at Zone C, m^{3} zone^{-1} year^{-1}
VRI	Variable Rate Irrigation
VT	Volume of trunk, m^{3} palm^{-1} year^{-1}
VWC	Volumetric Water Content, %
WF	Water Footprint
WGS84	World Geodetic System 1984
Wi-fi	Wireless fidelity
WMO	World Meteorological Organization

WP	Water Productivity
WS	Wind Speed
x	Emitter discharge exponent for flow rate
x1	Data in hex
Y	Yield dry matter, kg $palm^{-1}$ $year^{-1}$
y1	Data in mV
y2	Data in pressure, cbar
α	index of soil structural stability
μ	Dynamic viscosity of fluid (N s m^{-2})
υ	kinematic viscosity of fluid (m^2 sec^{-1})
f	Friction factor
h_f	Head loss, m

CHAPTER 1

INTRODUCTION

1.1 General background

Life is dependent upon water. For many years, water has been utilised arbitrarily and neglected. A growing human population correlates with a corresponding increase in the demand for water and food produced by agriculture. Additionally, increased production per unit area is necessary; as a result, the demand for water resources increases. In such circumstances, a trade-off arises between water availability for human consumption and water requirements for crops, especially in drought or El Niño. Therefore, it is essential to research water conservation and other forms of water efficiency to guarantee that crops will continue to produce superior outputs for human consumption. Irrigation is a method used to address the issue of insufficient soil moisture. Various irrigation techniques can be employed based on the crop type, slope, water availability, and other relevant factors. However, its application is restricted to specific areas due to significant factors such as cost implementation and economic scale.

In the oil palm industry, it is typical to schedule irrigation based on the evapotranspiration rate, giving less importance to the condition of the soil. Nevertheless, contemporary technological advancements, including real-time sensing through soil moisture and the progress of Internet of Things (IoT) systems, enhance the appeal of transitioning to Precision Irrigation (PI) systems for sustainable production. The higher capital costs associated with PI systems may pose challenges in implementing for oil palm, given that oil palm is a commodity product and the producer lacks price control. The benefits of PI in oil palm should be realised by either increasing production per unit of resources or saving resources for more extensive irrigation area implementation.

1.2 Statement of the research problem

Oil palm production is commonly affected by soil moisture deficit, as described by many researchers. Moisture deficit can affect oil palm physiology in terms of sex differentiation, floral abortion, and bunch failure (Caliman & Southworth, 1998; Woittiez et al., 2017). In addition, a direct reduction of up to 20% in the yield of fresh fruit bunch (FFB) (Caliman & Southworth, 1998) and oil (Cornaire et al., 1994) can occur due to water deficits. Hartley, 1988 suggests that there is broadly a 10% reduction in FFB yield for each 100 mm increase in the soil water deficit. Due to climate change, El Niño can affect FFB yield and crude palm oil (CPO) production, which was reported to significantly decline by 10-16 % and 8-14%, respectively (Azlan et al. 2016).

Implementing an irrigation system in the field is one strategy for mitigating the impact of soil moisture deficit. However, due to the high initial cost, irrigation system adoption remains low. Irrigation capital costs may vary, but it has been reported that drip irrigation can be as high as RM 18,000 ha^{-1} (Afandi et al., 2022). As one of the commodity crops, the farmer cannot control their product price, and as a result, any additional cost for their production is considered crucial and strictly controlled. Another bottleneck issue could be a lack of available water sources. Practitioners prefer surface water because it is less expensive than establishing groundwater infrastructure (JMG, 2024). During the drought season, these water sources become depleted, and when this happens, irrigation is used below its potential. Because of these factors, common irrigation practices are limited to small dedicated land, 50-200 ha $estate^{-1,}$ compared to a typical plantation size of 1000 - 3000 ha $estate^{-1}$.

Dedicated irrigation land, for example, up to 200 ha $estate^{-1}$, may be attributed by various soil properties, which are later translated to the same or different soil series. A conventional irrigation system treats an area uniformly, ignoring some factors that influence water input requirements such as soil, climate, and topography variability. Variations in soil properties with geospatial references may result in variations in soil-water holding capacity (Bordoloi et al., 2019). When irrigation is treated uniformly, water is either under- or over-supplied.

Irrigation scheduling for oil palm is usually done to meet crop evapotranspiration (ETc) demand and is often assumed constant at 5.0 mm day^{-1} (Corley & Tinker, 2016). This concept is according to crop water requirement and depends on Reference Evapotranspiration (ETo), Crop Coefficient (Kc) and local conditions. Limited local climatic data may impede the accurate calculation of evapotranspiration demand and soil water sensors being used to recalibrate the error. However, the sensor's capability to demonstrate water scheduling in an oil palm plantation and its impact on water usage is still lacking for future reference.

Emitter is one of the main components to get high uniformity across the field. Excellent emitter performance, such as pressure compensated type, has a smaller orifice that requires a certain level of filtering system and costs more. As the water quality is inconsistent, clogging may occur and farmers require a workforce and time to deal with this problem, making the irrigation management inefficient and tedious. Hence, it builds up a misconception, and they face low motivation to use irrigation for their practice. In order to get proper irrigation installation, farmers need to work with engineering-based vendors, which typically incur extra costs and require specific procedures. Low-cost micro-sprayer emitter is economical besides wide-range availability. However, it lacks certified specifications and requires some investigation to assess its usefulness.

This thesis emphasises the importance of implementing Irrigation Management Zones (IMZ) based on soil water holding capacity. IMZ is used to demonstrate that differential irrigation can be achieved rather than homogeneous irrigation input, enabling more sustainable future water use. A well-designed irrigation system in agricultural areas is essential for improving conventional irrigation, and a good irrigation system is reflected by high uniformity. Thus, irrigation software is utilised to simulate uniformity based on the hydraulic features of low-cost emitters. In today's world, the significance of real-time sensor cannot be disregarded, and measures must be taken to realise its benefits, particularly in the palm oil industry. Hence, the proposed project consisted of spatial analysis for zoning purposes, in-situ irrigation sensor, and assessment of the plant and system, which is Soil Variability-Based Irrigation (SBI) system believed to meet certain criteria for the PI concept.

1.3 Objectives of the study

The main objective of this study was to develop a physical model of a SBI system for oil palm plantations and act as a reference centre for the oil palm industry. The current study was carried out with the following specific objectives:

1) To delineate irrigation management zones (IMZ) based on the spatial variability of soil water holding capacity and precipitation.

2) To characterise low-cost micro-spray emitter and design an irrigation system by using the IrriPro software for hydraulic and uniformity studies.

3) To effectively monitor water application for increasing oil palm yield, growth, and efficient water usage using tensiometer within a soil variability-based management zone.

1.4 Scope and limitations of the study

The scope of this study was to develop a SBI system for oil palm at a plantation scale, backed by data such as soil physical, soil water retention capacity and rainfall with the aid of irrigation software. IrriPro software is a commercial software used in this study because it is able to provide hydraulic calculations for the layout at a reasonable price. The importance of SBI was shown through the Food and Agriculture Organization of the United Nations - CROPWAT (FAO-CROPWAT) software 8.0 simulation. Scheduling of irrigation is based on a multi-location plot basis according to tensiometer sensor readings. Later on, the system installed accessed water uniformity, water usage, oil palm growth and yield.

This study started with soil sampling during oil palm at three years old. Other activities, such as growth measurement taken at six years old and the yield recording reflect the oil palm at 7-8 years old. The study was done in a dry area rainfall regime location central in Peninsular Malaysia. The location was selected to gain a good response from the oil palm yield. The soil has been mapped with a semi-detailed soil survey, namely the Rasau soil series under riverine alluvium type of soil. To gain a clear comparison, the last objective of this study focused on Zone A and Zone C, despite three selected irrigation management zones. The period of this study was from

2016 until 2022, whereby yield recording and growth measurement was only carried out from 2020-2022, i.e., after SBI system installation was completed.

1.5 Significance of the study

In the early stage, soil sampling covered an area up to 20.3 ha, and the location was delineated to represent a semi-commercial scale. Irrigation management zones were derived from the soil's physical properties, which eventually reflect water-holding capacity. These methods are simple, straightforward and repeatable at a plantation level, yet provide powerful tools to segregate an area to respective IMZ. This study used tensiometers as sensors to monitor water demand based on pre-determined IMZ. Based on their mechanism and direct measurement, tensiometers reflect moisture needed around the root zone, making it the most sensitive device to justify irrigation scheduling. The location of this trial was selected at a dry region compared to other areas, such as in the southern or eastern areas of Peninsular Malaysia, to gain a better translation of response to soil moisture availability.

A total of three zones namely Zone A, B and C were classified in this study. Zone A has an Available Water Holding Capacity (AWHC) ranging from 125 – 167 mm, Zone B from 100 – 125, and Zone C from 79 – 100 mm. Regarding yield and vegetative growth data collection, comparisons were made between Zone A, Zone C and non-irrigation (NIR) plots. It was done to provide a distinct and more apparent response to the treatment. Zone A and Zone C focused on different ranges of AWHC, whereas the NIR plot provided a control for where irrigation was not being put into context. There is a lack of evidence on how irrigation software can help farmers to develop a good irrigation system. From a layman’s perspective, hydraulic and uniformity performance are some of the most challenging and technical aspects to be covered by the irrigation system owner. However, as shown in this study, software usage can help predict hydraulic performance, uniformity, and ease of billing activity. This study provides inventive steps for growers or researchers to implement PI in oil palm plantations to optimise resources.

1.6 Organization of the thesis

The current study mainly involved field oil palm trials in mature areas to achieve the targeted objectives. The thesis consists of five chapters. Chapter 1 discusses the general background of this study and its significance to science. In addition, there is a statement of the research problem, objectives of the study, and limitations of the study. Chapter 2 consists of reviews for all related key terms involved in this study. Generally, all the findings from other researchers related to soil-based irrigation, FAO-CROPWAT, oil palm, and others are discussed. Chapter 3 consists of detailed information on where this study was done and describes the methodology for this study. Chapter 4 is related to collected data and its discussion; all data are summarised, analysed, and presented in a way to emphasise the findings from the scope of the system, palm response and how it can be suitable for the oil palm sector. Chapter 5 comprises of a summary of the whole thesis, conclusions of the current study, and recommendations for future work.

CHAPTER 2

LITERATURE REVIEW

2.1 Introduction

Irrigation is unnecessary when there is abundant water or soil moisture in a particular place. However, some areas suffer from prolonged drought periods and or uneven rainfall distribution. The centre of oil palm cultivation is mainly in Asia, Africa, and America. Generally, rainfall in Malaysia is considered sufficient for oil palms, with a range of about 1,900-3,600 mm annually. Meanwhile, precipitation in Africa ranges from 1,100-3,500 mm; in America, the rainfall ranges from 1600-3600 mm. Despite a good amount of rainfall, some parts of these areas experience dry periods that can last more than three months. Some areas, such as Benin, Africa have a dry season lasting up to 4 months consecutively. Other places such as Colombia, have a 'dry season' consisting of 5 months of minimal rain with only an annual rainfall distribution of about 1000-1600 mm (Corley & Tinker, 2016). In Asia, Southern Thailand has been reported to have low rainfall between December and March, with an average 214 mm water deficit (Palat et al. 2000).

The concept of differential irrigation was introduced in the 1990s in the United States of America when farmers started to use central pivot systems or lateral irrigation machines. Several reasons are that fields are not uniform, the application of conventional irrigation is constant and any excess water that comes from irrigation may be lost through leaching and surface runoff, which might bring chemicals and nutrients along. Most non-uniform irrigation work aims to increase water use and economic efficiency. In most literature, researchers tend to expect a reduction in water use. High field variability and high crop prices are required to make it profitable in addition to the useful life of the equipment. Data collection to measure spatial and temporal variability for use in this concept was typically plant-based sensing, soil water sensing, weather sensing, or any combination of these factors.

2.2 Impact on water deficit to oil palm

Oil palm will react to water stress via different levels of adaptation, also termed a 'self-defense mechanism' against drought. The first reaction would be for an oil palm tree to close its' stomata during maximum evapotranspiration. The rate of leaf opening will be slower and the spear leaf extension rate will be reduced; this mechanism will minimise transpiration. However, a palm can rapidly recover if rain and moisture become available (Henson 1991). During longer periods of water stress, in order to maintain respiration and bunch development, starch or other polysaccharides available in the trunk will start to be converted into sugar. In more severe water stress situations, older leaves will desiccate prematurely. Developing bunch and inflorescence will be aborted to reduce carbohydrate sink. Based on Maillard et al. 1974, this is a four-stage process.

The first stage is an accumulation of 5-6 unopened spears instead of 2-3 spears under normal conditions. Later on, the second stage occurs where 4-6 leaves snap, and in addition, bunches will dry out and several bunches fail to achieve full ripeness. In the third stage, all leaves at the base of the crown will dry out and leaves at the upper parts will topple. Lastly, the fourth stage is the death of the oil palm.

The effect of water deficit on yield is acceptably known, but how much of the reduction is caused by the water deficit depends on the seriousness of the water deficit. Several researchers have done studies in the field to examine how oil palms react when a water deficit develops. In earlier years, studies by Olivin (1968) and Ochs and Daniel (1976) found that yield reductions between 10 and 20% were pronounced when the water deficit was at 100 mm, depending on soil quality. Later on, Hartley (1988) calculated the water deficit based on the Institut Recherche Huiles Oleagineux (IRHO) method and also concluded that a 100 mm water deficit in a year may reduce yield by 10%. Using a complex model, Caliman et al. (1987) and Caliman (1992) supported the fact that a 10% reduction from the potential yield occurs with a 100 mm water deficit over the years.

Many studies show that water stress reduces oil palm production through a lagged effect. It does not have a direct impact, and rather it affects the physiological process from the period of flower initiation to fruit harvesting. Based on the study by Caliman and Southworth (1998), crop loss caused by 100 mm water stress results in an impact equivalent to a 1-3% reduction of FFB production through floral initiation and the lagged period is 33-36 months. After which, drought or moisture stress reduces FFB production to 3-4% because of sex differentiation with lagged months of 19-25 months. Lastly, abortion of FFB may occur with an 8-10% reduction in FFB production from an 8-11 months lag (Corley et al., 1995).

Cheng Xu et al. 2011, who carried out a study to investigate the physiology of oil palm to water and nutrient stress, reported that water and nutrient stress would significantly affect palm growth in terms of dry matter allocation and partitioning. They also found that water stress more strongly influenced the root: shoot ratio than nutrient stress. Another interesting finding was that relative water content was significantly reduced with water stress only. This was similar to Chlorophyll a/b content and this was more obvious when nutrient stress was included. However, this study only represented the seedlings of palms up to 90 days and consisted of test palms planted in a closed pot.

Jazayeri et al. (2015) carried out a study using potentially drought-tolerant planting material seedlings in pots compared to normal seedlings. Each of the materials was tested with regular watering setting at field capacity (FC) (-0.042 MPa) while the other one represented drought stress (-1.50 MPa) effect, consisting of withholding water for up to 8 weeks to look at physiological changes in oil palm. They found that stomatal conductance was reduced to as low as 0.05 mol H_2O $m^{-2}s^{-1}$ due to drought stress after eight weeks. However, well-watered treatment was able to maintain the stomatal conductance of seedlings at 0.30 mol H_2O $m^{-2}s^{-1}$ in the same period. A similar trend was observed for photosynthetic activity.

2.3 Irrigation as a practice to reduce water deficit

The effect of irrigation on increasing oil palm yield was first reported by Ochs and Daniel (1976) through experiments done at Ivory Coast. The irrigation plot for this study achieved about 225% extra FFB yield compared to the standard plot. In 1979, Chan (1979) reported various increments after using different irrigation techniques in terms of oil contents which were 17%, 11%, and 8% by using drip, furrow, and jet irrigation respectively. This trial was done in Guthrie Plantation, Negeri Sembilan, and is also the first reported study of irrigation in Malaysia. A trial conducted in Southern Peninsular Malaysia showed a yield increment of about 5% by using a hose on 12 year old palms (Corley and Hong 1982). In other regions, Lim (1988) reported that there was a 140% increase in yield for nine year old palms by using drip irrigation. Later, irrigation trials located at a Sime Darby Plantation in Johor reported an increment of yield after the fifth to the seventh year of irrigation practices. From these experiments, drip irrigation with fertigation increased yield by 9% and 19% with palm oil mill effluent application (Roslan & Haniff, 2004).

In the early 1990s, FGV Agri Services Sdn Bhd (FGVAS) adopted a surface irrigation called the furrow or flatbed system. This system gives water input in large quantities: about 9,000 litres hour^{-1} depending on the number of palms within the same frond rows. This method is considered low-cost and less technical compared to other irrigation techniques. For this technique, Lee and Izwanizam (2013) reported that oil palm yield was improved from 33% to 56% when it was done in the dry region compared to the NIR plot. Concurrently, irrigation was set up at Pusat Perkhidmatan Pertanian Tun Razak using a flatbed system from 1999 until 2014. However, this trial only exhibited a lesser response of only approximately 3% extra yield. Good rainfall distribution with no clear drought season at the trial site was believed to contribute to this low yield improvement. They also reported that output increased by the improvement of bunch number rather than bunch weight and suggested that the trend of the yield did not change between irrigated and non-irrigated palms, but irrigation reduced the fluctuation of the yield. It is also reported that irrigation improves oil to mesocarp and thus increases oil content (Corley and Hong 1982; Lee and Izwanizam 2013; Ochs and Daniel 1976; Van der Vossen 1974).

In Thailand, Palat et al. 2000 studied and reported a series of comprehensive irrigation trials in oil palm plantations. The trial was set up in 1990 to compare two different rates of water input by using either a standard or double rate of fertiliser. Another set of trials was set up to test methods of irrigation consisting of drippers, sprinklers, micro-sprayers, and contour furrows. The third set of trials was done in 2000 to compare two different rates of fertiliser with standard or double fertiliser by fertigation. They reported that the drip irrigation method at 240 litre palm^{-1} day^{-1} gave the highest yield (26.6 t ha^{-1} year^{-1}) while the other method also gave a good response compared to the non-irrigated plot (19.5 t ha^{-1} year^{-1}). By looking at the means of the yield combined for every technique, 240 litre palm^{-1} day^{-1} gave a slightly higher yield than 360 litre palm^{-1} day^{-1}. For the second phase of the same trial, they obtained an even better yield with a double dose of fertiliser (28.0 t ha^{-1} year^{-1}) by using 450 litres palm^{-1} day^{-1} and recorded an almost 35% increase in yield. This trial showed that the interaction of fertiliser with water supply is significant.

2.4 Adoption of differential irrigation for better water management

Farmers adopted irrigation for their crops and the intention is typically to have uniform water application. Indeed, many studies related to irrigation focus on the uniformity of the system. However, soil is heterogeneous and it may vary considering many factors such as topography, soil texture, organic matter (OM), and others. Because of that, there are conditions where overwatering or underwatering may occur. If overwatering, water is wasted, and there is a high chance of drainage or leaching particularly from the next irrigation itself or from subsequent rainfall. However, if underwatering, there is a chance of nutrient leaching not being taken up by the plant effectively.

Most differential irrigation concepts have been used in arid and semi-arid climates where water scarcity was the primary issue and needed to be addressed, hence the development of differential irrigation is not progressive in temperate and humid climates areas. In Malaysia, where the rainfall is considerably well distributed, site-specific irrigation may be one of the approaches to adopting sustainable usage of energy or resources. Daccache et al. (2015) suggested that in a humid area, the spatial variable rate of irrigation would be impracticable and uneconomic, especially when applying such a fine resolution of soil Available Water Capacity (AWC) variability. They also mentioned that the essential factor was to define the scale and resolution of IMZ that are compatible with the current system and approaches to scheduling.

Integration of SBI with new technology will promotes PI usage. Several pieces of literature on PI bring up a range of definitions (King et al., 2006; Raine et al., 2007; Sadler et al., 2005). However, the definition consists of 'differential irrigation' as opposed to uniform irrigation underlaid in traditional ways. The concept of PI integrates information, communication, and technology to control the irrigation process and optimise water resources. It may involve spatial and temporal soil properties, plant responses, and weather variables and is controlled via the IoT to achieve water savings and yield improvement (Bitella et al., 2014). However, it is a system approach rather than a specific technology. PI is a convergence of advanced technology with sensing, modelling and controlling aspects and may incur a high capital cost. This matter leads to the perception that PI is about high technology, however it is not universally true (Smith & Baillie, 2009). In the same report, they also emphasise that the keys to successful PI are water saving and cost reduction, better management of resources, optimization of the economic value of water and optimization of crop production.

There are no exact standards for how the complexity of PI should be carried out. Evans et al. (2007) describe automated sensing of soil electrical conductivity through a wireless network of sensors linked to a microcomputer control and spraying equipment. However, the fundamental component of the PI concept includes the examination and application of water to a precise location and at the exact dose.

According to Smith et al., 2010, the PI concept is just the beginning and requires a lot of concurrent data, experiments and investigation for their feasibility and applicability through various crop and climatic regimes. Several obstacles that give potential barriers to PI are a lack of understanding of various crop interactions when applying PI, cost of inputs, and constraints in operating management. Other obstacles are that this technology is considered to be at its infancy and many equipment and services are still at high prices. To assess the feasibility of the crops, PI needs to be proven and demonstrated in the field. Due to the aforementioned factors, there is a scarcity of studies dependent on crop simulation.

Jobbágy et al. (2011) compared conventional water application and PI. After the soil sampling, the application map was produced consisting of an irrigation zone based on spatially variable soil moisture. Irrigation was done using reel hose machines. Five irrigation rates were applied during the entire growing season according to the principles of PI. They found that PI contributed to water savings of 478.56 m^3 ha^{-1}, electric power savings at 249.68 kWh ha^{-1} and cost-saving of 23.8%.

Several studies regarding PI have shown promising results. One example is a study by King et al. (2006) that compared site-specific irrigation management (SSIM) with conventional uniform irrigation practices. The area was divided into management zones called sub-areas of field. The total yield produced under SSIM was 4% greater but not significantly different. The output per unit of water for SSIM was greater than 4-6%. The gross income obtained from SSIM practices was about half the actual cost of implementing commercial SSIM. To realise the economic benefit of SSIM, the yield of other crop rotations needs to improve since this study only recorded the yield of tomatoes for just two years.

In view of oil palm, there is a lack of studies reported on the benefit of SBI or any differential irrigation system. Therefore, this study is intended to be as irrigation trial utilising the concept of delineation of soil properties as supportive to site-specific irrigation with the addition of real-time sensors. Without a proper trial, there is no evidence to prove whether this approach is worth the effort.

2.5 Soil sensor for SBI system

A soil moisture sensor is an essential device to monitor soil moisture status in real-time. Today, this device is placed in the field and installed at desired locations, connected to the control panel to make observations and quick monitoring. In SBI, the installation of a soil moisture sensor is a compulsory and reliable tool to maintain the objective of providing a good moisture level at all times.

There are two categories of sensor types, which are the soil volumetric water content sensor and the soil water tensiometer. Capacitance and Time Domain Reflectometry

(TDR) are normally two types of probes to measure volumetric water content. Meanwhile, a tensiometer is used to measure water tension in soil.

Capacitance works by polarizing the surrounding medium with an electromagnetic field with a low frequency between 20-300 MHz, while TDR and transmissometry work in the GHz range frequencies (Vaz et al., 2013). Then, measurement is made depending on the imposed frequency, the electrode configuration, and the dielectric permittivity of the porous medium. Meanwhile, for the TDR concept, its probe uses a voltage step pulse to generate a high-frequency electromagnetic wave that propagates along a transmission line. However, a study by Dettmann and Bechtold (2018) has shown that both probes experience increased uncertainties when the dielectric value is more than 40, which generally occurs in porous media.

Dukes and Scholberg (2005) tested two scheduling treatments: one using initiation and termination based on an installed TDR sensor 5 cm above the dripline, and another treatment was scheduled based on consistent daily irrigation. They found that a similar yield was achieved by using a subsurface buried at 23 cm depth and sprinkler irrigation, and water usage was reduced by up to 11%. However, the yield when the subsurface was buried at 33 cm was poor due to the movement of irrigation water below the root zone in a sandy area. They also found that irrigation for subsurface water use efficiency using the scheduling-based sensor increased by 19% compared to the sprinkler method.

Tensiometers consist of a water-filled tube attached to a vacuum gauge at the upper end and a ceramic cup at the lower end of the device. It will measure the tension created in the soil; soil with drier conditions will suck the water inside the tube and increase the gauge value. Tensiometers are the only devices that measure soil matric potential and give a direct connection between soil and water inside the tube. Therefore, the tensiometer requires no site-specific calibration and is a good tool for a wide range of applications (Thalheimer, 2013). The disadvantage of this device is that it needs regular checking and maintenance compared to capacitance and TDR.

Almarshadi and Ismail (2011) cultivated alfalfa located in arid climates and used three different types of irrigation, namely sprinkler, surface drip, and subsurface drip, and all methods were controlled precisely using water electric modules technology. In these modules, water requirement was calculated based on available soil moisture at the root zone area by using a watermark tensiometer. They reported that surface drip irrigation can save up to 29% of water, while sub-surface drip irrigation saves up to 36%. These two methods also had a yield increase from 16 to 45% compared to sprinkler irrigation.

In the past ten years, there have been many studies involving irrigation monitoring with advanced control systems. The control system connects with several IoT-based sensors using the Arduino board (Divya, 2019; Krishna, 2017; Kumar et al., 2017; Nageswara & Sridhar, 2018). According to Shigeta et al. (2018), a capacitance-based sensor is applicable for practical measurement for real-time monitoring sensing. It was done by correlating the Volumetric Water Content (VWC) of the soil and the capacitance with reasonable accuracy. According to Abioye et al. (2020), TDR sensors have an accurate sensing approach. TDR uses an electromagnetic pulse radiating from the sensor rod. However, it can be a high cost to farmers because it requires a high number of readings to get a better representative value of the field.

The application of sensors may incur a high cost for proof of the technology. However, some researchers have reported approaches to get lower prices. Bitella et al. (2014) proposed low-cost monitoring by using multisensory measurements using dielectric probes. The sensors interfaced with the Arduino Uni microcontroller and used a wireless fidelity (Wi-Fi) module to transmit data to the internet for data logging purposes. Many other researchers are also using Arduino as a controller (Jha et al., 2019; Salvi et al., 2020; Yashaswini et al., 2018).

Other than using Arduino and Wi-Fi, Hebbar and Prasad (2017) utilised a Global System for Mobile communication (GSM) network and infrared communication to offer automatic water supply. They used a programmable interface microcontroller coupled with a capacitance-based soil moisture sensor. With the emergence of technology, soil moisture monitoring using sensor layout network technology was integrated with iPhone Operating System (IOS) and Android applications (Işik et al., 2017).

2.6 Matric potential of Field Capacity (FC) and Permanent Wilting Point (PWP)

FC is defined as the water left in the field soil profile after free drainage for up to 48 hours. It is also considered to be an upper limit of water storage by the soil. Water in the soil will continuously be removed and finally reach the PWP, which is typically at matric potential -1500 kPa and this is called a lower limit. At this level, the plant can no longer extract water. According to Veihmeyer and Hendrickson (1949), FC is the amount of water remaining in the soil after saturation and drainage of the excess water when reaching a minimum rate of downward movement. It is has been widely accepted that FC is -33 kPa for finer textured soil and -10 kPa for coarser textured soil. There are many arguments regarding the value of FC. Kirkham (2014) stated that soil scientists now realise that the FC is imprecise and is not rigid nor unique because the equilibrium is never reached. The movement of water does not stop at a specific time, but it will continue at a reduced rate for a long time. In fact, there are no absolute values for FC. However, there are a range of values associated with it.

Previously, tensions of 10 kPa (Araujo et al. 2004; Silva et al. 1994) and 33 kPa have commonly been used to estimate moisture at FC. Klein et al. (2006) carried out a study on clayey oxisol, where several levels of tension starting from -0.006 MPa, -0.008 MPa, -0.01 MPa, and -0.033 MPa were compared with drainage methods. They found that soil treated with pressure using porous plate funnels with -0.01 MPa obtained similar and not significantly different results from internal drainage treatment, which is believed to best describe soil water content at FC. Veihmeyer and Hendrickson (1949) suggested that FC is not an equilibrium value but instead is based on a time drainage value curve. The curve is almost horizontal, further suggesting that the FC is not a unique value. This non-rigid value is also shown in examples used by Victoria Lab, Australia which set -0.02 MPa as an upper limit for AWHC calculation representing FC (J. Brouwer & Anderson, 2000).

PWP refers to water content in the soil under high soil retention where the plants wither and do not recover turgidity even in a humid atmosphere (Briggs & Homer, 1912). It may differ between plants and is also affected by soil texture: for example, PWP for potatoes is -1000 kPa while for wheat is -30 kPa. PWP is less speculated because when the PWP value is too high; the value of water content is almost negligible since the soil water retention curve for the wilting point is very steep.

Determination of the value of FC and PWP can be done in several ways using a laboratory, field, or statistical approach. In the laboratory method, pressure is gradually applied to saturated soil samples from 0 to 1500 kPa by using a pressure plate. An increase in pressure will force water to be expelled from the soil body and the sample weight will be taken to calculate the amount of water lost after pressure has been applied. The percentage of water at -10 kPa or -33 kPa represents FC while -1500 kPa represents PWP.

Measurement of FC using a field approach can be done by watering a quadrat of area (2m x 2m) and filling it with 200 L of water and leaving it for 48 hours (Foster, 1984). After that, a soil sample is taken at the desired soil depth. Finally, the sample is dried and the weight is then compared to the initial weight. However, Liang et al. (2016) commented that field sampling is notoriously tricky to measure in situ, the result is often not repeatable, and it is also labour and time-consuming. This argument was also in agreement with (Reichardt, 1988; Van Lier, 2000) with an addition that FC determination in the field has a set acceptable minimum drainage amount and has lateral losses caused by horizontal flow.

The inflection point has also been used as an idea to determine FC. Some work was done by Barros et al. (2017) using information extracted from the available literature. They estimated FC by using an equation based on the moisture retention curve and found that the inflection point can be considered a good estimator of FC. To that extent, several studies using Oxisols have shown that tension at an inflection point is lower than -0.06 MPa (Mello et al., 2002; B. M. Silva et al., 2014).

Statistical approaches are one of the options to predict FC and PWP values. Foster (1984) found a good correlation with an equation to calculate FC and PWP by using soil physical data analysis. He found that moisture content at PWP for mineral soil gave the best multiple correlations (R^2 = 0.865) with clay and Organic Matter (OM) but was independent of depth. Meanwhile, moisture content for mineral soil at FC was also best correlated with clay content, and the removal of OM improved the correlation

(R^2 = 0.784). These studies are useful since the experiment was done in the context of Malaysian soil type.

On the other hand, Saxton and Rawls (2006) produced good modelling for FC, PWP, and other soil physical parameters by using more than 2000 samples from U.S. Department of Agriculture (USDA) soil collection, and the verification was performed using an independent and wide range of datasets of soil textures. From the modelling, one software was produced, named Soil Water Characteristic and Soil-Plant-Air-Water (SPAW) software, and it is freely available on their web page (Saxton, 2009). This statistical approach is helpful if the data on soil physical is ready and there is an unavailability of pressure plate apparatus.

2.7 AWHC for IMZ

The amount of water held between FC and PWP is called AWHC (Foster, 1984). This term is interchangeably called Available Water Capacity or Available Moisture Capacity (Goyal 2015; Silva et al. 2014) or Available Water Content. AWHC is affected by the soil texture and structure and therefore, it might be different between layers of the soil. Valdivia et al. (2017) suggested that water holding capacity is a critical factor for irrigation management since it is related to the amount of water to be applied, timing, and frequency of irrigation. Knowledge of spatial variation of soil properties is an essential factor in SBI. Implementing differential irrigation water management according to field spatial variability can enhance the cost-effectiveness of irrigation (Liang et al., 2016) and improve water use efficiency, thus reducing nutrient leaching.

In China, Zhao et al., (2017) conducted a study to look at crop yield and Water Productivity (WP) at different variable irrigation rate management zones. There was a total number of three Variable Rate Irrigation (VRI) zones based on AWHC by using centre pivot irrigation. They found that plant height, Leaf Area Index (LAI), yield and WP of winter wheat and summer maize were different among management zones. In the field, they used a TDR (Trime T3-IMKO Ltd., Etlingen, Germany) to determine the trigger point for irrigation based on Management Allowable Depletion (MAD) of 0.45 AWHC. However, maximum and WP are not always in the highest AWHC zone because of the existence of layered textural soils among management zones. One study in Brazil to look at the potential of PI was done for IMZ based on AWHC. In this study, Souza & Rodrigues (2022) realised the potential for saving water, energy and crop yield, respectively equal to 1.85 % (4,770 m^3), 1.75 % (2,154 kWh) and 0.41 % (18.2 kg ha^{-1}). Interestingly, an additional result is that they found that small grid dimensions between 25 m^2 and 225 m^2 do not have a significant influence on conducting PI. Thus, a balance must be sought between optimal efficiency and feasibility in operational terms.

2.7.1 Relationship AWHC with other soil properties

Characterization of soil texture is important as it influences water-holding capacity, soil porosity, air-water circulation, and soil density (Chakraborty & Biswaranjan, 2015). AWHC is also affected by the presence of rock fragments, soil depth, and restrictive layer. Organic matter may increase soil to hold more water while compaction increases Bulk Density (BD) and reduces pore volume, consequently reducing AWHC (USDA, 1998).

Zebarth et al. (1999) reported that organic manure applications improve water retention but do not necessarily improve AWHC. This is because when OM is applied, the BD may reduce volumetric water content, which is the main component of calculating AWHC. A study done by (Asghari et al., 2009) showed that organic manure increased micropores (>75 µm) and decreased the number of macropores (<30 µm), thus promoting better water-holding capacity.

Foster (1984) carried out a study to determine AWHC for various parent materials up to 90 m depth for Malaysian soils. He found that AWHC for acid igneous rock, sedimentary rock, estuarine and riverine alluvium, marine alluvium, and peat is approximately 100, 127, 175, 236, and 413 mm m^{-1} respectively. Laterite soil has a low capacity depending on the volume of gravel. Based on his work, he demonstrated that AWHC can be determined by using a relevant fitted regression equation.

Debnath et al. (2012) reported that variables such as Organic Carbon (OC), clay and volume expansion had a positive relationship with water holding capacity. Conversely, variables such as BD, particle density, sand content and silt content had a negative relationship. They even predicted water holding capacity using an equation with R^2 = 0.923 after considering OC, sand content, silt content and clay content.

Pachepsky and Timlin (2001) looked into the relationship between topography and water retention properties. They found that the relationship between water retention and sand or silt starts emerging at 2.5 kPa. There was a strong relationship (R^2 = 0.703) between water content and silt content at pressures of 10 and 33 kPa. Meanwhile, by using generalised Least Square Regression, water retention and topography were highly correlated with R^2 = 0.671 and R^2 = 0.605 for 10 kPa and 33 kPa respectively.

Water holding capacity also has a good relationship with Apparent Electrical Conductivity (ECa), apparent canopy temperature and Normalised Difference Vegetation Index (NDVI). Bauer (2019) carried out a comparison between these three techniques: ECa was mapped using an EM38-Mk2 survey on bare soil while the newer alternatives (apparent canopy temperature and NDVI) were acquired via an Unmanned Aerial Vehicle (UAV) map. He found that apparent canopy temperature gave R^2 from 0.649 to 0.742, corresponding to linear regressions with Practical Available Water-Holding Capacity at 50 cm soil (PAWC50), whereby NDVI regression with PAWC50 was up 0.700 only when leaf desiccation. ECa had an $R^2 = 0.63$ when interpolated with PAWC50 but somehow managed to get $R^2 = 0.85$ when there was high soil salinity and a persistent soil saturation point.

2.8 FAO-CROPWAT model and its component

FAO-CROPWAT 8.0 is a computer program used as a tool of decision support for the calculation of crop water requirements and irrigation requirements based on soil, climate, and crop data. The program was developed by FAO and allows the development of irrigation schedules for different management conditions and the calculations of scheme water supply for varying crop patterns. FAO-CROPWAT modelling was intended to be used for food crops suggested by FAO, and this modelling does not include oil palm, which is only cultivated in some countries. It is crucial to obtain the precise water input to increase the irrigation efficiency. Several parameters are used to calculate ETc and Crop Water Requirement (CWR) in the FAO-CROPWAT software. It has eight different modules which are climate, rain, crop, soil, crop pattern, CWR, schedules, and scheme. The data input modules for the user are climate, rainfall, crop, soil, and crop pattern, then the software will automatically calculate crop water requirement and irrigation scheduling.

FAO-CROPWAT software is occasionally used to ascertain the suitability of an area for the cultivation of a crop. A study done by Ibrahim and Alaga (2016), proposed using FAO-CROPWAT modelling to calculate irrigation water requirements for oil palm in a different region within their country. Their results showed that a large percentage of Southwest Nigeria is suitable for oil palm cultivation. The water requirement increased from the humid forest zone to the Sahel savannah and it corresponded to increases in maximum temperature. The simulation result showed that the irrigation requirement per hectare ranged from 361 to 764 m^3 ha^{-1}.

Diakhate (2014) used FAO-CROPWAT as one of the tools to simulate crop water requirement and net irrigation for maize and sorghum in the Province of Kaolock, Senegal, for the rainy and dry seasons. He found that net irrigation for maize and sorghum was different for two different planting times. Maize uses more water than sorghum. Therefore, an earlier quantity of water can be predicted, and the best crop selection can be made.

Another study done by Surendran et al. (2017) looked at crop water needed for sustainable water resources in a pilot study for the Kollam District in India. His study attempted to simulate water used for rice, coconut, rubber, pepper, banana, brinjal, tomato, tapioca, cardamom, tea and others. By using FAO-CROPWAT, he found the current gross irrigation demand for the district was at 1045 Mm^3, of which 920 Mm^3 was supplied by groundwater sources, and the remaining was supplied by using surface water. From this study, they suggested a projected future total water demand, comprising irrigation, drinking, and industrial purposes, of 2667 mm^3. Therefore, there is a deficit in water if a new area is to be brought under irrigation.

Several studies have been done using FAO-CROPWAT as a tool to calculate the oil palm water footprint that is being used in the life cycle of a particular product, typically in terms of FFB. FAO-CROPWAT was directly used to compute crop water requirement and net irrigation for blue and green elements in water footprint calculation. Mungkalasiri et al. (2015) conducted a study for two districts, i.e., Pathamtani and Chonburi. He found that the water footprint for Pathamthani was 678.8 m^3 $tonne^{-1}$ while at Chonburi was 1070 m^3 $tonne^{-1}$. Then, he also compared the blue water simulated from FAO-CROPWAT to the actual amount of irrigation water applied by the farmers. Additionally, a study was done in Malaysia by Hashim (2014) based on inventory data from 281 plantations (equivalent to 441,000 ha planted area). They found that 3.56 blue, 1055 green, and 107 grey m^3 ton^{-1} of FFB had a total water footprint of 1175 m^3 $tonne^{-1}$.

2.8.1 Effective rainfall

Effective Rainfall (ER) is an estimate based on total rainfall (mm $month^{-1}$) by using a formula. This is because not all rainfall is available to the plant; some of it is lost by deep percolation, surface runoff, and evaporation. In irrigation practices, ER is the portion of the total precipitation retained by the soil and is available for use for crop production. However, the actual amount of rainfall that infiltrates the soil is commonly affected by initial soil water content, slope, soil types, and crop canopy. Generally, the efficiency of rainfall will decrease with increasing rainfall amount. For most rainfall values below 100 mm $month^{-1}$, the efficiency will be approximately 80%.

Several methods used are the U.S Department of Agriculture – Soil Conservation Service (USDA-SCS) method, the Evapotranspiration-Rainfall ratio method, the United States Bureau of Reclamation (USBR) method, the Soil Water-Balance Method, and the Renfro equation. Dastane (1976) described other empirical methods that have been used to estimate ER for different countries, typically used for both non-rice and rice crops. It is based on experience and is satisfactorily accepted, but it may specify the condition in which they were developed, for example, the Indian-1 and Indian-2 method (rice), the Japanese method (rice), the Vietnam method (rice) and the Burma method.

The USDA-SCS method was designed for monthly calculation and does not include rainfall intensity, irrigation, and slope factor (Ali & Mubarak, 2017). However, the USDA-SCS method takes into consideration soil, crop, and aridity factors. It is found to be suitable for areas with a low intensity of rainfall and high infiltration rate (Dastane 1976; Adnan and Khan 2012). It gives a lower value of ER compared to the Soil Water-Balance approach (Mohan et al. 1996).

The Evapotranspiration-Rainfall ratio method is considered a simplified semi-empirical method that does not essentially use soil properties or aridity. This method considers water storage capacity, runoff, and soil properties (Adnan & Khan, 2012). It may be suitable for broad planning purposes but not suited for instantaneous use for different crops with various soil properties and climatic conditions (Ali & Mubarak, 2017).

The United State Bureau of Reclamation (USBR) method is recommended for arid and semi-arid regions. It can be used for general planning purposes but is not suitable for instantaneous uses as the current or future climate may deviate from the past (Ali & Mubarak, 2017). This method is not considered satisfactory since it does not take into account the type of soil, nature of the crop, and frequency and distribution of rainfall (Adnan & Khan, 2012).

The soil water-balance method is considered an accurate way to estimate ER. This method takes into account evapotranspiration (ET), soil water storage, and runoff characterization. However, the disadvantage is that it requires significant input from meteorological data (Ali & Mubarak, 2017). Of all the methods, the Renfro equation is empirical and may not suit many situations (Ali & Mubarak, 2017). Furthermore, the accuracy of this method is low and too empirical (Adnan & Khan, 2012).

In the FAO-CROPWAT module, ER is one of the significant parameters used to estimate available soil moisture for the determination of total net irrigation (TNI). The option available for the calculation of ER is based on a fixed percentage, dependable rain (FAO/AGLW formula), and the USDA-SCS method. The calculation for ER based on a fixed percentage of rainfall is custom by accounting for losses from runoff and deep percolation, which is usually around 10-30%. Based on this value, the percentage is 0.7-0.9. Dependable rain is based on an analysis carried out for different arid and sub-humid climates developed in FAO/AGLW (Smith 1992). It is a combined effect of dependable rainfall and estimated losses due to runoff and percolation. A study conducted in Pakistan found that the FAO method obtained the best result for estimating ER in humid conditions (Rahimi et al. 2013).

Another vital factor accounted for ER is an interception of rainfall by vegetation which is later on loss through evaporation (Dastane, 1976). However, the interpretation of ER may differ among researchers according to their specialists in the field, and some of the methods do not take into account different types of crops (Ali and Mubarak, 2017). In oil palm, some of the studies do focus on ineffective rainfall due to canopy interception. A study done by Chong et al., 2018 has shown that interception by oil palm canopy was 27% of rainfall which is slightly higher (11-17%) than the estimated value by (Kee et al., 2000). Banabas, 2007 remarked that these differences might be caused by the angled of leaves during the high and low crop seasons.

2.8.2 Rooting depth

The root is essential and critical as it serves as the ability of the palm to absorb surrounding water and maintain its physiological activities. Nutrients are also taken by the root system through several processes, namely root interception, mass flow, and diffusion. Oil palm is categorised as a monocotyledon plant and the roots are an adventitious system classified by their size (Tinker, 1976). Primary roots are 5-8 mm, the secondary roots are 1-4 mm and develop from primary, a Tertiary (1.2 -1.7 mm) root arises from secondary and quaternary are unlignified roots on the tertiaries. Tailliez (1971) suggested that the greatest quantity of roots is to be found at soil depths of 20 and 60 cm and most absorption of nutrients is through quaternary roots and absorbing tips of primary, secondary, and tertiaries at this depth. (Ruer, 1967) reported that the density (g m^{-3} of soil) of all classes of roots in the top 60 cm of soil usually decreases with distance from the palm base, but for mature oil palms the total dry weight of absorbing roots from successive surrounding circles to a radius of at least 3.5-4.5 m.

Generally, roots are affected by the amount and availability of water in the soil (Carr, 2011). Descending roots mainly play a part in the absorption of water and when they are cut, the stomatal opening is reduced significantly (Ruer, 1969). However, too much water will also have an adverse effect on oil palm roots. Excessive water in the root zone may cause anoxia and usually kills younger palms. Nevertheless, fibrous roots spread and have greater tolerance to waterlogged periods as the oil palms grow older (Sharma, 2013).

The availability of water in the form of soil moisture may effect root activity (Nelson et al., 2006). Root activity is defined as comprising root density, length, and dry mass. Nelson et al., (2006) found that the highest activity of water uptake was under the weeded zone, which is closest to the palm stem, slightly lower for the area of stakes pruned frond, and lowest at the harvesting path.

In relation to water, the growth of oil palm roots can also be affected by several factors. When the soil is compacted, secondary root production is increased but then compensated with longer and thicker quaternary roots (Yahya et al., 2010). However, the exact root concentration depends on the soil type (Chan, 1977). In limiting conditions such as gravel conditions, the primary root tends to become twisted and constricted, the root system lies nearer to the surface, and tertiaries and quaternaries become coarser and lignified (Tailliez, 1971). In tropical soil, sometimes a hardpan can exist especially in ex-sugarcane areas where continuous tillage occurs, the roots are unable to penetrate this layer; thus oil palms are prone to wind damage (Paramananthan, 2013).

Therefore, it is essential to know the physiology of the oil palm rooting system. With regard to irrigation strategy, the placement of emitters would depend on where the most roots are available. In younger palms where the root is still limited, the emitter should be placed adjacent to the circle. However, in mature oil palms where the canopy is already overlapping between adjacent palms, the placement of the emitter can be anywhere but certainly needs to be considered operational-wise.

2.8.3 Kc Value

The ratio between ETc and ETo is known as the Kc. ETo is defined as the rate of evapotranspiration from a hypothetical crop with an assumed height of 0.12 m, with a surface resistance of 70 sec m^{-1} and an albedo of 0.23, closely resembling the evaporation from an extensive surface of green grass of uniform height, actively growing with unlimited water supply. In contrast, the Kc value is a crop coefficient that varies between crop development stages. It also varies between crop types. It is thought of as a fraction of reference crop ET that is used by the actual crop. Value of Kc for selected vegetables, roots and tuber, legumes, perennial vegetables, fibre crops, oil crops, cereals, forages, sugar cane, tropical fruits, and trees are available to be used (Allen et al., 1998).

Kc values available that are for closely related species and somewhat similar to oil palm morphological structure are date palms and other palm trees. (Allen et al., 1998) suggested that Kc for Date palm was 0.80-0.85 while for palm trees, it was 0.85-0.90. Several studies reported on the Kc value for oil palm using the water balance method and micrometeorological station method. Early work was done by Silva (1985) who reported an oil palm crop factor of 0.75 but the basis behind this value is not well documented.

More detailed work on the Kc value for oil palm has been carried out by Henson (1995), who suggested that Kc is equal to 1.00, but this value may decline to 0.90 when solar radiation exceeds 20 MJ m^{-2} day^{-1}. This is presumably because of stomata closure when the vapour pressure deficit increases. He also reported that the Kc value was 1.05 for 11 year old palms, estimated from a micro meteorological station located in a moist coastal area during late 1994 (Henson 1999). In the study, a micrometeorological station was set up in the centre of a 94 ha block. He measured Potential Evapotranspiration (PET) and ET, and ET was divided into two, i.e., above and below the canopy. The ratio of ET to PET, which can be interpreted as the Kc value, was 0.93 for the average data on the selected days in October and December. Additionally, ET below the canopy was only 12% of ET above the canopy.

In 2003, a study was conducted in Northern Malaysia, which routinely experiences dry spells starting in mid or late December and ending in March. Data measurement represented oil palm at the age of 27-34 months after planting (immature palm). PET was calculated from the measurement of net radiation, wind speed, and atmospheric vapour pressure deficit using the standard Penman Equation. In contrast, actual evapotranspiration (AET) was calculated by using water balance and was valid just for the dry season (as no measurement was made for deep drainage or runoff during excessive rainfall). AET/PET was found to be at 1.0 in January and started to decrease to lower than 0.2 in late February. Then it began to increase back to 1.0 from April onwards. The reduction was believed to be caused by the closure of stomata as it was highly related to low to no rainfall during the period of the middle of January to the middle of March (Henson and Harun 2005).

In another report from the same trial site, measurement of data continued from February 2004 to June 2004, when the palm reached the age of 4 years old. The measurement recorded a relatively higher rainfall amount compared to the previous paper. They found that Kc was 0.30 in February (low rainfall) and started to increase to 0.81 in April (highest rainfall). Kc continued to increase to 0.87-0.90 from May to June (Henson and Harun 2005).

A study in Cote d'Ivoire by Dufrene et al., (1992) reported that the Kc value during the rainy season was 0.81 and this value was lower during the dry season, which was only 0.56 for oil palms aged 14-17 years old.

In some situations, the Kc value was not directly reported. Hong, 1979 carried out a study on water usage of oil palm in the form of ETo using the Lysimeter technique from 1976-1978. ETo was calculated using the Penman-Monteith equation using data from a nearby meteorological weather station. It was concluded that the Kc value for immature oil palm (1-3 years) ranged from 0.81 to 1.14.

Safitri et al., (2018) carried out a study on various soil types and oil palm ages. They used calibration between the soil moisture change model based on Richard's equation and soil moisture sensor data placed at the root zone. They found that Kc was between 0.68 and 0.70 for oil palms aged from 7 to 13 years old. Overall, it can be said that the Kc value for oil palm can be improved further. There are many factors that might contribute to its variation, such as palm age, soil type, temporal weather, and changes in the selection of planting material.

2.8.4 Infiltration

Soil infiltration rate is the quantity of water that can pass through the soil surface at a given time. According to Richards (1952), infiltration is defined as the downward entry of water into the soil. This is associated with two events; the passage of water through the soil surface (intake) and the movement through soil mass (permeability). It is sometimes called soil intake rate. Fine-textured soil has more pore space and can hold water longer than sand-textured soil. Typical infiltration rates in one hour are shown in Table 2.1. The infiltration rate is affected by the amount of calcium, salt, tillage, vegetation on the soil surface, microorganisms, and the amount of OM in the soil. Soil compaction may also reduce the infiltration rate. The infiltration rate is high when the soil is dry, but after that, the rate decreases as it achieves a steady state.

Table 2.1: Basic infiltration rate, mm hour^{-1} according to soil type

Soil Type	Basic Infiltration rate (mm hour^{-1})
Sand	Less than 30
Sandy Loam	20-30
Loam	10-20
Clay Loam	5-10
Clay	1-5

(Brouwer et al., 1985)

Infiltration needs to be described quantitatively but nonlinearly at the same time. This led to the development of an empirical expression relating to infiltration rate over time. The most widely used is the model suggested by Horton in 1933. The widely used empirical equation for surface irrigation is the Lewis-Kostiakov-Mezencev set of equations (Assouline, 2013). Kastiokov's model suggests a formula that assumes that when the time, t = 0, then the infiltration rate is infinite, whereas at the time = ~, the rate approaches zero (V. P. Singh & Yu, 1990). Kastiokov's models are quite popular because of their simplicity in use and proficiency.

Soil infiltration rate is an important aspect and it affects the surface irrigation uniformity and efficiency because it describes how the water is being distributed and transferred from surfaces to soil profiles (Rashidi et al., 2014). Rashidi et al., (2014) made a good argument and established a model to predict infiltration rate based on the soil's physical properties. Infiltration behaviour determines essential variables such as inflow rate, length of run, application time, depth of percolation, and tailwater run-off in the irrigation system (Adeniji et al., 2013).

Patle et al., (2018) carried out a study using a double-ring infiltrometer and found that sandy loam soil had a basic infiltration rate from 24 to 168 mm hr^{-1}, compared to loamy sand soil which had a basic infiltration rate of 3.0-138 mm hr^{-1}. By using regression analysis, they suggested sand, particle density, and OC have a positive correlation with infiltration rate whereas silt, clay, BD, and moisture content have a negative correlation.

Mustafa et al., (2003) conducted a study regarding infiltration. He calibrated the Kostiakov model with the observed infiltration rate for local conditions. At the beginning of the experiment, cumulative infiltration was less compared to the Kostiakov model, but at the elapsed time of 180 minutes, the calculated infiltration rate became equal to the observed value. Another observation by Adindu et al., (2014) has found that data simulated using the Kostiakov model showed a closed relationship with measured infiltration rate for different locations on the soils of Umudike, Abia State in Nigeria.

Hasan et al., (2015) conducted a study on clay-loamy soil without any tillage practices and had typical soil vegetation. They also compared the observed data with the estimated data from Kostiakov's model. The average value of the error percentage was 0.134. Values of log (a), alpha, and b were 0.178. 0.683 and 0.145, respectively and these values are below 1, following the requirement of the modified Kostiakov's model.

2.8.5 Critical Depletion

At a certain fraction of AWHC, there are points in which plants can suffer or experience water stress conditions before entering the wilting point and it varies between crop type, crop age, and growth. Hence, the term critical depletion (CD) was introduced to represent the limit of depletion that is allowed before irrigation refills water losses in the system. On the other hand, Allowable Water Deficit (AWD) is the amount of water that can be temporarily withheld from plants before they suffer irreversible damage or the difference between the current soil moisture content and the CD.

For oil palm, very few studies report on CD at different growing ages. Rey et al., (1998) said that CD for oil palm was around 70% of the AWHC as they found that no stomatal closure occurred until 70% of AWHC had been used. As suggested by Smith (1992), critical soil moisture level is when moisture stress occurs and affects ET and crop production. The value is expressed as a fraction of AWHC and is typically between 0.4-0.6; the lower values are taken for sensitive crops with limited root systems, while the higher values are for deep and dense rooting crops. Henson et al., (2005) investigated the extension of spear leaf emergence with the percentage of available soil water content. Based on his findings and if reliably accepted as an indicator, the spear extension rate rapidly declines when the available soil water content is between 75% and 80% (0.75-0.80). These values are also quite similar to the 0.70 value reported by (Rey et al., 1998).

2.9 Micro-sprayer irrigation method

Previously, the furrow system was implemented with canals constructed between planting rows (Lee and Izwanizam 2013) and this method lasted for almost 15 years. A previous adaptation of such a method was selected to minimise interference in daily activities. When the micro-sprayer method is being considered, the selection of lateral intensity, as well as emitter placing is likely to become a significant problem. This is due to possible complications for activities in the field such as harvesting, manuring, weeding, and others. These activities are often manually, semi-, or fully-mechanised.

In addition, the palms will get taller over time. At 25 years old, typical oil palm trees will be almost 15.0 m in height. When harvesting is done, several fronds will be cut down from the palm crown, and this brings pruned fronds to the ground from a height of at least 5 meters, resulting in a very high impact fall and could damage emitters placed nearby. The same situation applies to harvesting bunches that can sometimes weigh up to 30 kg bunch^{-1}. This activity will occur at least twice a month for every palm, therefore there is a high probability that harvesting activity could damage the irrigation system.

In Thailand, Palat et al., (2008) reported on several types of irrigation systems including furrow, drip, micro-sprayer, and sprinkler. They noted that the furrow system was considered low cost but did incur additional costs to place bridges and maintain the furrow itself. Drip and sprinkler systems had a low cost of running the system but were offset by high capital costs. Meanwhile, the micro-sprayer had the highest price and required regular attention to run smoothly. They also reported that the sprinkler and micro-sprayer methods occupied 90% and 28% of the total area, respectively. However, the yield for sprinklers was slightly lower than for micro-sprayers. In comparison, the drip system had a higher yield when a rate of up to 360 litres palm^{-1} was applied. Therefore, the results of the study indicated that there were no differences in terms of coverage occupied by spray patterns.

Concerned by the factors mentioned above, a micro-sprayer was selected for this study. In addition, it served as a reference point as results from this project could be compared to micro-sprayer irrigation projects done at other estates. Drip irrigation may be good, but it is prone to clogging and requires an intense monitoring schedule since it is impossible to monitor it from a distance with the naked eye. In contrast, the micro-sprayer system is easy to observe from a distance and has a relatively larger orifice size than the drip system; hence there is a lower risk of clogging. A study done by Li (2015) showed that the discharge ratio for a given time increased linearly with the pathway width, length, area, and filtration area, indicating that the sensitivity to clogging was inversely proportional to the abovementioned parameters. He also revealed that an emitter model with a smaller pathway area or a lower manufacturing coefficient of variability was more susceptible to clogging. Emitters are installed on the same level as the ground without any stand like in the sprinkler system, thus reducing the damage risks from human activities such as pruning and harvesting. Single emitters will also minimise pressure loss in the system and avoid low uniformity.

For this reason, emitters were installed on a single point facing the palm trunk. The decision to place one emitter for every palm was based on the hydraulic properties of the emitter itself. Typically, oil palm blocks have 10-20 palms per planting row. The increase in emitter numbers for a lateral line will increase irrigation output and require a larger diameter size of lateral pipes to reduce friction loss. Ame et al., (2022) demonstrated that lateral cost accounts for a large portion of irrigation cost, which is highly related to lateral diameter and length, emitter flow rate, and water irrigation quota.

2.9.1 Low-cost emitter as point sources of water

Emitters are used to distribute water to plants, and they come in various types. The classification of emitters is usually determined by flow rate and operating pressure.

One type of emitter is pressure compensated (PC), which only allows a relatively equal amount of water at the range of pressure. While these features are outstanding and can give numerous advantages, they are sometimes prone to clogging due to improper installation of filters or unclean water sources. Emitter clogging is highly dependent on the labyrinth or water pathway inside the emitter. Aboamera et al., (2017) found that the turbo key emitter had the lowest percentage of clogging compared to long-path and PC emitters. Another study by Zaghluol et al., (2014) found that the Katif and Micro Jet emitters stand out as there was no clogging at all when 2.0 gram litre^{-1} of sand particles (diameter <0.1mm) were used. Drip irrigation or pressurised irrigation typically requires higher initial costs, which are attributed to components of the drip line, emitter, and filtering system (Polak et al., 1997), and sometimes the parts are not available at local hardware shops. The high initial cost of irrigation restricts the efficiency of the irrigation system in some developing countries or small farmers who prefer to adopt cheaper alternatives (Postel et al., 2001). A study done by Chirgwin and Sutton (2019) has shown that low-cost micro-irrigation emitters performed well under all indices compared to conventional emitters. In Nigeria, a study was conducted to evaluate the substitution of imported emitters for drip irrigation systems, which were fabricated using cheap and readily available materials. They reported that Emission Uniformity (EU) was at 74% and can be improved with further improvement (Sobowale et al., 2015).

2.9.2 Uniformity assessment for micro-sprayer irrigation

For uniformity, it is the concept of 'how equal' or 'unequal' the application rates are. The low value of the coefficient indicates application rates are significantly different while a high value of the coefficient suggests application rates are very similar and evenly distributed. One of the earliest indices that were introduced is the Christiansen's uniformity (UCC), which is used to check water distribution in sprinkler systems. Andrade et al., (2022) reported that wind speed negatively impacted UCC with r^2 = 0.75.

Keller and Karmeli (1974) suggested a new equation for calculating the non-uniformity in drip or microsystems, which consider additional components, i.e., emission uniformity based manufacturing variation and pressure differences or EU. This formula used the ratio of the minimum emission rate to the average emission rate multiplied by the low quarter of emitter flow rates caused by manufacturer variation (Amer & Gomaa, 2015). For the EU, data below 90% was considered unacceptable and this parameter was the most sensitive compared to other indices. Nakayama et al., (1979) considered the manufacturing coefficient of variation to be 0.05-0.50, but these days, it is likely to improve with a typical value of 0.02-0.06 (Burt, 2004).

Distribution uniformity (DU) is one of the indices used for sprinkler systems, but it is also applied to micro or sprinkler irrigation systems (Irmak & Haman, 2017). This type of measurement is used to show variation, utilising the ratio of the minimum to the mean. A DU percentage of less than 60% indicates that the irrigation water is unevenly distributed. In comparison, a high DU of more than 80% indicates that the application is relatively uniform over the entire field. (Burt, 2004) reviewed the DU values (he used the term low quarter distribution uniformity) for drip and micro-irrigation systems in many irrigation systems in Califonia, USA. He reported that in the early days, pre-1996, the average drip DU value was 0.73-0.75 and for micro-sprayers, DU was 0.63-0.65. However, this value has improved significantly to 0.85 for the Drip and 0.80 for the micro-sprayer.

Another performance indicator used by researchers is the Statistical Uniformity Coefficient (Us), which is based on the assumption that the emitter flow is normally distributed. Bralts and Kesner (1983) developed a graphical technique called the nomograph to simplify the statistical method used to estimate the coefficient of variation. The determination of probability in each tail was one-sixth bell-shaped, which included the upper and the lower values of the distribution. The nomograph showed emitter flow rate for the range <60% was unacceptable, between 65% - 70% was considered poor, 75 - 80% was fair, 85% - 90% was good and 95% - 100% was excellent (Lamm et al., 1997).

2.10 Irrigation software for planning purposes

One of the critical processes in irrigation planning is to design an irrigation layout. This process can be cumbersome and requires a high level of technical expertise, especially when involving hilly topographic conditions and a limited cost of implementation. Some of the available software are IrriPro, IRRICAD, and IrriLab. Each of the mentioned software has its advantages and limitations. Baiamonte et al., (2021) described that Irrilab lacks features to check the uniformity goodness of the emitters, the pressure head's distribution, and the emission uniformity. Furthermore, Irrilab only permits rectangular sector shapes, unlike IrriPro, which can be used to design any sector shape.

The IrriPro and IRRICAD software are able to calculate the cost required for particular designs, thus enabling the user to find different solution costs (Baiamonte et al., 2021; Brennan 2008). However, IRRICAD is relatively expensive and does not handle situations found in many irrigation systems, such as loops and multiple pumping stations (Andrade et al. 1999).

IrriPro is a software produced by Irriworks Ltd. To design irrigation layouts and simulate the hydrology of the system based on numerical solutions. It provides a tool for analysis and diagnostics needed to evaluate the effects of each design choice made by the user. It can identify potential malfunctions and allows users to create graphical presentations of the result. Several features owned by IrriPro are that it can calculate hydraulic properties and interpret the data in a visual form so that the user can identify the acceptable and unacceptable areas based on their hydraulic characteristics.

This software uses rigorous algorithms to solve equations of continuity and equations of motion by combining hydraulic and geometric boundary conditions, distribution of the plano-altimetric network, geometric and hydraulic characteristics of pipelines and installed emitters by using the basis of Darcy-Weisbach equation. The step-by-step procedure elaborates on details by (Provenzano & Pumo, 2004) and later on improved by simplified procedures (Provenzano et al. 2005), making this software are able to estimate the head losses along the pipe and localised caused by installed emitters along laterals pipe. In comparison to other software, the IrriPro software claims that it does not use the criterion of constant speed to calculate the size of the pipeline. Instead, speed is calculated as a variable at every point (Irriworks, 2022).

Arshad et al. (2014) carried out a study using the IrriPro in a greenhouse to test the operational reliability, efficiency, dependability, and harmony of the drip irrigation system. The irrigation system used PC-type emitters with a lateral length of 16 meters. They compared the existing drip irrigation with the simulation done by the IrriPro. The observed UCC for the system was 96.50% compared to the simulated 99.98%. For the DU, the observed data was found to be 94.36%, while the simulated data was 99.88%. They also found that the EU for the observed data was 99.22% while 99.99% for the simulated data. Uncertainty was found to be less than 10%, which indicated the accuracy of the system.

Di Dio et al. (2008) studied the IrriPro application in relation to an existing drip irrigation plant with an irregular shape and variable slope. They compared simulated pressure heads and flow rates with the corresponding measured values in the field planted with olive trees. They first did a laboratory experiment to ascertain the flow rate-pressure head relationship and manufacturer's variation coefficient and found that the emitter was a self-compensation emitter. They also reported that simulated and measured pressures in the sub-main pipe were quite similar, expressed as a percentage related to less than 9%. The EU simulated by IrriPro was 95%, slightly higher than the value of 91% measured in the field.

2.11 Summary

Spatial variation in the soil in terms of soil physical properties is highly correlated. Many studies have shown that sand, silt, and clay have a direct relationship with water retention. Based on this, the oil palm could potentially have different irrigation responses at different management zones delineated by soil-water holding capacity. The determination of AWHC delineation can be done through ECa, but extra tools and effort are required to cross-check samples, which is still needed for verification. Apparent canopy temperature and NDVI are interesting to explore, but they are pretty complex at an estate level that does not have access to geospatial and technical knowledge. Delineation of the zone by using soil data is more straightforward, requires fewer steps and reduces procedural error.

Irrigation in oil palms requires a high initial cost and an additional workforce to monitor the system. By using a low-cost emitter, replacements can be cheaper and do not require high-end filtration systems, thus reducing a big chunk of initial cost. Low-cost emitters are considered fast alternatives since they are widely available in the market, but the downside is a lack of technical data to use in hydraulic calculation for irrigation pre-assessment. Evaluation of its properties may help practitioners understand which emitter would be suitable for their main objectives and improve the hydraulic condition of the whole system.

Irrigation design software such as the IrriPro software has proved its reliability in designing and analysing the system before any project starts. A previous study showed that the differences between simulated uniformity by the IrriPro and actual measurements were relatively small, and it is strongly related to the advantages of pressure-compensating emitters, which are not prone to pressure variation. Since this study is done to support limitations on operational issues, the helpfulness of irrigation software to maximise the usage of a low-cost emitter is proposed. In contrast, topographic variation in the study plot may add complexity to the software to calculate the hydraulic of the system.

This study uses IMZ to manage water resources at the field level better. The placement of the soil water potential meter shows how the water demand varies among the zones. The implementation of a soil sensor, IoT for control, and irrigation based on soil spatial delineation has met the requirements for the concept SBI system. Many studies have been conducted on SBI, particularly on other crops, but not specifically on oil palm. It is necessary to reassess the irrigation methods used in oil palm cultivation and as a foundation for future research. Additionally, this study will provide effort for the optimization of resources towards sustainable agriculture.

CHAPTER 3

MATERIALS AND METHODS

3.1 General description of experimental works

In general, the experimental work was divided into four main categories, which are the delineation of the study area into irrigation zones and its impact on TNI, experiments of the emitter, uniformity evaluation for installed layout by using commercial software and finally, assessment of the oil palm and water use efficiency. Experimental works began with soil samplings at three different depths from 28 points of location. Several lab analyses were done to determine the soil's physical and water-holding properties. Then, all the values were analysed on a computer using Geographic Information System (GIS) software to delineate the study area into appropriate AWHC zones. In order to get a contrast analysis, only two selected zones representing the lowest and highest range of AWHC were chosen for the installation of irrigation. A commercial irrigation software, namely the IrriPro software, was used in this study to design an irrigation system and to analyse the uniformity between simulation and actual measurement in the field. In-house experiments and field data regarding emitter properties and infiltration rates were collected to serve as supporting data in the IrriPro software. Once the installation of irrigation was complete, actual uniformity data was collected and compared with the simulation data produced by the IrriPro software. Meanwhile, the older piping network was also evaluated using the IrriPro software. The FAO-CROPWAT software was used to look into calculated irrigation water requirements and it was compared to historical irrigation input that was previously done by the estate. Upon completion of the irrigation system, irrigation was carried out based on information from the sensor located on the lowest AWHC value for each irrigation plot. Additionally, after completion of the irrigation setup, bunch number, bunch weight and oil palm growth were measured during intervals. All these parameters were assessed as an indication of palm response. A brief summary of the activities carried out in the current study is shown in Figure 3.1.

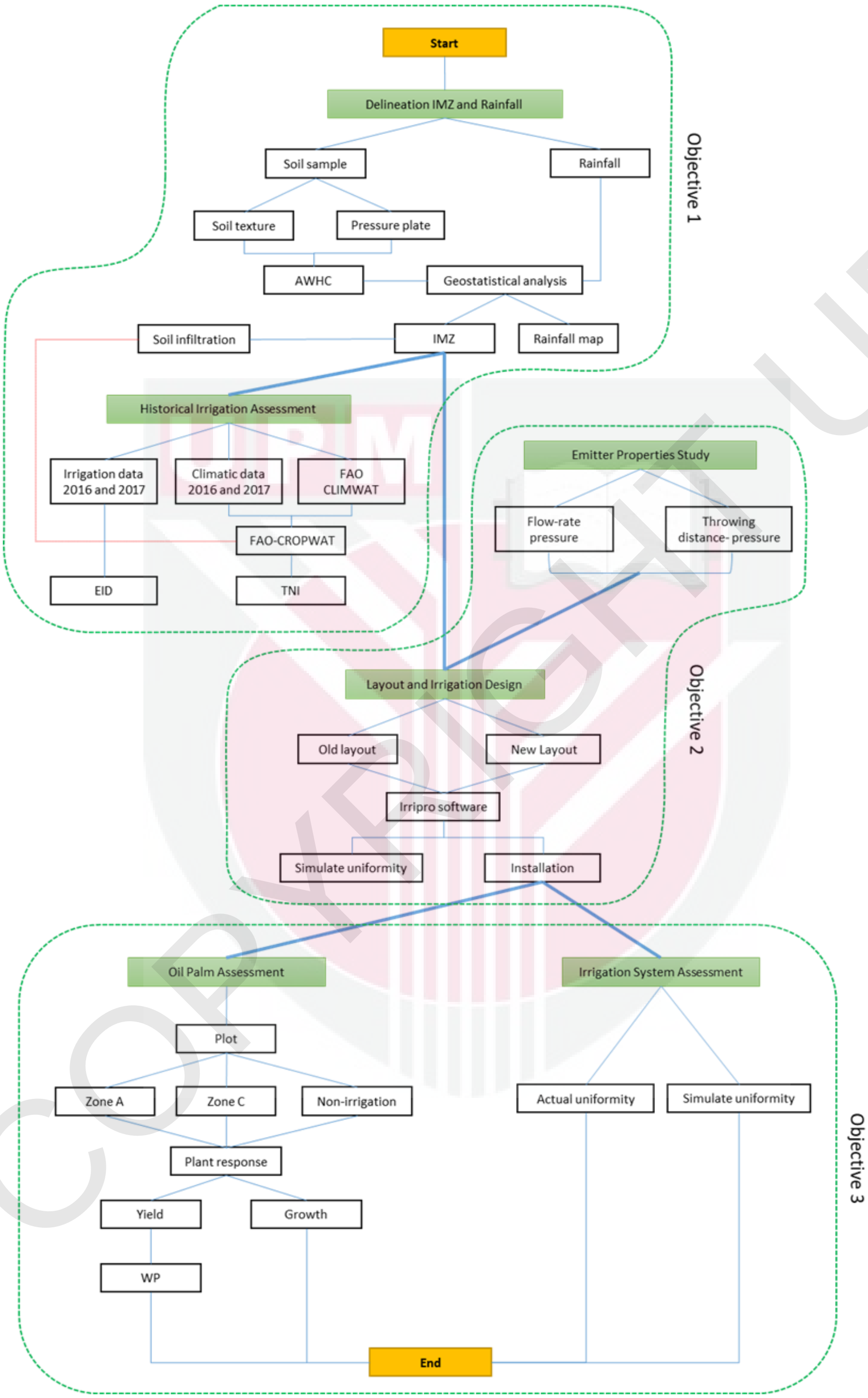

Figure 3.1: General outline of activities involved in this study

3.2 Location of the experimental site

The study was carried out in Serting Hilir Estate, FGVAS (2.950266°N, 102.489499°E), Negeri Sembilan, which consisted of 46 – 52 m of elevation from sea level. This area is categorised as a dry region with an annual rainfall distribution below 1600 mm $year^{-1}$ and a flat to gently undulating topography. Paramananthan (2015) produced a semi-detailed soil map and reported that the soil series in this area, called the Rasau Series, is classified as Haplic Nitisols (FAO, 2014), or Typic Kandiudult according to Malaysian Taxonomy Classification (Paramananthan, 2020). Soils of the Rasau Series are deep, well-drained soils developed over sub-recent alluvium. They are characterised by their brownish-yellow fine sandy clay loam subsoils. These soils occur on undulating terrain (4-12% or 2-6° slopes). The topsoils of the Rasau Series consist of a brown (10YR5/3) fine, sandy clay loam. The subsoils, up to 100 cm, are a uniform brownish yellow (10YR6/6), fine, sandy clay loam. Structures are weak to moderate, medium subangular blocky and consistently friable. Patchy clayskins occur on ped faces.

At the start of this project, the oil palm cultivation had already entered the second generation of the replanting cycle. A total of 13 plots separated by two different blocks were selected for assessment. Ten plots located at Block 1 represented irrigation treatment, while three plots located at Block 2E represented non-irrigation treatment (Figure 3.2). In order to reduce the complexity of the SBI setup, two plots from Block 1 were excluded and eight plots were retained for the palm growth assessment. However, the number of plots for the non-irrigation treatment remained unchanged. Historically, Block 1 was treated with irrigation since 1991 by using the furrow system until palms were felled for replanting purposes. Starting in 2014, the estate has implemented a micro-sprayer irrigation system, and the boundary of the system is indicated in Figure 3.3. Meanwhile, the red coloured line represents the boundary limit for the grid system of this current project. Details of the study area are shown in Table 3.1.

Figure 3.2: Location of the study area and its semi-detailed soil map

Figure 3.3: Map of the trial plots for the study

Table 3.1: Details background on study area at Serting Hilir estate, FGVAS

Treatment	Irrigation Plot	NIR Plot
Estate	Serting Hilir Estate, Negeri Sembilan	
Area	20.3 ha	3.30 ha
Block	1	2E
Year of planted	December 2014	
Topography	Flat (0°) to Undulating (3°)	
Irrigation	Micro-sprayer method	Nil
Plot Number	8	3
Plot Size	4 x 4 palms	3 x 3 palms

3.3 Field sampling and determination of AWHC

The MapInfo Professional, Pitney Bowes Software Inc, Version 12.0 was used to create a 100 m × 100 m grid system of the study site consisting of 28 main sampling points Figure 3.4. Locations for each point used the World Geodetic System 1984 (WGS84) longitude and latitude projection system, which was later converted into the Kertau (RSO) projection system. A copy of the map that included cross sections for each point was saved as a portable document format (PDF) and uploaded to a smartphone. The Avenza map application, Avenza System Inc, Toronto, Canada, was used to track locations at the study site.

A grid system is more organised and has substantial data collection from a statistical view, as grid point sampling is better for detecting patterns of variability. It can construct contour maps of each soil test parameter and provide a detailed look at the tested variable with georeferenced points (Dawson & Knowles, 2018). It can be seen that the actual points sometimes deviate from the pre-determined points, resulting in an uneven straight line. This occurred due to uncontrollable factors in the field, such as minor roads, the presence of rocks, drainage lines, or the original point being placed at the planting row. When this happens, the initial point needs to be adjusted to reduce the sampling error due to disturbed soil factors.

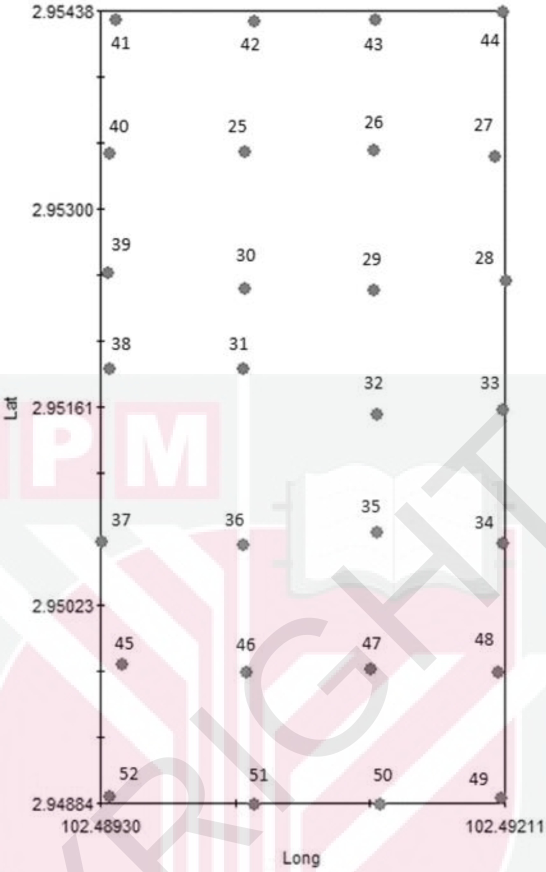

Figure 3.4: Soil sampling points by using a WGS84 projection system

Soil samples were collected by digging with a chisel, and then a set of ring cores were used to gather the soil samples. There were three sub-samples for each point, i.e., samples from 0-30 cm, 30-60 cm, and 60-90 cm of soil depth, making a number for sampling 84 samples. A measuring tape was used to determine the depth of samples.

After the soil samples were removed, they were sealed in a ring cover to preserve their shape and condition before being weighed on a digital scale. Samples were sent to the soil physical laboratory at University Putra Malaysia (UPM) to establish key soil physic parameters such as BD, soil water content, FC, and PWP. First, the total weight of the ring core with fresh soil samples was measured. Then, about 10 grams of soil was taken from the ring core and dried in an oven at 105°C for 1 to 2 days. After that, the soil was weighed using a digital scale and the final weight was recorded. Then, the remaining soil in the ring core was removed and divided into five parts for the soil-water retention procedure. Each part was placed on five ceramic plates according to the sampling number. After that, the soil was saturated with water for 16-24 hours (Figure 3.5).

Figure 3.5: Saturation process before sample transfer into the pressure chamber

Figure 3.6: The arrangement of the sample in the pressure chamber

Four ceramic plates that contained saturated soil samples were then placed in different pressure chambers (Figure 3.6). The remaining plate was left at room temperature for 24 hours. The four-pressure chamber was set at 1, 10, 33, and 1500 kPa, respectively. Within the pressurised period, the pressure gauge was monitored to maintain desirable value, especially in the early stage of the desaturation process.

All samples were left in a pressure chamber for 4-5 days, depending on water overflow from the chamber. When there was no excess water, the samples were removed from the pressure plate apparatus. All samples were removed from the pressure chamber and weighed using a digital scale. Then, samples were dried in the oven at 105°C for 16-24 hours. After that, samples were weighed again by using a digital scale to determine the final dry mass in gravimetric percentage for preset (1, 10, 33, 1500 kPa) pressure and samples that were left at room temperature as well.

AWHC was calculated based on Equation (1) where the FC point was for a sample at pressure 10 kPa, while PWP was for a sample at 1500 kPa. Each point had three data points to represent 0-30 cm, 30-60 cm, and 60-90 cm soil depth. Data for each soil depth was summed to get the value of AWHC up to 90 cm. In this equation, BD is bulk density in g cm^{-3}, FC is field capacity and PWP is permanent wilting point. Both represent gravimetric soil moisture in percentage, and depth is soil thickness during sampling in mm, Dw is water density, which is 1.0 g cm^{-3}. Meanwhile, AWHC data was analysed according to depth using Statistical Analysis Software (SAS) software, SAS Institute Inc. USA. All AWHC data were tested by using the Shapiro-Wilk test for normality. The null hypothesis variable is normally distributed and will be rejected if the p-value < 0.05.

$$AWHC = \frac{FC - PWP}{100}\ x \left(\frac{BD}{Dw}\right) x\ depth \quad (1)$$

3.4 Interpolation of AWHC

3.4.1 Creation of a working layer in MapInfo

Several layers were selected as working layers for interpolation. The most critical layer was the collection of data, which consisted of location, point of sampling, and AWHC value. All vector and raster files were created as a working layer in MapInfo software. There were several files, namely boundary data, plot data, and table data. Table data was a source of information stored in table form consisting of location, point number, the value of AWHC for each sampling point, and others. Boundary data consisted of a vector line drawing acting as a boundary of the layer for interpolation (Figure 3.7).

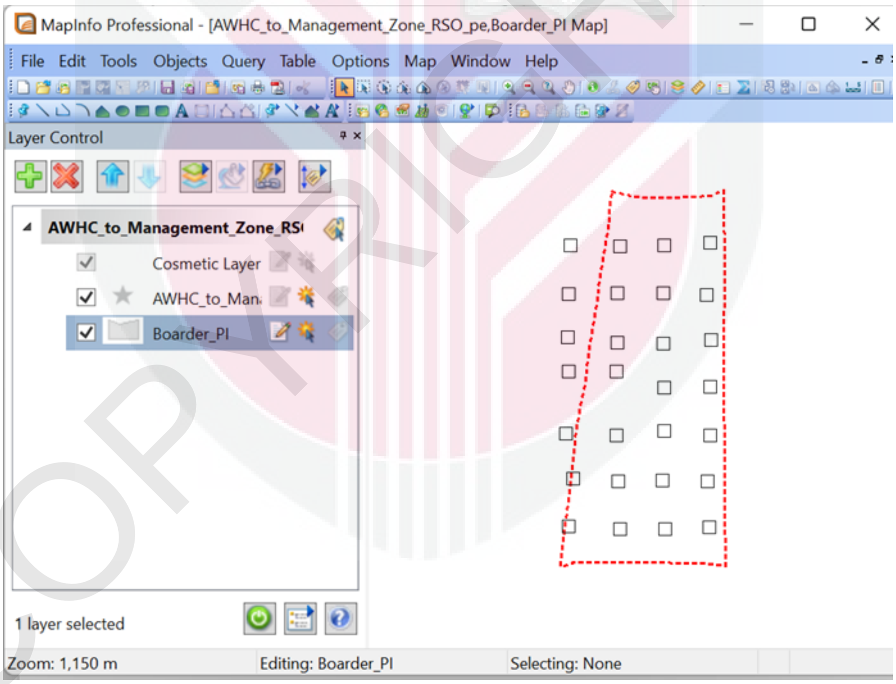

Figure 3.7: The process of inserting the working layer in the Map Info software

Plot data consisted of a polygon file to represent ten selected plots with a number of 16 cluster palms. Table data was first inserted into the MapInfo Software. File > Open > Select Excel type of file > browse and select file > ok > and set ‘float’ for all column types. Then, a point was created by using that table by following these sequences:

Table > Create points > Choose WGS84 projection. By doing this, MapInfo was created as a file that contained points and was able to be opened by this software.

3.4.2 Determination of best-fit semivariogram model by using GS+ Software

The table form in Excel that contained all the AWHC data and its location was imported to the Geostatistics for Environmental Sciences Software (GS+ Software), Version 7, Gamma Design, USA, to determine the best-fit model for interpolation. The appropriate columns were assigned to each parameter according to the X, Y coordinate and Z as a column of AWHC. A summary of the data can be viewed by clicking on Data > Summary statistic > Primary Variate. Calculation on the semivariogram was done by clicking on Autocorrelation > Variogram > Primary variate > Calculate. Values for Active lag distance and lag class distance interval were manually inserted and confirmed by clicking on the 'Calculate' button again. For this analysis, the value of 'Active Lag Distance' was set at 600 m while the 'Lag Class Distance Interval' was set at 120 m (Figure 3.8). Under the variogram menu, the 'Model' button was clicked and the best model for the variogram was selected based on the highest R^2 value. All properties were recorded and used in the mapping process using the ArcMap Software, Esri Inc, USA.

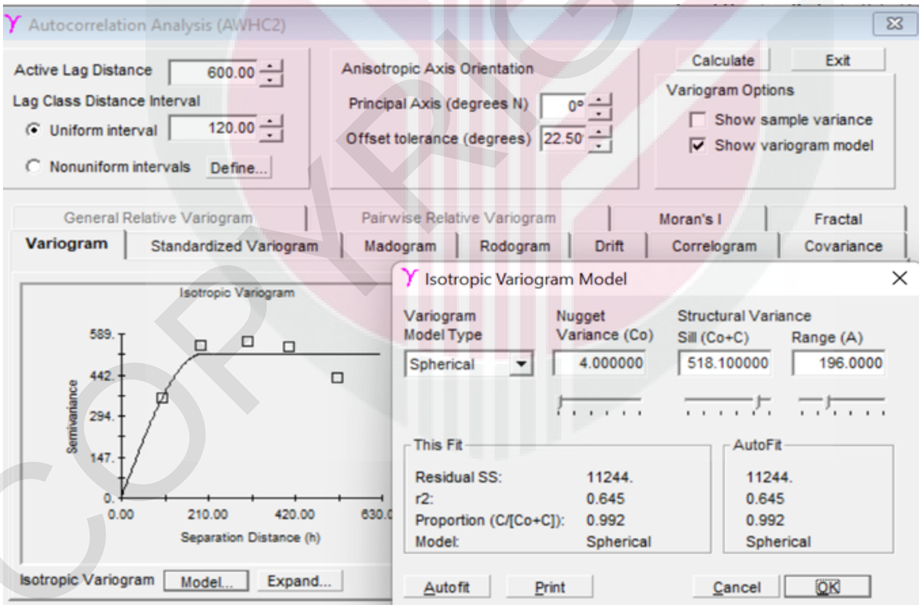

Figure 3.8: The user interface of GS+ software for geostatistical analysis

3.4.3 Preparation of layer for ArcMap Software Interpolation

To use the ArcMap software, the .tab file had to be converted into a .shp file. It was done using a translation tool in MapInfo software. The translation process in the MapInfo Software began with the selection of Tools > Universal translator > Universal translator > File > Translate. Under reader selection, the existing .tab file was selected by clicking on the 'Dataset' button. Under 'writer selection', the new location of the .shp file was set, and then the new location was determined by clicking on the 'Dataset' button. Finally, the 'OK' button was clicked to initiate the translation process, resulting in a new .shp file layer being created and ready to be used in the ArcMap software.

In the earlier stages, all parameters for the determination of the best-fit model in the GS+ Software were based on Kertau (RSO) projection. Therefore, some steps were used to change the .shp layer file with WGS84 projection and used in the ArcGIS map in the Kertau (RSO) projection form. Using the ArcMap software, the 'Convert Coordinate Notation' menu was selected using the following steps: ArcMap > Arc Toolbox > Data Management Tools > Projections and Transformations > Convert Coordinate Notation. Under this menu, a table that consisted of AWHC data was located using the 'Input table' button. WGS84 projection was selected for the 'Input Coordinate System' menu. In 'Output Feature Class', a new folder was set as the target folder of a new file with the Kertau (RSO) Projection system. Then, the Kertau (RSO) coordinate system was set by selecting 'Output Coordinate System' > Projected Coordinate System > National Grid > Malaysia and Singapore > Kertau (RSO). X and Y coordinates were properly selected and finally, the 'OK' button was clicked to perform the translation process. For another layer, such as the plot layer, the boundary layer was also converted to the Kertau (RSO) Projection system by using the same step under the 'batch' button menu. Finally, all the layers were compiled together and tabulated in the ArcMap software (Figure 3.9).

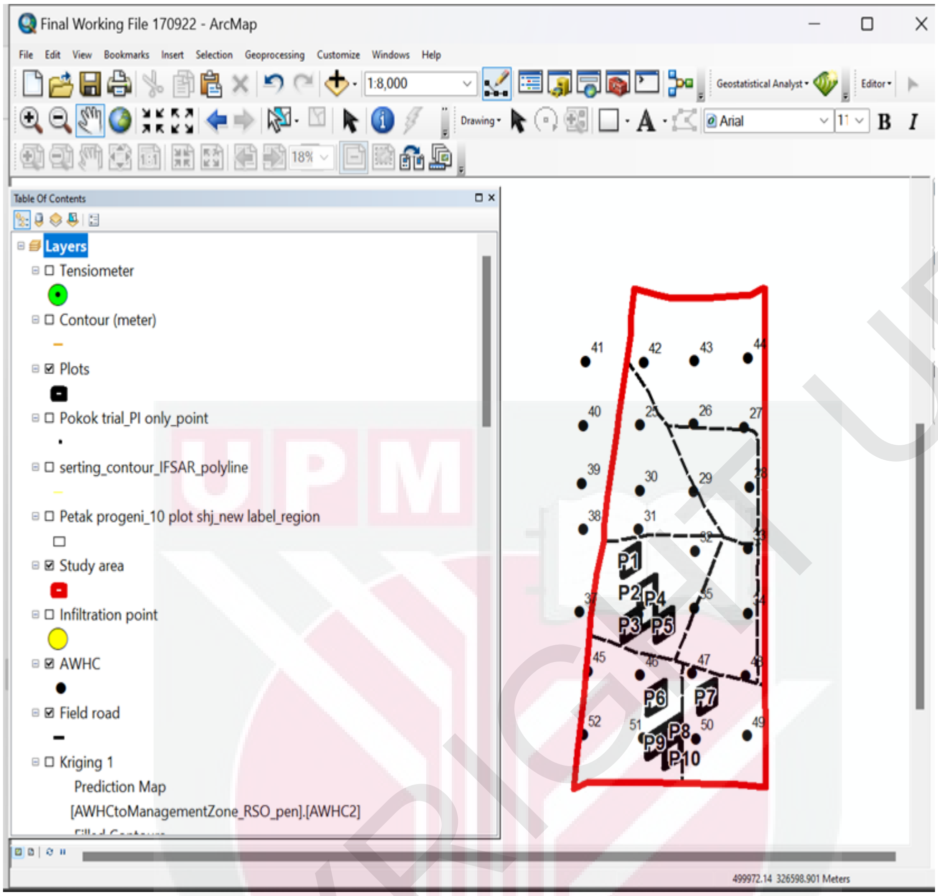

Figure 3.9: Layer use in ArcGIS map software

3.4.4 Interpolation by using ArcMap Software

The 'Geostatistical analyst' module was enabled to make an interpolation in the ArcGIS map software by using these steps: ArcMap > Customise > Extension > Geostatistical Analyst. After that, the 'Geostatistical analyst' box was opened by selecting ArcMap, then Customise Toolbars, and then 'Geostatistical Analyst' was clicked. Initially, Geostatistical Wizards was opened under Geostatistical Analyst. The kriging method was selected, and the correct column of AWHC was set up using the Data field drop-down menu. The procedure was continued by clicking on the 'Next' button, and then 'Ordinary kriging' was set. The menu at 'Calculate nugget' was set as False and the value of nugget was set at 4 (Figure 3.10). Under the Model #1 menu, a model was set at spherical type and the major range was set at 196. Then, the Partial sill was set at 518.1 after subtracting the value of Nugget from the sill. The lag size was set at 120 m, while the number of lags was set at 5. This is equivalent to 'Active Lag Distance' or 600 m (Lag size * a number of lags) that was previously set in the

GS+ software. Finally, the SAS software was used to determine whether the intended zones were statistically reliable or not.

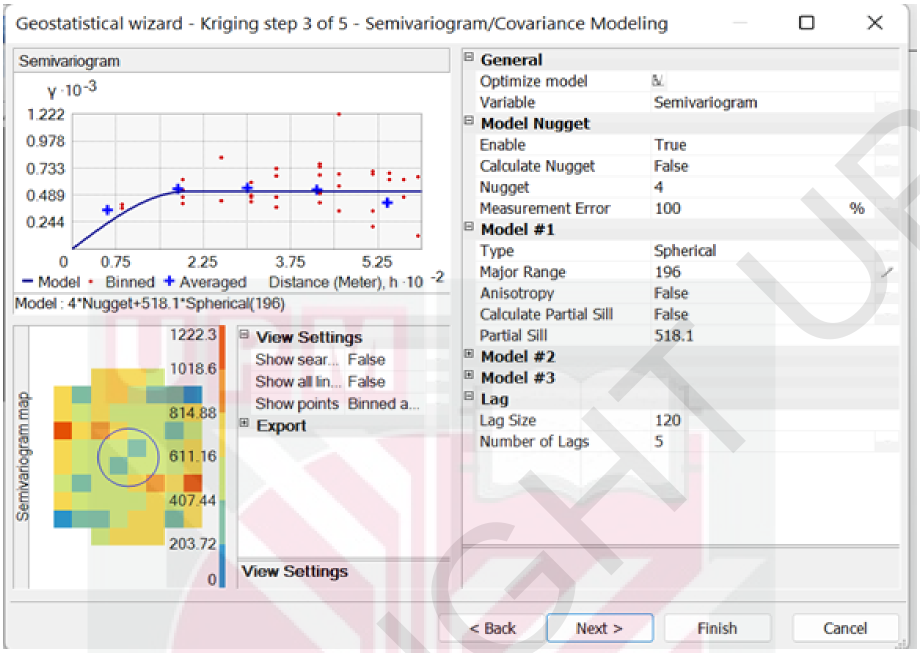

Figure 3.10: Geostatistical wizard in ArcMap for Interpolation step

3.4.5 Reclassification of management zone

Reclassification was done using an existing method in ArcMap software to make the irrigation management zone reliable. In the ArcMap software, 'Prediction Map' was clicked, followed by the 'Classify' button under the symbology menu. Under the classification menu, the geometric interval method was selected. Initially, 15 default classes were reported by ArcMap software and those were then reduced to three classes (Figure 3.11). ArcMap software automatically sets the range from 79.00-96.51 mm, 96.51-123.96 mm, and 123.96-167.00 mm. This range was edited manually to make a value rounded to the nearest whole number, i.e., 96.51 was changed to 100 mm, and 123.95 mm was adjusted to 125 mm. The zones were classified into three categories labelled as Zone A, Zone B, and Zone C with the range of 125-167 mm, 100-125mm, and 79-100 mm, respectively (Figure 3.12). Finally, a statistical analysis was run to solidify the result of the geometric interval method.

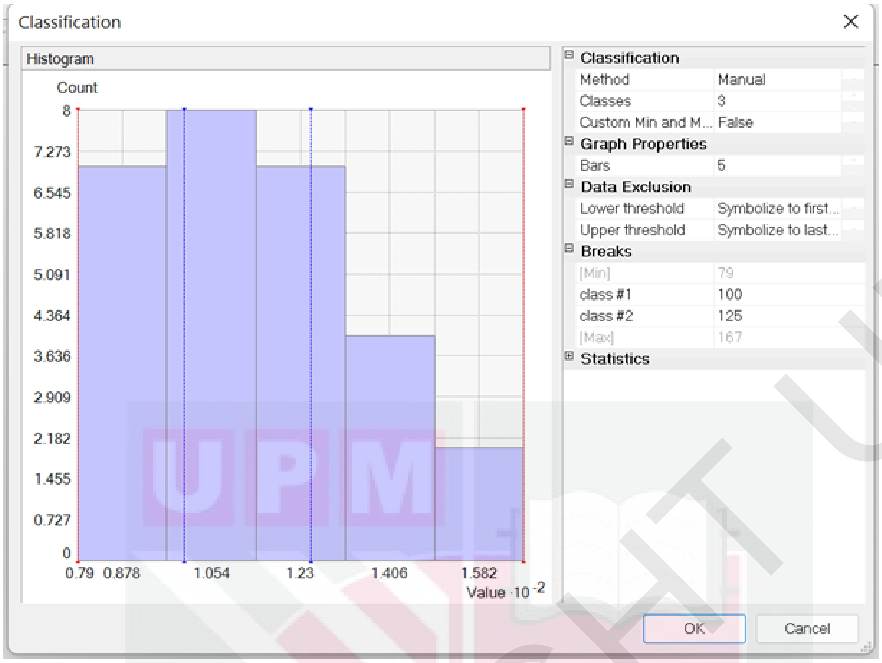

Figure 3.11: Classification menu for manual or auto-calculated data entry by ArcMap

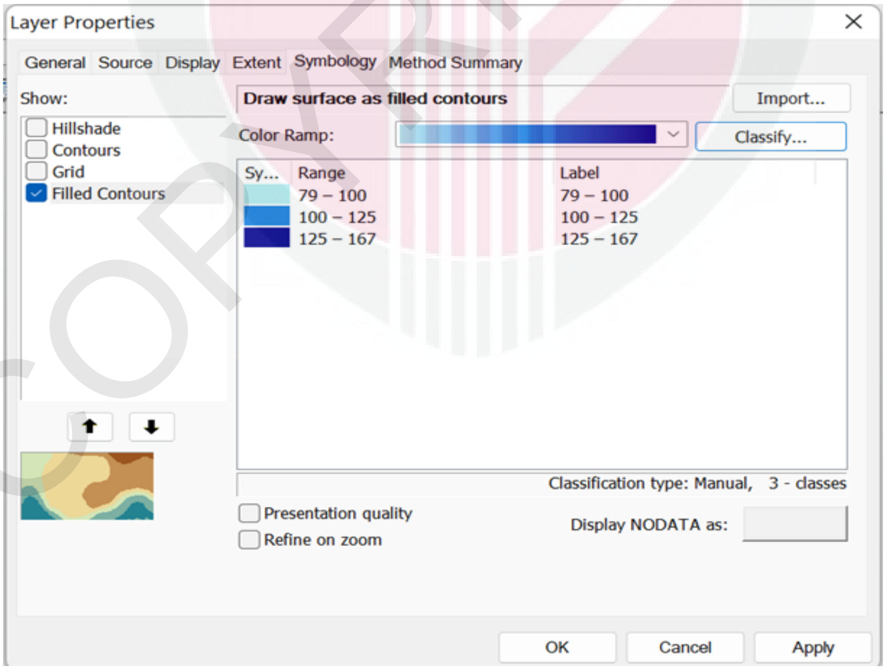

Figure 3.12: Final classification based on nearest value for three classes

3.5 Analysis of soil physical properties

Samples were collected using an auger at three points to represent 0-30 cm, 30-60 cm, and 60-90 cm soil depths (Figure 3.13 and Figure 3.14). Soil samples were kept in a plastic bag and sent to the FGV Laboratory at Jerantut, Pahang. In this lab, the soil sample underwent soil mechanical analysis according to Malaysia Standard (MS) 840: Part II (1983). Some of the samples, depending on location, were analysed to determine Total Organic Carbon (TOC) according to the MS 678: Part III (1980). Determination of soil OM was done according to the procedure of the MS 678: Part III (1980).

Figure 3.13: Soil was dug by using a chisel to open enough space for sampling purposes

Figure 3.14: Sample in the ring that will be enclosed with the lid to send to the laboratory

3.6 Interpolation of rainfall data from various meteorological stations

The coordinates of the study location were determined using a handheld Global Positioning System (GPS). All meteorological stations were identified by the Meteorological Malaysia Department (MMD), complete with their coordinates. Using Google Earth Pro software, each location was pinned to the map. A station within a 55 km radius of the study location was selected and the data was used for the interpolation process. Figure 3.15 shows the location of the stations selected as data sources, which are indicated by blue pins. First, each meteorological station coordinate had to be converted into a Kertau (RSO) projection system. Historical rainfall data from 1997 to 2016 was purchased from the MMD. Once the data were collected, they were analysed for basic properties, and the normality test was run using the Shapiro-Wilk test.

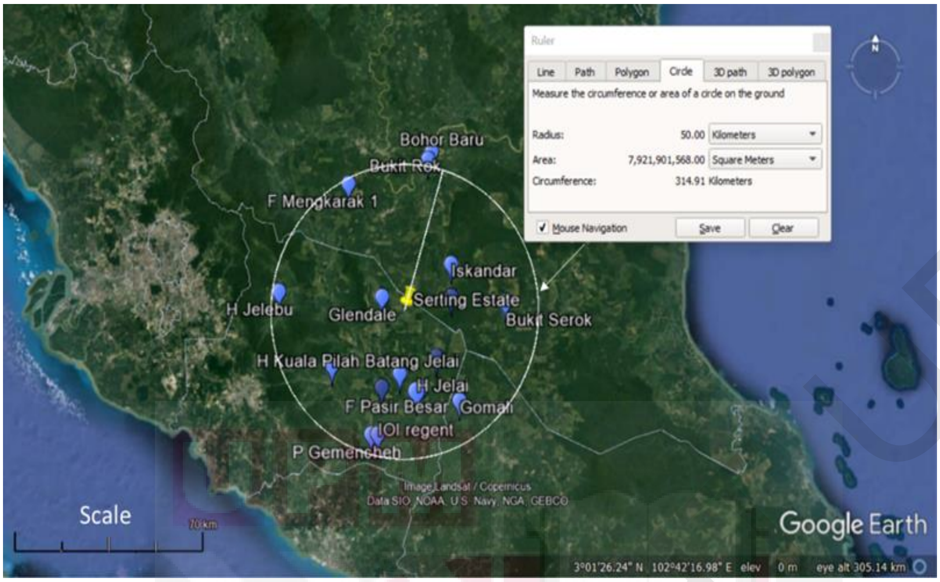

Figure 3.15: Location of meteorological station for rainfall data analysis

By using the MapInfo software, a table was created consisting of a summarization of yearly rainfall complete with station identification, longitude, and latitude. The points were made using the WGS84 projection, and the .tab file type was generated and used in the ArcMap software.

The analysis of the semivariogram was performed using the GS+ Software and ordinary kriging. Active lag distance and lag interval of the variogram were adjusted manually to get the highest value of R^2. For these cases, the active lag distance was set at 70,000 m while the lag class interval was set at 14,000 m. Details of the steps for point creation and variogram modelling are the same as described in Section 3.4.

The interpolation map was drawn using the ArcMap software. Firstly, the points with a .tab type file were translated to .shape file by using the MapInfo software translate menu. Then, .shape file was opened in ArcMap software and the projection of the file was changed to the Kertau (RSO) system. The geostatistical analyst menu was selected, and interpolation was done using ordinary kriging. For this analysis, the number of lag was set at 5, and the lag size was 14,000 m. The value of the nugget and range was set at 360 m and 56,700 m, respectively. Details of the procedure for converting projection and interpolation are the same as described in Section 3.4.

It is essential to look at rainfall distribution at the study site, whether it is homogenous or not, between the beginning and far end of the research plot. If there are differences, two or more rain gauges need to be allocated to record the data. Uneven rainfall distribution will affect soil moisture status and, therefore, irrigation scheduling. Some studies demonstrated the necessity of having more rain gauges to reduce sampling error. Xu et al., (2013) conducted a survey comprising 100 configuration networks from 181 random rain gauges. They found that poor model performance will be obtained when the rain gauge density falls below 0.4 over 1000 km^2. A recent study by Gyasi-Agyei (2020) utilised grid radar rainfall records. Based on their investigation, they suggested the optimum rain gauge network density varied from 14 km^2 $gauge^{-1}$ to 38 km^2 $gauge^{-1}$, with an average of 25 km^2 $gauge^{-1}$. Mishra (2013) indicated that 4–6 rain gauges give reasonable accuracy in daily rainfall estimation in a 50 km x 50 km area. Based on this, if a minimum of 4 rain gauges is selected, 17 rain gauges can cover almost 10,625 km^2. Therefore, 17 rainfall stations were chosen in this study to give a reasonable number for data interpolation since all stations were located within 9,700 km^2. The density of these 17 rain gauges was also according to World Meteorological Organization (WMO) standard, which states that precipitation gauge networks in Type II_a regions, which include tropical zones, is 600-900 km^2 $gauge^{-1}$ (Liang and Wang 2019).

The value of total rainfall averaged for 20 years at each station is shown in Table 3.2. The lowest value was from the Gemencheh Station, with a record of only 1,495 mm $year^{-1}$. The highest one, Bohor Station, recorded 2,000 mm of rainfall per year.

Table 3.2: Average rainfall data for every station from the years 1997-2016

Number	Station	Longitude, X	Latitude, Y	Rainfall (mm year^{-1})	SE
1	Bohor	102.583	3.383	1990	±69
2	Rokan Utara	102.417	2.667	1724	±58
3	Mengkarak	102.299	3.287	1945	±97
4	Palong 5	102.641	2.742	1925	±118
5	Pasir Besar	102.550	2.650	1716	±82
6	Tembangau 6	102.650	2.933	1940	±72
7	Gomali	102.667	2.617	1633	±92
8	H. Jelai	102.546	2.629	1611	±70
9	H. Jelebu	102.058	2.951	1696	±85
10	Glendale	102.417	2.933	1618	±78
11	Jelai	102.467	2.700	1668	±81
12	Bukit Rok	102.567	3.367	1680	±61
13	Iskandar	102.650	3.033	1745	±117
14	Gemencheh	102.383	2.517	1495	±73
15	IOI Regent	102.404	2.514	1525	±69
16	Bukit Serok	102.833	2.917	1759	±73
17	Kuala Pilah	102.249	2.727	1528	±58

3.7 Determination of infiltration rate at different irrigation management zones

A total number of three random points were selected to represent each IMZ. The infiltration rate for each location was determined using a double-ring infiltrometer. Firstly, any physical obstacles, such as oil palm debris, dead roots, and others, were removed within the radius of the double-ring apparatus. During the selection of the measurement point, some of the points were eliminated by selecting the points that were not near traffic or roadside and were clear of vegetation and organic biomass. In addition, areas with oil palm oil residue and possible insect nests were also avoided. There were three points for each irrigation management zone, which are indicated by yellow dots in Figure 3.16.

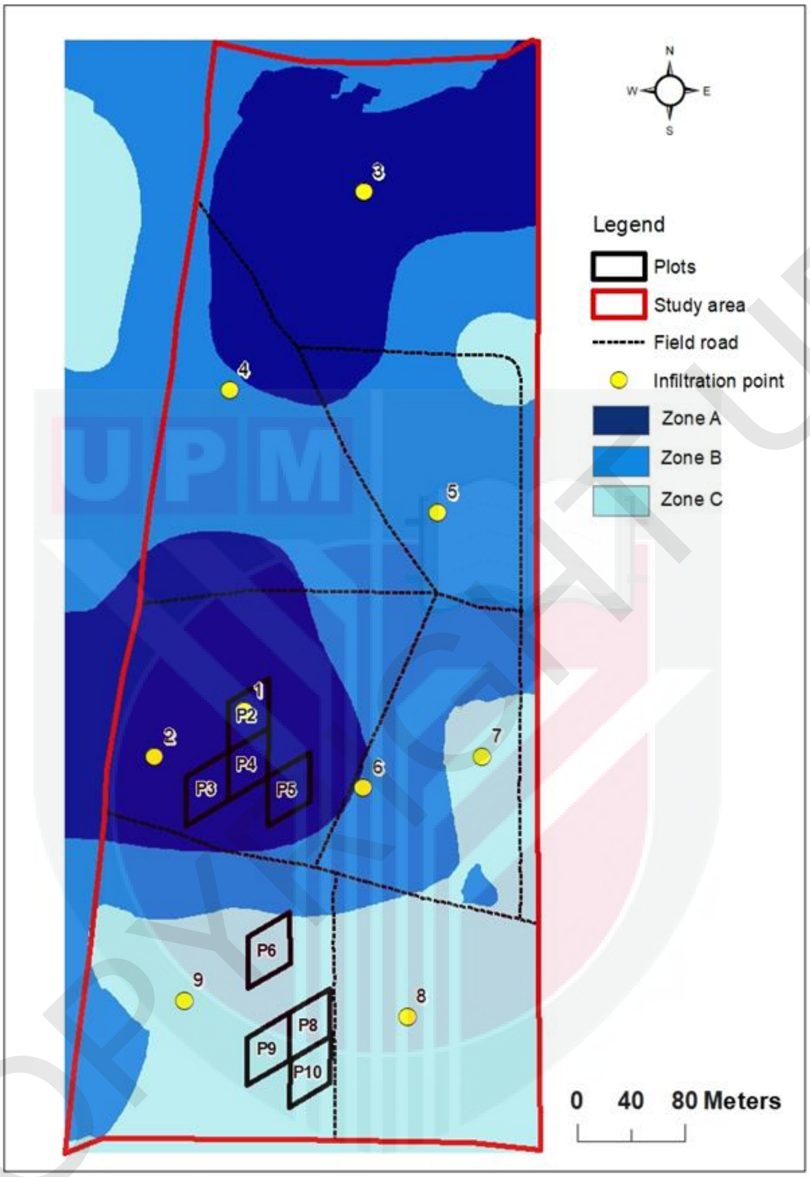

Figure 3.16: Selected point for infiltration data collection according to IMZ

The inner and outer rings with cutting edges were placed facing down on the ground. Then, the stainless steel metal accessories were placed across the inner and outer rings according to the mark. After that, the stainless steel metal parts were hammered with an impact-absorbing hammer until the base of the rings was buried 25 cm from the soil surface. Then, a measuring bridge with a measuring rod was placed on the inner ring (Figure 3.17).

Water was added to the outer ring until the water level reached the indicator mark. This step was then repeated for the inner ring. Measurement was taken immediately from the inner ring to determine the infiltration curve. The reading was recorded as soon as possible since the initial infiltration rate was speedy. Initially, the infiltration rate was set at close intervals, which was every 5 minutes. However, after 30 minutes, the interval increased, and infiltration was recorded every 10 minutes. Reading was taken for one and a half hours or until the value was constant.

Infiltration capacity was calculated based on Equation (2), and Equation (3) was used to estimate infiltration for an unknown cumulative time. The value of c, t, and α was determined by inserting two known times and infiltration rates into the log equation (Mbagwu, 1994). In this equation, I is the cumulative infiltration rate, c is a measure of the initial rate of infiltration, t is the time elapsed, and α is an index of soil structural stability.

$$\text{Infiltration capacity} = \frac{\text{Infiltration rate (mm)}}{\text{Infiltration time (minute)}} \quad (2)$$

$$\mathrm{I} = \mathrm{ct}^{\alpha} \quad (3)$$

Taking the logs of both sides
Log I = Log C + α log t

Figure 3.17: Double-ring infiltrometer setup for each location

3.8 Comparison of TNI with historical irrigation data

3.8.1 Collection of climatic data for FAO-CROPWAT simulation

Irrigation at FGVAS Serting Hilir estate was considered a commercial area where estate workers managed irrigation effort. Water input solely depended on rainfall and soil surface conditions. Irrigation scheduling was based on rainfall data from the previous day. Generally, 5 mm of water is used as a rule of thumb; if there was no rainfall on the last day, water was irrigated until 5 mm, whereas if rainfall was 10 mm per day, there would be no irrigation for two days. As a comparison, the FAO-CROPWAT software was used to predict the irrigation requirement in the study area based on historical rainfall data.

Firstly, daily rainfall data was collected from FGVAS Serting Estate for the years 2016 and 2017. Pre-required monthly data, which are Minimum Temperature (MinT), Maximum Temperature (MaxT), Relative Humidity (RH), Wind Speed (WS), and Sunshine Hours (SH) were used to predict radiation and ETo. Unfortunately, the estate did not record any of the data above except for rainfall.

Data for the four mentioned parameters was collected from various meteorological stations. A total number of four national meteorological stations namely Hospital Seremban (101.944°E, 2.706°N), Federal Land Development Authority (FELDA) Palong 5 (102.641°E, 2.742°N), Kuala Pilah (102.249°E, 2.727°N) and Ayer Hitam (102.417°E, 2.933°N) were selected to serve as data sources as depicted by green pins in Figure 3.18. All the stations are located within a 60 km radius of the study site, and the elevation of all stations is shown in Table 3.3.

However, SH was still missing and not recorded by these four stations. Hence, SH was imported from the FAO Climwat 2.0 database for nine nearby stations around the trial site, depicted by the red balloon shape in Figure 3.18. These stations were namely Bentong (101.910°E, 3.510°N), Kuantan (103.210°E, 3.610°N), Raub (101.850°E, 3.780°N), Mersing (103.390°E, 2.450°N), Malacca (102.250°E, 2.260°N), Tampin (102.230°E, 2.460°N), Port Dickson (101.800°E, 2.530°N), KL Subang (101.550°E, 3.110°N) and Kepong (101.630°E, 3.230°N).

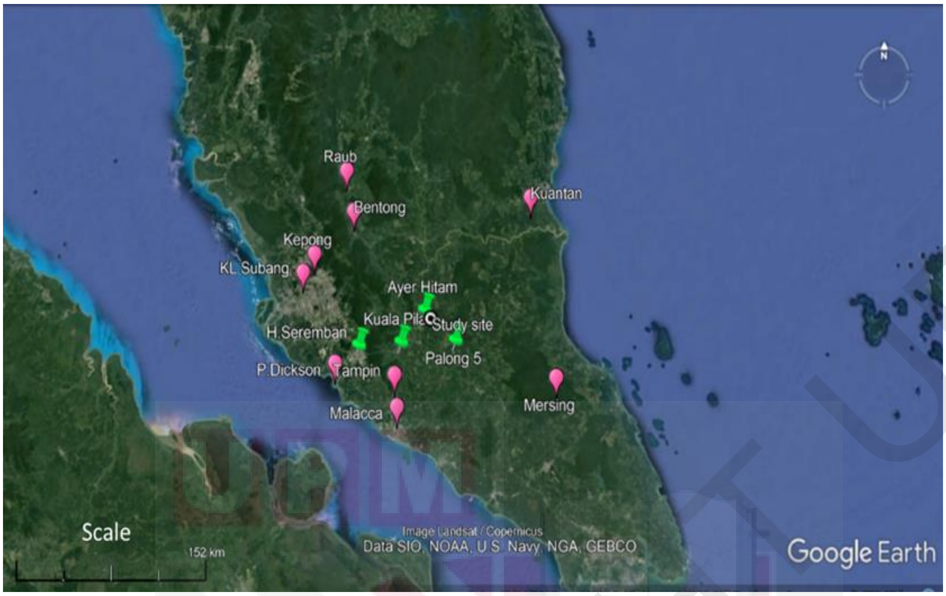

Figure 3.18: The location of all meteorological stations used as a source of the data

Table 3.3: Elevation of all meteorological stations used in this study

Station	Elevation
Hospital Seremban	64 m
FELDA Palong 5	71 m
Kuala Pilah	144 m
Ayer Hitam	59 m
Bentong	96 m
Kuantan	16 m
Raub	157 m
Mersing	45 m
Malacca	9 m
Tampin	61 m
Port Dickson	9 m
KL Subang	22 m
Kepong	97 m

3.8.2 Module data for FAO-CROPWAT software

Generally, there are four main modules in the FAO-CROPWAT model: Climate/ETo, Rain, Crop, and Soil. Data collected from selected stations comprised MinT, MaxT, RH, WS, and SH were copied in the Climate/ETo table menu, and its user interface is shown in Figure 3.19. Before that, information regarding the station's country, altitude, and coordinates was inserted into the model. Then, the Rain module was selected, and all rainfall data was copied into the table form. The ‘Option’ button was selected, and Dependable Rain (FAO/AGLW formula) was used to change the calculation method for ER.

In the third module (Figure 3.20), all information regarding the oil palm crop was inserted accordingly. The planting date was set at the beginning of the year, and the harvest date was set at the end of the year. The value of Kc was set at 0.80, as it was the suggested value for mature oil palm. Meanwhile, rooting depth was set at 0.60 meters based on the most significant quantity of roots available, as indicated by Tailliez, 1971. Then, the ‘Soil’ module button was selected, and all data related to AWHC was filled in the appropriate blank column. For the purpose of this evaluation, the lowest AWHC value for each classification was inserted to simulate how much water is needed according to Section 3.4.5. Initial soil moisture depletion was set at 100% to assume the initial soil was dry. For the irrigation simulation, the irrigation depth was set at 5 mm, considering 80% irrigation efficiency. In the FAO-CROPWAT, the calculation of CWR was made based on a decade (10-day interval) and finally summed up for the entire year.

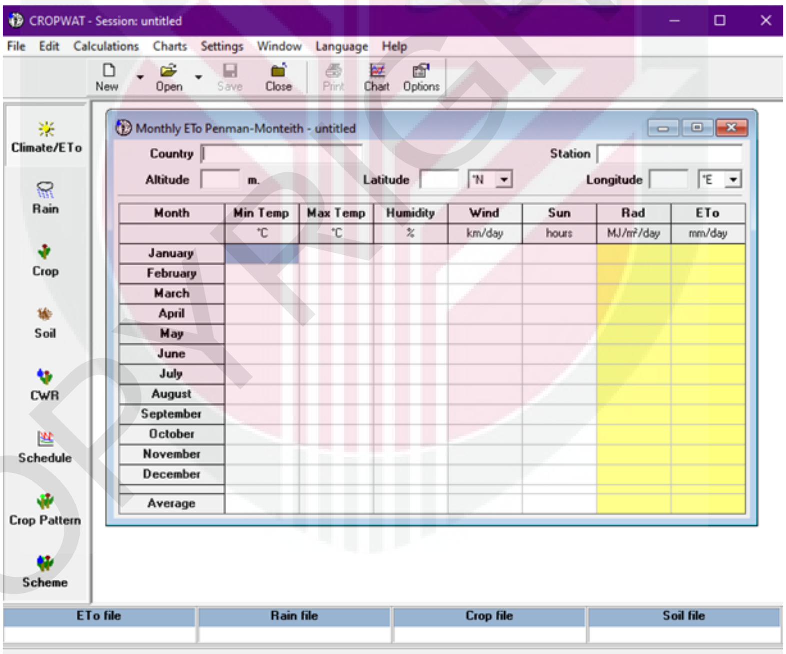

Figure 3.19: Climate/Eto module interface in FAO CROPWAT

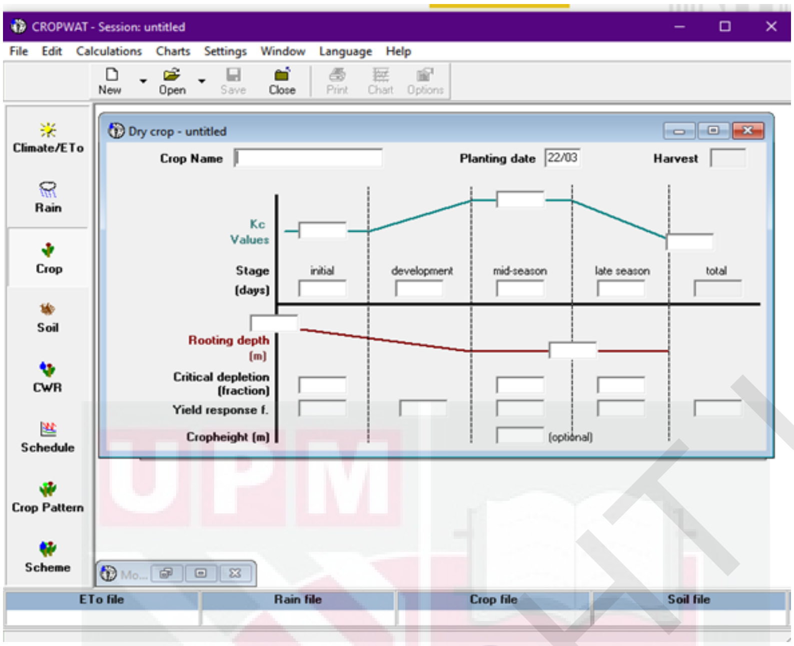

Figure 3.20: Crop module interface in FAO CROPWAT

3.8.3 Irrigation Water Supply Practices by the Estate

Before this, there were no attempts to assess whether the irrigation input given to the field was sufficient or oversupplied. Irrigation was carried out by workers who depended on the previous day's rainfall and some knowledge of soil surface conditions. The rule of thumb is that there will be no irrigation if the previous day's rainfall exceeds 10 mm. The irrigation schedule is based on how many hours the engine is running throughout the day. Therefore, there is no exact figure of how much irrigation input is given to the crop. For this study, basic information on irrigation activities was collected from the estate. Vital information collected was irrigation time, schedule of the block, and block interval time for the years 2016 and 2017. All of the data were summarised on a monthly basis.

Further calculation was made based on the assumption that there was no leakage or pipe damage, and each emitter gave a constant output of water at 60 Litre hour^{-1}. Based on operation hours, the Estimated Volume of Water for the existing irrigation area (EVW) was calculated for each year based on Equation (4). Then, the value of EVW was converted into Estimate Irrigation Depth (EID) for the existing irrigation area, as shown in Equation (5).

EVW is the function of monthly operation time in hours, area of irrigation (A) in a hectare, number of emitters (n) per hectare, and a nominal emitter flow rate (Q_e) in litre hour^{-1}. EID involved the occupied area of oil palm based on canopy radius (r) in meters

(Roslan and Haniff, 2004) and density of palms per hectare (d). In 2016, the palm was at three years of planting, and the value of r was set at 3.43 m, whereas in 2017 the value of r was 4.58 m (FGVAS, 2019).

$$EVW = \text{Operation time x A x n x } Q_e \quad (4)$$

$$EID = \frac{EVW}{\pi r^2 \; x \; A \; x \; d} \quad (5)$$

3.9 Characterization of several generic micro-spray emitter's properties

3.9.1 Determination of Emitter head-discharge (H-Q) relationship

The design layout for this experiment was adopted from (Hezarjaribi et al., 2008). The primary piping system layout was constructed using high-density polyethylene (HDPE) with a nominal diameter of 20 mm (Figure 3.21). This pipe will represent a lateral pipe under field conditions. A total of two pressure gauges were installed at the start and end of the lateral line. Household water grade that was connected to a water tank was used as a water source. The piping system was also linked to the booster pump.

One piece of the emitter was installed in the middle of the lateral pipe. This evaluation used several generic micro-spray emitter colours: blue, black, and orange. Before measurements were recorded, the water was turned on and left running constant for several minutes until it achieved the desired pressure. Different levels of pressure were applied to the emitter, starting from 0.5 bar until 2.5 bar with an interval of 0.5 bar. A unique cone was used to block the dispersion of water from the top of the emitter. Meanwhile, a plastic container was placed at the bottom of the emitter point to collect the water.

The collection of the water by using a specialised cone was carried out for 1 minute and repeated for different colours and pressures of the emitter. The volume of water collected within one minute was measured by using a measuring cylinder and recorded using a dedicated form. X is the parameter that characterises the flow from an emitter as a power function of operating pressure (pressure differential) with the formula $Q_e = KH^x$ as Equation (6) (Solomon, 1979). Value of Q_e is emitter flow $hour^{-1}$, K is emitter discharge coefficient for flow rate, H is operating pressure, and x is emitter discharge exponent for flow rate. The values of K and x were determined by analysing the data using the power function in the SAS software. To find a linear relationship between these two variables, Qe and H were changed to a log function of Equation (7) to resemble y = mx + c and analysed for a linear relationship model by using the SAS software.

$$Q_e = KH^x \quad (6)$$

$$Log (Qe) = xLogH + LogK \quad (7)$$

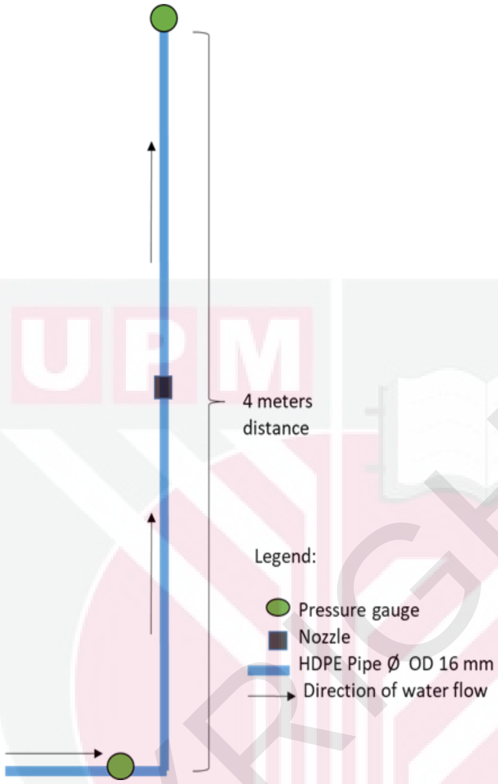

Figure 3.21: Diagram of basic layout for emitter head – discharge curve determination

3.9.2 Determination of Emitter head-throwing distances (H-T) relationship

This evaluation was carried out in the plant house building to avoid any errors due to the wind effect and the experiment was adopted from (Aris 2014). The lateral pipe was raised 10.0 cm from the ground by using a unique stand. Two pressure gauges were installed at the start and end of the lateral line. One piece of the emitter was placed in the middle of the lateral pipe. The system was given different sets of pressure starting from 0.5 bar and continuing to 2.5 bar with an interval of 0.5 bar (Ravi et al. 2016). The maximum throwing distance with a 90° angle from the emitter was measured using measuring tape at the right and left sides of the emitter. Data were averaged and analysed using the SAS statistical software. The value of the emitter constant for radius (Gk) and emitter exponent for radius (Gx) for throwing distance properties were determined using Equation (6). Meanwhile, Localised Application Depth (LAD) in mm $hour^{-1}$ was calculated by dividing the emitter flow rate, L $hour^{-1}$ at a specific pressure by the area of water dispersion in m^2, as shown in Equation (8). Later on, the area of water coverage $hectare^{-1}$ in percent was estimated using Equation (9).

$$LAD = \frac{Q_e}{\pi(radius^2)} \quad (8)$$

$$Coverage\ ha^{-1} = \left(\frac{LAD\ x\ 148}{10000}\right)\ x\ 100 \quad (9)$$

3.9.3 Determination of wetted pattern for the emitters

An open container with a diameter of 6.2 cm and a height of 10.0 cm was prepared to collect water dispersion from the emitter. These containers were arranged in a grid form with a size of 0.457 m x 0.457 m, and the emitter position was in the centre of the grid (Figure 3.22). A total number of 81 containers were involved, and each of them was labelled with an appropriate number to ease recording purposes. For this experiment, only a 1.5 bar level of pressure was applied to the system as it is close to the value that will give high uniformity for micro-sprinkler or spray-type emitter, as suggested by Boman (1989). The pressure was applied to the system for 20 minutes, and three replicates were used in this experiment. Once finished, each container was weighed again. The volume of water in millimetres was determined by subtracting the weight of the container with water (g) from the weight of the container without water (g).

All the data were tabulated in the table using Microsoft Excel. The distance of the container from the centre of the grid was used to represent the X-axis and Y-axis. The container placed at the bottom of the emitter with number #41 was set as ‘0,0’. The right side indicated ‘+ value’ whilst the left side indicated ‘- value’. The upper side of the container was tagged as ‘+ value’ whilst the bottom container, in relation to the emitter, was labelled as ‘- value’. All the data was inserted into the SURFER software© Colorado for spatial spraying pattern determination (Rovelo et al., 2019) by using the Kriging method.

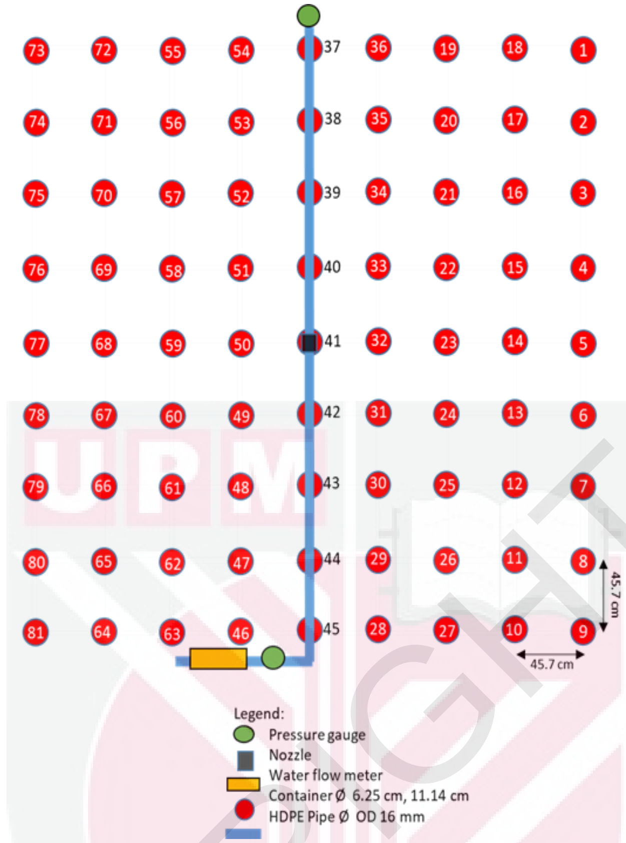

Figure 3.22: Containers were arranged in a grid form around the centre of the emitter

After the contour map was generated, the Distribution Characteristic (D_C) value was calculated based on Equation (10) (Dipak et al. 2020). The area that received more than average depth was extracted using the 'volume' function under the 'Grids' menu. The value of average depth for each emitter was set as Z value as a constant. In this assessment, the Z scale factor was set at 1.00. In the report, the value of 'Positive Planar Area' was used as a total area with more than average depth. Meanwhile, the 'Contour/Vol Area' function was used to determine the total wetted area represented by 'Planar Area Above Contour' with '0' contour value.

$$D_C = \left(\frac{\text{The area receiving more than average depth,m}^2}{\text{Total wetted area,m}^2}\right) x\ 100 \qquad (10)$$

3.10 Analysis of existing irrigation system by using computer-aided software

3.10.1 Drawing existing piping network into IrriPro software

Firstly, all data associated with the UAV image (Figure 3.23) and Interferometric Synthetic Aperture Radar (IFSAR) contour map (Figure 3.24) were collected. IFSAR data was used as a topography layer in the MapInfo software. This layer was combined with a UAV image file for the study site. The map contours were then saved as a .jpg file type and were later used as a reference to drawing contours in the IrriPro Ver 4.5.1 software, IRRIWORKS, Italy. All the information and manual maps for the irrigation system layout were collected from the estate management. All details on piping accessories, such as sources of water, pipe size, pipe type, filtering system, and type of emitter, were recorded.

In the IrriPro software, 'Design/Manual' was selected in the first selection window to open the design wizard. On Palette tools, the existing .jpeg image containing topography and base map was loaded into IrriPro by using the 'Load map' button. The procedure to do this was using this step: Layer > Add layer > Browse for .jpg file > Open. The image was scaled by selecting the 'Scaling tool'. The actual distance between two selected points was inserted. Then, the scaled image was imported inside IrriPro by clicking on 'File> Import' in the software. UAV file with .jpg file type was loaded into the load map selection under the Palette panel.

Contour lines needed to be drawn on the map for the system to recognise any differences in elevation. Once the map was imported into IrriPro software, a contour line was drawn onto the map by using the 'Contour line' at the Palette panel. Contour lines were drawn according to the pre-drew line in the images one at a time. An Interval of 1.00 meters was used as a guideline. The main pipe was drawn by selecting the 'Main pipe' at the 'Edge' palette. A line of pipe was drawn on the map starting from the sources of water indicated by a rectangular purple box until the last point where the main pipe should be. For this assessment, the actual 'water Source' was collected from an artificial pond. This main pipeline was connected to 'Sources'. Failing to do this will cause the error 'Associate a water supply to the sector,' and the software will not undergo further process. Before further processing, 'Nodes' was added to the main line to represent a diversion from the main pipe to the secondary pipe. This step was done by selecting the Generic node under the 'Nodes' palette and placing it on the main line.

Initially, the pipe size was set according to the software's default value. Then, the pipe size was changed according to the installed system. The 'Add new sector' button was selected to draw a sector, followed by the 'Start' button and then 'Manual Design'. In order to associate the water source with the sector, any nodes that existed within the main line were selected and set as sources of the sector.

‘Restore wizard’ was selected to return to the selection menu. Once in this menu, several variables were adjusted according to the properties of this sector. The input of emitter spacing and plant row spacing was inserted by typing the actual value in the boxes ‘a’ and ‘b’, respectively. For this analysis, ‘a’ was set at 7.65 m while ‘b’ was set at 8.84 m. Based on the oil palm arrangement in the field, triangular on even lateral was selected as the geometry of planting. The ‘Next’ button and Generic sector shape were selected. Once again, the ‘Drawing area’ was selected to insert the shape of the sector. On the palette panel, ‘terrain’ was selected, and a polygon line was drawn at the desired place. It served as a boundary of the piping system.

Once again, the ‘Restore wizard’ was clicked, and then the value of the lateral angle was added. In this case, ‘Angle’ was selected on the Palette panel. Any line was drawn starting at any place, starting from the lateral inlet at any length. The angle of the lateral line was captured automatically by the software. The emitter and Lateral Data window was entered by clicking on the ‘Next’ button. The ‘Spray/Mini sprinkler’ button was selected. Properties of the emitter from the previous study (Section 4.5) were manually inserted into the emitter's additional feature selection. Nominal pressure was set at 0.5 bar, nominal flow rate was set at 60 litre hour^{-1}, and the range value was set at 1.70 m. The ‘Advanced’ button was clicked to manually insert the value of the emitter exponent and emitter constant (k, x, Gk and Gx) variables that were derived from Section 4.5. The k value was set at 17.797, the x value was set at 0.467, Gk was set at 0.854 and lastly, Gx was set at 0.284. The process was continued by clicking on the ‘Next’ button to enter the pipe size data. For this study, pipe sizes of 96.4 mm, 55.1 mm, and 28.1 mm were selected for secondary pipe, sub-main pipe, and lateral pipe, respectively, to represent the inner diameter of the pipe. The process above was repeated to insert the remaining sectors. All the sectors were appointed based on three shifts as operated by the estate (Figure 3.25).

Figure 3.23: Drone image of study location at FGVAS Serting Hilir, Phase 1

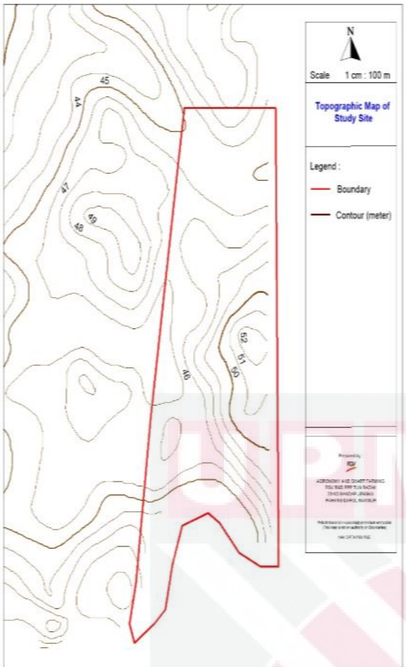

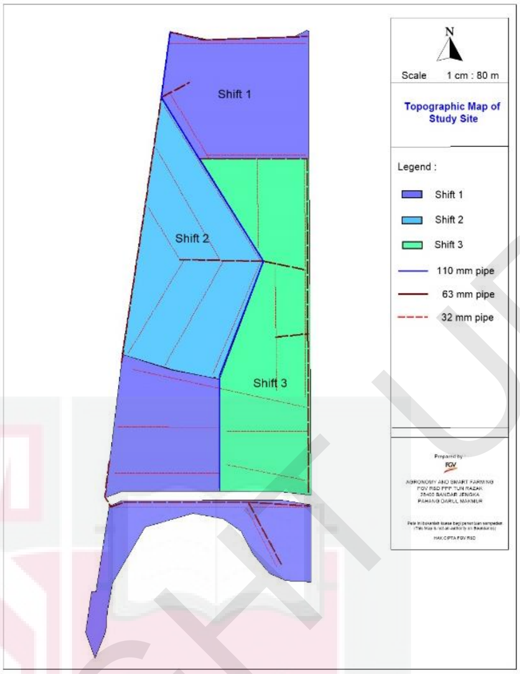

Figure 3.24: Contour map of the study area

Figure 3.25: Irrigation scheduling based on three shifts (practiced by the estate)

3.10.2 Simulation of hydrology properties

Once all sectors were inserted in the IrriPro software, the main valve was consigned to each sector. The step involved selecting the ‘Valve’ features in the node selection. Then, a valve was put at the beginning of the secondary pipes. The shift of irrigation was created based on the estate's actual irrigation schedule. Each shift was evaluated according to the following steps. On the main menu, the Advanced tab ‘Calculate’ button was selected to ensure the software made a calculation; this process took some time. Under the results menu, this software gave simulation results based on two types of uniformity coefficients, which are the UCC (Lopes et al., 2019) and EU (Barragan et al. 2006; Nakayama et al. 1979). Their formulas are shown as Equation (11) and Equation (12) respectively, where Q_i is the flow rate of a single emitter, Q_m is the average value, Q_{min} is the minimum flow rate of an emitter, Q_{med} is the medium flow rate of an emitter, n is a number of emitter for each tree and CVT is the coefficient of technology variation.

$$UCC = 1 - \left(\frac{\sum_{i=1}^{n} |Q_i - Q_m|}{n \times Q_m} \right) \times 100 \quad (11)$$

$$EU = \left[\left(1 - 1.27\ x\ \frac{CVT}{\sqrt{n}}\right)\ x\ \frac{Q_{min}}{Q_m}\right] \text{x } 100 \qquad (12)$$

3.11 Installation of SBI for the recording plots

The ideal situation is to set up a new SBI network independent from the current system. However, due to some limitations such as water sources, electricity point sources, and selection of research plots, the SBI network for the present study was set up to co-exist with the commercial irrigation system. Only two distinct IMZs were selected, and they represented the lowest and the highest IMZ categories. Four plots represented each zone, and each plot contained 16 palms that were recorded for uniformity assessment and palm measurement. The general layout of the SBI system is shown in Figure 3.26. The SBI consisted of four major components, which were piping, control, automation, and data segmentation (Figure 3.27). The piping consisted of a reservoir and piping layout, i.e., water distribution for the plot. The control component was made up of a photovoltaic panel, inverter, and Hunter iCore. The automation component consisted of a tensiometer to get the real-time soil water potential (SWP) reading and a solenoid valve. In contrast, the data component consisted of a data logger to log and store the data according to 5-minute intervals.

SBI system scheduling activities can be divided into automated and manual. In ideal conditions, scheduling is done automatically, starting with a signal from the tensiometer. The signal is sent to the iCore when the reading exceeds 30 kPa suction pressure (label at tensiometer pressure gauge) or less than -30 kPa SWP. Then, iCore translated the message and communicated with the solenoid valve at each plot's secondary pipes. Opening the valve will reduce the pressure inside the pipe, and the electrical pump will be started automatically to deliver the water into the plot. This process will continue until the solenoid valve is closed and the pressure in the pipe is built up, thus turning off the pump according to the presetting pressure value.

However, manual operation takes place to run the irrigation instead of automatic operations if any obstacles exist. Operators read the tensiometer value for each plot and open the non-solenoid valve intentionally installed at every plot to ease the manual irrigation process. For this case, tensiometers were being read every day in the early morning between 8.00 and 9.00 am, and the operator decided to start the pump if the tensiometer reading was more than 30 kPa. Regarding irrigation timing, operators shut off the valve for a particular plot when the tensiometer gauge shows a value lower than 30 kPa. However, irrigation timing is slightly influenced by the actual time required by the operator to move plot-by-plot. In this situation, irrigation will be done within 30 minutes to 2.5 hours, depending on the SWP's magnitude. Brief activities involving scheduling are shown in Figure 3.28.

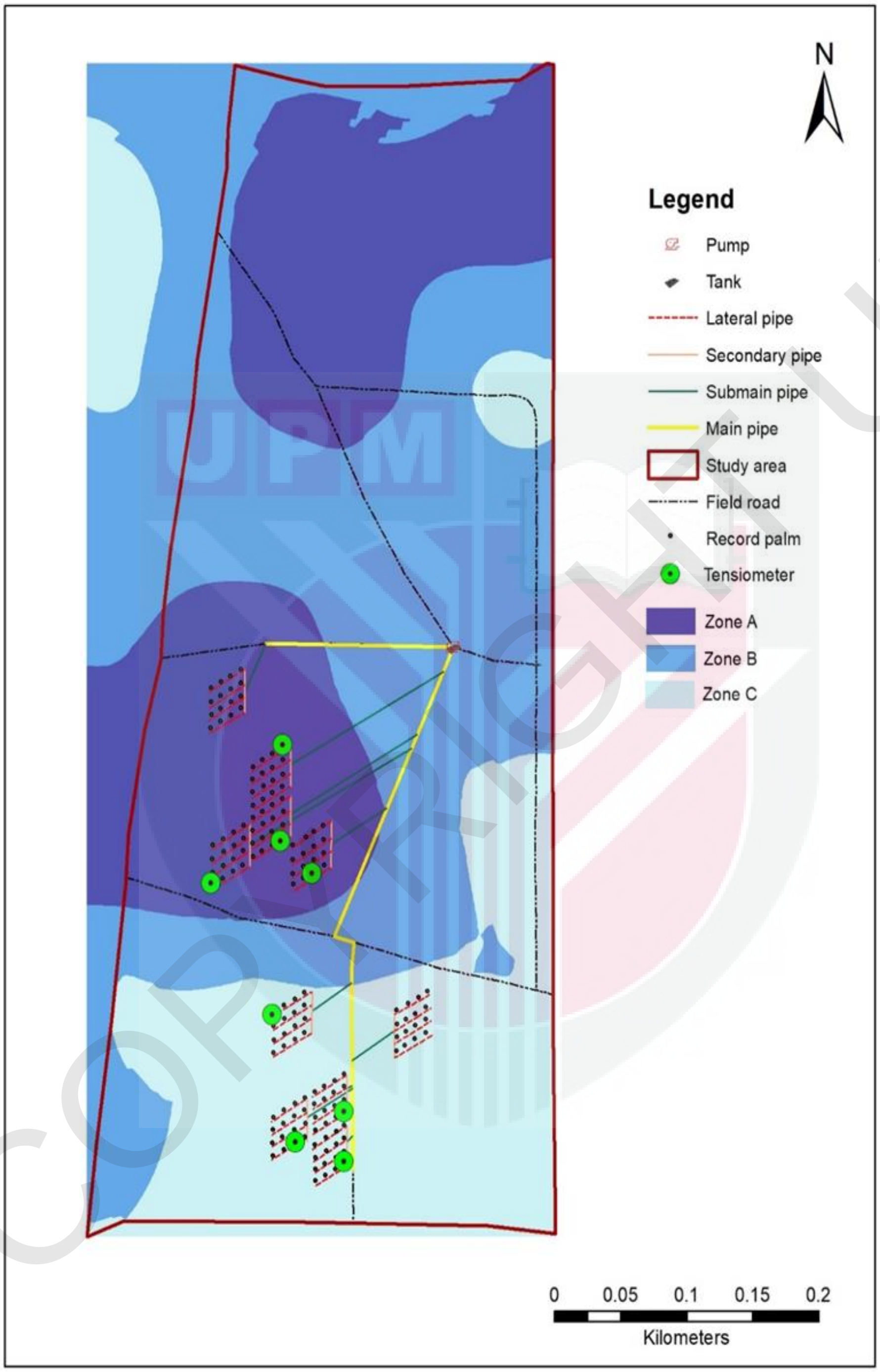

Figure 3.26: Diagram of irrigation system drawing including location of tensiometer for each plot

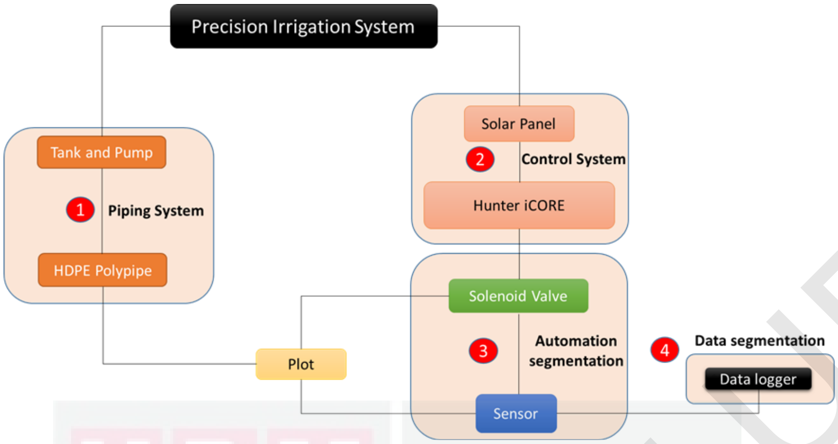

Figure 3.27: Segmentation of the SBI system layout

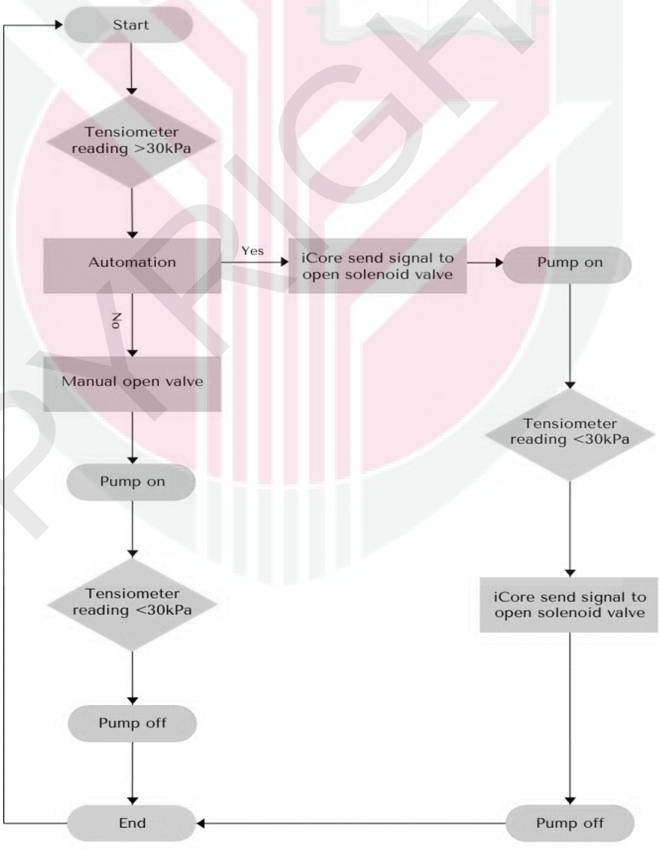

Figure 3.28: Flow chart of SBI scheduling under automatic and manual operation

3.11.1 Basis calculation for piping size

The piping size is manually calculated first before being drawn into IrriPro software. Drone images and topography contours were used for IrriPro software, and the procedure was the same and described in Section 3.10.1. Peak water requirement was calculated based on Equation (13), where P is the number of plots, N_p is the number of palms, and Q_e is the emitter flow rate (L $hour^{-1}$). This value served as a reference to decide the volume of water storage for the system.

$$\text{Peak water requirement} = \left(\text{P x } N_p\right) \text{ x Qe} \tag{13}$$

Friction is the most important part that contributes to head loss in the system and it involves three main steps. The first step was the determination of the Reynold Number (R_n) to decide whether the fluid had a laminar or turbulent flow as shown in Equation (14); if R_n < 2300, then the flow is categorised as Laminar flow, if R_n > 4000, the flow is classified as turbulent flow. In this equation, R_n is unitless, V is the Velocity of fluid (m s^{-1}), ID is the internal diameter of the pipe (m), and v is the kinematic viscosity of fluid (m^2 sec^{-1}), which can be referred to Table D.1.

$$R = \frac{V\ x\ ID}{v} \tag{14}$$

After the determination of R_n, friction factor (f) was determined by using Equation (15) if the flow was laminar and Equation (16) if the flow was turbulent. Equation (16) is also called the Colebrook-White Equation. In these equations, f is a frictional factor, R_n is the Reynolds number, k is the roughness of pipe (m), and d_h is the hydraulic diameter (m). Due to the complexity of the calculation, the Moody diagram (Figure D.1) sometimes being referred to determine f value for turbulent flow.

$$f = \frac{64}{R_n} \tag{15}$$

$$\frac{1}{\sqrt{f}} = -2 \log \left[\frac{2.51}{R_n \sqrt{f}} + \frac{\frac{k}{d_h}}{3.72}\right] \tag{16}$$

To use the Colebrook-White Equation, the k value, which refers to absolute roughness (m), was determined by using Table D.2. Once k was identified, Relative Roughness, as shown in Equation (17), was calculated by dividing k with D_h (inside diameter of the pipe, m). Once the f value was determined, the friction head of specific pipe length and diameter was determined by using the Darcy-Weisbach formula in Equation (18). In this equation, h_f is head loss (m), f is friction factor, L is the length of pipe (m), ID is the internal diameter of the pipe (m), V is the velocity of the fluid in m sec^{-1}, and g is the acceleration due to gravity or 9.81 m sec^{-2}.

$$\text{Relative roughness} = \frac{k}{D_h} \tag{17}$$

$$hf = f \times \left(\frac{L}{ID}\right) \times \left(\frac{V^2}{2g}\right) \tag{18}$$

3.11.2 SBI: Piping segmentation

Water sources for SBI were stored in HDPE tanks with a capacity of 8,000 gallons or 30.3 m^3. However, the primary water source that fed water to the tank was a diesel engine 0.60 km away from the tank. This diesel engine was used to fill the tank whenever necessary. The main HDPE pipe was sent in spiral form from the factory. Then, it was stretched and straightened using a pickup (Figure 3.29) before being laid on the ground for the jointing process using mechanical fittings.

Figure 3.29: The coiled HDPE was stretched along the main road

Then, it was arranged at the edge of the main road so that it could be buried in the soil to avoid damage by any mechanical machines operating in the field. Eight outlets were constructed from the main pipe. These outlets served as a sub-main pipe, with the same piping size as the main pipe, and were connected to the main pipe using saddle clamps. The total number of 8 sub-main pipes also represented the eight number of plots.

Four sub-main pipes distributed water to Zone A (near the water source), while the remaining pipes were for Zone C (farthest from the water source). The sub-main line was laid at the edge of the frond path and continued until the centre of the plot. Before entering the plot, there was a small section that contained several fittings for data collection purposes. The components attached to this section started with a solenoid valve followed by a mechanical water meter, disc filter, and pressure gauge.

Water was drawn by the electrical pump unit located near the tank. The water was delivered to the main pipe, which was 63 mm HDPE (ID 55mm). After that, water flowed through the sub-main pipe, which was the same size as the main pipe. The sub-main was connected to the secondary pipe, which was divided into four lateral lines. Secondary and lateral lines had a similar size of 32mm (ID 28mm), and each of the lateral lines delivered water for the palms row. For this trial, a total number of 16 palms were selected with a configuration of 4 x 4 rows of palms. Each palm was irrigated by using one orange-coloured micro-sprayer emitter installed at the lateral lines placed approximately 1.0 meters from the palm circle. It is to maximise water uptake by the palm, as shown by (Nelson et al., 2006), who suggested that rooting activity for water uptake was high within 2.0 meters from the palm bole.

The existing semi-commercial irrigation project used a diesel engine to generate power for the pump. However, in this case, electricity was introduced into the system. Installation work for the electric cable and poles was done by Tenaga Nasional Berhad (TNB). Poles were buried in the soil and were used to connect the cable with the nearest source near the estate. After which, the cable was connected to the main board, where the electric meter, distribution box, main switch, and circuit breaker were placed (Figure 3.30). Wall switches and plug sockets were installed below the distribution box. The maximum output for this station was 240V. It was more than enough to generate the power for the 2.0 HP Booster pump that was used in this system.

Figure 3.30: An electrical control board was installed near the water tank

3.11.3 SBI: Control segmentation

The control segmentation was equipped with a photovoltaic panel, Hunter iCORE (230 V), and surge protector. One solar panel was installed in the middle of the zones, which contained four plots in Zones A and C. A small tower was built by using a scaffold rig with a height of 3.0 m. It was to prevent solar panels from being shaded by the oil palm canopy. Therefore, the power system for the two zones was independent and not related to each other. The specifications of the solar panels are shown in Table 3.4.

The energy tapped by the panel was about 42-46 Volts of Direct Current (DC) and sent to the inverter inside the bunker. The inverter (with serial ISI-501) converted the DC into an Alternate Current (AC) and made it a practical power source for the Hunter iCORE. Meanwhile, a 12V DC was used to charge the battery. Photon Solar (PGEL 100-12) 12V 100Ah was used as a battery and was charged accordingly.

Table 3.4: Specification of the solar panel (Model ODA200-36-M)

Variables	Details
Peak power (Pmax)	200.00
Maximum Power Voltage (Vmp)	38.71
Maximum Power Current (Imp)	5.17
Cells efficiency (%)	18.48
Module efficiency (%)	15.66
Power Tolerance	0±3%
Nominal Operating Cell Temperature (°C)	47±2
Cell Type	Mono-crystalline 125 x 125mm
Number of cells	72 (6 x 12)
Dimensions	1580 x 808 x 35 mm

3.11.4 SBI: Automation segmentation

3.11.4.1 Tensiometer as a real-time sensor

By using the ArcMap Software, the lowest point of AWHC for each plot was referred from the interpolation map produced in Section 3.4. It is common to put a sensor on the lowest AWHC in the field and the greatest risk of droughtiness (Peters et al. 2013). This point was used to bury tensiometers and monitor soil moisture status. The location of each point is shown in Figure 3.26. Two tensiometers were installed in each plot to represent 12” (30 cm) and 24” (60 cm) soil depth. The type of tensiometer used was the Irrometer SR Model manufactured by IRROMETER Company under the Remote Sensing Tensiometer (RSU-V) type. There was a brass tee connected to the tensiometer output for automation cable and data collection cable. The tensiometer was soaked in the water nightly to saturate the ceramic cup with water to ensure there was no air bubble in the ceramic cavity and to maintain capillary force between soil and water inside the tensiometer. The tube of the tensiometer was filled with water mixed with IRROMETER fluid colour concentrate to ease the process of operating and viewing the water level.

During the transfer, the ceramic cup section was covered with plastic and tied with a rubber band to avoid water loss from the tube. The location for placement of the tensiometer was selected using a GPS device with slight adjustments to avoid sloppy and bumpy areas, palm debris, and mechanization path to minimise errors. Alignment with a predetermined location was done whenever necessary. In addition, the tensiometer was placed within 30 cm of the emitter to ensure the ceramic cup represented the root of the oil palm. The holes were dug using a coring tool kit supplied by the manufacturer with an auger size of 22 mm x 90 cm. A number of two holes were drilled according to the length of the tensiometer.

Meanwhile, excessive soil from the holing step was collected and put into the piles to make a slurry solution. Once the tensiometer was placed in the hole, the slurry solution was poured inside the edge of the tube until there was no empty space. It was to ensure that good contact was established between the soil and the ceramic cup. A tiny stick was inserted in the hole repeatedly to expel excessive air space. After the tensiometer was buried in the soil, the cap of the tensiometer was opened, and the suction cup of a hand vacuum was placed at the edge of the tube. The syringe was pulled, and the entrapped air in the tube was evacuated by releasing the air bleed suction cup slowly. It was done to ensure no sudden force was experienced by the gauge. Finally, a small cage was constructed by using wire mesh with a size of 30 cm x 30 cm x 30 cm to protect tensiometers from physical contact or other hazards.

3.11.4.2 Solenoid Valve

There was one solenoid valve to control water flow for each plot. The type of valve used was the Hunter Professional Grade Valve (PGV-101G), and it was installed correctly at the sub-main pipe with a size of 32 mm. In this study, a small screw was adjusted to attain the trigger point at 30 kPa. The screw was rotated clockwise to increase and anticlockwise to decrease the level of the trigger point. For the adjustment, the cap of the tensiometer was opened, and a hand pump was used to suck the air within the tensiometer tube. When the gauge showed 30 kPa, the pump was put on hold, and the small screw was rotated until the solenoid 'clicked.' It is indicated that the sensor triggered the solenoid. Finally, the solenoid valve was covered by using a specific case supplied by the manufacturer. In an actual situation, water drawn from the tensiometer tube will create a vacuum pressure inside the tube and increase the gauge slowly. Once the trigger point (30 kPa) is reached, the automatic switching mechanism closes and sends electricity to the solenoid valve. Electricity will magnetise the solenoid, and the plunger will rise decreasing the pressure at the top of the diaphragm and allowing water to flow into the field.

The tensiometer power cables come in black and red colours. A connection was made where these two wires from both 12" and 24" tensiometers were connected parallelly together. The black wire was connected to the blue wire and ran to the solenoid valve first before being connected to the Hunter iCORE. Meanwhile, the red wire was connected to the yellow wire and directly to the Hunter iCORE. For the data cable, there were a total of six wires from two tensiometers with colour codes of red, black, and white. All of these wires were joined to four core data cables from the Watermark 900 data logger. Pairs of red wire were joined together and connected to the red-green wire.

Meanwhile, a pair of black wires were joined together and connected to a yellow-blue wire. Two white wires were connected to a yellow-green wire and a yellow-dark green wire separately. Then, all cables were laid on the ground and inserted into the heavy-duty conduits. The wires were buried in the soil at about a 4-inch depth to protect them from hazards.

3.11.5 SBI: Data segmentation

Watermark Monitor 900M was used to log and record the reading of the tensiometer in five-minute intervals. The logger was set up by connecting laptops with the logger using a Universal Serial Bus (USB) cable. Prior to that, the WaterGraph software was downloaded and installed on the computer. In the WaterGraph software, the "Setup Datalogger" button was selected. The program connected to the device and retrieved the current configuration. Basically, the data was stored in the logger in the form of Hexadecimal data (Hex), and a green button was pushed to view it in the Watermark liquid crystal display (LCD) in the 'volts' form (Figure 4.31). Data was downloaded from the logger in two ways: either by using a USB or a Shuttle device port.

The trend of the data over time can be viewed in the WaterGraph software once it is downloaded into a computer. Calibration was done to ease interpretation by converting voltages to Centibars or kPa units. The step involved selecting "Option" > "Sensor Config" in the software. On the special calibration menu, each channel type was changed to Voltage Remote Sensing Unit ("RSU-V") and "save configuration" was clicked.

The raw data that was transferred to the computer was still in the 'volts' unit. In order to explore the data using other software, some procedures were required to convert it into a kPa unit. In the working file, Equation (19) was used to convert Hexadecimal (Hex) data into millivolts (mV) data. Then, mV data was converted into pressure in the cbar unit by using Equation (20). In these equations, x1 is data in Hex, y_1 is data in mV, and y_2 is data in pressure (cbar) (Irrometer, 2020).

Figure 3.31: LCD display shows the value of the data

$$y_1 = 19.608\ (x1) \quad (19)$$

$$y_2 = 0.023\ (y1) - 11.625 \quad (20)$$

3.12 Assessment of SBI system for hydrology and uniformity

Before finalising the design, a simulation of the layout was tested using the IrriPro software. Generic emitter input found in Section 3.9 was inserted into the layout one by one. After insertion, the simulation was run, and the result was summarised in an Excel file according to plot number. The selection of generic emitter to use in the system was based on the lowest headloss and the highest simulation uniformity.

Measurement of the actual flow rate for uniformity calculation was done twice a year after the installation of the generic emitter. The irrigation system was turned on and left for several minutes to allow the pressure to stabilise. A special plastic container was made to serve as a protective cap for water droplets emitted by the nozzles. The protective case was placed on top of the emitter while the other container was used to collect the trickled water. The water is collected in a container that is designed to contain precisely 1.0 litres of water.

By using the protective case, the time to fill the water container was recorded. The selection of emitter was based on the location at the front, middle and back end of the plot. Generally, there were at least three samples of emitter for each plot. So, 30 data points were collected during this test. A total number of four tests were done during the study period at six-month intervals. All of this data was compared with the data simulated for the same emitter in the IrriPro Software.

Besides UCC and EU uniformity indices, two other indices used for the comparison were the DU, as shown in Equation (21) and the Statistical Uniformity Coefficient (Us), as shown in Equation (22) (Bralts & Kesner, 1983). DU is typically used to characterise the irrigation water distribution for surface irrigation systems, but it can also be applied to micro and sprinkler irrigation systems (Irmak et al., 2011). Q_m is the average emitter flow rate in L $hour^{-1}$, Q_{25} is the average low quarter of flow rate in L $hour^{-1}$, and Q_{SD} is the standard deviation of the emitter flow rate.

$$DU = \frac{Q_{25}}{Qm} \text{ x } 100 \quad (21)$$

$$Us = 100 \left(1 - \frac{Q_{SD}}{Q_m}\right) \quad (22)$$

3.13 Assessment of SBI in view of oil palm yield and response

3.13.1 Oil palm yield record

Oil palm will produce FFB continuously, but harvesting is typically done two to three times on a monthly basis. The standard operating procedure of this study was to select a ripe bunch based on colour, which is orange in colour, with more than two numbers of loose fruit. Bunches were harvested using a sickle, and sometimes, pruning of the palm was needed to ease the process of harvesting. Once the bunch was harvested, research workers weighed all the bunches, along with loose fruit, using a 50 kg weight scale. The number of bunches was also recorded during this activity. At the end of the year, cumulative weight was calculated, and data was converted into yield (t ha^{-1}) by using Equation (23). In this equation, BN is a bunch number and ABW is an average bunch weight, kg $bunch^{-1}$.

$$\text{Yield, t } ha^{-1} = \frac{BN \text{ x } ABW \text{ x } 148}{1000} \quad (23)$$

3.13.2 Measurement of oil palm growth variables

A total number of 155 palms were measured to record growth. Several variables were selected, such as frond number production, leaf width, leaf length, canopy length, leaflet number, rachis width, rachis thickness, palm height, and trunk diameter. All of these variables were measured at six-month intervals and used as primary data for other empirical growth estimations.

The production of frond numbers was calculated with a reference mark at frond number #1 from the previous measurement. The determination of frond number #1 was based on the youngest frond that had a fully opened frond (Figure 3.32). In order to measure leaf width and leaf length, a determination of the middle part of the frond was required. The selection of the middle frond part was made based on the location of the adjacent V-shape on the upper rachis part (Figure 3.33). Leaf width and leaf length were measured at two leaves representing the right and left leaf positions. Leaflet numbers were calculated from the base of the petiole until the end of the frond. The starting point was from the first vestigial laminae (spine look), which is either on the right side or left side, depending on the longest one.

Figure 3.32: Youngest fully open frond

Figure 3.33: 'V' shape of the upper part of the rachis

For the width of the leaf, each leaf was folded in half and measured, and the measurement was made based on the folded leaf part. Petiole width was measured at the location of the first vestigial laminae with spines. A similar point was used to measure petiole thickness. The height of the palm was measured from the base of frond #41 until ground level by using a measuring tape. A calliper was used to measure the diameter of the trunk at a height of 1.0 meters from the ground level to determine the trunk diameter.

In addition to these variables, 15% of palms were selected from each zone to undergo frond destructive analysis. The frond was cut down and chopped into small pieces, then all parts of the frond were weighed, and data was recorded. Then, all segments of the frond were put into plastic bags and sent to an oven for the drying process. The drying process was continued until no changes in weight were observed. Finally, the dry weight of an individual frond was obtained, called the actual frond dry weight. All these data were pooled and analysed by linear correlation with Petiole Cross-Section (PCS). This linear relationship was calculated using Equation (24), called the Leaf Dry Weight (LDW) in kg palm^{-1}, and was adjusted from the older equation proposed by (Corley et al. 1971).

$$LDW = 0.06541\ PCS + 0.34553 \quad (24)$$

3.13.3 Calculation of derivative oil palm growth indices

Additional growth indices were used to study how water-holding capacity affects oil palm growth. Measurements of these indices were done from August 2020 until July 2021, along with the growth variables measurement that was done annually in February and August. From the LDW value, other variables calculated were Vegetative Dry Matter (VDM) (Equation (26), Yield Dry Matter (Y) (Equation (27), Bunch Index (BI) (Equation (28), and Crop Growth Rate (CGR) (Equation (29). For the Y calculation, FFB is yield in kg $palm^{-1}$ $year^{-1}$. Estimation of VDM required Trunk Dry Matter (TDM) obtained from Equation (25), where VT is the volume of trunk increase by measurement interval and T is palm age in years. VDM and TDM have the same unit, which is kg $palm^{-1}$ $year^{-1}$.

$$TDM,\ kg\ palm^{-1}\ year^{-1} = VT\ (7.62\ T + 83) \quad (25)$$

$$VDM,\ kg\ palm^{-1}\ year^{-1} = ((LDW\ x\ frond\ production) + TDM) \quad (26)$$

$$Y,\ kg\ palm^{-1}\ year^{-1} = 0.5470\ FFB - 0.372 \quad (27)$$

$$BI = \frac{Y}{(Y+VDM)} \quad (28)$$

$$CGR,\ t\ ha^{-1}\ year^{-1} = \frac{Y+VDW}{1000}\ x\ Density \quad (29)$$

3.14 Water productivity for the oil palm

In this study, WP was adopted from Stone et al., 2016 and expressed as crop yield divided by water input for both irrigation (IR) and effective rainfall (ER), as shown in Equation (30). Crop yield is FFB in kg $palm^{-1}$, and both IR and ER are in m^3 $palm^{-1}$. In this study, the FAO/AGLW formula was used for the calculation of ER in Equation (33) and (34), d in density of palms per hectare.

$$WP,\ kg\ m^{-3} = \frac{Yield}{IR+ER} \quad (30)$$

$$ER,\ mm = (0.6 \times Rainfall) - 10, for\ Rainfall \leq 70\ mm\ month^{-1} \quad (31)$$

$$ER,\ mm = (0.8 \times Rainfall) - 24, for\ Rainfall > 70\ mm\ month^{-1}$$

$$\text{Converting ER in mm to m}^3\ \text{palm}^{-1}, \qquad (32)$$

$$\text{ER, m}^3\ \text{palm}^{-1} = \frac{ER,\ mm \times 10}{d}$$

3.15 Cost benefit analysis

The cost-benefit analysis calculation involves several components, such as net profit, return on investment (ROI), and net present value (NPV), as in Equation (33), Equation (34) and Equation (35) respectively. These indices are used to show whether the investment is profitable or not. The total cost of production consisted of the capital cost of the system and operation cost. The capital cost involves costs for the establishment of the system, such as the installation of electrical components, engine and water pumps, piping system, and IoT installation. Meanwhile, operational costs are subject to yearly terms and involve utility, workforce, and system maintenance. By the nature of oil palm crops, the analysis involved calculation from the year '0', which was when the system was established and extended to 25 years of palm age. During this tenure, several non-fixed variables are subject to change, such as FFB price, extra yield, salary, and others. The average yield for Zone A and Zone C was used as the actual yield for the first three years (2020 – 2022). The same goes for the FFB price which reflect the actual average price reported by the government agency (MPOB, 2020, 2022).

Net Profit = Total revenue (RM) – Total cost of operation (RM) (33)

ROI, % = (Net Profit / Total cost of operation) x 100 (34)

NPV = Total profit x Discount rate at 10% (35)

3.16 Statistical analysis

In this study, several statistical analysis procedures were selected to study relationships between treatments and or independent variables. At the earlier stage of the current study, geostatistical analysis was done to delineate IMZ and rainfall data. For most analyses, the Analysis of Variance (ANOVA) test was used to differentiate or compare the variables by using SAS software, SAS Institute Inc. USA. ANOVA was used to (i) compare between soil physical comparison and three sampling depths, (ii) compare the classification of AWHC according to IMZ and rainfall pattern, and (iii) analysis emitter experiments and oil palm performance evaluation according to the treatment given. Correlation analysis was used to study the relationship between soil physical variables and AWHC. Regression was used to (i) study the relationship between infiltration capacity and time for each point of sampling, (ii) determine the relationship between pressure with flow rate and throwing distance for each emitter colour code, and (iii) establish a relationship between actual frond dry weight and PCS of oil palm growth. An Independent t-test was used to compare most of the variables between Zone A and Zone C. Among the variables were water usage, the volume of events, WP, events of irrigation, and volume of water usage.

CHAPTER 4

RESULTS AND DISCUSSION

This chapter illustrates the results of field experiments, discussion of these results, and compares the results from other findings. This chapter consists of eight sections as follows:

1. Determination of irrigation management zone based on soil-water holding capacity.
2. Interpolation of rainfall data for the study site.
3. Assessment of soil infiltration for each irrigation management zone.
4. Comparison of historical water usage and FAO-CROPWAT simulation data.
5. Assessment of emitter hydraulic properties.
6. Assessment of existing irrigation system by using IrriPro Software.
7. Field assessment of water uniformity under the SBI system.
8. Evaluation of SBI with respect to palm response and irrigation water use.

4.1 Determination of irrigation management zone based on soil-water holding capacity

4.1.1 Soil physical properties according to soil depth

Table 4.1 shows the result of descriptive analysis of the three depths of the samples. BD ranged from 1.59 to 1.67 g cm^{-3}. The value of BD was relatively high, indicating that the soil was typically compacted. In comparison, the range of typical soil BD for sand or compact clay soil is 1.40 – 1.80 g cm^{-3}, loose silt loam or clay is 1.00 – 1.40 g cm^{-3} and Organic soil has extremely low bulk densities between 0.20-0.80 g cm^{-3} (McCarty et al. 2016). The latter is due to low particle densities and a large amount of pore space. At all dedicated soil depths, soil moisture was reduced with the increase of pressure applied. Soil moisture ranged from 23.0% to 24.5% (g/g) at saturation point (0 kPa). The highest water percentage (g/g) was found to be 31.73%, while the mean was 24.5% at depths of 30-60 cm. The saturation point represents a condition when there is no pressure at all when pores are filled with water. After free drainage, the remaining water in soil pores reaches FC.

For soil physical analysis (Table 4.2), the selected variables were clay, silt, coarse sand (Csand), fine sand (Fsand), Total Sand (Tsand), OM, and OC. The percentage of clay increased with increasing depth from 28.1% to 43.7%. Clay has smaller soil pores than other particles but has relatively more water-holding capacity. This particle has quite a broad range of values, indicated by a high SD value, but it is clear that the percentage of clay increased with higher depth. However, the percentage of silt was low, only 14.0-15.5%. It is the second smallest particle in soil and can also hold water. The data shows that silt distribution was not more than 35% up to 60 cm soil depth. The data indicates that sand was the most dominant particle in the study site, with a range from 42.3 % to 56.3%. Most of the sand fractions are made up of Fsand, which is up to 80% of Tsand. From these analyses, soil classification for depths of 0-30 cm and 30-60 cm was fine loamy and fine clayey for depths of 60-90 cm.

Table 4.1: Descriptive analysis of different moisture content at various depths by using the pressure plate method, negative value to annotate soil water potential (SWP)

Descriptive Statistics for Depth = 0-30 cm							
Variable	**N**	**Mean**	**SD**	**SE Mean**	**CV**	**Minimum**	**Maximum**
BD	28	1.61	0.10	0.02	6.16	1.44	1.83
Water content at equilibrium							
0 kPa	28	23.1	3.45	0.65	14.98	17.06	29.91
-1 kPa	28	19.2	2.30	0.43	11.95	15.46	24.69
-10 kPa	28	17.5	2.20	0.42	12.63	13.72	24.12
-33 kPa	28	13.3	3.51	0.66	26.40	7.76	23.14
-1500 kPa	28	11.1	3.07	0.58	27.72	6.91	21.39

Descriptive Statistics for Depth = 30-60 cm							
Variable	**N**	**Mean**	**SD**	**SE Mean**	**CV**	**Minimum**	**Maximum**
BD	28	1.67	0.14	0.03	8.35	1.24	1.90
Water content at equilibrium							
0 kPa	28	24.5	3.52	0.67	14.39	19.64	31.73
-1 kPa	28	20.2	2.64	0.50	13.04	15.68	29.10
-10 kPa	28	18.6	2.58	0.49	13.90	14.66	28.19
-33 kPa	28	14.4	3.63	0.69	25.26	7.10	24.82
-1500 kPa	28	11.8	2.98	0.56	25.26	6.36	19.56

Descriptive Statistics for Depth = 60-90 cm							
Variable	**N**	**Mean**	**SD**	**SE Mean**	**CV**	**Minimum**	**Maximum**
BD	24	1.59	0.16	0.03	9.98	1.28	1.85
Water content at equilibrium							
0 kPa	24	23.9	3.77	0.77	15.76	17.9	31.08
-1 kPa	24	22.4	4.04	0.82	18.04	16.64	30.86
-10 kPa	24	18.1	3.65	0.75	20.19	12.61	25.10
-33 kPa	24	15.8	3.46	0.70	21.80	9.56	23.00
-1500 kPa	24	7.3	4.28	0.87	57.95	1.85	16.37

Note: SD – Standard deviation, SE – Standard error, CV – coefficient of variation

Table 4.2: Descriptive analysis for soil physical analysis at different depths

Descriptive Statistics for Depth = 0-30 cm							
Variable	**N**	**Mean**	**SD**	**SE Mean**	**CV**	**Minimum**	**Maximum**
Clay	28	28.13	9.76	1.84	34.69	16.80	50.30
Silt	28	15.54	6.56	1.24	42.23	5.40	31.80
Csand	28	9.74	4.95	0.94	50.79	2.10	18.00
Fsand	28	46.58	12.57	2.37	26.96	17.30	70.90
Tsand	28	56.32	13.88	2.62	24.65	19.40	73.80
OM	28	0.95	0.46	0.09	47.96	0.36	2.79
OC	28	1.65	0.79	0.15	48.02	0.62	4.82

Descriptive Statistics for Depth = 30-60 cm							
Variable	**N**	**Mean**	**SD**	**SE Mean**	**CV**	**Minimum**	**Maximum**
Clay	28	34.93	10.11	1.91	28.94	22.60	61.10
Silt	28	14.84	6.72	1.27	45.30	4.90	34.90
Csand	28	9.43	6.52	1.23	69.11	2.00	30.90
Fsand	28	41.58	12.98	2.45	31.23	12.10	63.90
Tsand	28	51.01	13.69	2.59	26.84	15.20	69.90
OM	28	0.53	0.46	0.09	86.31	0.20	2.61
OC	28	0.91	0.79	0.15	86.37	0.34	4.49

Descriptive Statistics for Depth = 60-90 cm							
Variable	**N**	**Mean**	**SD**	**SE Mean**	**CV**	**Minimum**	**Maximum**
Clay	28	43.70	11.22	2.12	25.67	23.1	65.40
Silt	28	14.04	6.10	1.15	43.44	6.1	29.90
Csand	28	7.54	5.45	1.03	72.24	0.6	19.10
Fsand	28	34.71	12.19	2.30	35.12	8.6	55.50
Tsand	28	42.25	14.00	2.65	33.14	10.7	64.00
OM	28	0.38	0.21	0.04	55.89	0.16	0.28
OC	28	0.66	0.37	0.07	56.11	1.24	2.13

Note: SD – Standard deviation, SE – Standard error, CV – coefficient of variation

Volumetric Water Content (VWC) is an expression of the volume of water per unit volume of soil. It was calculated by multiplying gravimetric water content with BD. The S-curve graph often defines the relationship between VWC and pressure applied. In this type of graph, the X-axis starts from 0.1 kPa instead of 0 kPa to allow the log-scaled chart to be plotted as shown in Figure 4.1. Based on the S-curve graph, it was indicated that the water progressively dried at a non-linear trend according to the pressure applied. At saturation point, the upper part of 0-30 cm soil depth was 37% VWC, 41% for 30-60 cm, and 38% for 60-90 cm. Soil samples from 30-60 cm depth had an almost similar trend to 0-30 cm soil depth but had a higher capacity for holding water. It is noteworthy that the curve for 60-90 cm is likely to deviate from the s-curve trend. This layer gave a saturation point of 37.5% and gradually decreased with increased pressure applied. At -1500 kPa, the percentage of water was very low (11.4%) compared to the soil layer up to 60 cm.

This graph is essential to serve as a fundamental sensor benchmark data. Two tensiometers were buried in the soil to read soil water potential at depths of 0-30 cm and 30-60 cm. By having two sensors, each of them will act as a check and balance where the valve would open if any of them are below the triggering point. Even though the upper sensor is wet, the lower one is not; water is still irrigated until the flow enters the 30-60 cm zone. Meanwhile, if the lower sensor is wet but the upper one is not, irrigation will take place to moisten the upper part of the area.

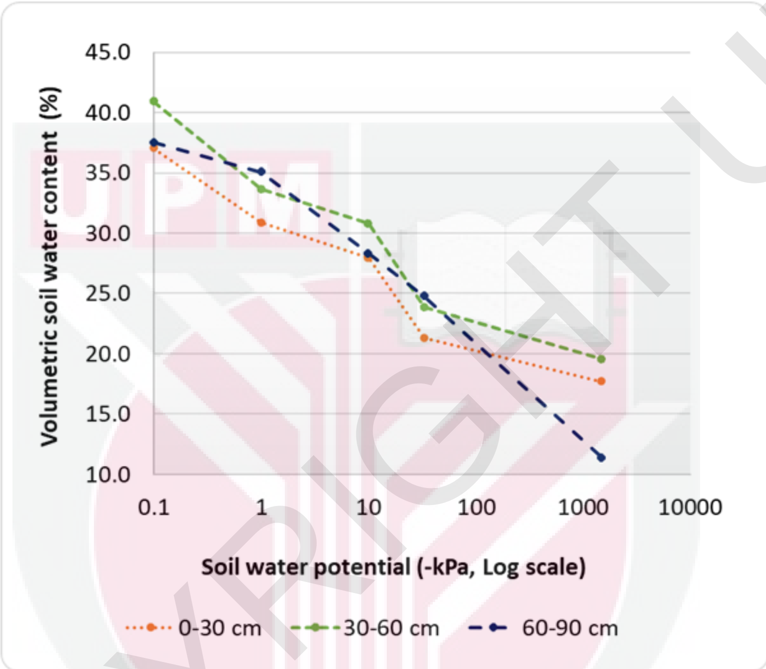

Figure 4.1: Soil water retention curve according to various soil depth

Data were analysed using an ANOVA test to look for differences in soil physical analysis according to soil depth. The four variables, namely clay, Csand, Fsand, Tsand, and OM, were statistically significantly different (Table 4.3). Clay particles increased with the increase in soil depth. Silt particles were not significantly different at various soil depths, while Csand was slightly reduced with an increase in depth but was not statistically significant. The Fsand was dominant and had the highest contribution, up to 47% in terms of whole particles. Like Csand, the Fsand percentage also decreased with increasing soil depth.

OM decreased at increasing depths of more than 30cm and was statistically significantly different for the depth of 0-30 cm. It could be due to OM from fronds, leaves, and other biomass in the field. Meanwhile, the OC also had the same trend as OM, decreasing with increasing soil depth.

Table 4.3: ANOVA result for each of soil particles according to soil depth

Soil depth (cm)	Clay	Silt	Csand	Fsand	Tsand	OM	OC
				(%)			
0-30	28.13±1.8 c	15.54±1.2	9.74±0.9	46.58±2.4 a	56.32±2.6 a	0.95±0.09 a	1.64±0.15 a
30-60	34.93±1.9 b	14.84±1.3	9.43±1.2	41.58±2.5 ab	51.01±2.6 ab	0.53±0.09 b	0.91±0.15 b
60-90	43.70±2.1 a	14.04±1.2	7.54±1.0	34.71±2.3 b	42.25±2.6 b	0.38±0.04 b	0.66±0.07 b
Mean	35.6	14.8	8.9	41.0	49.9	0.6	0.7
P value	<0.01	0.6845	0.2963	<0.01	<0.01	<0.01	<0.01
CV	29	44	64	31	28	63	63

Noted: Different letters in the same column indicate significant differences between means according to Tukey's test

4.1.2 Determination of AWHC

AWHC is direct and can be translated as the difference between FC and PWP. PWP refers to the water content under high soil retention that causes the plants to wither and lose turgidity even in a humid atmosphere (Briggs & Homer, 1912). Generally, PWP is widely accepted as a -1500 kPa pressure level. It differs between crop species, developmental stage, soil condition, and climate (Reimar 1995; Romano and Santini 2002) and is usually determined in a laboratory. However, the determination of FC is proposed to be measured in the field where the soil is undisturbed (Reichardt 1988). It can be hampered by the practical difficulties of lateral losses through horizontal flow, which are laborious and time-consuming (Mello et al., 2002). Although -33 kPa is often used as an estimation for FC, some arguments have been raised about that (Kirkham, 2014). He stated that soil scientists realised that FC was an imprecise term and not a unique value because equilibrium was never reached.

Sometimes, FC is usually determined by applying tension from 10 – 33 kPa for sandy to loamy soils (McCarty et al. 2016). FC can be determined by calculating an equation referred to as an inflection point (Liang et al. 2016). Zotarelli et al. (2010) suggested that the FC point can be assumed to be between the 'rapid' and 'slower' decrease of the soil water content of the soil moisture curve. During this phase, water is drained out from macropores and replaced by air, leaving the remaining water at smaller pores (micropores) to supply the moisture needed by the plant. In the case of this study, inflection points are potentially located adjacent to -10 kPa (Figure 4.1) for the curves for 0-30 cm and 30-60 cm. However, the inflection point for the soil depth of 60-90 cm was not clear due to a non S-curve trendline. The reason behind this is unclear. Based on these results, -10 kPa was selected as the best FC to be use in this study for determination of AWHC.

Data for the AWHC values ranged from as low as 79 mm up to 167 mm (Table 4.4) and the mean of the AWHC data was 113 mm. The Shapiro-Wilk test did not show evidence of non-normality of the data ($W = 0.9625$, $p = 0.3997$). No significant outliers were detected in the AWHC data since the largest Z-value, 2.35, is not more than the Critical Z-value, 2.88.

Table 4.4: AWHC value for 90 cm soil depth according to points of sampling

Point	BD ($g\ cm^{-3}$)	Water content at equilibrium ($g_{water}\ g_{soil}^{-1}$)					AWHC
		0 kPa	1 kPa	10 kPa	33 kPa	1500 kPa	
25	1.70	21.0	17.7	15.5	10.8	7.0	130
26	1.66	27.7	23.1	20.6	17.1	11.6	132
27	1.56	22.8	22.2	18.9	15.1	12.5	88
28	1.75	20.0	18.2	15.1	11.2	7.8	116
29	1.61	23.0	20.2	20.2	14.5	11.7	120
30	1.64	24.5	20.6	18.3	13.9	11.2	105
31	1.64	24.1	20.4	18.7	11.2	8.6	149
32	1.65	19.7	18.8	17.3	13.4	10.5	102
33	1.61	20.5	17.7	15.3	10.4	7.6	113
34	1.56	22.6	22.0	19.9	16.6	13.3	88
35	1.74	19.7	17.1	15.6	10.7	7.5	126
36	1.59	24.1	21.6	19.4	12.3	7.8	167
37	1.61	23.5	21.5	18.7	12.6	8.0	155
38	1.50	21.7	20.0	17.8	10.2	9.3	115
39	1.73	29.1	19.6	15.8	13.2	8.3	118
40	1.60	28.5	20.0	19.3	16.6	12.7	95
41	1.59	23.4	19.0	17.7	14.5	11.8	85
42	1.61	26.8	21.4	18.1	16.4	8.3	135
43	1.64	25.2	19.3	16.4	13.7	7.5	129
44	1.66	24.4	18.6	17.2	14.3	8.0	136
45	1.47	23.5	20.1	16.8	14.7	9.0	101
46	1.71	22.7	20.7	16.9	15.5	10.2	102
47	1.60	25.7	22.2	20.1	18.5	13.0	103
48	1.82	21.1	15.9	14.0	12.6	7.8	101
49	1.38	29.3	28.0	25.6	23.1	19.1	79
50	1.50	27.0	24.8	21.4	20.3	15.4	81
51	1.64	23.9	21.4	16.6	13.7	10.9	84
52	1.65	23.6	21.5	17.6	16.5	10.3	109
Mean	1.62	23.8	20.5	18.0	14.4	10.2	113

The matrix correlation table between analysed soil variables and AWHC is shown in Table A.1. A strong negative relationship was found between Fsand and clay particles (r =-0.814). It is indicated that one variable is inferior while another is dominant. Fsand was found to be negatively correlated with soil depth and had a high percentage of almost 82-83% of Tsand. Therefore, it was higher (r= 0.93) compared to the Csand (r= 0.46). AWHC reflects the capability of the soil to retain water, and it is related to total pore space. Higher pore space generally holds more water. It is aligned with the positive relationship between soil depth and clay particles. Clay, which is known as the smallest particle in soil, has the smallest pore spaces called micropores. Due to the greater number of pores, there were more total pore spaces than other particles. Micropores give greater capillary action than macropores in sand particles. Therefore, clay can retain more water but is typically poorly drained and not well aerated. Clay particles also swell when wet and shrink when dry.

In addition, OM has a moderately negative correlation with soil depth. High OM in the upper part of the soil is expected since a lot of plant debris and other OM will remain at the top of the soil, and only a small fraction can enter soil bodies. OM is accepted worldwide as a factor in improving soil water holding capacity. However, the results of this study showed no solid positive relationship between OM and AWHC, and there was a negative correlation. Minasny and McBratney (2018) conducted a study and proved that the effect of OM on improving available water capacity is very limited or overestimated. They also proposed that the increase is more pronounced in sandy soil, followed by loam and least in clay. Therefore, the contradictory result of this study could be due to decreasing OM availability over increasing soil depth, which is further compounded by the distribution of clay particles.

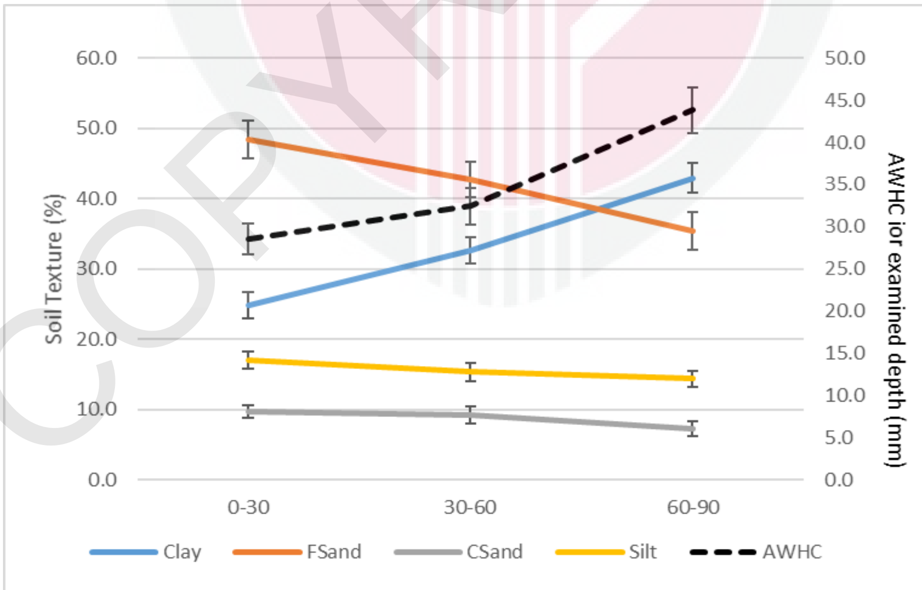

Figure 4.2: Average soil physical percentage according to soil depth

A simple view of the percentage of soil physical and AWHC over soil depth is shown in Figure 4.2. It is clearly demonstrated that the dominant soil physical, which is Fsand, was negatively correlated with clay. AWHC increased with an increase of Clay. However, the r value was low (0.137) and not statistically significantly different as shown in Table A.1.

4.1.2.1 Interpolation of AWHC

The total number of grid intersections was 28 points across a 20.3 ha area. During marking, the projection used for the coordinate system was WGS84. Somehow, the projection was converted into Kertau (RSO) to ease the post-process analysis, such as interpretation and interpolation. The data summary section in the GS+ Software contained a summary of statistics of the selected variables, such as the AWHC (Figure 4.3). Data transformation was not done because the data was normally distributed.

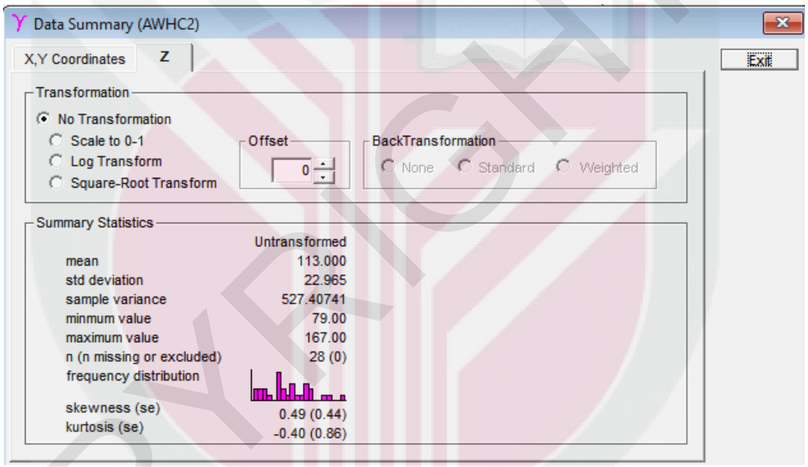

Figure 4.3: Output summary from GS+ software for interpolation of AWHC

The active lag distance was selected at 600 m at a uniform interval of 120 m (Figure 3.8). The value of lag distance followed the practical rules suggested by (Journel & Huijbregts, 1978). According to them, the first rule is that the number of pairs needs to be greater than 30, and the second rule concerns the 'distance of reliability' for an experimental variogram is $h < \frac{D}{2}$, where D is the maximum distance over the field of data. However, the second rule cannot be applied in this study. The minimum lag interval must be more than 100 m since the sampling is a grid point. If $h < 350$ m is selected as active lag distance (700 m is the maximum distance between points of sampling), then the number of lag classes is below 5, and $R^2 = 1.000$ (too perfect for the model). It should also be noted that the minimum number of lag classes in the ArcMap software is five. When the active lag distance is at 600 m, the best-fit model is a spherical isotropic variogram with a range of 196 m, and the value for R^2 is acceptable, which was 0.645 (Figure 4.4). The isotropic variogram means that the spatial structure of the variable is consistent in all directions. This data is considered to have a strong spatial dependence as the nugget semi-variance percentage is 0.77% and it falls below 25% (Cambardella et al., 1994). This software also suggested that the range was 196 m. It is means that an effective range before no spatial dependence existed was 196 m, and distances of 100 m between the sampling points were acceptable.

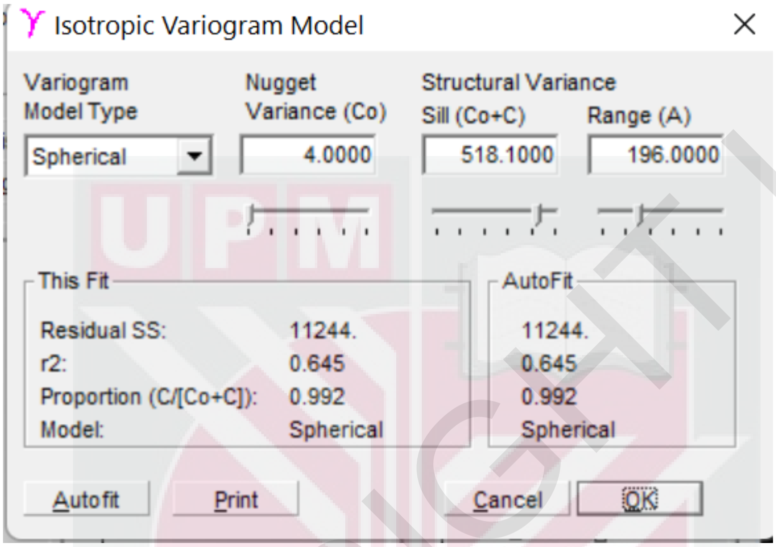

Figure 4.4: Result and parameter of best-fit model for the data

The ArcMap software is very interactive software that makes interpolations with intuitive graphics and various preferences. The first image of interpolation is shown in Figure 4.5 with a multi-colour graphic scheme. However, the different colour schemes do not help ease the determination of the irrigation zone. The irrigation zones need to be concise, smaller numbers without compromising underlying objectives to distinguish soil into different but manageable zones and, at the same time, be operationally wise.

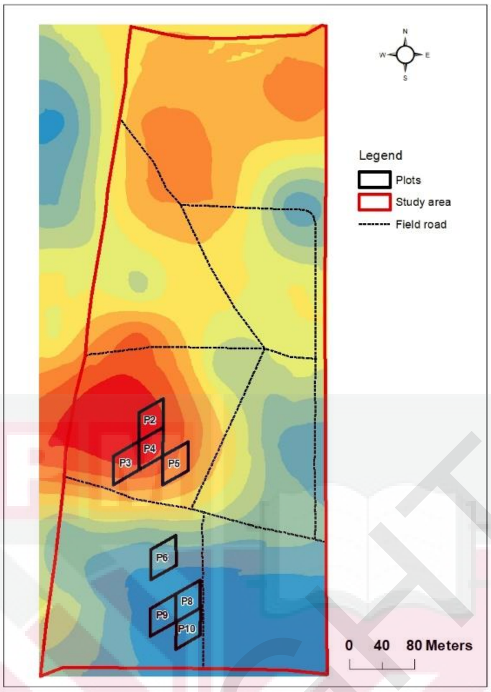

Figure 4.5: First interpolation map for AWHC data across the study field

4.1.2.2 Classification of management zone

Irrigation requires much effort in terms of management activities. It is consists of knowledge to overcome any problem that arises due to leakage, damage, maintenance, and others. For non-moving irrigation systems, several zones were suggested based on differences among the AWHCs studied. Management zones need to be practically different amongst themselves and prove to be statistically different. The number of management zones also needs to be decided based on factors such as ease of irrigation management and cost of establishment.

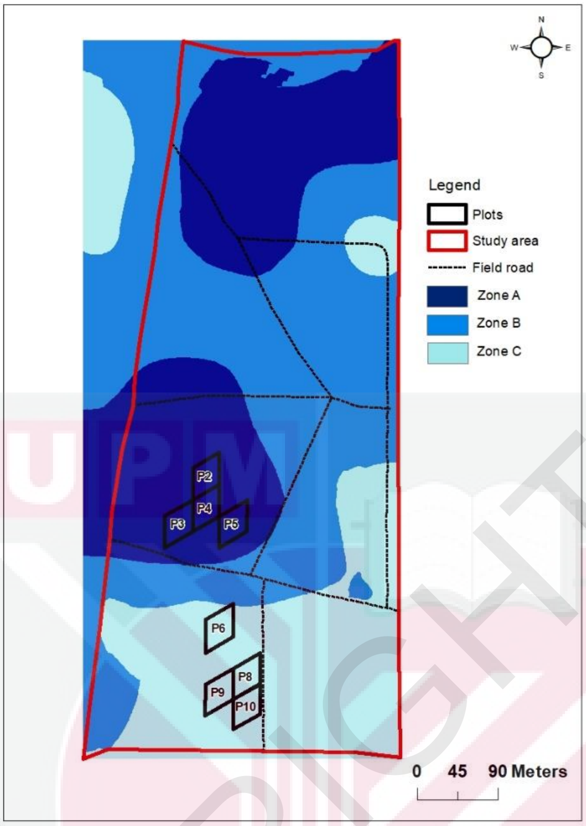

Figure 4.6: Layout view reclassified interpolation map

An effort was made to classify IMZ using ArcMap, and as a result, three classes of IMZ were produced to represent the lower-end, intermediate, and higher-end classes. Finally, three distinct management zones were created, namely Zone A, Zone B, and Zone C (Figure 4.6). Generally, an irrigation event will take place once the CD of AWHC is achieved. For example, if normal evapotranspiration is 5.0 mm and CD is 50%, Zone A would require 7-8 days, Zone B about six days, and Zone C would need about 4-5 days of irrigation interval.

By using the suggested IMZ from the ArcMap software, nine values of AWHC fall into Zone A, 12 AWHCs fall into Zone B, and seven AWHCs fall into Zone C (Table 4.5). One-way ANOVA test analysis resulted in values of F = 65.63 and P <0.001, which suggested that each classification group was highly statistically significantly different. Further analysis using Tukey's test showed that the most extensive region was Zone B, which was 9.23 ha, followed by Zone A, which was 7.62 ha, and lastly, Zone C, which was 6.57 ha.

Table 4.5: Statistical analysis of every AWHC zone after reclassification process

Zone	AWHC Category (mm)	N	Mean	Standard deviation	Standard Error of the mean	Area (ha)	%
A	125-167	9	140 a	13.9	4.6	7.62	33
B	100-125	12	109 b	7.1	2.0	9.23	39
C	79-100	7	86 c	5.3	2.0	6.57	28
Total						23.43	100

Noted: Different letters in the same column indicate significant differences between means according to Tukey's test

Previous studies have shown that IMZ values can be delineated using Sentinel-2 images or field property data (Liakos et al., 2018; Oldoni & Bassoi, 2016). In this study, IMZ values based on AWHC data were considered stable and, as a result, can be used for many years as initial guidelines for growers or irrigation planners; however, the produced IMZ maps cannot be used to provide real-time soil moisture status information. Based on this study, it is suggested that the period of water in each zone reached the soil deficit limit at different times from each other. Each management zone should have a different irrigation schedule and water requirements. The establishment of these three management zones is manageable and reliable compared to a higher number of categorisations.

4.1.2.3 Other factors contributing to the reclassification of the management zone

The only main road is indicated as black lines in the map shown in Figure 4.6. This road had a considerable impact on the piping network plan. This road is mainly used for daily activities such as transportation of FFB, fertiliser, maintenance, and many other things. The current main pipe or sub-main pipe generally follows this route and is buried at the side of the road. Meanwhile, there is another crucial path in oil palm estates called the mechanization path. It is mainly used to carry loads such as FFB to the collection point at nearby main roads (Figure 4.7). Any decision on the management zone for SBI system needs to address this since this path is used by machines such as tractors and rotor slashers. It will be a limiting factor for any level of pipe arrangement as it is compulsory to bury pipes to minimise the impact of activities done on this path, thus avoiding pipe damage.

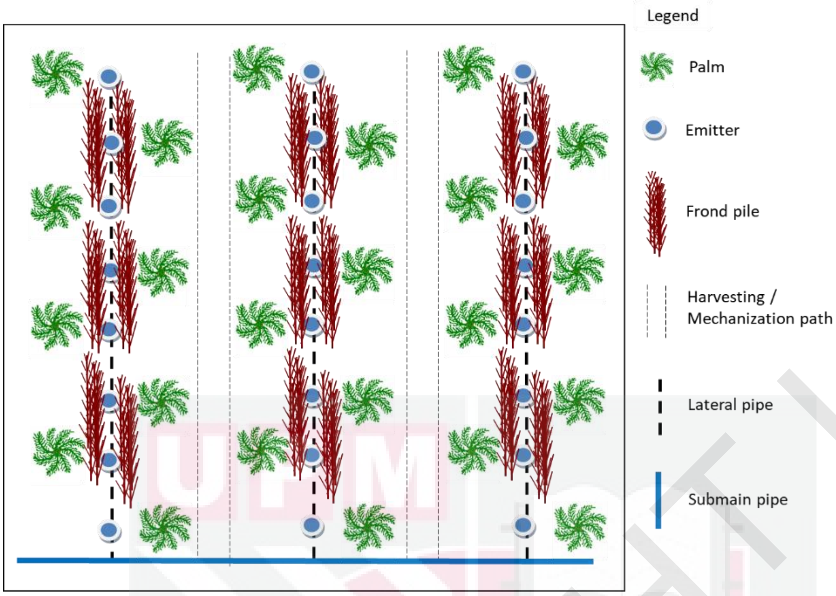

Figure 4.7: Illustration of mechanization path and frond pile in the oil palm field

4.2 Spatial variability of annual rainfall

The rainfall pattern per year is shown in Figure 4.8. Two distinct seasons occur in a year, which are the dry period and the monsoon period. The former period consists of low rainfall distribution, usually below 150 mm month^{-1}, and starts from January until February. The second season of the dry period occurs between June and September, but it is relatively much better than the dry season in February. The monsoon period typically starts from October until December, with a higher amount of rainfall of more than 290 mm month^{-1}. No irrigation is needed for these months as soil water status is more than sufficient.

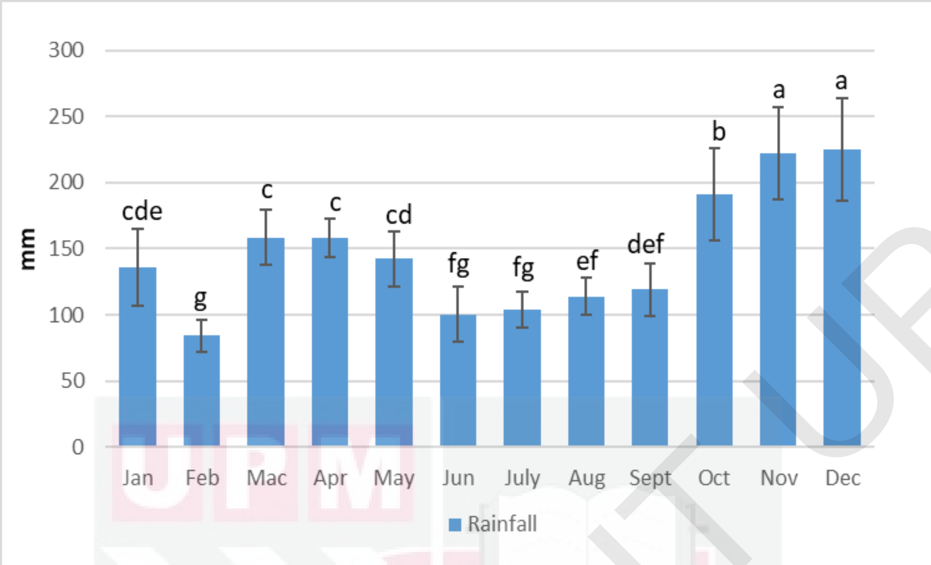

Figure 4.8: Average rainfall distribution by month for 17 meteorological stations

Table 4.6: Descriptive analysis of rainfall data

Variable	N	W	P	Skew	Kurtosis
Rainfall	17	0.9234	0.168	0.431	-0.8503

Rainfall data for the 17 selected areas was normally distributed with $P > 0.05$ and skewness close to zero (Table 4.6). From the semivariance analysis, the value of the nugget was 360, the Sill was 24,960, and the range was 56,7000 m with the R^2 value of 0.960 and of the exponential variogram type. The spatial structure of the variable was consistent in all directions and fell below the isotropic variogram. The result also suggested that rainfall data among all stations had a strong spatial dependence as the nugget semivariance percentage was 1.4% (Cambardella et al., 1994). A map based on the rainfall data is shown in Figure 4.9. The current study area is located in an area with an average rainfall amount of 1696-1720 mm $year^{-1}$ (represented by the yellow-coloured areas in Figure 4.9). Therefore, rainfall is relatively homogenous within the study area. Ghazalli and Nieuwolt (1982) presented four agroclimatic regions in Malaysia based on the length of the dry period. Later, Goh et al. (1994) modified this category for oil palm into three areas according to yield profile. This current study site falls into the region with a prolonged dry period.

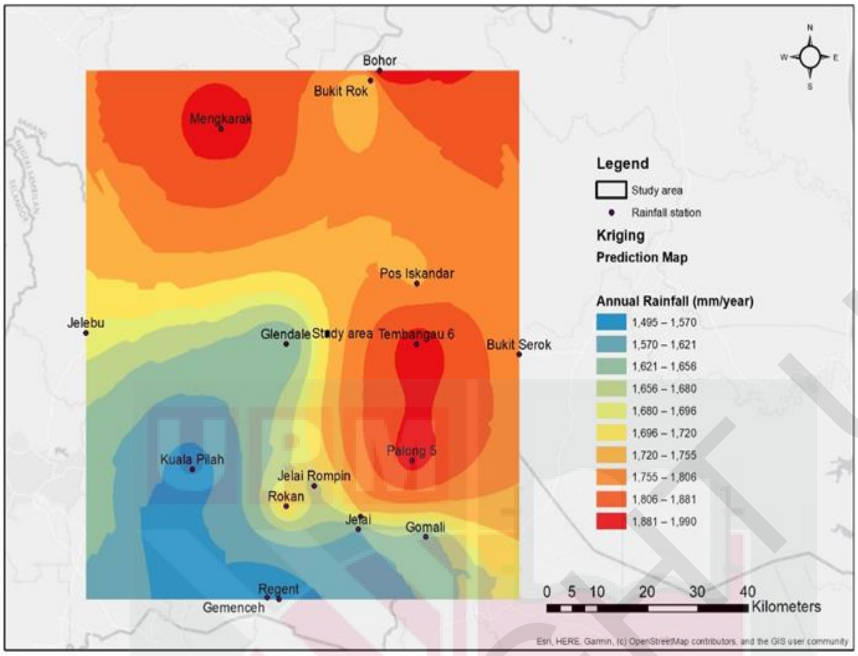

Figure 4.9: Interpolation rainfall map indicating study site falls under 1696-1720 mm year^{-1}

4.3 Assessment of soil infiltration for each irrigation management zone

Infiltration rates have various consequences in irrigation management, such as scheduling and flow rate selection. Random locations were selected to reduce human error and bias in the data. It also meant minimizing the hefty work of collecting the field data because the infiltration test requires a considerable amount of time. The primary data for infiltration capacity is shown in Figure 4.10 - Figure 4.18. Generally, from nine locations, two locations, i.e., Location 3 and 6, gave outlier results and did not follow the typical infiltration capacity trend over time (Assouline, 2013). Locations 1 and 2 (Zone A) gave satisfying results with R^2 values of 0.7750 and 0.8751, respectively (Figure 4.11). At Zone B, Location 4 gave R^2=0.6171, and Location 5 gave R^2=0.7372. Zone C gave perfect curve lines from all locations, which are Location 7 (R^2=0.9365) and Location 8 (R^2=0.9051), and the highest was at Location 9 (R^2=0.8951).

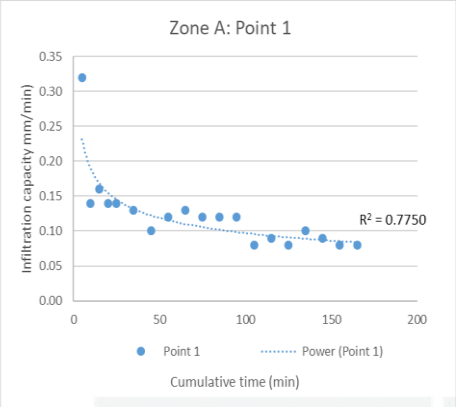

Figure 4.10: Infiltration capacity for Zone A-Location 1

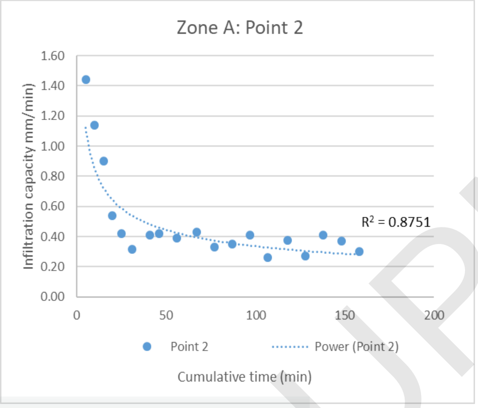

Figure 4.11: Infiltration capacity for Zone A-Location 2

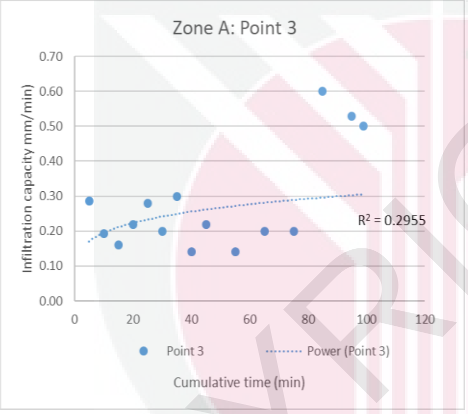

Figure 4.12: Infiltration capacity for Zone A-Location 3

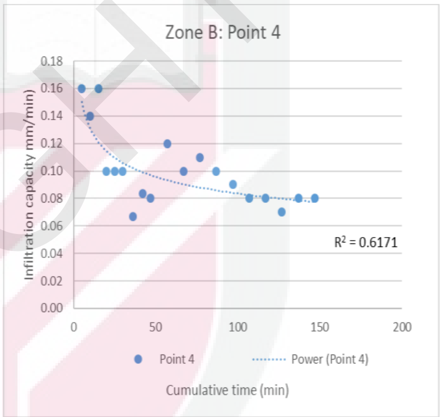

Figure 4.13: Infiltration capacity for Zone B-Location 4

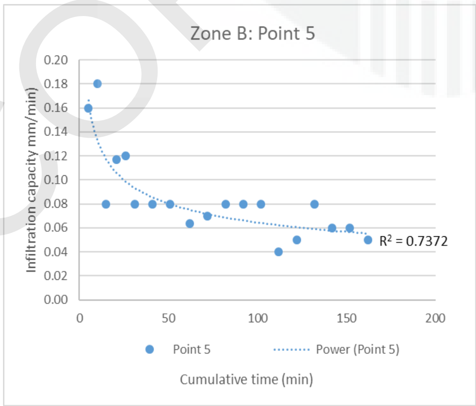

Figure 4.14: Infiltration capacity for Zone B-Location 5

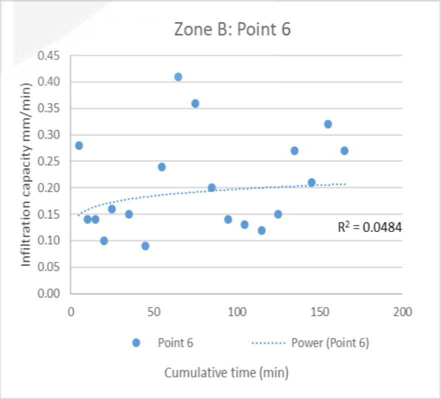

Figure 4.15: Infiltration capacity for Zone B-Location 6

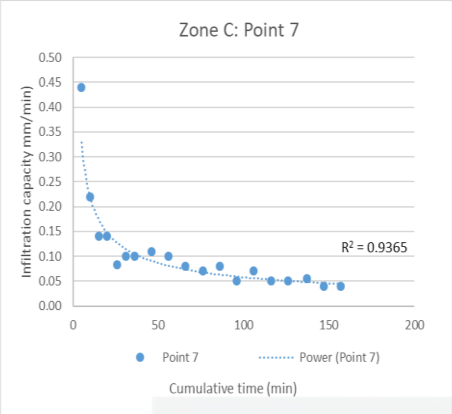

Figure 4.16: Infiltration capacity for Zone C-Location 7

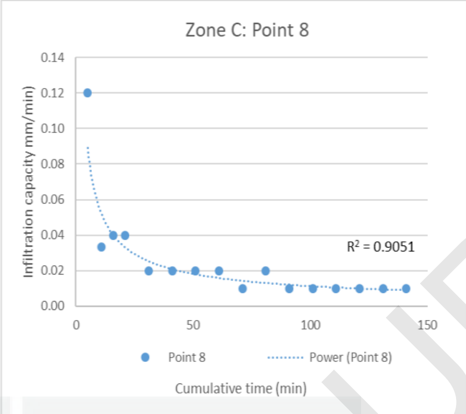

Figure 4.17: Infiltration capacity for Zone C-Location 8

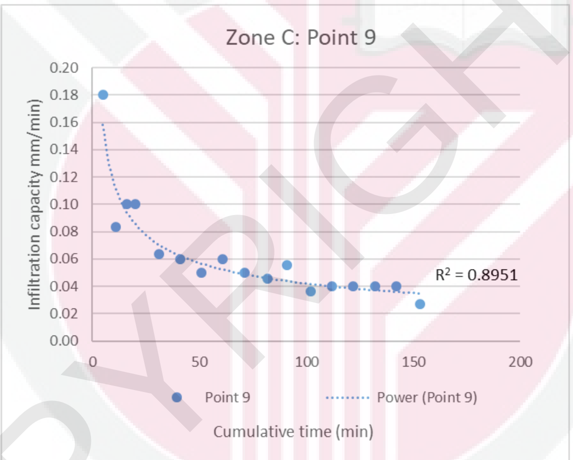

Figure 4.18: Infiltration capacity for Zone C-Location 9

Table 4.7 shows the field-measured cumulative infiltration depths and the rates for each location. Zone A had a cumulative infiltration rate from 2.57-8.23 mm hr^{-1} by excluding data from Location 3. Meanwhile, Zone B had a lower cumulative infiltration that ranged from 2.35-3.51 mm $hr^{-1,}$ which was also obtained with the exclusion of Location 6 from the assessment. Location 8 (Zone C) had a very low infiltration capacity despite a good R^2 value, as shown in Figure 4.17. Based on Hillel (2004), the lowest infiltration rate for clayey soil should be in the range of 1.0-5.0 mm $hour^{-1}$ and because of this, Location 8 was also treated as outlier data. Therefore, the infiltration rate for Zone C was from 1.01-1.06 mm hr^{-1} after excluding Location 8.

Table 4.7: Cumulative infiltration for each point calculated by using Equation 5

Location	Zone	Longitude	Latitude	I (mm day^{-1})	I (mm min^{-1})	I (mm hour^{-1})
1	A	102.4904	2.9510	87.3	0.043	2.57
2	A	102.4898	2.9507	300.1	0.137	8.23
3*	A	102.4912	2.9544	398.2	0.275	16.50
4	B	102.4903	2.9531	99.0	0.058	3.51
5	B	102.4917	2.9523	71.2	0.039	2.35
6*	B	102.4912	2.9505	253.6	0.162	9.70
7	C	102.4920	2.9507	47.1	0.018	1.06
8*	C	102.4915	2.9490	8.7	0.003	0.17
9	C	102.4900	2.9491	37.0	0.017	1.01

Note: * Data are considered as outliers based on typical soil infiltration range

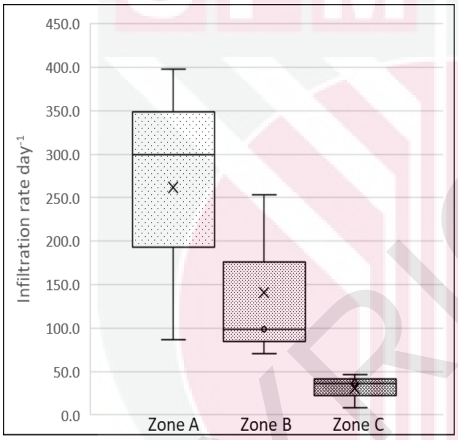

Figure 4.19: Distribution of infiltration per day according to IMZ

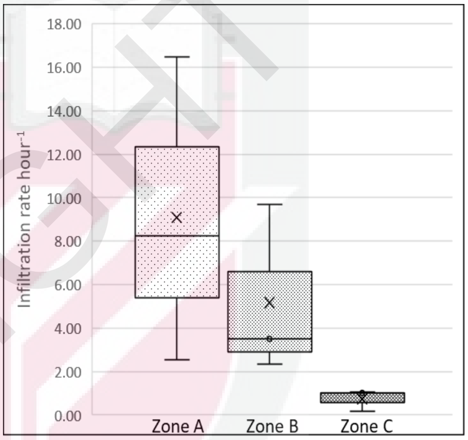

Figure 4.20: Distribution of infiltration per hour according to IMZ

Zone A exhibited an extensive range but still overlapped with Zone B. However, Zone B produced consistent datasets similar to Zone C. In addition, Zone C also had a non-overlapping dataset with both Zone A and Zone B. Each management zone had its specific maximum infiltration rate with the corresponding sequence of Zone A > Zone B > Zone C, as shown in Figure 4.19 and Figure 4.20.

Many factors impact soil infiltration rate. Generally, it can be divided into three groups which are surface conditions, soil characteristics, and cultural practices. In detail, the factors are the crop root system, organic debris, mulching, burrowing animals, insects, surface moisture content, frost heave, salts, digging cracks, interstitial air, and temperature (Folorunso & Aribisala, 2018). Higher infiltration rates in Zone A and Zone B of this study can be caused mainly by variations in soil texture, which has a significant influence on the value of infiltration capacity (Cleophas et al., 2021).
In general, Zone C had a higher percentage of clay and significantly higher silt at a depth of 0-30 cm, as shown in Figure 4.21. Zone C also showed a higher clay

percentage for the rest of the examined depths (Figure 4.22- Figure 4.23). For the 0-30 cm soil depth, fine texture, such as a combination of silt and clay, may impede the flow of water due to lower saturation conductivity (Adhikary et al., 2008). Clay is characterised by small particles (<0.002 mm) and contains micro-pore space, thus holding water more tightly. In the case of Zone A and Zone B, sand has a larger particle size and a larger pore size than clay particles. Larger pore sizes have more permeability capacity and allow a higher amount of water to infiltrate the soil (Shaari et al., 2017).

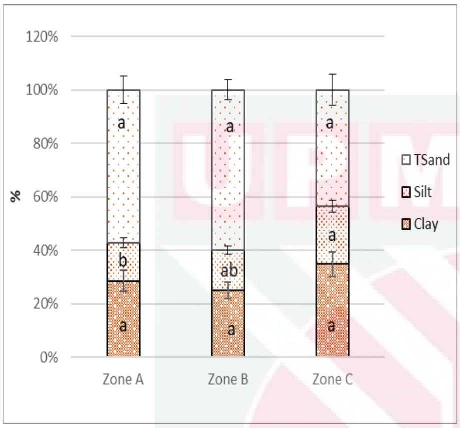

Figure 4.21: Distribution of soil physical for IMZ at 0-30 cm soil depth

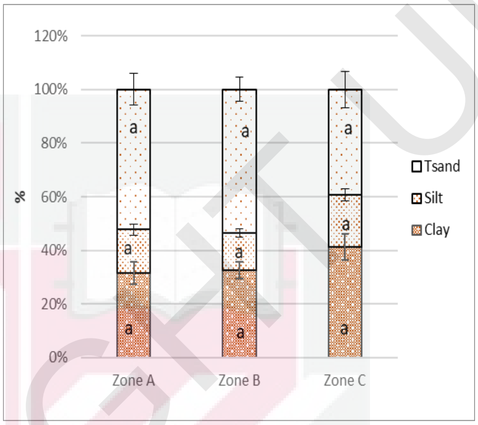

Figure 4.23: Distribution of soil physical for IMZ at 30-60 cm soil depth

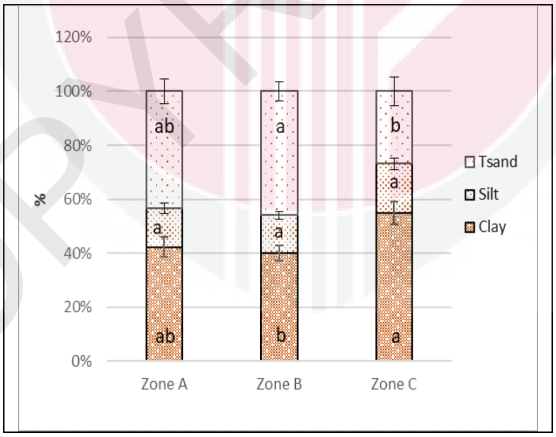

Figure 4.23: Distribution of soil physical for IMZ at 60-90 cm soil depth

As mentioned in Section 3.8, FAO-CROPWAT requires a maximum infiltration rate in a day as one of the inputs from the user. Maximum rain infiltration rate in FAO-CROPWAT will allow for an estimate of surface runoff or ER calculation, which will affect the TNI value (Smith 1992). Based on these findings, the cumulative infiltration for a day ranged from 37 to 300 mm day^{-1} by excluding erratic data from Locations 3, 6 and 8. However, it was found that this range did not affect TNI.

Despite reasonable procedures taken during data recording, the first 'actual' data might be 'unrecorded' due to the speedy absorption of water by the soil during the water-filling process. Perrier and Salkini (1991) stated that a double-ring infiltrometer had the same disadvantages as a single-ring infiltrometer. This device required pounding the ring into the soil (a difficult task) to a depth that can fracture dry soil. It will cause soil to crack and allow water to seep, increasing the value of the estimated infiltration rate. If this happens before a steady reading can be taken, the gradient of the curve trend may be lower and result in low cumulative infiltration capacity. Additionally, one study has suggested that the occurrence of termite colonies may increase the infiltration capacity of the soil (Mando et al., 1996). Termite colonies frequently may exist in the soil and feed on wood or dead plant matter, especially decayed roots of oil palms.

4.4 Comparison of historical water usage and FAO-CROPWAT simulation data

FGVAS Serting Estate established irrigation as soon as the replanting program finished in 2014. In 2015, irrigation was still in the development phase, and the operation started in 2016. In 2016, the plantation experienced very low rainfall, with the total amount of rainfall being only 992 mm (Table 4.8). Whereas in 2017, this area received a considerably huge downpour with a total amount of 2084 mm $year^{-1}$. Based on the recorded data by the estate, the EVW applied as irrigation was 41,265 m^3 in 2016, which decreased to 29,614 m^3 in 2017. When EVW was translated into EID, the total was 322 mm for the year 2016 and reduced to 130 mm for the year 2017. Generally, the massive difference between these years was because of the opposing trends of rainfall availability. The depth of monthly irrigation is shown in Figure 4.24 and Figure 4.25. In 2016, the highest EID was in February and April, which were 86 mm $month^{-1}$, whilst the lowest was in May, which was only 6.0 mm $month^{-1}$. There were no irrigation activities toward the end of the year because the amount of rain was sufficient due to the typical monsoon period. Thus, the soil was considered wet almost all the time. The value of 120 mm was set as a baseline to represent the minimum value for ETc, as suggested by IRHO (Surre, 1968).

The year 2016 was the warmest year for Malaysia and was strongly influenced by the Super El Niño, which occurred between February and May (MMD 2016). Ironically, EVW was very low in March even though rainfall was low that month. In this case, EID was limited to only 15 mm due to the shortage of water sources that originated from a nearby river. The total input for water in March 2016 was only 21.8 mm $month^{-1}$, which was only 18% of the baseline value. Based on previous records, the level of river water was too low and below the suction drawing point thus, irrigation was impossible to be carried out. The issue of limited water sources is strongly considered a bottleneck factor for any irrigation adoption. Alternative water sources such as groundwater can incur a very high capital cost, and the decision to use them requires further analysis and thorough study. According to Azrina et al. (2011), only 1% of total groundwater is being exploited in Malaysia. Lack of exploitation is due to the failure to recognise groundwater potential, a misconception that groundwater is not sustainable and a lack of assessment of these resources (Mohammed & Ghazali, 2009).

In 2017, there was no irrigation from the period of January to March and November to December (Figure 4.25). The rainfall amount in November was as high as 600 mm month^{-1}. The gap between the water deficit (June and September) was much closer to the baseline. Based on (MMD 2017), the El Niño Southern Oscillation (ENSO) index was neutral starting from January 2017 till the end of November 2017, followed by a weak La Niña condition that began in December 2017. Thus, Malaysia did not experience long-lasting hot and dry weather throughout 2017.

Table 4.8: Irrigation input, requirement and rainfall during 2016 and 2017

Year	EVW (m^3)	EID (mm)	Rainfall (mm)
2016	41,265	322	992
2017	29,614	130	2084

Note: For 23.5 ha irrigation area with 148 stands per ha and 60 L per hour emitter output

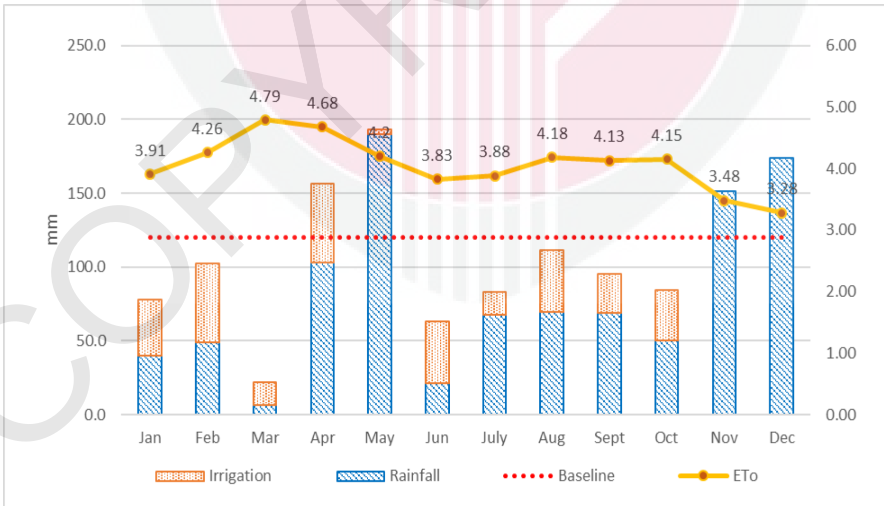

Figure 4.24: Monthly EID and rainfall distribution for FGVAS Serting Hilir Estate in 2016

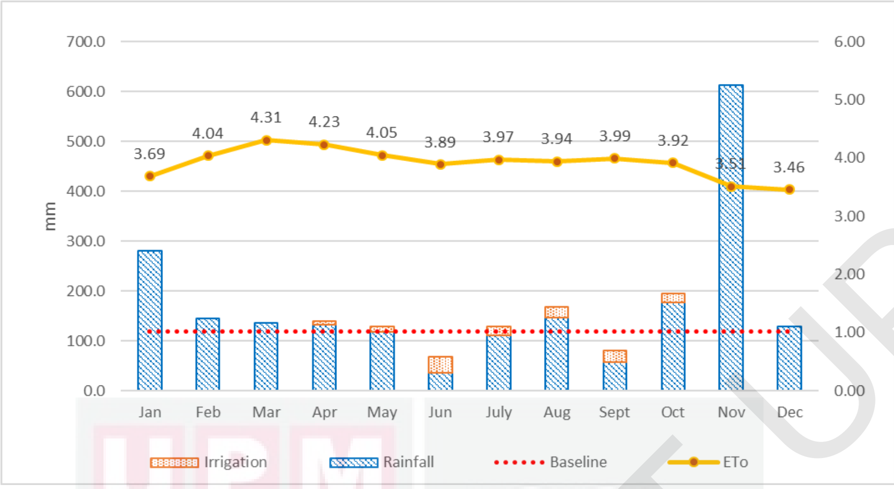

Figure 4.25: Monthly EID and rainfall distribution for FGVAS Serting Hilir Estate in 2017

Several factors have an adverse effect on irrigation scheduling. Human factor bias or error is a major factor since the operation is mainly done manually by the workers. Without proper management and supervision, irrigation activities tend to be inconsistent. There are some cases where irrigation cannot be done due to the engine or system failure. With time, a mechanical engine requires maintenance and replacement of parts, which sometimes cannot be recovered within a short period. Fortunately, some minor breakdowns or damage can be solved by experienced workers equipped with basic engineering skills. Apart from that, knowledge of overcoming or operating routine problems regarding emitter clogging, fundamental hydrology, and filtering systems is a must-have skill for responsible workers.

FAO-CROPWAT model simulated crop water requirement based on climatic conditions. Table 4.9 shows CWR for both years and the values for 2016 and 2017 were 1129 mm and 1065 mm, respectively. It was derived from estimated ETo based on provided meteorological data without considering soil factors. CWR according to decade which represented each 10-days per month requirements for 2016 are shown in Figure 4.26 and for 2017 as shown in Figure 4.27.

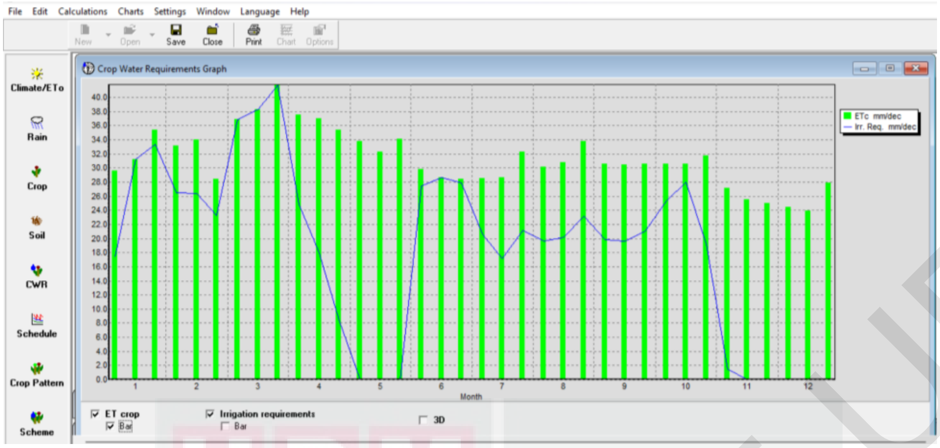

Figure 4.26: CWR graph with calculated ETc according to decade value for 2016

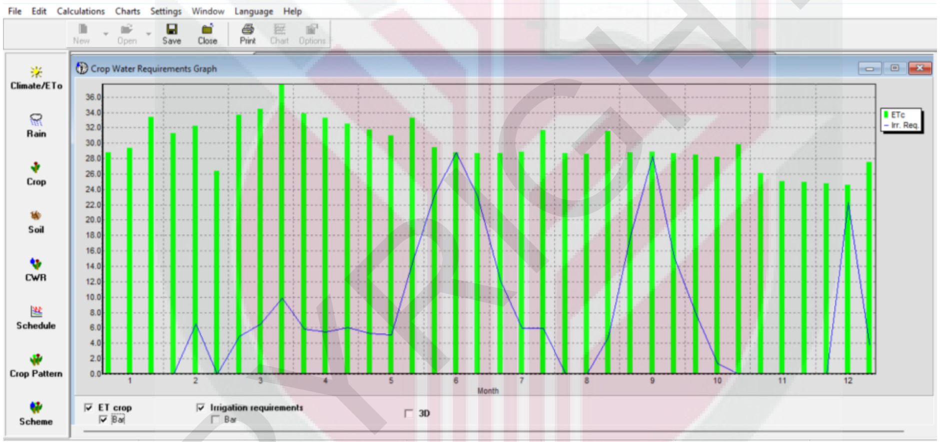

Figure 4.27: CWR graph with calculated ETc according to decade value for 2017

Table 4.9: Value of rainfall amount and CWR for the years 2016 and 2017

Year	ETc (mm year^{-1})	ER (mm year^{-1})	Irrigation requirement (mm year^{-1})
2016	1129	549	667
2017	1065	1389	283

Regarding TNI, the estimated value takes into account soil water holding capacity and irrigation practices. Different AWHCs vary the capability of water holding, which affects the timing of irrigation. The soil AWHC result from different IMZs from Section 4.1 was used in this assessment. From the analysis, irrigation in 2016 was below TNI, ranging from 73 mm to 93 mm (Table 4.10). EID for 2017 was 130 mm, but the maximum TNI was only 75 mm. This translates to surplus EID from 55 to 90 mm. Insufficient EID in 2016 was partly because of the limited water source, as mentioned before.

Table 4.10: Comparison of estimated water need and estimated irrigation depth given to the field

Year	2016			2017		
Zone	TNI (mm)	EID (mm year^{-1})	Surplus (+) or deficit (-) in mm	TNI (mm)	EID (mm year^{-1})	Surplus (+) or deficit (-) in mm
A	395	322	–73	40	130	90
B	405	322	–83	55	130	75
C	415	322	–93	75	130	55

Irrigation scheduling for current practices based on rainfall amount is probably the basic guideline for operators to ease decision-making for them. The water balance approach can be used to keep track of the soil water deficit by accounting for all water additions and subtractions from the soil root zone (Andales et al., 2011). Meanwhile, many types of soil moisture sensors can provide real-time and continuous data (Bitella et al., 2014; IAEA, 2008; Sui, 2017) and thus improve water use efficiency. Increasing the scheduling efficiency offers the opportunity to conserve water resources (McCready & Dukes, 2011). Over-irrigation means that extra energy resources are required, such as gasoline, human resources, and maintenance. It also results in nitrogen leaching and runoff, an increase in weed pressure, vulnerability to diseases, and delayed growth and yield (Irmak & Rathje, 2008). Therefore, as occurred in 2016, water could be diverted and stored for the use of irrigation purposes at critical times. Meanwhile, the water requirement is sometimes low due to a high excess of water from rainfall, such as in the case of 2017. In this situation, water can be diverted elsewhere by harvesting rainwater using various methods so that water can be used whenever necessary (Pala et al., 2021).

4.5 Hydraulic performance of selected micro-sprayer emitter

Back in the 1990s, this estate adopted irrigation using the furrow method. Almost 20 years later, when replanting took place, the irrigation method was replaced with pressurised irrigation. However, the adoption of pressurised irrigation was not well studied and fully understood. Micro-sprayer type of emitter was widely used despite differences in their colour code. The unavailability of specifications of generic emitters in the market worsened the situation. Usually, manufacturers will provide a head-discharge curve for their products but seldom publish information related to the pressure-to-emitter discharge component (Hezarjaribi et al., 2008).

There were no data sheets or any specifications given related to the products used in this study, but the cost was significantly cheap, which was Malaysia Ringgit (MYR) 0.20 emitter^{-1} compared to more than MYR 1.00 emitter^{-1} from other well-established products or brands. Information related to the emitter is essential since it is related to the calculation of water output, pressure, and determination of pump size. In this study, emitter properties need to be used as one of the inputs of the software to improve the hydrology calculation of the system and basic specifications are shown in Figure 4.28.

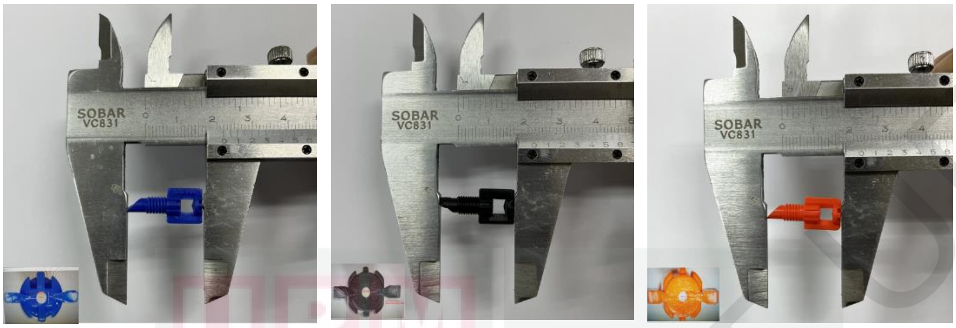

Blue Emitter	Black emitter	Orange emitter
Length: 2.14 cm ± 0.2%	Length: 2.14 cm ± 0.4%	Length: 2.19 cm ± 0.4%
Width: 1.02 cm ± 0.0%	Width: 1.01 cm ± 0.4%	Width: 0.95 cm ± 0.4%
Orifice: 1.806×10^{-6} m^2	Orifice: 1.265×10^{-6} m^2	Orifice: 1.243×10^{-6} m^2

Figure 4.28: Specification of a low-cost emitter according to colour code

4.5.1 Emitter head-discharge (H-Q) relationship

From the result, the difference in emitter H-Q curves is apparent and the sequence from lowest to highest is as follows; Orange < Black < Blue (Table 4.11). In Table 4.13, the pressure unit in terms of meter head of water was used to complement the further analysis of the IrriPro software. The mean values of the flow rate for every incremental pressure applied were significantly different. For this experiment, the flow rate of the emitter ranged from 39 – 125 L hour$^{-1,}$ which falls into the range of 20 – 150 L hour^{-1}, making this emitter fall into the category of micro-sprayers or non-rotating type of static micro-jets (Goyal, 2015).

Table 4.11: Emitter flow rate based on various operating pressure

Emitter	**Pressure (Meter)**				
(litre hour^{-1})	0.50	10.2	15.3	20.4	25.5
Blue	56 ± 2.3a	74 ± 0.7a	92 ± 0.4a	114 ± 3.4a	125 ± 0.5a
Black	46 ± 0.4b	63 ± 0.4b	75 ± 0.1b	86 ± 0.0b	99 ± 0.4b
Orange	39 ± 0.2c	51 ± 0.4c	63 ± 0.0c	73 ± 0.1c	81 ± 0.0c
CV	4.17	1.39	0.61	3.70	0.43

Noted: Different letters in the same column indicate significant differences between means according to Tukey’s test

The non-linear graph using the power function ($Q_e = KH^x$) is shown in Figure 4.29, and it was used in the IrriPro software for the design simulation. Q_e is the emitter flow rate in litre hour^{-1}, K is the emitter discharge coefficient, H is the pressure head and x is an emitter exponent. The exponent, x is an indirect measure of the sensitivity of flow rate to the change in pressure.

The constant value, K, for the Blue emitter is 22.082, the Black emitter is 20.599, and the Orange emitter is 17.797 as shown in Table 4.12. The value of x typically ranges between 0 and 1.0, where a lower value indicates a lower sensitivity and a higher value shows a higher sensitivity (Mangrio et al., 2013). Keller and Karmeli (1974) suggested that emitters have absolute flow regulation if x = 0.0 and some degree of regulation if x <0.50. They also indicated that x can be used to characterise the regime of emitter flow as summarised in Table 4.13. Based on this, the flow regime of all tested emitters was turbulent, and emitters had a considerably medium sensitivity to pressure differential. In the IrriPro software, this value can be added manually in the catalog and then used in the simulation to create better insight for the irrigation design.

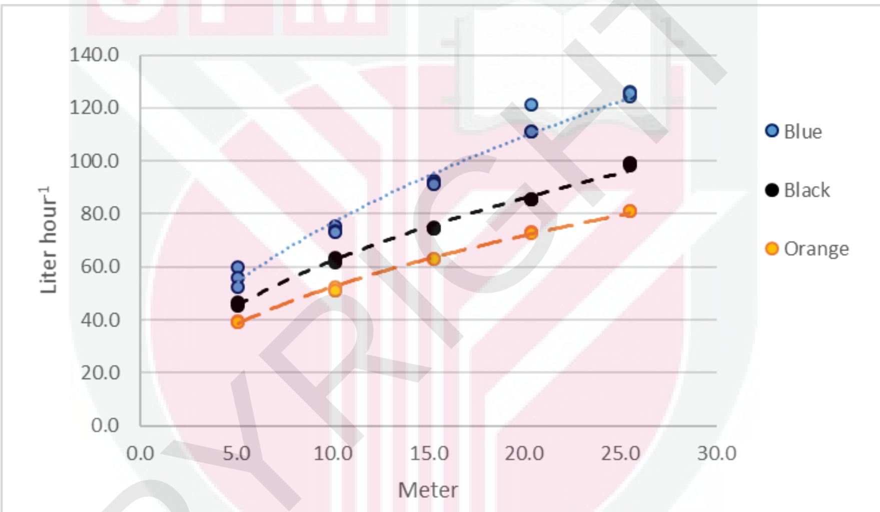

Figure 4.29: H-Q relationship for different micro-sprayer emitters

Table 4.12: Detail of regression analysis for different colour codes of emitter

Emitter	Blue	Black	Orange
K	22.082	20.599	17.797
x	0.536	0.478	0.467
Pseudo R^2	0.977	0.994	0.997

Table 4.13: Classification of emitter state of flow based on emitter exponent value

Value of x	State of Flow
=0.50	Turbulent
0.50 < x < 0.70	Partial Turbulent flow
0.70 < x < 1.00	Unstable flow regime
=1.00	Laminar flow

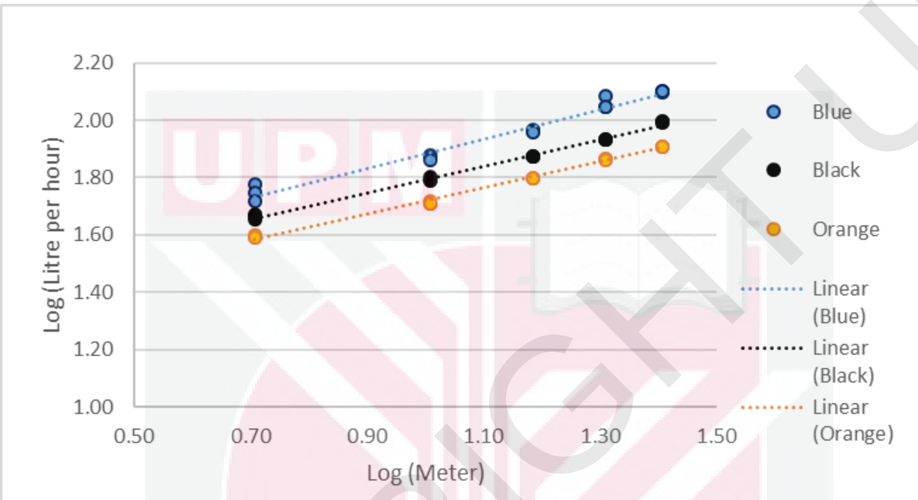

Figure 4.30: Flow rate of an emitter according to its colour and operating pressure, in Log scale

The high number of R^2 observed, almost all of them exceeded $R^2 = 0.90$, suggesting a high correlation between flow rate and applied pressure. The flow rate does not show a horizontal line, meaning that this type of emitter does not have PC characteristics (Figure 4.30). The results of this study show that the relation between each emitter and applied pressure had significant differences (Table 4.14). It was expected due to the relatively cheap cost of the emitter. However, the usage of these emitters may require attention since they are more vulnerable to non-uniform application in the field. The flow rate at the far end of the lateral pipe may be slower compared to the emitter nearest to the water source. The length of the lateral line is critical since it will affect the pressure and result in a low flow rate at a far lateral distance. The variation of the emitter flow rate is hydraulically based on pressure variation along the lateral line represented in the flow exponent of the emitter (Amer & Gomaa, 2015).

Table 4.14: Linear regression component between Log meter (X-axis) and Log Flow rate (Y-axis)

Emitter	Blue	Black	Orange
Constant	1.372	1.329	1.265
Coefficient of Log (Meter)	0.513	0.465	0.454
R^2	0.976	0.995	0.997
P value	< 0.01	< 0.01	< 0.01

4.5.2 Emitter head-throwing distance (H-T) relationship

In the IrriPro software, the range of water dispersion can be used as an input for a particular emitter if the range function with pressure is obtained. When it comes to throwing distance, all emitters throw distance range below 3.0 m. The blue emitter had the broadest range, from 1.67 m – 2.74 m (Table 4.15). According to Post et al., (1986), micro-irrigation spray and spinner emitters were characterised by having a throw distance ranging from 0.75 to 5.00 m. Black and Orange emitters produced an almost similar range of water dispersion, which was generally from 1.47 m to 2.22 m, and did not significantly differ from others with the same operating pressure.

Table 4.15: Emitter throwing distance based on various operating pressure

Radius (meter)	Pressure (Meter)				
	0.50	10.2	15.3	20.4	25.5
Blue	1.67 ± 0.06a	2.30 ± 0.04a	2.36 ± 0.04a	2.00 ± 0.07a	2.74 ± 0.05a
Black	1.57 ± 0.03ab	1.63 ± 0.04b	1.71 ± 0.07b	2.54 ± 0.07b	2.15 ± 0.01b
Orange	1.47 ± 0.01b	1.55 ± 0.07b	1.74 ± 0.03b	2.03 ± 0.06b	2.22 ± 0.04b
CV	3.92	5.66	5.09	3.45	3.05

Noted: Different letters in the same column indicate significant differences between means according to Tukey's test

Although water droplets can be seen up to 25.5 meters emitter head, these droplets are in mist form and are not ideal for field conditions. One study found that droplet size decreased as operating pressure increased (Chaya & Hills, 1991). In mist form, water droplets can evaporate and be lost from the system, therefore reducing the efficiency of irrigation. It worsens when there is wind, as this affects the trajectory of water distribution and results in a reduction of irrigation uniformity. Pradeep (2021) carried out a study on micro-sprinklers of varying heights and heads and reported that uniformity decreased with an increase in wind speed and the uniformity coefficient was at maximum when the riser height was low.

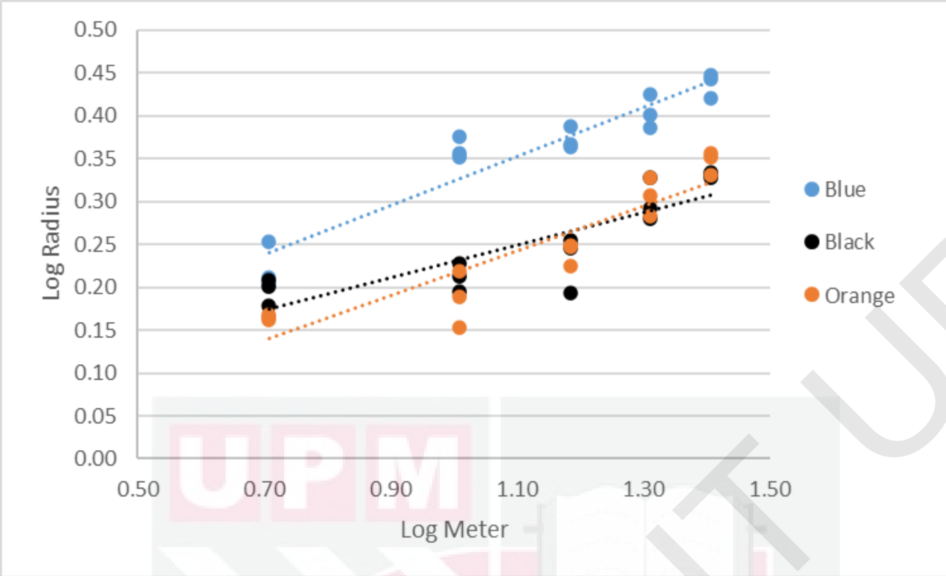

Figure 4.31: Radius (log) of emitter according to its colour and operating pressure (log)

There was a big gap in radius for the Blue emitter compared to the others as shown in Figure 4.31. However, the Blue emitter produced a smooth line that was close to the fitted line and had the highest R^2, which was 0.895. The orange emitter also had a strong relationship between radius and pressure with $R^2 = 0.830$, while the Black emitter had the lowest R^2, which was only 0.717. All the linear trendlines were statistically significant and had a P value lower than 0.01.

Table 4.16: Result of linear regression between Log meter (X-axis) and Log Radius (Y-axis)

Emitter	Blue	Black	Orange
Constant	0.031	0.040	-0.044
LogPress	0.293	0.190	0.262
R^2	0.895	0.717	0.830
P value	< 0.01	< 0.01	< 0.01

Similar to the previous assessment, a non-linear graph was constructed using the power function ($Q_e = KH^x$), as shown in Figure 4.32. Indicators for emitter constant and exponent were changed to Gk and Gx, respectively, to differentiate them from the previous assessment. Gk value for the Blue emitter was 1.133, 1.052 for the Black emitter, and 0.854 for the Orange emitter, and all these values were used for further simulation in the IrriPro software (Table 4.17).

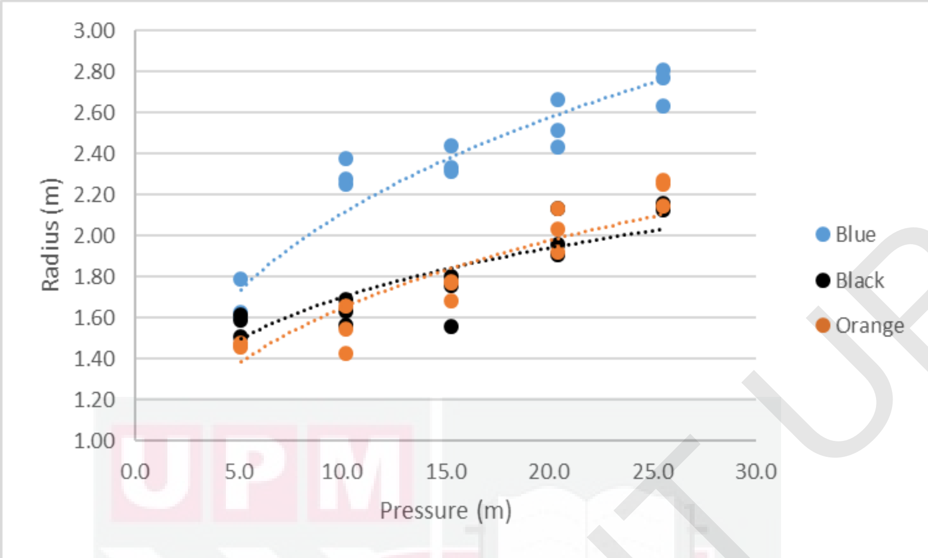

Figure 4.32: H-T relationship for different micro-sprayer emitters

Table 4.17: Detail of regression analysis for different colour codes of emitter

Emitter	Blue	Black	Orange
Gk	1.133	1.052	0.854
Gx	0.273	0.207	0.284
Pseudo R^2	0.900	0.746	0.851

4.5.3 A wetted pattern of the emitter

In most cases, retailers purchase generic emitters in bulk quantities and repack them into smaller packages to be sold. There is the possibility of missing information as it is not included in the packaging. Some of the best emitter types, complete with information found on the web, were from Rain Bird Corporation (2023) and local manufacturers (KMB, 2024). From the results of this study, it was found that the blue emitters do not have a uniform pattern of distribution and have the broadest coverage, i.e., it could be more than 2.00 m, as seen in Figure 4.33. The intensity of flow rate observed at the centre (not more than 130 ml $hour^{-1}$) and patches at the bottom left side of the figure was up to 62 ml $hour^{-1}$.

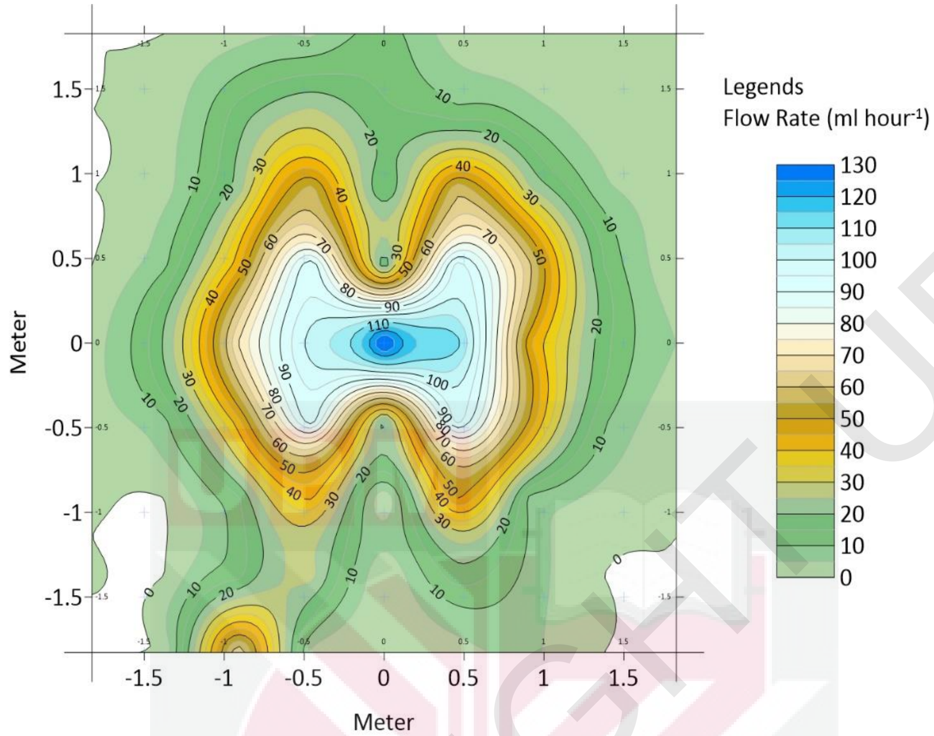

Figure 4.33: Blue emitter spraying pattern at operating pressure 1.5 bar

The Black and Orange emitters showed higher intensity at the centre than the Blue emitter (Figure 4.34 and Figure 4.35). Measurement for X-axis width radius was 1.50 m and Y-axis width diameter was more than 2.00 m. Unlike the Blue emitter, the highest intensity for both of these emitters was 190-200 ml hour^{-1} and was located around the centre of the grid. Despite the similar pattern of area distribution, the Orange emitter produced less intense precipitation at the outer layer and had a slight variation in terms of its form, particularly at the lower right section of the grid.

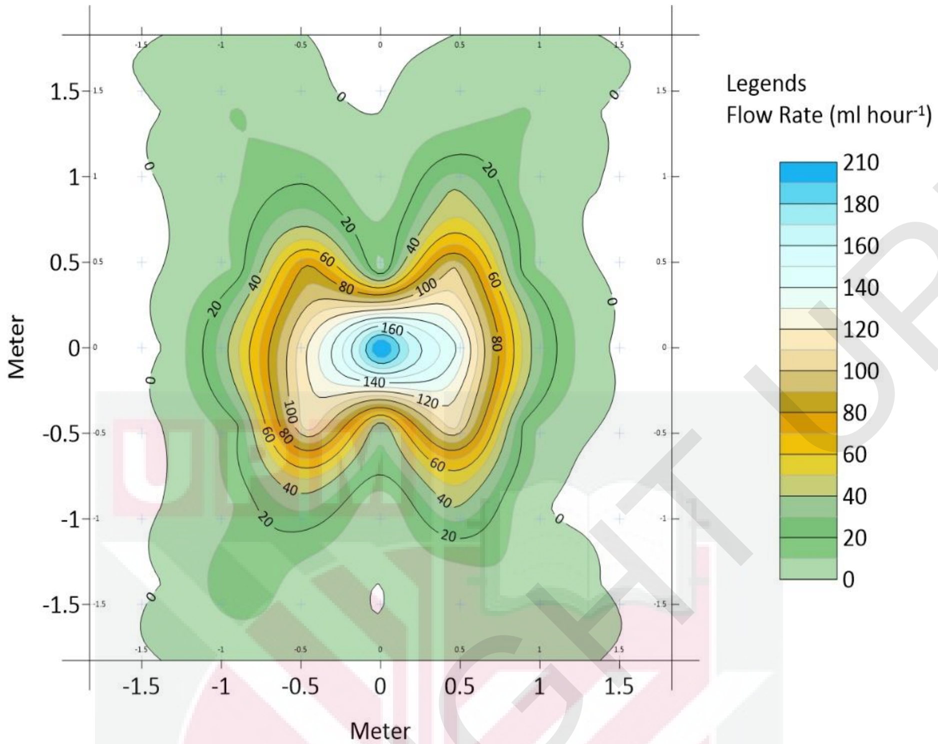

Figure 4.34: Black emitter spraying pattern at operating pressure 1.5 bar

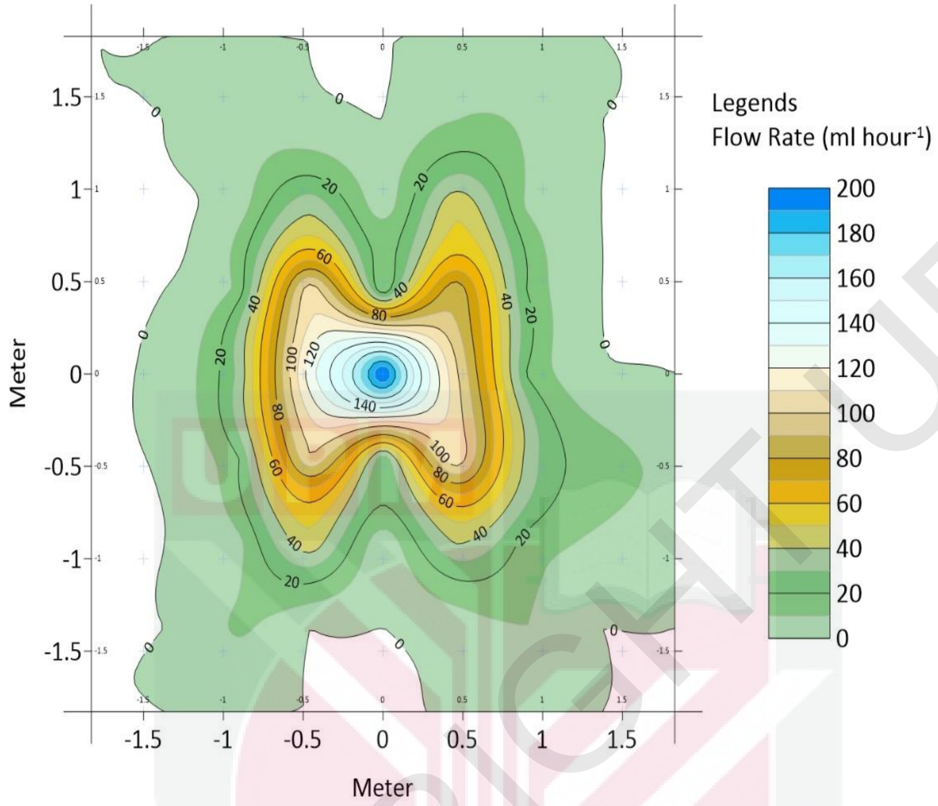

Figure 4.35: Orange emitter spraying pattern at operating pressure 1.5 bar

Based on the findings of this study, the Blue emitter showed a wider radius of throwing distance compared to the Black and Orange emitters, in line with previous findings from Section 4.5.1. Zhang et al., (2018) investigated the relationship between throwing distance and nozzle size. They suggested that with a larger ratio of pressure to nozzle size, there would be smaller droplet size and reduced flight distance. The Blue emitter definitely had a larger nozzle size compared to the Black and Orange emitters when operating at the same pressure. All emitters showed some variation between the left and right sides of the grid, indicating that the manufacturing design was not uniform. The sources for the variation could be passage size, shape, and final finish due to inconsistent raw materials, pressure, and temperature during moulding and the welding process (Hezarjaribi et al., 2008). All emitters showed peak precipitation within a 1.00 m radius, similar to the results of the study carried out by Jeon et al. (2018).

Table 4.18: D_C value for all tested emitters

Emitter	Maximum Flow Rate ml hour^{-1}	Average Flow Rate ml hour^{-1}	Area m^2	Area more than average m^2	D_C %
Blue	134	67	12.67	1.67	13.2
Black	200	100	10.01	0.84	8.4
Orange	198	99	10.49	0.70	6.6

According to Merriam and Keller (1978), D_C related to uniformity is the portion of the central wetted area that may contribute to deep percolation losses even under good management, and values greater than 50% are considered satisfactory. However, in this study, the D_C values ranged from 6.6 to 13.2% only. It is indicates that the depth of water that was larger than the average depth was more concentrated at the centre of the wetted area. A study done by Boman (1989), consisting of various types of emitters, reported that the sprayer and spinner types of emitters did not produce more than 50% of D_C. Additionally, they found that D_C did not show appreciable differences when operated at varying pressure tests.

4.5.4 Coverage by the emitter

To the best of the author's knowledge, the decision to pick the most suitable emitter has never been made before. Based on the evaluation of emitters in Section 4.5, all of their properties are shown in Table 4.19. The Blue emitter had the highest flow rate, with a water radius dispersion from 1.77 to 2.74 m. It is translated LAD to at least 5.3 mm hours^{-1} with a maximum coverage of almost 35% per ha. On the other hand, the Black emitter had the second highest flow rate with a radius range from 1.47 to 2.05 m. However, the Black emitter had a high LAD, which was 6.6-7.3 mm hour^{-1}. A smaller radius translates to smaller coverage, which is only 19.5% with a head pressure of 25 m. The Orange emitter had the lowest flow rate per hour and water dispersion. However, due to the smaller radius, it had a moderate LAD among emitter colour codes. As it has the smallest radius of water dispersion, the percentage of coverage per hectare was generally lower than other emitters, i.e., only up to 21%.

Infiltration and soil physical properties may serve as crucial factors when deciding the type of emitter. Based on findings from Section 4.3, the infiltration rate was from 1.01 mm hour^{-1} at Zone C to 9.27 mm hour^{-1} at Zone A. Meanwhile, the application rate for all emitter colour codes ranged from 5.3 to 7.3 mm hour^{-1}. Zone C will have a slight issue where the spraying rate is higher than the infiltration rate. Higher spraying rates will have problems, especially in slope areas where the water will flow to the lower slope and carry along sediment. This problem can be overcome by replacing emitters with those of a lower application rate or digging a small drainage around the emitter point to increase water penetration.

In mature oil palms, fronds are overlapping, and evapotranspiration is at a minimal rate. A study done by Henson (1999) has proved that the portion of ETc below the canopy is only 12.6% of total ETc. When the age of the palm increases, the root system will be extensive, dominate the below-ground area and be able to absorb water nearby or far from the emitter. A study by Zaharah et al. (1989) using P32 demonstrated that oil palm roots in mature oil palm areas extend up to 35 m. Therefore, it is suggested that a higher LAD than infiltration rate for tested micro-sprayers is not critical for mature oil palm.

Table 4.19: Coverage of micro sprayer emitter to flow rate and distribution radius

Emitter code	Pressure curve		Range curve		Pressure	Flow rate	Radius	LAD	Coverage	Coverage
	k	x	k	x	m	Litre per hour	m	mm	m^2	% ha^{-1}
Blue	22.082	0.536	1.133	0.273	5	52.9	1.77	5.4	1453	14.5
					10	76.7	2.14	5.3	2121	21.2
					15	95.3	2.39	5.3	2647	26.5
					20	111.2	2.58	5.3	3097	31.0
					25	125.3	2.74	5.3	3498	35.0
Black	20.599	0.478	1.052	0.207	5	44.5	1.47	6.6	1002	10.0
					10	61.9	1.69	6.9	1335	13.4
					15	75.2	1.84	7.0	1579	15.8
					20	86.2	1.96	7.2	1779	17.8
					25	96.0	2.05	7.3	1951	19.5
Orange	17.797	0.467	0.854	0.284	5	37.7	1.35	6.6	846	8.5
					10	52.2	1.64	6.2	1254	12.5
					15	63.0	1.84	5.9	1579	15.8
					20	72.1	2.00	5.7	1859	18.6
					25	80.0	2.13	5.6	2111	21.1

4.6 Assessment of existing irrigation system by using the IrriPro Software

The IrriPro software is one of the software used to plan irrigation and perform hydraulic calculations within a relatively short time. Estate management typically requires several trial-and-errors to obtain the best irrigation shifts that match the piping, engine, and pump capacity before a steady state is achieved. Luckily, the terrain in the study site is considered as 'flat to undulating', thus minimizing pressure loss due to elevation changes. This estate comprised a 23.5 ha area that was divided into three primary irrigation shifts (Table 4.20). There was a total number of three shifts due to the total working hours available in a day. Maximum irrigation time is about 2.5 hours for every shift, making it possible to complete all shifts within a day. Shift #1 is the largest and comprises 15 sectors with an area of 10.6 ha. Shift #2 and Shift #3 had an area of 5.78 and 7.08 ha with 7 and 6 sectors, respectively.

Table 4.20: Separation of the sectors and shift for irrigation scheduling in FGVAS estate

Group	Shift 1	Shift 2	Shift 3
Sector	1,2,3,4,5,6,20,21,22,23,24,25,26,27,28	14,15,16,17,18,19	7,8,9,10,11,12,13
Number of sectors	15	6	7
Total Area (ha)	10.6	5.78	7.08

Figure 4.36 shows the re-drawn irrigation model for FGVAS Serting Hilir's estate using the IrriPro software according to its shifts. The hollow area on the upper part represents the water reservoir for the system. Support units such as pump house, engine, water pump, and water filter were also located near the reservoir.

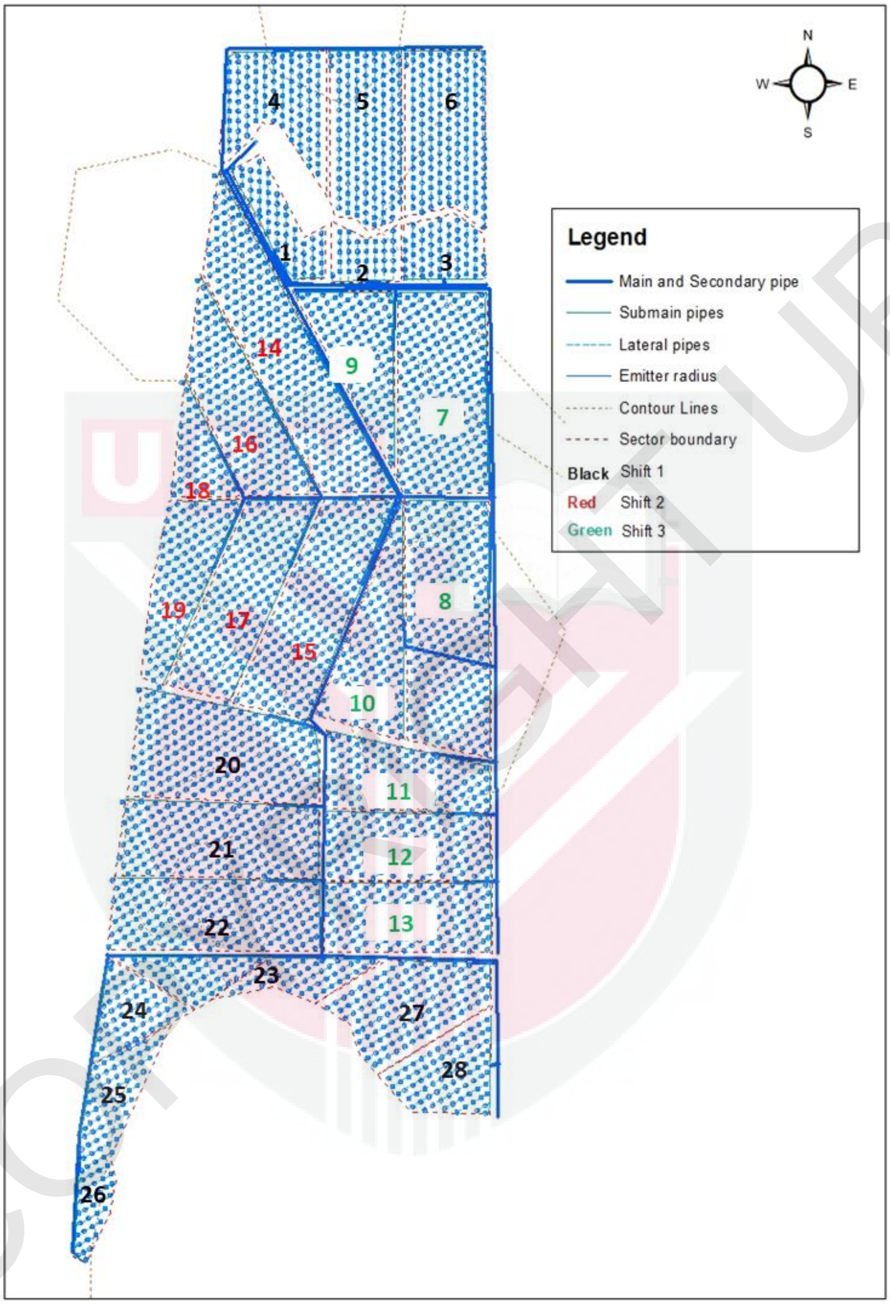

Figure 4.36: Piping network after all data insert in the IrriPro Software 3.0

4.6.1 Piping Network

The length of main pipes (OD 160 mm) used in this study was 781 m, secondary pipes (OD 90 mm and 110 mm) was 1,295 m, sub-main pipes (OD 63 mm) was 4,672 m and lateral pipes (OD 32 mm) was 1,688 m. The length of pipes was crucial since it determined the cost of irrigation. In this case, irrigation was started during the immature phase of oil palms. During this time, the oil palm root was still near the palm base, so lateral pipes were placed beside the palm for each planting row. Another researcher (Haniff et al., 2014) also made this arrangement, placing piping 1.0 meters from the palm base. As a result, the total length of lateral pipes was double the amount as compared to the mature stage, where the lateral lines were only placed in an alternate row arrangement.

Shift #1 was the most extensively covered area and had the highest number of emitters. The number of emitters was relatively straightforward as it reflected the number of palms per ha^{-1} multiplied by the coverage area. Emitters were placed one for each palm partly due to operational factors. For example, a study by Norhajijah and Darius (2021) reported that mechanization for the harvesting process was only adopted at a level of 2.36%, and a majority of estates still use chisel and sickle for this activity. Multiple emitter placement, whether in a linear or circular arrangement around the palm base, will put the emitters at risk of damage from daily activities such as frond removal, harvesting, herbicide and pesticide spraying, and many other things. Emitters are typically placed at the ground level to ease the estate management's monitoring of tasks such as pipe and emitter replacement. In terms of irrigation method selection, it is sometimes beyond the efficiency indicator. Burt (1999) mentioned that the factors affecting the preference for irrigation systems include divisibility, maintenance, risk, management skill, management effort, and ruggedness.

Many irrigation types can be used in the field. In the early evaluation of irrigation, oil palm plantations used the furrow system (Lee and Izwanizam, 2013), where the water streams were at a dedicated drainage centre between planting rows. However, the furrow had several disadvantages, such as low efficiency, which ranged between 55-77% (Martin, 2011). Typically, pressurised irrigation, such as micro-irrigation, claims to produce a higher yield compared to the furrow method, in addition to its more efficient water usage (Rogers et al., 1997). Other factors that make the application method preferable are adequate system design and proper installation, operation, and maintenance. Subsurface irrigation is another typical method applied in the field. It is reported to have the highest water use efficiency than drip and sprinkler irrigation systems (Almarshadi & Ismail, 2011). However, it has disadvantages such as a huge investment cost, the requirement of special instruments during installation, an inflexible design, and prone to rodent attacks (Payero et al., 2005).

4.6.2 Hydraulic Properties

Shift #1 and Shift #2 had almost identical uniformity values based on the two uniformity tests. In terms of UCC, Shift #1 and Shift #2 were within the acceptable range with values more than 90%, whilst in terms of EU, these two shifts were below 90% and were not satisfactory. Shift #1 had the higher flow rate with a range of 60.0 - 76.2 Litre hr^{-1} and an average of 72.9 Litre hr^{-1}, whilst Shift #2 had a slightly lower range of 53.4 - 63.7 Litre $hr^{-1,}$ and the average was 60.1 Litre hr^{-1}. Shift #2 produced a better and closer to the nominal value of the emitter flow rate, i.e., 60 litre hr^{-1}. Shift #1 also had a higher speed of water and pressure head compared to Shift #2. This is possible because Shift #1 had a larger area and needed to deliver a larger volume of water per unit of time. As a result, the speed was higher and the friction in the pipe increased. However, water velocity is still below the critical speed, which was only 0.38 m sec^{-1} compared to the reference value of 1.5 m sec^{-1} – 3.0 m sec^{-1} (Clark & Haman, 2017). Shift #1 had two distinct areas, i.e., near the water pump and the other was the farthest area from the water pump. Referring to the graphical presentation from the IrriPro software (Figure 4.37- Figure 4.38), the former area results are in blue colour, indicating very high pressure, and the farthest consisted of blue, green, and reddish hues, showing that the flow rate varies from very high pressure (P > 10%) to very low pressure (P < -10%). However, Shift #2 is much more consistent despite having a different colour scheme, thus resulting in better uniformity (Figure 4.39).

Table 4.21: Simulation result by IrriPro software for each shift (Automatic calculation)

Variable	Unit	Shift 1	Shift 2	Shift 3	P value
UCC	%	97.1±1.1	97.3±0.7	56.1±19.8	0.117
EU	%	89.0±3.9	88.4±4.8	54.4±19.2	0.200
Max Flow Rate	L hr^{-1}	76.2±2.6b	63.7±1.3b	442.0±74.7a	<.0001
Min Flow Rate	L hr^{-1}	60.0±5.9b	53.4±3.0b	333.4±96.7a	0.005
Av. Flow Rate	L hr^{-1}	72.9±3.0b	60.1±0.9b	433.8±76.1a	<.0001
Max Speed	m sec^{-1}	0.38±0.0b	0.25±0.0b	2.90±0.1a	<.0001
Min Speed	m sec^{-1}	0.03±0.0b	0.02±0.0b	0.24±0.0a	<.0001
Av. Speed	m sec^{-1}	0.17±0.0b	0.12±0.0b	1.25±0.1a	<.0001
Max Pressure head	m	10.0±0.7b	7.0±0.3b	364.9±91.0a	0.001
Min Pressure head	m	8.5±0.8b	4.7±0.9b	279.6±99.2a	0.008
Av. Pressure head	m	9.3±0.7b	6.3±0.2b	358.3±91.4a	0.001
Area	ha	10.6	5.8	7.1	
HeadLoss	m	7.1	3.5	560.0	

Flow rate, pressure head and head loss for Shift #3 were very high and too far from the other two shifts, making Shift #3 significantly different from the others (Table 4.21). For example, data for flow rate and speed were hundreds of times more than the other shifts. Data from head loss was considered erratic and it is believed that it did not portray the actual conditions. The IrriPro software calculation of the variables may have overestimated the actual value.

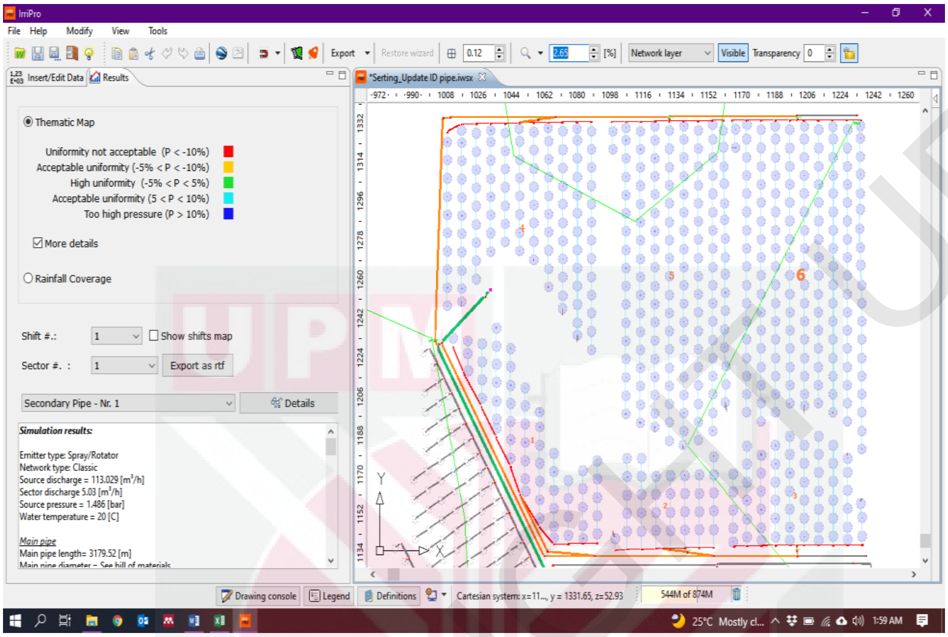

Figure 4.37: Shift #1 (nearest to water sources)

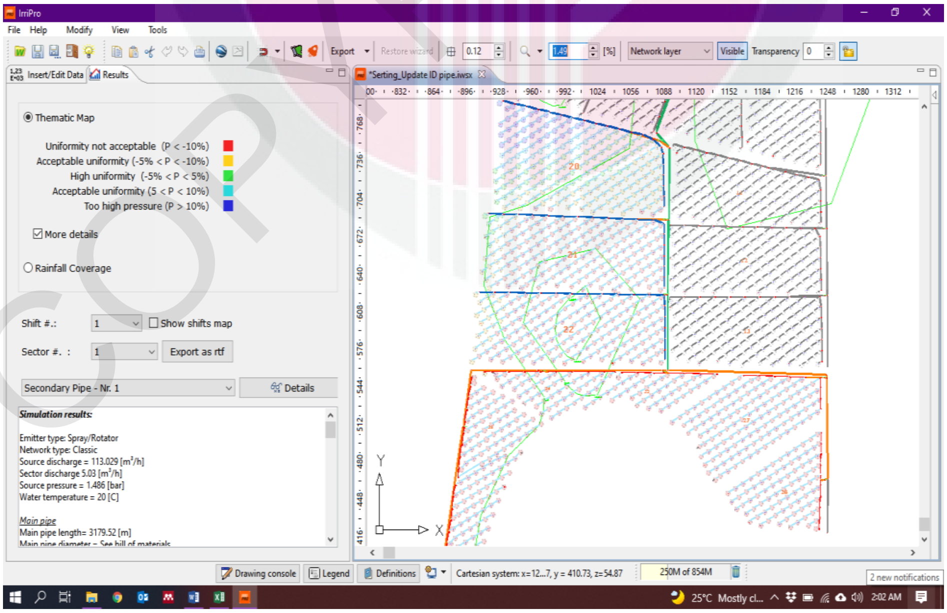

Figure 4.38: Uniformity thematic map for Shift #1

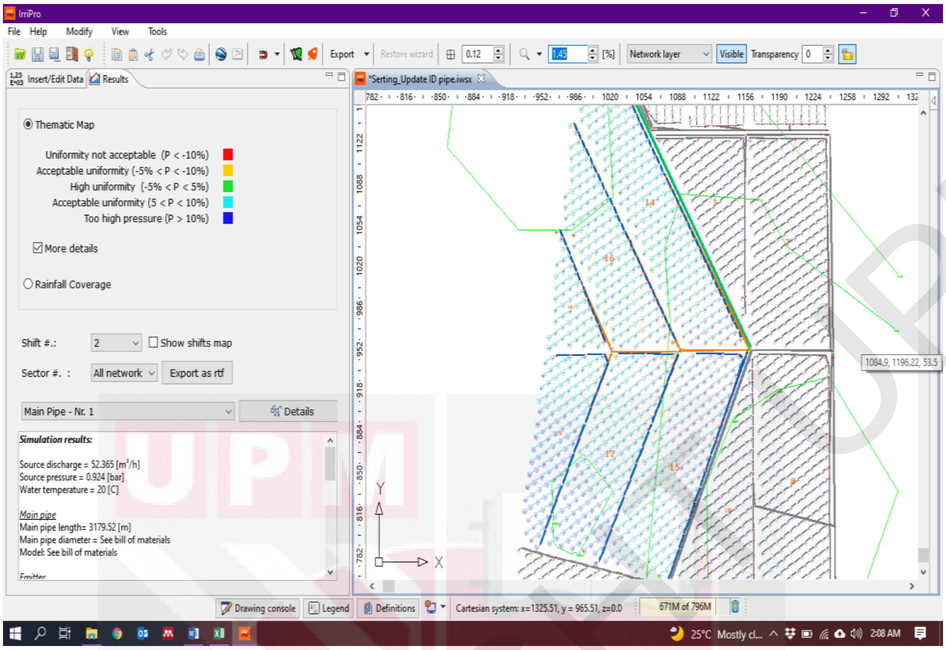

Figure 4.39: Uniformity thematic map for Shift #2

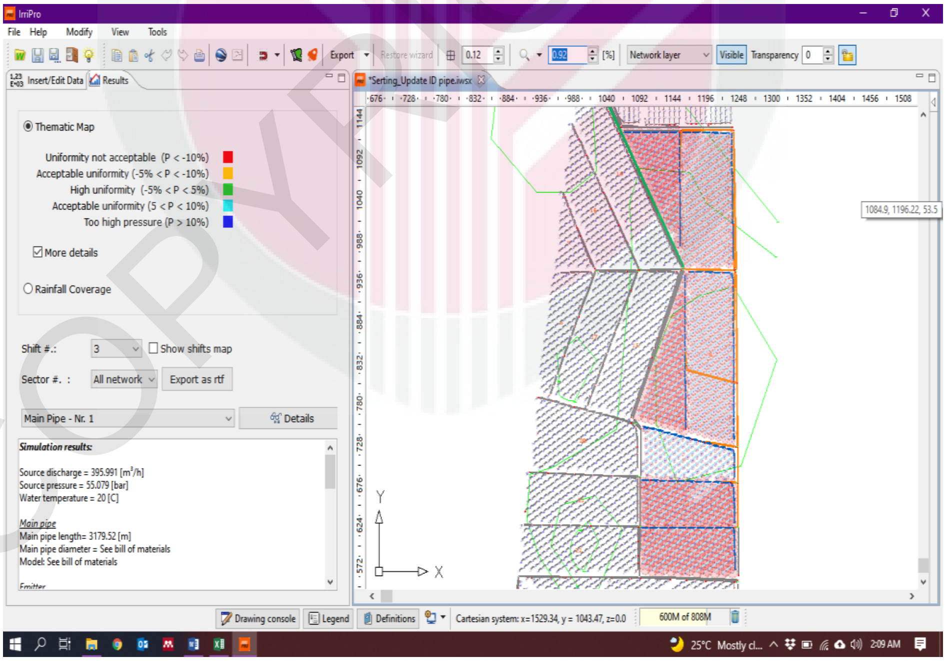

Figure 4.40: Uniformity thematic map for Shift #3

UCC was only 56.1%, whilst EU was only 54.4%. Although the value for variables was high, it is believed that the low uniformity coefficient was caused by low pressure. Compared to the other shifts, Shift #3 was located at a higher slope, with a difference of about 6.0 m from the lowest elevation (Figure 4.42). As seen in Figure 4.40, uniformity was below 10% and was considered unacceptable by the software.

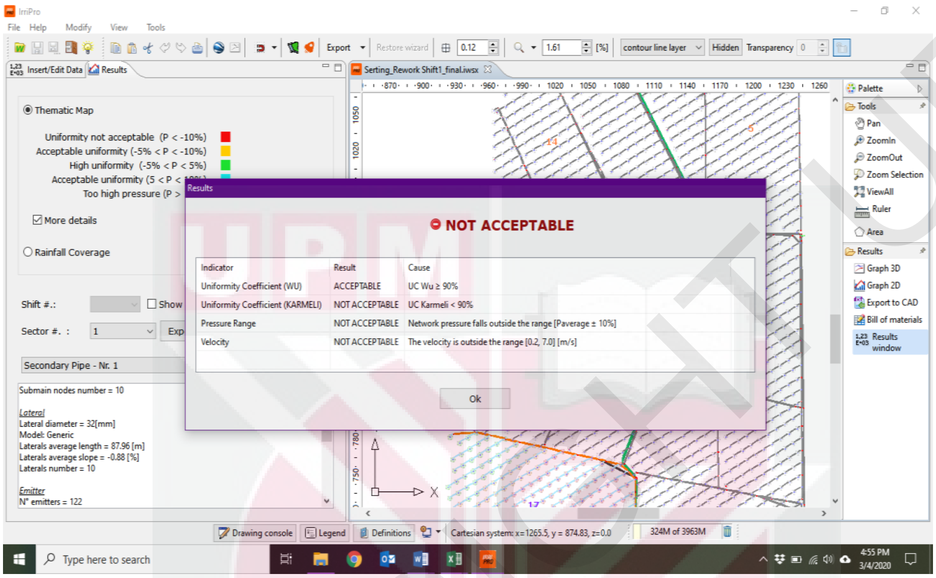

Figure 4.41: Results windows interface for the whole irrigation system

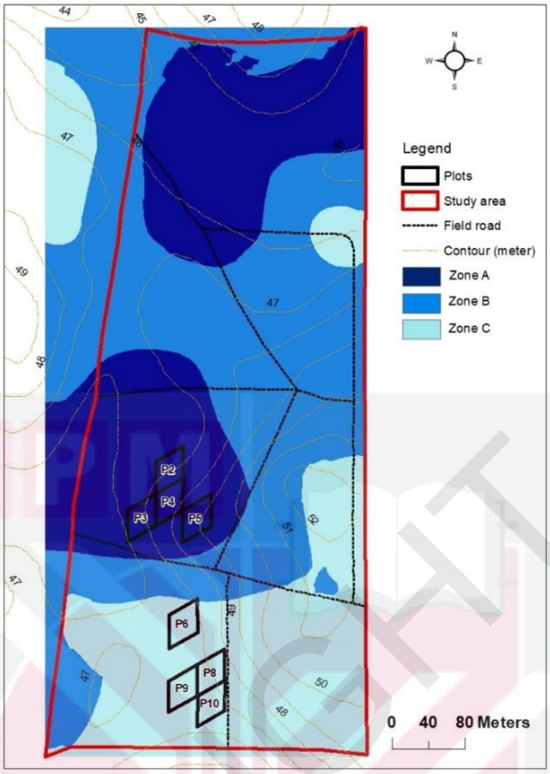

Figure 4.42: Contour map for the study area

In the last section (Figure 4.41), this software showed results on whether the irrigation layout was acceptable or not. The interface took three variables into consideration, i.e., uniformity, pressure range, and velocity. For the first criterion, the EU uniformity index was below 90%. The pressure range at Shift #3 was unreasonable and up to 365 m, making the criteria for number two unfulfilled. For the third criterion, minimum velocity was found at 0.03 and 0.02 m sec^{-1} for Shift #1 and Shift #2, respectively, thus falling outside of the recommended range value (0.20 – 7.00 m sec^{-1}).

4.7 Assessment of new irrigation system for SBI plot

4.7.1 Hydraulic properties of SBI plot

In the previous section outcome, the evaluated emitters in this study are the non-PC type. This simulation shows the sector discharge rate based on the different emitter colours (Figure 4.43). The blue emitter produced the highest sector discharge, followed by the Black and, lastly the Orange emitter. Trends of discharge were the same for every plot. In the early plot (P1), sector discharge was the highest compared to other plots, and the trend slowly decreased until P5. In P6, discharge increased a little before a sharp reduction at P7. Sector discharge increased again in P8, P9, and P10.

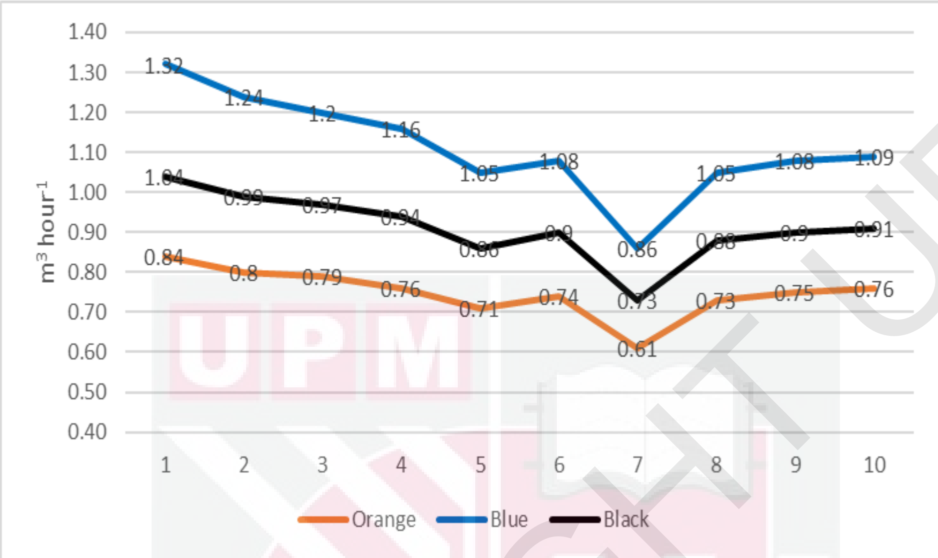

Figure 4.43: Sector discharge for every plot according to different emitter selection

The sharp reduction at P7 could be due to the differences in elevation at the field. From the topography map, P7 was at the highest elevation, i.e., elevation at 50 m and higher compared to the rest of the plots. The large volume of discharge at the earliest plot is highly likely due to the close distance to the pump and minimum head loss. As water travels across the pipeline to other plots, the head loss increases as a result of the friction in the pipe. The flow rate was also proportional to the remaining head available and that explains the decrease in flow rate from plot to plot as the distance from the water pump increased. Figure 4.44 shows the minimum and maximum flow rates based on the plot available. Once again, the flow rate trend was according to sector discharge. A plot with the highest sector discharge would also have a higher flow rate. Differences between maximum and minimum flow rates in this study were not too contrasting. In terms of speed, each plot had an acceptable value and none were higher than 1.5 m sec^{-1} (Figure 4.45). A maximum flow velocity of 1.5 m sec^{-1} is recommended to minimise excessive surge pressures (Clark & Haman, 2017). Additionally, a minimum flow velocity of 0.3 m sec^{-1} is recommended to ensure that suspended materials can be adequately flushed (Puig-Bargués & Lamm, 2013). However, all plots in this study recorded speeds of less than 0.3 m sec^{-1}.

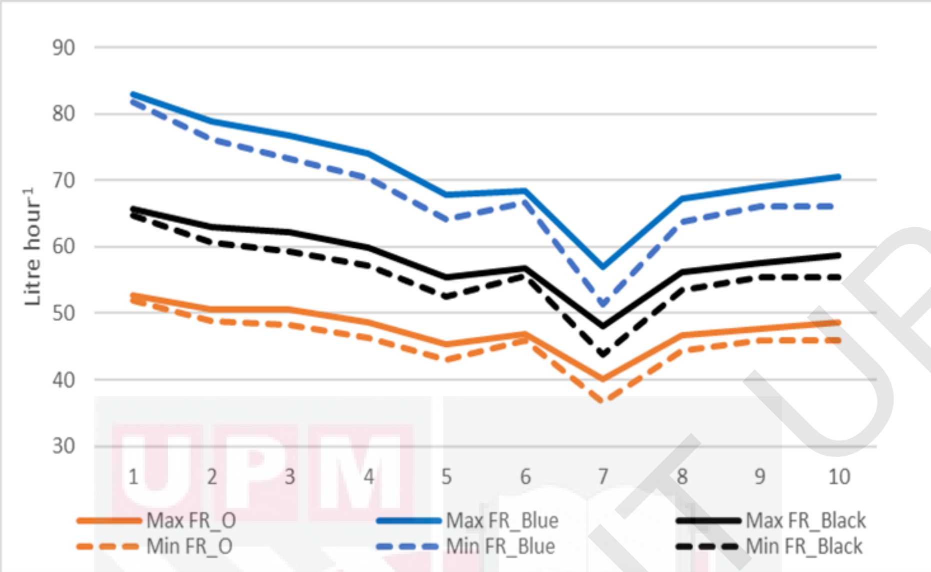

Figure 4.44: Minimum and maximum flow rate for every emitter installed

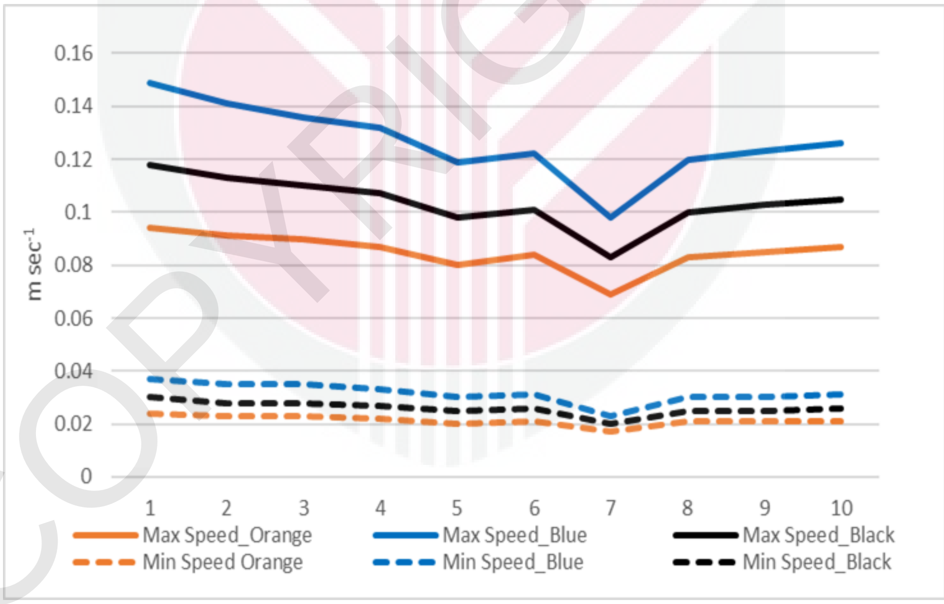

Figure 4.45: Minimum and maximum speed of water for every plot

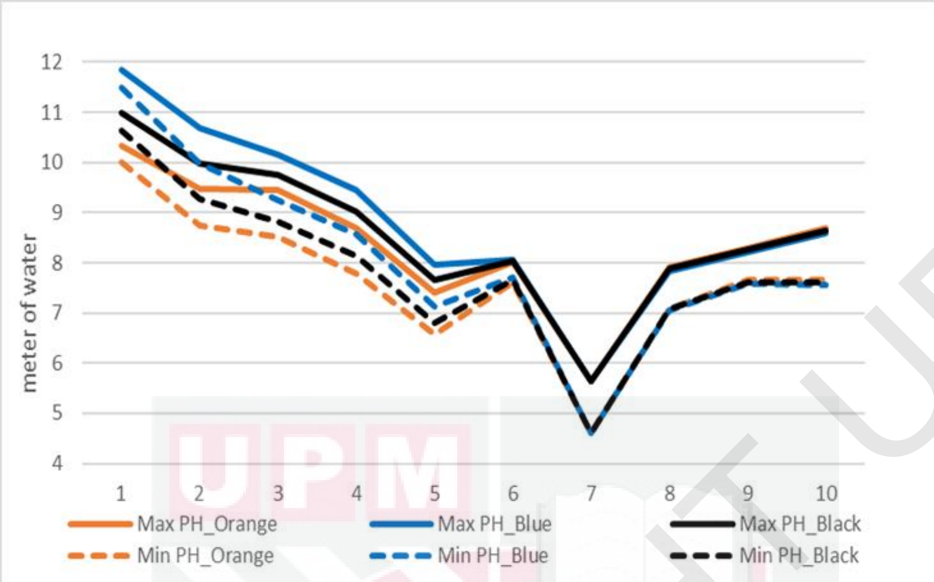

Figure 4.46: Maximum and minimum pressure head for every plot

The maximum and minimum pressure heads were highly related to sector discharge. As the pressure head increases, the discharge also increases according to the power function of the emitter. An interesting result, as shown in Figure 4.46, was that the trendline for each emitter colour code showed different values until P5. However, from P6 onward, the difference between each emitter was not noticeable. At P7, the minimum and maximum pressure heads were the lowest because of higher elevation. The similar trendline for the minimum and maximum values from P6 onward still cannot be explained.

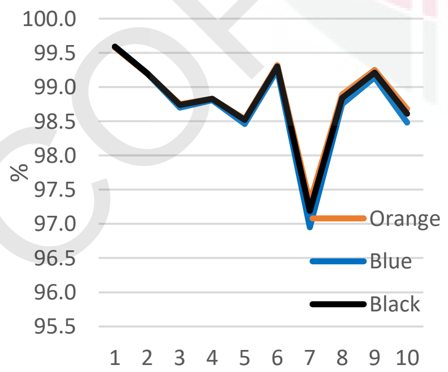

Figure 4.47: Uniformity coefficient by using the UCC formula for every plot

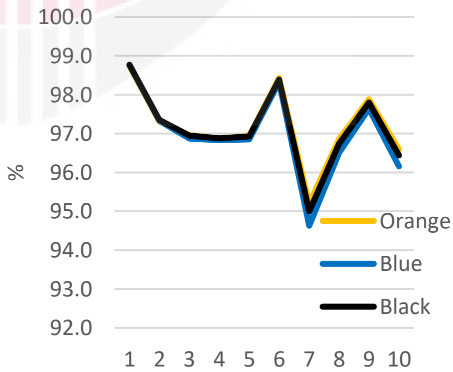

Figure 4.48: Uniformity coefficient by using EU formula for every plot

Uniformity coefficients for each of the plots are shown in Figure 4.47and these values are used for plot-by-plot evaluation based on each of the 16 emitters. UCC was very high, from 96.9% to 99.6%, whereas EU (Figure 4.48) was considerably high, ranging from 94.6% to 99.0%. It can be seen that P7 had the lowest percentage of uniformity coefficient for both calculations. As mentioned, the study used non-PC emitters that allowed different flow rates with the function of the pressure head. P7 was located at a higher elevation of about 4-5 meters compared to the other plots. The elevation changes are believed to affect the emitter flow rate and cause a reduction of the uniformity coefficient.

The result of the uniformity coefficient for every plot did not adequately reflect the overall performance of the irrigation design. Compared to the above results, Figure 4.49 shows the uniformity coefficient value by pooling the data from P1 to P10 altogether. This graph compiled the result of different emitter colour codes used in the system rather than reported by individual plots. Previously, EU for the plot basis was around 94.6% to 99.0%. However, as a whole system, the EU was far lower and the design only managed to obtain values of 73.3-77.8%. Simulation-based on the emitter colour code shows the orange emitter had the highest EU, followed by the Black emitter and lastly the Blue emitter. One of the essential variables in this assessment is system head loss as indicated by the red circle. Among the three emitters, the lowest head loss was with the orange emitter, followed by the Black and then Blue emitter. Head loss in this assessment was the difference between the minimum pressure head and the pressure at the source. It was calculated by IrriPro consisting of slope changes and friction loss. The latter is related to velocity, quantity, pipe diameter, pipe length, gravity, and fitting friction.

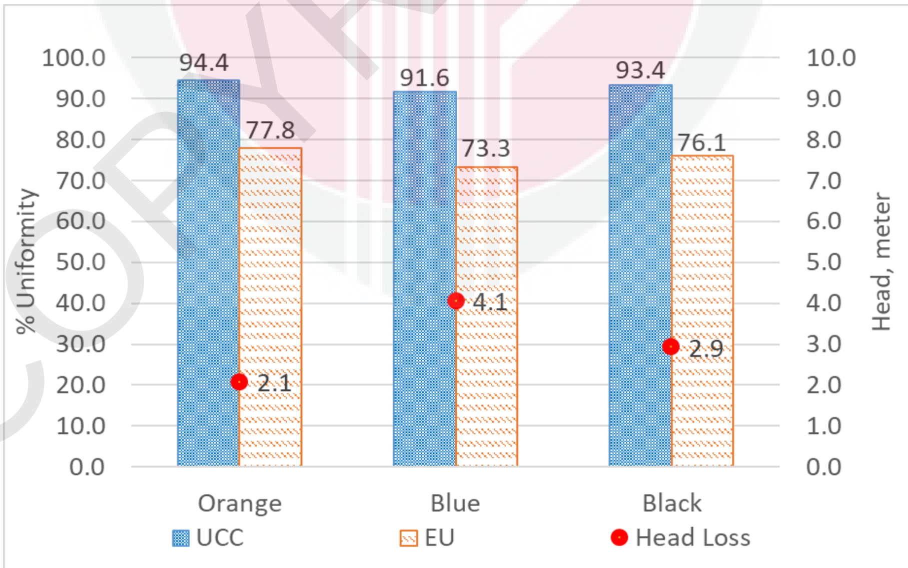

Figure 4.49: Average performance for two efficiency categories of all plot

The orange emitter generally produced a better result. It had the highest uniformity in terms of UCC (94.41%) and EU (77.82%) and the least head loss at only 2.08 meters.

The orange emitter resulted in the slightest source discharge (7.487 m^3 hr^{-1}) and water velocity (0.053 m s^{-1}) according to the plot-by-plot data, thus giving an overall better performance compared to the other emitters. Based on this result, the orange emitter was used in SBI.

4.7.2 Actual uniformity of the system

The previous assessment based on a calculation by the IrriPro software was based on an innovative algorithm to analyse complex irrigation systems while maintaining necessary scientific accuracy with a sensible reduction of the computation time (Provenzano et al. 2005). Comparison data between the actual emitter flow rate and simulated data from IrriPro are shown in Figure 4.50. This graph contains a 1:1 line to show the deviation of actual data from the IrriPro simulation.

The deviation between actual and simulated data could be due to the system itself. In actual field conditions, the system may face issues such as leakage, clogging, or imperfect connection between the joints. In the IrriPro software, the Coefficient of Manufacturer Variation (CV_m) had a default value of 0.004, which was used in this simulation and this value was far from the value suggested by (Solomon, 1979). However, in this study, no actual CV_m was measured and it is believed the deviation between actual and simulated data can be improved further by testing actual CV_m.

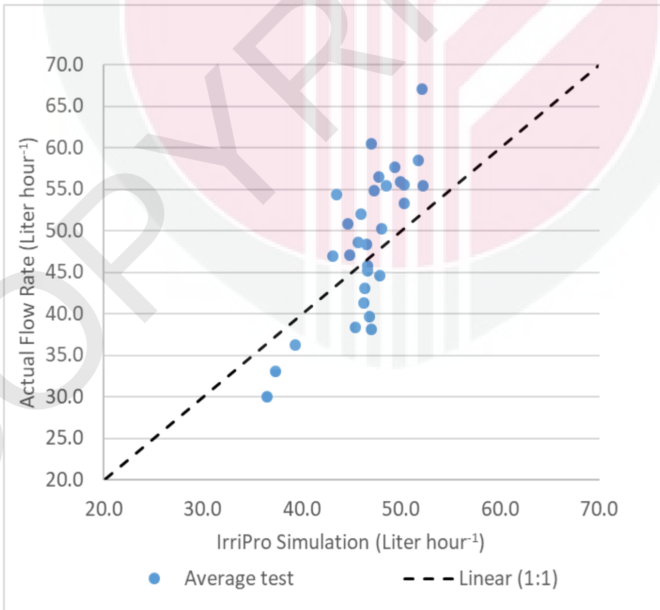

Figure 4.50: Average of four test data collected from 30 emitters

The IrriPro software analysed two uniformity indices called the UCC (Arshad et al. 2014) and the EU (Barragan et al. 2006; Keller and Karmeli 1974). Two other uniformity indices were also analysed, i.e., DU and Us. Based on the four assessments, all uniformities measured gave slight improvement compared to the earlier result. UCC showed good values of more than 80% for all data, and any value of more than 70% indicates that the measured data have a normal distribution (Maroufpoor et al., 2010). Actual test 1 was measured just after the system was installed in the field. At this point, UCC was below 90%, and EU was at the lowest point, i.e., 28%. Except for the UCC and Us (Actual tests 3 and 4), all data assessments were below 80% (Table 4.22). Over time, the uniformity coefficient for Actual test 2, Actual test 3, and Actual test 4 increased. During the last evaluation, the Actual test 4 flow rate managed to achieve 83% UCC, 66% EU, 78% DU, and 83% Us. An increasing trend for all uniformity indices proved that the system was still in the improvement process. In an early setup, all accessories and fittings may still be imperfect, and there might be some connections that need to be adjusted and tightened. Some of the emitters were plugging because of leftover residue during the installation of the pipe. After some time, all of these errors are minimised, resulting in the improvement of all uniformity ranges. Despite the non-PC emitter, UCC showed that the flow rate was normally distributed. However, EU which is the most sensitive parameter, still performed below 70%, although it was predicted to be 78%. The EU formula proposed by Keller and Karmeli 50 years ago compromises hydraulic variation, manufacturer variation and emitter grouping (Barragan et al. 2006). Similar to the previous argument, the low coefficient of EU might be due to the considerable variation in the actual CV_m of the tested emitter. According to Solomon (1979), CV_m with a value of more than 15% (0.15) is considered unacceptable. Barragan et al. (2006) demonstrated that the calculated EU dramatically changed to 65% when CV_m was reduced to 0.20. In this study, the study site particularly Zone C had a higher elevation of 6.0 m in comparison to the lowest elevation. This could have contributed to the low EU, as reported by (Ella et al. 2008) who carried out a study using the drip system and noted that the EU dropped abruptly when the steep was more than 20%.

In this evaluation, 78% DU was recorded for the last measurement, indicating that the system was slightly below ‘uniform’ performance, as suggested by Irmak et al. (2011). A thorough evaluation was reported by Burt (2004) using more than 300 systems involving drip and micro-irrigation. They reported that the DU for drip systems was 85%, while 80% for micro-irrigation systems. They also suggested that 45% of the non-uniformity was due to pressure differences, 52% was due to "other causes", 1% due to unequal drainage, and 2% due to unequal application rates. The last measurement indicating Us fell between “Fair” and “Good’’ and so the installed irrigation was considered satisfactory (Bralts and Kesner 1983; Lamm et al. 1997).

Table 4.22: Uniformity results for the SBI system according to various uniformity indices

Data	UCC %	EU %	DU %	Us %
Actual test 1	81.9	27.7	69.2	76.3
Actual test 2	82.1	53.6	73.0	78.3
Actual test 3	85.0	65.7	75.8	82.2
Actual test 4	84.7	65.7	77.7	83.1
Mean Actual test	83.4	53.2	73.9	79.9
Simulated	94.4	77.8	89.9	92.0
% over simulated	88.4	68.4	82.2	86.9

4.8 Evaluation of SBI in terms of scheduling, growth and yield

4.8.1 Pre-settings and challenges

Tensiometers have been installed in the field since January 2020. The early period was still considered a familiarisation process due to the lack of experience and knowledge gap on how to operate tensiometers. Therefore, the amount of water being given to the palm was inadequate. In early installation, almost more than half of the tensiometers showed a 'zero' reading despite dry soil conditions. It happened because the cap was too tight, which caused the stopper below the lid to block the small pit in the air tunnel and prevented the gauge from responding to vacuum conditions that were created by a lower SWP. The water reserve remained in place and gave a false indicator that the soil was still wet (Figure 4.51).

Figure 4.51: Water remains at the reservoir due to the overtightening lid

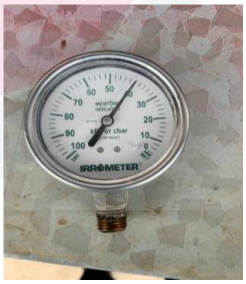

Figure 4.52: Tensiometer gauge needle stuck at a higher value

The use of the tensiometer to read SWP is accurate, relatively cheap, and has a simple theory behind it (Sadeghi et al., 2018). However, consistent maintenance and refill work are required to avoid cavitation (Smith & Kean, 2018). From March to May 2020, the activities for tensiometer monitoring were affected by the movement control order imposed by the government due to the coronavirus pandemic. In June 2020, some of the tensiometer gauges were stuck at a high value (>30 kPa). It is happened because the workers did not have access to the field, and when the soil became dry for too long, the gauge jammed and remained at a high reading. As this condition is prolonged, the gauge cannot revert to a normal reading even though the vacuum condition breaks (Figure 4.52). In August 2020, the affected tensiometers were sent for warranty claim.

Other than issues with the sensor, technical problems also arose from other factors. There were incidents of lightning strikes affecting the wiring that was buried in the soil (Figure 4.53), and in some instances, the condition was worse and affected inverters as well. In this study, lightning strikes caused the two-way data and communication from power sources to the solenoid and tensiometer to break down. Statistics from South Africa showed that 31% of photovoltaic solar damage was caused by lightning strikes Oelofse (2018) and this could be even higher for countries located along the Equator such as Malaysia. Syakura et al., (2018) estimated that the number of thunder days in Malaysia was an average of 139 thunder each year. Other damages that occurred can be classified as pest attacks with geckos hiding in the electronic module and causing the circuit board to burn during the startup of the system (Figure 4.54). These multiple issues were barriers to a fully automated process, and therefore, irrigation scheduling relied on manual observation of the sensor.

Power supply management is one of the most crucial aspects of an IoT system. A sensor must be installed in the core of the field, and a DC electrical system often powers it. As a result, it requires continuous power sources, either from a battery or from solar panels. To ensure sufficient power, a specific open area must be dedicated to minimise canopy enclosure. The oil palm growth rate for the height was 40-75 cm year^{-1} (Kushairi & Amiruddin, 2020). Thus, a mechanism is required to ensure that solar cell efficiency remains unaffected in the future.

Figure 4.53: Lighting strike affected wire buried in the soil

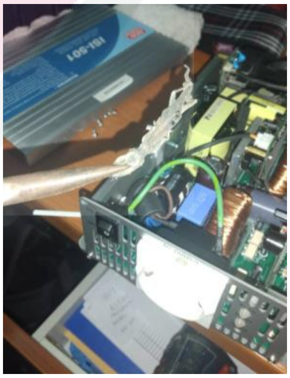

Figure 4.54: Inverter circuit board burns because of lizard

Despite proper arrangement and planning, automation is still not fully adopted. Thus, irrigation scheduling depends partly on human effort to allow for operation. Other researchers have demonstrated that tensiometers could successfully plan irrigation, but water deficits cannot be entirely eradicated due to pump failures or salinity of water (Rhebergen et al., 2019). In this study, automation will be the best solution for real-time monitoring of SBI; unfortunately, their potential cannot be fully realised, as hindered by the abovementioned.

4.8.2 Tensiometer data

Both graphs demonstrate daily fluctuations of SWP monitored by tensiometer at two depths between November 2021 and the end of December 2022 as shown in Figure 4.55 and Figure 4.56. Ideally, irrigation should be started when the triggering point is achieved, which is more than 30 kPa suction (label at tensiometer pressure gauge) or less than -30 kPa SWP. Due to oppressive issues, manual operation occurs, leading to certain inconsistencies indicated by delayed irrigation at lower SWP, denoted by peaks that surpass the MAD line. Again, this emphasised the importance and need to overcome the challenges of automation, thus reducing dependency on human factors.

In both graphs, four components are presented: FC, MAD, tensiometer readings at two depths, and water supply in litre palm^{-1}. FC is the water content after free drainage when soil pores are filled with water, represented by SWP (y-axis) at -10 kPa. This value was previously discussed in Section 4.1.2. In contrast, MAD at 70% is a percentage of VWC between FC (-10 kPa) and PWP (-1500 kPa) derived using data from Table 4.2. It is vital to note that MAD is recognised by VWC, not an SWP, which has no linear relationship. MAD is particular to each plant species and developmental stage. There are minimal studies on MAD levels in oil palm. In this scenario, 70% (Rey et al., 1998) was selected to represent the mature stage of the palm, which was 7-9 years old in 2021-2022. The modifications in MAD proportion throughout the year are unnecessary. This is because oil palm known as perennial crops, types of plants that do not have a specific growing season and can be harvested multiple times throughout the year.

From early November 2020 until January 2021, a lower trend of tensiometer readings was observed due to higher and more frequent rainfall. During this month, rainfall was recorded at 133 mm (16 days), whilst in December, the rainfall was 121 mm (12 days).

The tensiometer reading at Zone A (Figure 4.55) for the 0 - 30 cm soil depth was often below the trigger point as a response to water supplied by irrigation. However, the gauge for the lower depth sensor frequently showed values of more than 30 kPa (for example, in 2021) and several times up to 70 kPa in March, June to July. This indicates that SWP below 30 cm for Zone A was quickly reduced despite sufficient moisture provided at the upper layer of the soil.

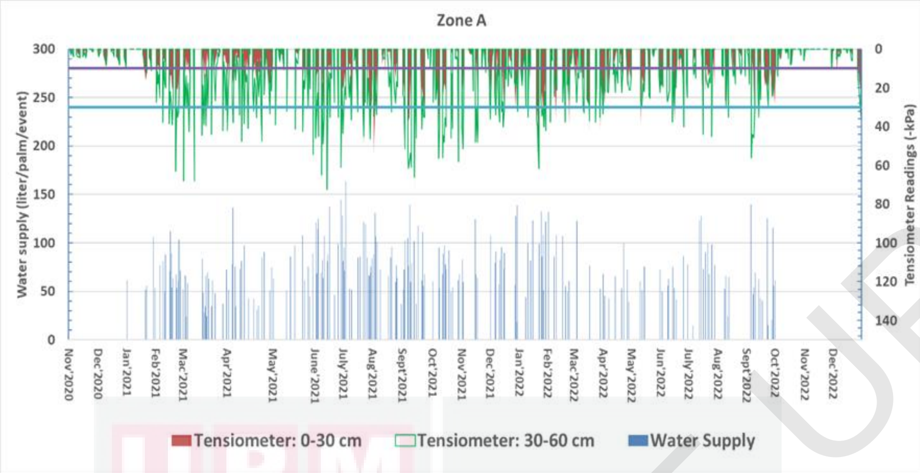

Figure 4.55: Trend of sensor reading at Zone A for depths 0-30 cm and 30-60 cm

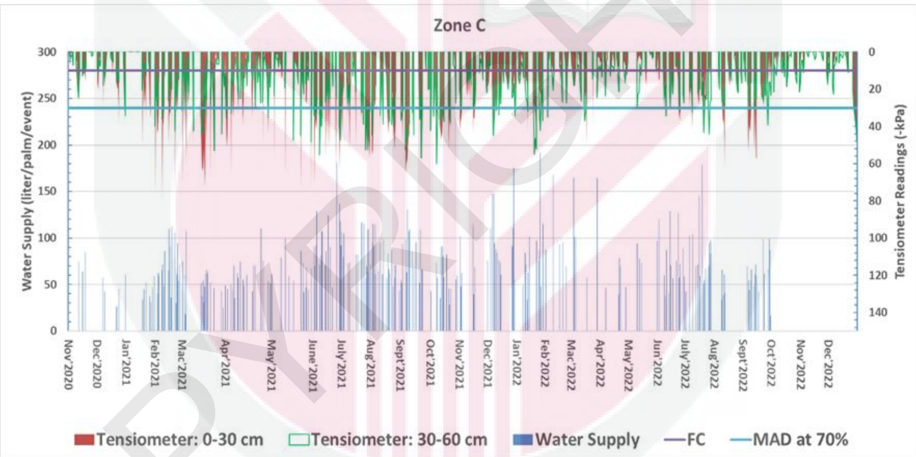

Figure 4.56: Trend of sensor reading at Zone C for depths 0-30 cm and 30-60 cm

At Zone A, water easily infiltrated through the soil from the upper to the lower depth due to a high infiltration rate, as shown in Section 4.3. Despite a higher AWHC, Zone A had higher BD (Figure 4.57) compared to other zones until 60 cm depth but was not significantly different except at 90 cm depth. Soil texture at Zone A was also dominantly filled with sand particles (Figure 4.21- Figure 4.22). It is generally believed that soil at lower depths dries quicker than at the upper depths because of a higher root density. Chan (1977) reported that the most significant quantity of roots was present at 30-60 cm vertically from the soil surface. Thus, higher root density may extract more water and reduce water storage. From previous research, the highest root activity in terms of water uptake was reported to be tremendously high at the weeding circle, up to 2.0 m horizontally and 1.0 meters vertically from the ground (Nelson et al., 2006).

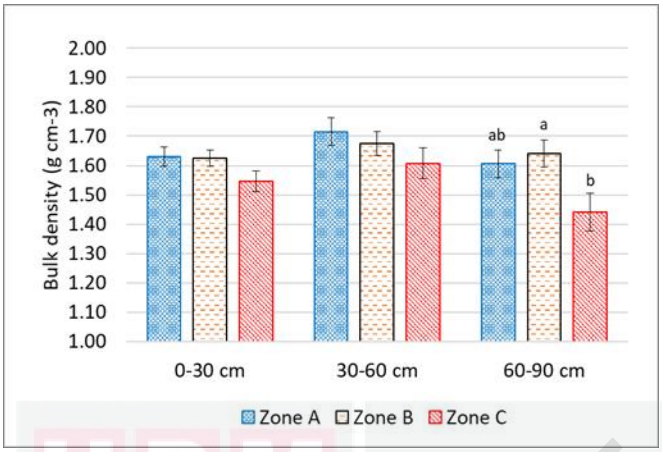

Figure 4.57: Bulk density (BD) for each zone according to their examined soil depth

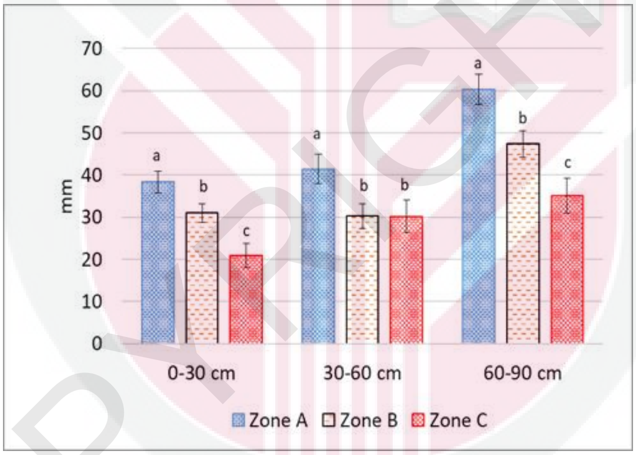

Figure 4.58: Available water holding capacity (AWHC) for each zone according to examined soil depth

Unlike Zone A, the sensor reading at Zone C was almost identical for soil depths and the difference between the upper and lower depths was not so pronounced (Figure 4.56). There were several occasions where lower depth, i.e., 30-60 cm, had lower SWP than upper depth, for example, in October 2021 and January to February 2022. However, the upper depth is more sensitive towards SWP.

Apart from BD, there was a noticeable difference at Zone C, which had a higher percentage of clay and a lower percentage of sand throughout 90 cm (Figure 4.21-Figure 4.22). It also had a slower infiltration rate at 8-11 times that of Zone A. Because of this, irrigation needed to be longer to restore sensor reading to below 30 kPa (confirmed from fieldwork, although no record was taken for the irrigation period). Based on Figure 4.58 it was clearly indicated that the upper depth for Zone C had a significantly lower AWHC compared to the lower depth and to other zones. This situation could explain the fluctuation of data trends in the upper depths.

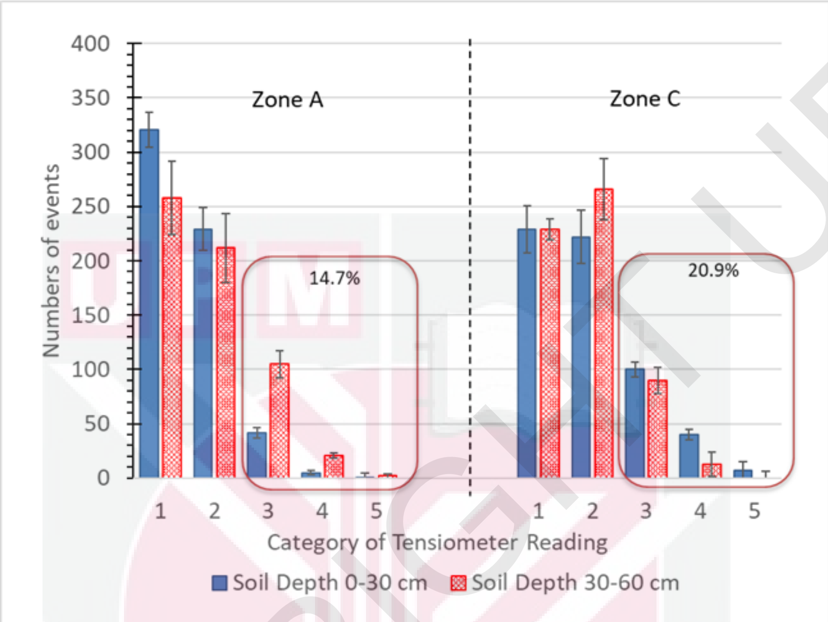

Figure 4.59: Sensor reading according to its category and separation by IMZ

Sensor records were summarised according to category, as shown in Figure 4.59, and their description of classification was shown in Table 4.23 (IAEA, 2008). The sensor placed at a lower depth of Zone A often had a SWP of less than -30 kPa (Category 3 – 5) than the upper zones. It is indicated by a higher percentage (70%) of Category 3-5 for tensiometer at 60 cm compared to tensiometer placed at 30 cm.

Zone C had a lower number of observations for Category 1 and 2 at the upper depths since it has a lower water retention capability, thus requiring more irrigation events. As discussed before, SWP at Zone C for the upper depth easily increased, proven by the higher percentage of Category 3-5, which was 34% compared to the lower depth which was 23%.

Basically, there are two outcomes from daily monitoring: either the gauge reading is higher or lesser than the trigger point (30 kPa on tensiometer gauge). Irrigation is done when the former situation occurs but is omitted for the latter case. Typically, irrigation is once daily (if it exceeds the trigger point) but can be more frequent, up to twice in a drier month. There are also some cases where irrigation was supplied in the morning, but a deficit built up toward the end of the day could cause the reading to surpass the trigger point for the next day. This explains the occurrence of multi-peaks for both zones.

Table 4.23: Description of each category of tensiometer readings (IAEA, 2008)

Category	Reading	Description
1	0-10 kPa	Saturation (0 kPa) to near saturation; this can occur following heavy rain or due to overirrigation. Plant roots may suffer from a lack of oxygen if readings in this range persist.
2	11-30 kPa	FC, no irrigation is necessary.
3	31-50 kPa	Mild stress on well-drained soils.
4	51-70 kPa	The soil is getting dry. The usual range to start irrigation is to ensure maintenance of readily available soil water and provide a safety factor to compensate for practical problems of delayed irrigation or inability to obtain uniform distribution of water to all parts of the field.
5	70-100 kPa	Stress ranges for many soils and crops, especially shallow-rooted crops. The readily available water may be below that required for maximum growth. Tension is likely to exceed the tensiometer's air entry potential, causing air to enter the tensiometer, which will stop functioning correctly, especially in coarser textured soils.

4.8.3 Irrigation frequencies and water usage

In the industry, the IRHO method (Surre, 1968) is widely used and the relationship between Potential Water Deficit (PWD) and rainfall is shown in Figure 4.60. In 2020, six months showed deficit value during the period from January to March and July to August. The IRHO method was initially developed to estimate oil palm suitability to rainfall regimes and yield profile investigations. However, it is not suitable to use for short-term estimates of water stress (Corley & Tinker, 2016). Data prior to November 2020 need to be ignored since there is too much interference from pre-setting and the mentioned issues. It has been proven that irrigation was still needed (especially in Zone C), even though no water deficit was shown according to the IRHO method, such as in November - December 2020, April 2021, November 2021 – January 2022, April 2022 and August 2022. According to the yearly trend, 2021 shows a lot of irrigation events compared to 2022.

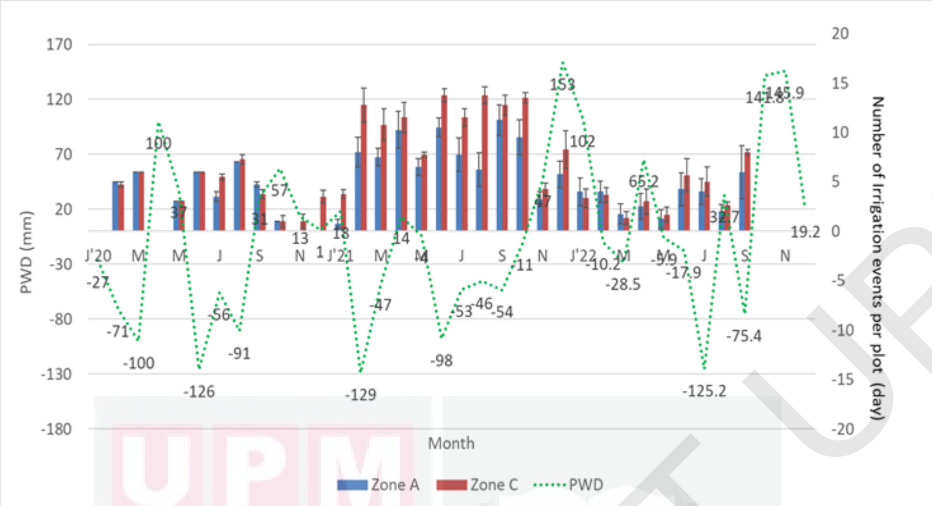

Figure 4.60: Average of irrigation frequencies monthly for all IMZ

Results for the average volumetric irrigation input are shown in Figure 4.61. Zone C used a higher quantity of water (13.28 m^3 $palm^{-1}$) than Zone A (9.72 m^3 $palm^{-1}$). The t-test analysis resulted in t = -3.86 and a p-value of 0.0084, i.e., the irrigation volume of the two zones was statistically significantly different. In terms of the number of irrigation days, Zone A had fewer events (156 event $plot^{-1}$) than Zone C (212 event $plot^{-1}$) as shown in Figure 4.62. The t-test analysis, t = -4.54, p-value = 0.0039, showed that the number of irrigation events at the two zones was statistically significantly different. These results were expected due to the distinct ability to hold water. Zone A was expected to hold a higher quantity of water starting from the field capacity point, and it took more days to reach critical depletion at the same PET rate.

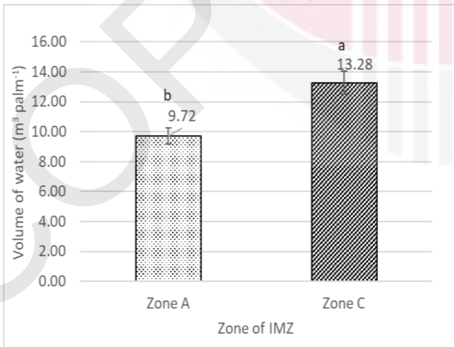

Figure 4.61: Comparison of total water usage (m^3 $palm^{-1}$) for Zone A and Zone C from November 2020 until December 2022

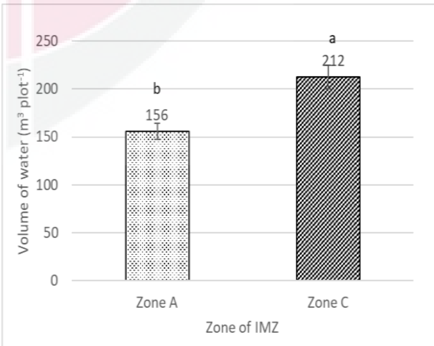

Figure 4.62: Comparison of the number of irrigation events for Zone A and Zone C from November 2020 until December 2022

It is noteworthy that the volume of irrigation for Zone A was not significantly higher, i.e., 84 Litre event^{-1} palm^{-1}, compared to Zone C at 78 Litre event^{-1} palm^{-1} as shown in Figure 4.63. This situation could be due to an uneven pressure head. Zone A was closer to the water tank and pump location than Zone C. In addition, the previous uniformity assessment showed that all Zone A plots had higher operating pressure and slightly higher emitter flow rate hour^{-1} than Zone C (Figure 4.44). From the earlier result, it was found that the emitter type is non-pressure compensated. Therefore, pressure variation in the system and emitters will vary, resulting in higher volume sprayed at the emitter as a function of the H-Q curve.

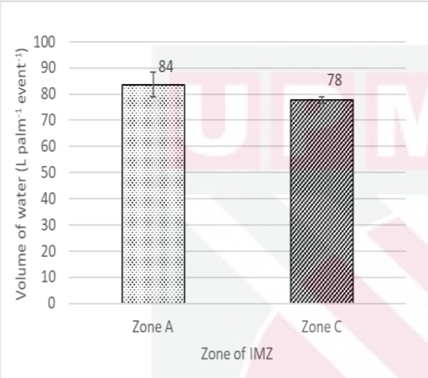

Figure 4.63: Comparison of water usage for each palm per event from November 2020 until December 2022

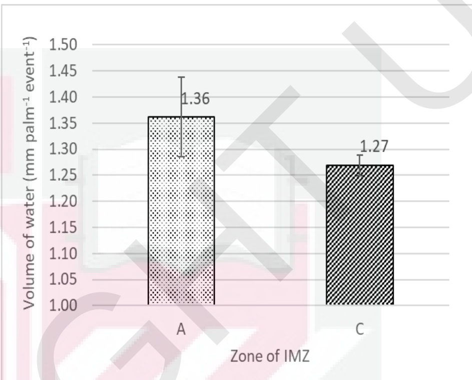

Figure 4.64: Comparison of water usage in mm for Zone A and Zone C from November 2020 until December 2022

During the process of closing the valve, the timing may not have been precise according to the set time when the gauge decreases to below 30 kPa. The soil may already be wet enough by the time workers arrive at the plot. Based on this factor, different times to shut off the valve could have influenced the water volume at Zone A to be higher than in Zone C. This element of human bias and error justifies the importance of SBI using an automated system and ultimately to be a PI system. The advancement of technology for irrigation scheduling is well documented, but certain areas need to be carefully looked at before it is adopted in the field. Some of the factors contributing to the effectiveness of the system are technical training and willingness of the farmers, well-designed systems and maintenance, and robust and cheap sensors (García et al., 2020).

From Figure 4.64, water input per palm was equivalent to 1.36 mm palm^{-1} event^{-1} and 1.27 mm palm^{-1} event^{-1} for Zone A and Zone C, respectively. However, there were occasions when the palm received more water due to additional rounds of irrigation from February to May 2021. This irrigation amount was relatively low compared to practices by other researchers. To put this into context, Lee and Izwanizam (2013) carried out irrigation from 4.0 – 5.0 mm day^{-1} using the furrow system, while another study (Rhebergen et al., 2019) reported 6.5 mm day^{-1} using the sprinkler system with an additional tensiometer to monitor SWP. Meanwhile, comprehensive trials done by Palat et al. (2000) used 3.5 – 6.7 mm day^{-1} using various types of irrigation systems.

Generally, water input from previous trials was mainly to replace PET due to climate conditions, which was typically 5.0 mm day^{-1}. Hence, it is wise to apply more than calculated if possible (Corley & Tinker, 2016). They also mentioned that frequency is not vital regardless of critical deficit is avoided.

Since the irrigation rate for this project was low (78 - 84 Litre palm^{-1} event^{-1}), it may raise the question of whether it is sufficient for oil palm. A study done by Mahadani and Foster (2007) to test minimal irrigation used only 108 Litre palm^{-1} week^{-1} (1.5 mm), and they found yield increased up to 4.0 t ha^{-1} or 13.6% due to higher efficiency of nutrient uptake. Therefore, the effect of irrigation on yield was not solely due to the improvement of soil moisture but also nutrient solubility to be taken up by the plant. Studies on the usage of tensiometers have been demonstrated by various researchers (Jeranyama et al., 2017; Toll et al., 2016). Studer and Spoehel (2019) also proved that irrigation scheduling using tensiometers was able to reduce water usage significantly by about 20%, compared to conventional farmer practices. Despite that, there is a lack of studies discussing the potential water saving using tensiometers on different AWHCs, except for the rough estimation suggested by Temizel (2016).

The low irrigation rate could be due to a single emitter point for each palm. The sensor is located near the emitter and only localised SWP is measured. Thus, the other portion of soil not covered by the emitter radius may still be dry. In an early study by Palat et al. (2000), he used two micro-sprayers for every palm with multiple irrigation rates from 120 – 360 L palm^{-1} as a predetermined rate without using a soil sensor. However, these two rates have no significant differences, and the average yield is around 24.0 t ha^{-1} yr^{-1}, which is likely similar to those found in this study. Considering this, partial replacement of ETo over a large area will result in a significant total production compared to a complete replacement over a smaller area under a limited water supply (Corley & Tinker, 2016).

In this study, there is no direct comparison to demonstrate water savings between conventional irrigation and SBI due to the limited plot number and complexity of the irrigation setup. Back in 2017, EID was estimated to be around 130 mm year^{-1} or 8.78 m^3 palm^{-1} year^{-1}, reflecting a PWD of -218 mm. Later, SBI resulted in water usage at 3.04 – 3.54 m^3 palm^{-1} for 2022 despite a slightly higher PWD at -263 mm for Zone A and C, respectively. It is indicated that water usage has been improved by using the micro-sprayer method with a tensiometer, and 60% water savings have been achieved.

The results of the relationship between the amount of rainfall (Rainfall), number of rainy days (Day), ER, PWD, and number of events at Zone A (EventA) and C (EventC), as well as water volume used at Zone A (VolA) and C (VolC) are interesting. As shown in Table 4.24, Rainfall had a strong positive relationship with ER and PWD but a moderate negative relationship with EventC, VolA and VolC.

However, the number of Raindays had a moderate negative relationship with EventC (r = -0.554, p<0.05) and VolA (r = -0.537, p<0.05). This relationship was getting stronger with VolC (r = -0.637, p<0.01). ER and PWD also showed a moderate negative relationship with any other significant variable. These results show the importance of a number of rainy days for irrigation scheduling, not the amount of rainfall or ER. A well-distributed rain will maintain soil moisture at the desired level and reduce SWP below the trigger point. Zone C showed a better relationship, probably because this area was more responsive to water deficit due to lower AWHC and infiltration rate than Zone A.

Table 4.24: Result of the relationship between irrigation and rainfall component

	Rainfall	Day	ER	PWD	EventA	EventC	VolA	VolC
Rainfall	1							
p-value	0.000							
Day	0.681	1						
	0.000	0.000						
ER	0.999	0.673	1					
	0.000	0.000	0.000					
PWD	0.984	0.766	0.982	1				
	0.000	0.000	0.000	0.000				
EventA	-0.473	-0.486	-0.479	-0.478	1			
	0.020	0.016	0.018	0.018	0.000			
EventC	-0.517	-0.554	-0.519	-0.528	0.929	1		
	0.010	0.005	0.009	0.008	0.000	0.000		
VolA	-0.509	-0.537	-0.508	-0.529	0.892	0.814	1	
	0.011	0.007	0.011	0.008	0.000	0.000	0.000	
VolC	-0.536	-0.637	-0.532	-0.580	0.828	0.853	0.932	1
	0.007	0.001	0.008	0.003	0.000	0.000	0.000	0.000

4.8.4 Palm growth and its relation to the yield

4.8.4.1 Vegetative measurement

Several growth variables have been used to look at the performance of the study plot. Within six-month intervals, palms can produce 12 -16 fronds for the six-month interval, which are equivalent to two to three fronds a month. Generally, no significant difference among all the treatments. However, Zone A had the highest frond number production until 12 months after treatment (MAT) and Zone C recorded the lowest frond production for the 12 - 30 MAT trial period (Figure 4.65). Frond number production is an important variable to look into when assessing the drought effect. Palm will naturally reduce the opening of the leaves to minimise water loss through transpiration. Higher frond number production indicates the palm is less stressed by water deficit. During water deficit, spears remain closed for a certain period until the condition is suitable to reduce transpiration. The existence of unopened spears and to a certain extent, yellowing and snapping of leaves were symptoms of water stress for oil palms in Costa Rica (Villalobos et al. 1992).

For girth size, no significant differences were observed in all treatments except during 18 MAT (Figure 4.66). At all times, NIR showed better girth size than Zone A and Zone C. The Girth size of the palm may exhibit how vigorous the palm is. A bigger girth size reflects that the palm is more stable and 'good looking' when it is supposed to be the storage organ for nutrients. During photosynthesis, assimilates produced by this process will be transferred to the entire organ and moved to the bunch for the production process. If any shortfalls of nutrients occur, the trunk will provide the buffering capacity for short-term imbalances (Corley and Tinker 2015). The NIR plot produced a low yield compared to the Zone A and C plots. The nutrient allocation was not for bunch formation and was stored in the trunk as a reserve, thus resulting in a bigger girth size.

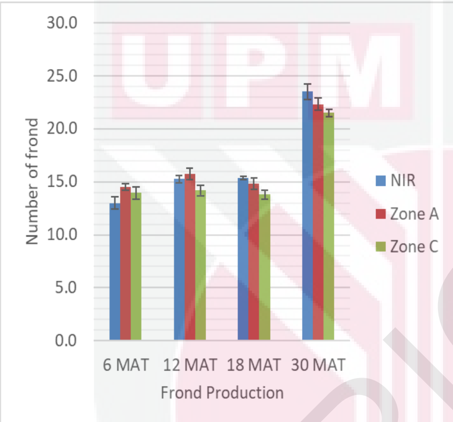

Figure 4.65: Frond production for each treatment

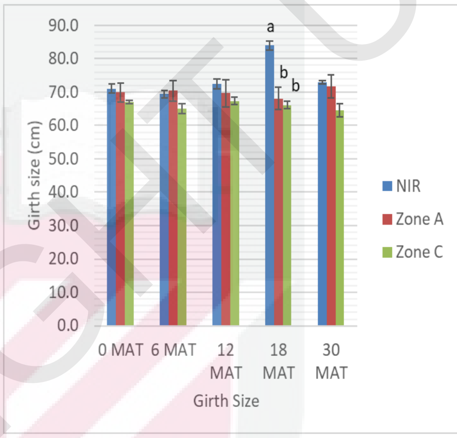

Figure 4.66: Girth size for each treatment

Palm height did not show a significant difference, although there were trends where Zone A was superior to Zone C and NIR. Meanwhile, Zone C and NIR had almost similar palm heights (Figure 4.67) except at 30 MAT. It has been generally accepted that height are also correlated with the number of leaf production and FFB component (Rafii et al., 2013). Thus, higher frond production in Zone A explains why it was taller compared to the other treatments and this was also applied when comparing NIR to Zone C. Apart from that, height increment could also be affected by internode length and planting density.

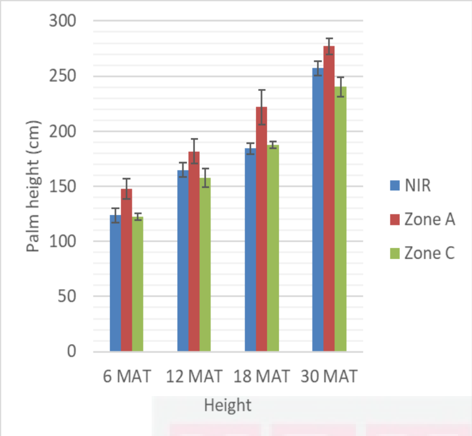

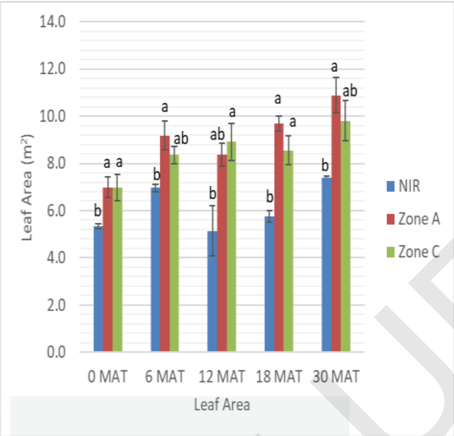

Figure 4.67: Palm height from ground to frond 41

Figure 4.68: Leaf area for each treatment

Leaf area is encompassing and generated from leaf width, leaf length, and number of leaflet frond^{-1}. Logically, a bigger leaf area will accommodate more chlorophyll and have a higher ability to translate energy from the sun to carbohydrates for better production. Zone A and Zone C did not show significant differences from each other, whilst the NIR plot had the smallest leaf area compared to irrigated plots (Figure 4.68). These features are affected by years, indicating that Zone A and Zone C had better conditions for promoting their growth. An early study by Hardon et al., (1969) found a positive correlation between leaf area and yield. Later, Henson and Chang (2000) reported that the leaf area was much lower for stressed palms than for unstressed palms.

PCS is one of the variables that indicate the healthiness of the palm. In this graph, Zone A had significantly larger PCS, followed by Zone C and lastly NIR (Figure 4.69). Prabowo et al., (2010) reported that FFB yield can be accurately predicted from leaf dry biomass, nutrient data, and palm age. PCS correlation with frond dry biomass can later be used to access the CGR and BI. Larger PCS sometimes do translate to superior yield, though Lee et al., (2014) showed that palm with a larger PCS value did not necessarily produce better yield in terms of bunch and oil production.

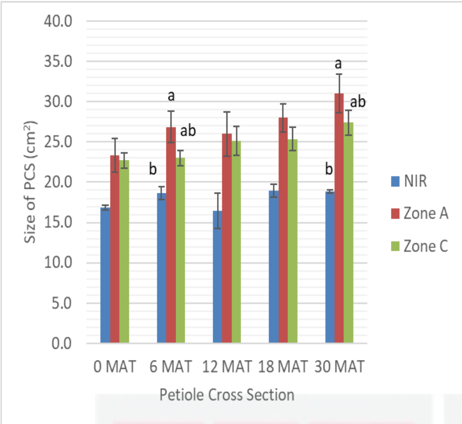

Figure 4.69: PCS area for each treatment

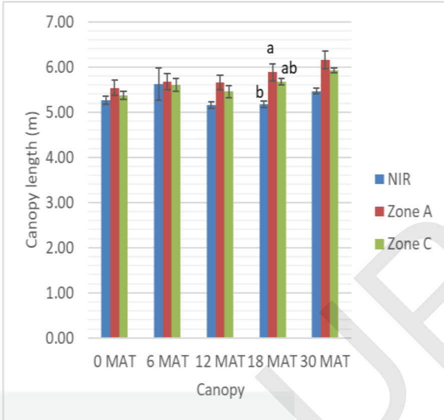

Figure 4.70: Canopy length for each treatment

Canopy length was the measurement taken to represent the opening of frond coverage from the centre trunk of the palm by determining the maximum distance covered by the leaf tip. It was clear that Zone A and Zone C had higher canopy lengths than the NIR plot for each examined interval, which was significantly higher at 18 MAT (Figure 4.70). NIR plot has a smaller canopy, indicating slower vegetative growth. It may be due to insufficient moisture reserves in the soil, especially during low rainfall. Zones A and C have been located at a dedicated irrigation zone since 2014; thus, soil moisture reserves remain low, although there were no tensiometers before 2020. Korom et al., (2016) reported that canopy diameter had a strong non-linear regression relationship with above-ground biomass (R^2 from 0.950 to 0.975) across various oil palm ages and from this study, higher above-ground biomass resulted in higher yield.

4.8.4.2 Refine frond biomass equation

At each IMZ, the whole frond number 17 was sampled to represent each treatment to differentiate the water percentage in the frond. Later, the percentage of water in the frond was used to estimate VDM and to estimate CGR. Zone A consistently had a higher percentage of water compared to Zone C and NIR except for 18 MAT (Figure 4.71). Overall, the gap between readings was very close, with differences varying from 0.5 to 1.5%. However, the difference could significantly impact the estimation of frond dry weight after multiplying the frond number production for each palm. If the same frond number production is assumed (32 number of fronds) with the same weight of frond (6.50 kg frond^{-1}) and same water percentage (70.5%), then there is an estimated 125 L of water stored in the frond only. Zone A probably had a higher water percentage from 0-12 MAT as the water uptake was not limited like in the Zone C and NIR plots.

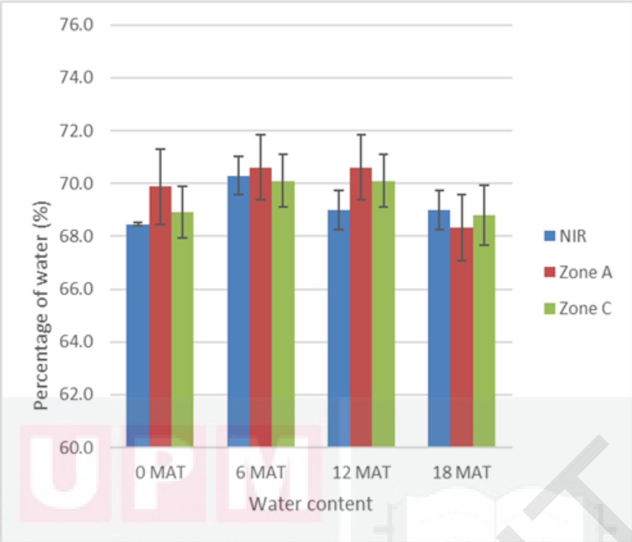

Figure 4.71: Percentage of water in the frond 17

For many years, the frond dry weight was estimated from the equation introduced by Corley et al., (1971). Recently, researchers have attempted to improve the equation (Aholoukpè et al. 2013; Henson and Dolmat 2003) as the procedure to obtain actual dry weight is a destructive and laborious method. Due to this, an empirical formula was used to calculate the dry matter biomass of the fronds.

In the current study, actual data of frond dry weight was pooled together for all intervals sampled and then correlated with PCS. From the analysis, R^2 was 0.7125, i.e., it is acceptable to say there was a strong correlation between frond dry weight and PCS (Figure 4.72). The model suggested by the linear relationship was Y = 0.06541 PCS + 0.34553. This formula was used to estimate frond dry weight precisely for this project; in comparison, the original model suggested by Corley et al., (1971) was Y = 0.102 PCS + 0.206. The old empirical formula used to estimate the biomass was 50% higher than the actual data obtained from this study; this is likely because the formula was established in the early 1970s and today, most of the planting material has been replaced by newer planting material that could give a different set of result. Zone A and Zone C consistently produced higher dry-weight frond biomass compared to NIR (Figure 4.73). This indicates that the water percentage did not significantly differ for each treatment. It shows that in terms of moisture, palms in favourable conditions produce better dry matter despite relatively constant water content in their organs. It is likely that nutrients were available, and uptake by the palm was able to meet compulsory requirements for production and vegetative matter. Corley and Tinker (2016) stated that the above-ground biomass follows the "Overflow model", and the yield depends on the excess assimilates once vegetative requirements are satisfied.

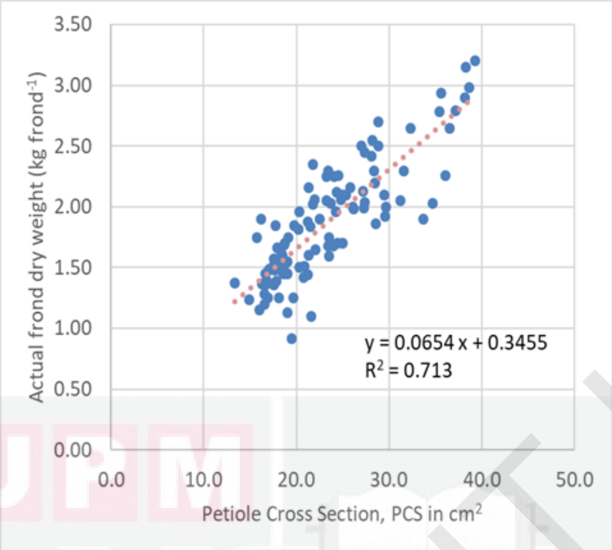

Figure 4.72: Linear regression line for actual frond dry weight and PCS

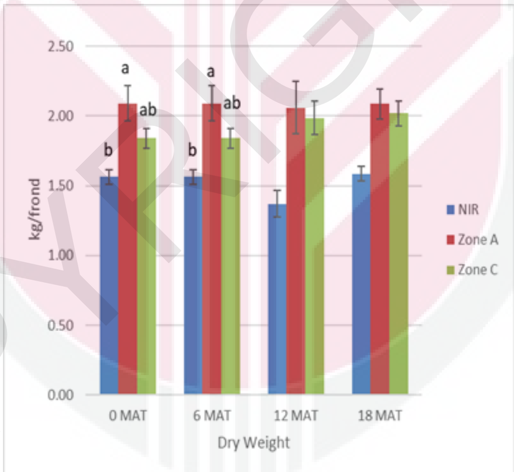

Figure 4.73: Actual frond dry weight estimation based on linear regression line

4.8.4.3 Derivatives growth indices

Previously, numerous studies only reported on the improvement of FFB in terms of a tonne for every hectare, i.e., bunch number formation. However, further research is needed to elaborate on the effects of irrigation on palm growth. Due to timing and interval schedules, there were 12 months (6 – 18 MAT) to access and measure derivative growth indices of the palm in terms of VDM, CGR and BI (Table 4.25).

Table 4.25: Several components of growth water productivity indices for selective timeframe

Treatment	FFB T ha^{-1}	VDM Kg palm^{-1}	CGR T ha^{-1}	CGR Kg palm^{-1}	BI ratio Index
NIR	18.9±1.5 b	67.2±5.5 a	22.53±0.1 b	152±16.5 b	0.44±0.02 b
Zone A	28.6±1.7 a	104.2±6.9 a	30.73±2.6 a	208±17.7 a	0.51±0.01 a
Zone C	28.1±1.8 a	100.9±7.0 a	27.65±1.3 b	187±8.8 b	0.53±0.02 a

Noted: Different letters in the same column indicate significant differences between means according to Tukey's test

In terms of VDM, Zone A and C were significantly higher than NIR by about 50-55%. Zone A and Zone C produced better and significantly different CGR compared to NIR. In addition, irrigated plots showed significantly higher BI with a range of 0.51-0.53, and the average dry biomass of fruit from irrigated plots was higher than NIR (0.44). In comparison, Corley et al., 1971 reported that the average BI from 11 tested progenies was 0.45.

From all the data above, it can be concluded that irrigation does improve either fresh or dry biomass and leads to higher BI for better yield. In most situations, Zone A had a higher value for growth indices (though in terms of BI, the difference was not significant with Zone C). The ability to hold more water content at Zone A showed that it provided better conditions for the palm to grow and produce a better yield.

4.8.5 Yield Component

Yield recording started after the installation of the irrigation system was completed. The results are shown in Table 4.26, representing seven and 8-year-old palms for 2021 and 2022, respectively. While the BN and ABW were measured directly, the tonnage was calculated by multiplication of BN, ABW, and palm density per hectare. In 2020, Zone A produced the highest yield with 24.1 t ha^{-1}, clearly surpassing Zone C and NIR plots, which recorded 17.8 t ha^{-1} and 14.9 t ha^{-1}, respectively. Zone A had the highest BN with almost 15 bunches palm^{-1} year^{-1}, which was 30% higher than in Zone C. It has led to extra tonnage despite Zone A recording a slightly lower ABW than Zone C. In 2021, the trend for BN and ABW was constant for Zone A. However, Zone C vastly improved for both variables. The difference was minimal between these two zones, but Zone C had the higher annual tonnage.

In 2022, all treatments have surpassed 24.0 t ha$^{-1,}$ which is considered a good achievement. It might be because of good rainfall distribution in 2022 and less water deficit two years before. However, cumulatively Zone A still produced a higher yield, i.e., 75.5 t ha^{-1}, compared to Zone C (69.1 t ha^{-1}) and NIR plot (51.4 t ha^{-1}). NIR treatment showed the lowest trend among all yield components for both years.

In another context, an average 21-year-old data record (1991-2011) for conventional irrigation using the furrow irrigation method yielded 30 - 36 t ha^{-1} (Lee & Izwanizam, 2013). This led to arguments and debates about the vast differences between the furrow method and the SBI system. However, a variety of factors, such as fertiliser rate and type, planting materials, estate maintenance, and microclimate changes, may all contribute to the differences.

SBI system only started in January 2020, and the system was optimised from November 2020 onwards. It is widely accepted that at least two years are required before any variable makes an impact on the physiological fruit development process of oil palms. Based on the previous discussion from Section 2.2, oil palm yields are sensitive to moisture up to 33-36 months, 19-25 months and 8-11 months prior to harvesting. Therefore, the difference in yield performance between Zone A and Zone C was attributed to the soil's capacity to hold moisture provided by rainfall and conventional irrigation scheduling before 2020. Zone A had the advantage of storing enough water and reducing the risk of water deficit impact compared to Zone C. This effect was clearly represented by the inferior yield from NIR plots where no irrigation was carried out to decrease the water deficit in the soil.

Another impact of moisture is through the availability of nutrients within the root zone. Moisture will help nutrients dissolve and turn into available forms for uptake by the palm and also act as a transport medium (Frank, 1972). For example, in irrigation trials done by Rhebergen et al., (2019), treatment of irrigation alone can increase yield by about 2% compared to non-irrigated plots without fertiliser. Additionally, the yield gap increased to 17% when there was a combination of irrigation and nutrients. This was similar to the report by Arifin et al., (2022), who highlighted that yield increase was about 17% when one to two folds of fertiliser were applied with homogenous irrigation treatment.

As can be seen in Table 4.26 – Table 4.27, Zone A has a sustained performance compared to the others. Lee and Izwanizam (2013) demonstrated that BN is a contributing factor that increases oil palm yield under irrigation treatment, leading to increased leaf production and, later on, improved sex ratio (Carr, 2011). A higher bunch number can also be affected by the planting environment. Henson (1998) reported that yield was 35% higher on wet sites than on dry sites, and this difference was entirely due to the number of components. Previously, Sparnaaij (1969) reported that BN and ABW were negatively correlated. However, current researchers report that in oil palm physiology, a balance between BN and ABW will be achieved because yield is generally ‘source limited’. Thus, if the palm has a high BN, ABW will be reduced as compensation due to the limiting sources (Corley & Tinker, 2016). Thus, the superior performance of Zone C in 2021 could be due to its ABW impact, as can be seen in 2022.

Table 4.26: Yield component from 2020 until 2021 for Zone A, Zone C and NIR

Block	2020			2021		
	BN n	ABW kg bunch^{-1}	Tonne t ha^{-1}	BN n	ABW kg bunch^{-1}	Tonne t ha^{-1}
Zone A	14.8 ± 1.7	10.0 ± 0.2	24.1 ± 2.4	12.7 ± 1.2	13.0 ± 0.5	24.9 ± 2.3 a
Zone C	10.5 ± 3.3	11.3 ± 1.1	17.8 ± 4.0	11.3 ± 0.9	15.2 ± 1.4	25.8 ± 0.8 a
NIR	7.6 ± 0.2	9.2 ± 0.8	11.8 ± 1.2	9.0 ± 1.5	11.2 ± 0.8	14.7 ± 1.8 b
p-Value	0.215	0.364	0.087	0.643	0.195	0.023

Noted: Different letters in the same column indicate significant differences between means according to Tukey's test

Table 4.27: Yield component for 2022 and cumulative for Zone A, Zone C and NIR

Block	2022			Cumulative (2020 – 2022)		
	BN n	ABW kg bunch^{-1}	Tonne t ha^{-1}	BN n	ABW kg bunch^{-1}	Tonne t ha^{-1}
Zone A	13.4 ± 0.6	13.2 ± 0.4	26.4 ± 1.3	40.9 ± 3.0	11.9 ± 0.3	75.5 ± 4.3 a
Zone C	12.9 ± 2.2	13.5 ± 1.0	25.5 ± 2.4	34.7 ± 6.3	13.5 ± 1.2	69.1 ± 5.7 ab
NIR	14.1 ± 0.7	11.5 ± 0.3	24.8 ± 1.5	31.0 ± 1.2	10.5 ± 0.7	51.4 ± 1.3 bc
p-Value	0.588	0.416	0.782	0.354	0.225	0.044

Noted: Different letters in the same column indicate significant differences between means according to Tukey's test

4.8.6 WP performance

The performance of oil palm in terms of WP is shown in Figure 4.74. Generally, NIR treatment has insignificantly less WP compared to Zone A and Zone C. Irrigation plot area able to get WP ranged from 2.05 – 2.66 kg m^{-3}. Water productivity can be increased through irrigation plots, with the exception of 2022, when Zone C has a marginally lower WP than NIR cumulatively. The primary constituent of WP is the ER, which represents the total annual rainfall. In 2022, rainfall amount was improved by up to 1834 mm year^{-1} (PWD equal to -263 mm year^{-1}). NIR is able to achieve a high yield, and WP is 2.08 kg m^{-3} higher than Zone C. It is probably, NIR plot revover when conditions are favourable and experiences peak crop or "bumper crop year" (Amirul Hadi et al., 2016; Corley & Tinker, 2016). This circumstance is thought to narrow the disparity between treatments and enhance the output in NIR.

The use of a tensiometer not only helps conserve water but also enhances crop output, as emphasised by researchers. In their study, Singh et al., (2017) presented different irrigation scheduling techniques for paddy cultivation. They discovered that employing a tensiometer for irrigation scheduling resulted in a significant reduction of water usage by up to 33%, while still maintaining the crop yield. Marwa et al., (2017) showed that the utilisation of a tensiometer resulted in water savings of 16 – 35% and a yield increase of 20%.

In an oil palm context, there is a lack of studies regarding WP, and thus, there is no study that directly compares the outcomes. Despite the lack of a WP study, some publications focus on Water Footprint (WF), which is a different conceptualisation that uses total water that accounts for evapotranspiration and other activities for the entire oil palm life cycle. Hashim et al., 2014 found that WF for oil palm was at 1165 m^3 t^{-1} FFB, equivalent to 0.86 kg m^{-3}. Meanwhile, (Safitri et al., 2018) have suggested that WF for oil palm in Indonesia is between 0.56 and 1.14 m^3 kg^{-1} for various plant ages and soil types, or equal to 0.87 – 1.79 kg m^{-3}. Another study done in Thailand by Mungkalasiri et al., 2015 found that WF for oil palm planted in two different fields were 787 and 1532 m^3 t^{-1} FFB, or equal to 0.65 and 1.27 kg m^{-3}, respectively.

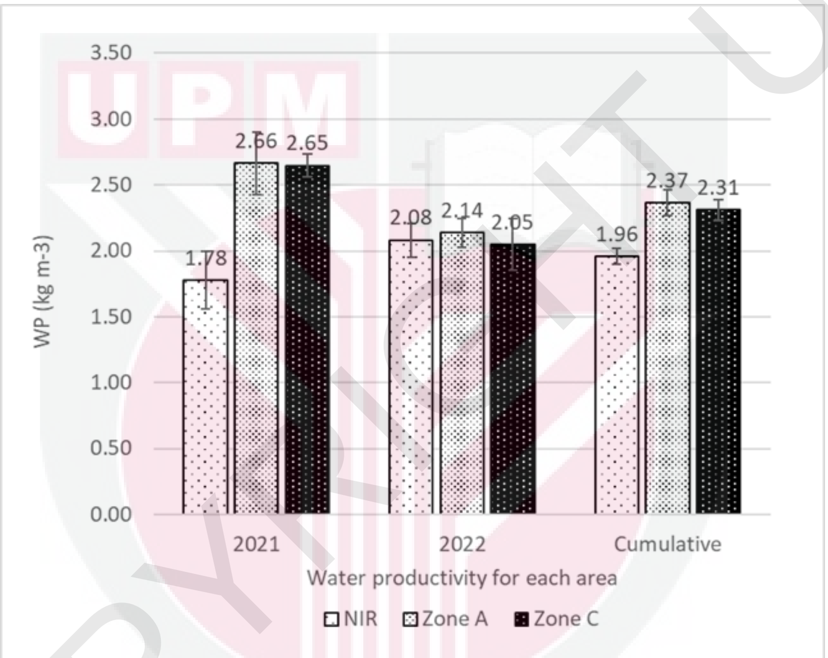

Figure 4.74: Comparison of WP for each treatment for 2021, 2022 and cumulative year

Based on the available WF study, water usage is around 0.65 – 1.79 kg m^{-3}, which is less or slightly more than the outcome of NIR treatment (1.78 – 2.08 kg m^{-3}). The differences could be due to the WF equation, which also included the usage of pesticides, herbicides, and water to remove pollutants in the grey WF calculation (Hoekstra & Chapagain, 2008). WF also used indirect and direct forms of water for FFB production rather than rainfall and irrigation alone. Higher water productivity reflects more efficient water use by the plant. In comparison to other types of crops, water productivity for grains under aerobic conditions was in the range of 0.8 – 1.0 kg m^{-3} (Kato et al. 2009), 2.8 – 3.3 kg m^{-3} for beetroots (Studer & Spoehel, 2019), and 1.5 kg m^{-3} for sugarcane (Haruna and Hanafiah 2017). Meanwhile, González et al. (2020) reported high water productivity up to 8.0 kg m^{-3} for potatoes but only 0.3 kg m^{-3} for beans. From the outcome of this study, Zone A and B have better WP compared to

NIR within a three-year data period. In the future, better indicators could be used by climatic data collection to estimate ETc and calculate water use efficiency (Clemmens & Molden, 2007; Sharma et al., 2006).

4.9 Cost Benefit Analysis

All costs associated with developing a SBI system for this project have been divided into three categories: capital cost, operational cost, and extra expenses incurred for each increase in tonnage, as shown in Table 4.28. This project has an area of 1.08 ha, which was calculated by dividing the total number of palms (160 palms) by the number of stands (148 per ha) and was later simulated to 20.30 ha to represent the boundary of the sampling block. This table is constructed in such a way that it allows for a better representation of things such as water pumps, IoT installation, electrical components, and manpower. During this study, all of the items stated above were purchased to meet the study plot requirements, but their operational capacity is much larger. Meanwhile, piping elements are proportionate to the area involved, while maintenance and repairs are scheduled every two years.

Table F.1 - Table F.2 in the appendix contains details on the cost analysis, and Table 4.29 shows a summary of the indices. ROI is a financial ratio that calculates the benefit an investor receives in comparison to their investment cost. The higher the ratio, the greater the benefit obtained. The ROI for this project is 5%, which takes into account the oil palm lifespan and the project timeline of 20 years.

Table 4.28: Components involved in each section of the cost for SBI system derived for 20.3 ha from actual 1.08 ha of area

No.	**Item**	**RM**	**RM**
Capital Cost (a)		Actual, 1.08 ha	Simulation, 20.30 ha
1	Engine and Pumping Unit	47,000.00	47,000.00
2	IoT Installation	113,550.00	113,550.00
3	Electrical source installation, such as Tenaga Nasional Berhad load charges, deposit and meter installation	8,180.00	8,180.00
4	Piping (Main, Sub-main, Secondary, Lateral and all fittings)	7,340.00	149,002.00
Total Cost (a)		176,070.00	317,732.00
No.	**Item**	**RM year^{-1}**	**RM year^{-1}**
Operational Cost (b)		Actual, 1.08 ha	Simulation, 23.00 ha
1	Utility	100.00	4,000.00
2	Manpower	5,000.00	18,000.00
3	Repair and Maintenance (every two years)	30,000.00	30,000.00
Total Cost (b)		35,100.00	52,000.00
No.	**Item**	**RM t^{-1}ha^{-1}**	
Operational Cost for every tonne increase (c)			
1	Harvesting	30.00	
2	Transporting	30.00	
Total Cost (c)		60.00	

Table 4.29: Economic indices for SBI system on 20.3 ha area

Indices	**Value**
ROI	5%
Payback period	4.5 years
NPV	RM 14,419

The payback period is the amount of time required for the return of the funds invested or to reach the break-even point. The payback period is approximately 4.5 years. This calculation indicates that oil palm age is a critical criterion for any irrigation project. Oil palm, which is more than 20 years old, is not recommended because there is a high risk of non-refundable investment or failure to achieve break-even. If the FFB price is higher than expected, the payback period will be much shorter. NPV is the difference between the present value of cash inflows and the present value of cash outflows over time. NPV is a calculation used in capital budgeting and investment planning to determine the profitability of the suggested investment or project. In this case, a 10% discount rate was used in the calculation, and the NPV was found to be positive, at RM 14,419. Because the NPV value is greater than zero, it can be concluded that this project is profitable.

CHAPTER 5

CONCLUSIONS AND RECOMMENDATIONS

5.1 Summary

Merely 10% of the water accessible in this world exists in the form of surface water. There is a rise in the human population, leading to a corresponding increase in agricultural production. Consequently, the demand for water for agricultural purposes also rises. Measures must be taken to enhance the efficiency of water utilization and achieve sustainable practices. This thesis focuses on optimizing water resource utilization by establishing irrigation management zones and using in-situ sensors for precise irrigation management. This approach demonstrates an innovative advancement in irrigation compared to a conventional method, which uniformly treated the entire area, disregarding the soil's characteristics for irrigation scheduling. The main goal is to demonstrate the direct influence of SBI system on oil palm plantations and establish the feasibility of differential irrigation rates, specifically in relation to the soil's AWHC. The current study involved many activities, but the main ones can be summarised as follows:

1. Finding the spatial variability of AWHC within 20.3 ha of the study area previously reported to have homogenous soil series.

2. Using an available model to determine the irrigation requirement for the study area and utilise irrigation software for installation and hydraulic calculation.

3. Assess oil palm response to irrigation at different IMZ using variables such as palm growth and yield component.

5.2 Conclusions

The following conclusions can be drawn from the current study:

1. It was found that IMZ can be classified into three distinct zones based on soil water-holding capacity, and there was no variation in rainfall within the study area.

2. It was found that generic emitters fall into the micro-sprayer type with non-compensating pressure characteristics. It can also deliver acceptable performance provided by comprehensive irrigation planning.

3. Computer-aided irrigation software, namely IrriPro, provided reliable simulations with detailed hydraulic properties of system design.

4. It has been confirmed that irrigation significantly differs in terms of water usage, number of events, yield water productivity and oil palm growth under variations of soil water holding capacity.

5.3 The novelty of the study and Contributions to Knowledge

Irrigation is crucial for enhancing crop productivity, especially in regions with limited rainfall. Insufficient research has hindered the comprehensive understanding of the advantages of soil sensors for irrigation scheduling, particularly in relation to oil palm yield, growth performance, and water usage. This study showed inventive steps towards the PI approach at an oil palm plantation scale. A combination of soil physical properties and geostatistical analysis techniques can be used to generate IMZ based on AWHC to improve water resources. The utilisation of tensiometers for irrigation scheduling based on IMZ yields novel insights and demonstrates the possibility of achieving differential irrigation even within areas classified under the same soil series. The selection of low-cost emitters often lacks sufficient technical specifications. This study provides a more precise understanding of the behaviour of low-cost emitters used in the previous micro-sprayer method and leveraging commercial irrigation software for performance evaluation. One section of this study also demonstrated a significant correlation between PCS and frond dry biomass, which is consistent with previous research. The new equation significantly improved the accuracy of estimating dry weight and minimised the error for future calculations.

5.4 Recommendations for Further Studies

Based on the results and conclusions from this study, further improvements can be made by paying attention to the following points:

1. IMZ can be established in other soil physical properties or maybe a combination of soil and rainfall data.

2. It is highly recommended that the coefficient of manufacturer variations of the emitter be determined as additional information for hydrology properties.

3. Developing models for estimation of water usage based on soil physical and rainfall factors.

4. ER estimation or specific value according to the study site might be good for obtaining a reasonable estimation of water productivity.

5. The type of sensor and IoT system for irrigation automation is critical to ensure precise input. Sensors that read soil moisture can be any kind, provided there is site-specific calibration.

6. A wire or cable connection for a control system can be low-cost, but its drawback can be a high risk of damage and increased complexity for setup. Wireless connections can be less complex, but challenges such as uneven topography and dense oil palm canopy can significantly hinder stable connection.

7. Sensor and IoT systems need power to maintain good connections with control systems and provide valuable real-time information. A dedicated space for solar energy to intercept radiation is needed for good power establishment.

8. Establishment of different types of irrigation systems, such as sub-surface and sprinkler irrigation systems, to look at water productivity.

REFERENCES

Abioye, E. A., Abidin, M. S. Z., Mahmud, M. S. A., Buyamin, S., Ishak, M. H. I., Rahman, M. K. I. A., Otuoze, A. O., Onotu, P., & Ramli, M. S. A. (2020). A review on monitoring and advanced control strategies for precision irrigation. *Computers and Electronics in Agriculture*, *173*(April), 105441. https://doi.org/10.1016/j.compag.2020.105441

Aboamera, M. A., Gomaa, A. H., & Ibrahim, K. A. (2017). Effect of Irrigation Water Quality on Emitter'S Clogging Percent. *Misr Journal of Agricultural Engineering*, *34*(4), 2121–2140. https://doi.org/10.21608/mjae.2017.96532

Adeniji, F. A., Umara, B. G., Dibal, J. M., & Amali, A. A. (2013). Variation of Infiltration Rates with Soil Texture. A Laboratory Study. *International Journal of Engineering and Innovative Technology*, *3*(2), 454–459.

Adhikary, P. P., Chakraborty, D., Kalra, N., Sachdev, C. B., Patra, A. K., Kumar, S., Tomar, R. K., Chandna, P., Raghav, D., Agrawal, K., & Sehgal, M. (2008). Pedotransfer functions for predicting the hydraulic properties of Indian soils. *Australian Journal of Soil Research*, *46*(5), 476–484. https://doi.org/10.1071/SR07042

Adindu, R. U., Igbokwe, K. K., Chigbu, T. O., & Ike Am, C. A. (2014). Application of Kostiakov ' s Infiltration Model on the Soils of Umudike , Abia State - Nigeria. *American Journal of Environmental Engineering*, *4*(1), 1–6. https://doi.org/10.5923/j.ajee.20140401.01

Adnan, S., & Khan, A. H. (2012). Effective Rainfall for Irrigated Agriculture Plains of Pakistan. *Pakistan Journal of Meteorology*, *6*(11), 61–72.

Afandi, A. H., Zulkifli, H., Nur Zuhaili, H. A. Z. A., Norliyana, Z. Z., Hisham, H., Saharul, A. M., Dzulhelmi, M. N., & Vu Thanh, T. A. (2022). Oil Palm Water Requirement and the Need for Irrigation in Dry Malaysian Areas. *Journal of Oil Palm Research*, *August*. https://doi.org/10.21894/jopr.2022.0052

Aholoukpè, H., Dubos, B., Flori, A., Deleporte, P., Amadji, G., Chotte, J. L., & Blavet, D. (2013). Estimating aboveground biomass of oil palm: Allometric equations for estimating frond biomass. *Forest Ecology and Management*, *292*(2013), 122–129. https://doi.org/10.1016/j.foreco.2012.11.027

Ali, M., & Mubarak, S. (2017). Effective Rainfall Calculation Methods for Field Crops: An Overview, Analysis and New Formulation. *Asian Research Journal of Agriculture*, *7*(1), 1–12. https://doi.org/10.9734/arja/2017/36812

Allen, R. G., Pereira, L. S., Raes, D., & Smith, M. (1998). Crop evapotranspiration: Guidelines for computing crop requirements. *Irrigation and Drainage Paper No. 56, FAO*, *56*, 300. https://doi.org/10.1016/j.eja.2010.12.001

Almarshadi, M. H., & Ismail, S. M. (2011). Effects of Precision Irrigation on Productivity and Water Use Efficiency of Alfalfa under Different Irrigation Methods in Arid Climates. *Journal of Applied Science Research*, *7*(3), 299–308.

Ame, M. A., Shouhua, C., & Khailah, E. Y. (2022). Optimal selection of lateral in drip irrigation system with pressure compensating emitters. *Ain Shams Engineering Journal*, *13*(4), 101715. https://doi.org/10.1016/j.asej.2022.101715

Amer, K. H., & Gomaa, A. H. (2015). Uniformity Determination in Drip Irrigation Lateral Design. *Misr J. Ag. Eng.*, *20*(April 2003), 405–431.

Amirul Hadi, A., Lee, C. T., Soh, K. Y., Sudharsan, S., Rosman, R., Izwanizam, A., & Palaniappan, S. (2016). Impact of El Nino On Palm Oil Production. *The Planter*, *1088*(92), 789–806.

Andales, A. A., Chávez, J. L., & Bauder, T. A. (2011). Irrigation Scheduling: The Water Balance Approach. *Colorado State University Extension*, *4*, 1–6.

Andrade, L. M., Pacheco, J. C. C., Costa, G. L. L., Alencar, C. A. B. de, & Cunha, F. F. da. (2022). Uniformity of water distribution by a sprinkler irrigation system on a soccer field. *Bioscience Journal*, *38*(February), e38012. https://doi.org/10.14393/bj-v38n0a2022-57028

Anonymus. (n.d.). Manuring The Oil Palm. In *Manuring The Oil Palm*. https://doi.org/10.1002/9781118953297

Araujo, M. A., Tormena, C. A., & Silva, A. P. (2004). Physical properties of a dystrophic Red Latosol (OXISOL) under crop cultivation and native forest. *Revista Brasileira de Ciencia Do Solo*, *28*(2), 337–345. https://doi.org/10.1590/s0100-06832004000200012

Aris Sistanto, B. (2014). The Study of Placement Pattern Micro Sprinkler Depends on Hanging Micro Sprinkler Irrigation Against the Value of Irrigation Efficiency. *International Journal on Advanced Science, Engineering and Information Technology*, *4*(5), 326. https://doi.org/10.18517/ijaseit.4.5.428

Arshad, I., Savona, P., & Khan, Z. A. (2014). Analysis of Trickle / Drip Irrigation Uniformity by IRRIPRO Simulations. *International Journal of Research*, *1*(8), 635–649. http://edupediapublications.org/journals/index.php/ijr/article/view/533

Asghari, S., Neyshabouri, M. R., Abbasi, F., Aliasgharzad, N., & Oustan, S. (2009). The effects of four organic soil conditioners on aggregate stability, pore size distribution, and respiration activity in a sandy loam soil. *Turkish Journal of Agriculture and Forestry*, *33*(1), 47–55. https://doi.org/10.3906/tar-0804-20

Assouline, S. (2013). Infiltration into soils: Conceptual approaches and solutions. *Water Resources Research*, *49*(4), 1755–1772. https://doi.org/10.1002/wrcr.20155

Azlan, A. H., Lee, C. T., & Soh, K. Y. (2016). Impact of El Nino on Palm Oil Production. *The Planter*, *92*(1088), 200–217.

Azrina, A., Khoo, H. E., Idris, M. A., & Razman, M. R. (2011). Major Inorganic Elements in Tap Water Samples in Peninsular Malaysia. *Malaysian Journal of Nutrition*, *December 2013*.

Baiamonte, G., Di Dio, P., & Elfahl, M. (2021). Verification of IRRILAB software application for the hydraulic design of a micro-irrigation system by using IRRIPRO for an apple farm in sicily. *Water (Switzerland)*, *13*(5). https://doi.org/10.3390/w13050694

Banabas, M. (2007). *Study of nitrogen loss pathways in oil palm (Elaeis guineensis Jacq.) growing agro-ecosystems on volcanic ash soils in Papua New Guinea*. Massey University.

Barragan, J., Bralts, V., & Wu, I. P. (2006). Assessment of emission uniformity for micro-irrigation design. *Biosystems Engineering*, *93*(1), 89–97. https://doi.org/10.1016/j.biosystemseng.2005.09.010

Barros, T. H. S., Farias, A. J., Almeida, A. M., Fraga, J. E. F., & Coelho, R. D. (2017). *Field Capacity Estimation From the Inflection Point of the Soil Moisture Retention Curve*. *October*. https://doi.org/10.7127/iv-inovagri-meeting-2017-res0250268

Bauer, J. J. (2019). *Methods of delineating irrigation management zones for variable rate irrigation*. Graduate Theses and Dissertations. https://harvest.usask.ca/handle/10388/12355

Bitella, G., Rossi, R., Bochicchio, R., Perniola, M., & Amato, M. (2014). A Novel Low-Cost Open-Hardware Platform for Monitoring Soil Water Content and Multiple Soil-Air-Vegetation Parameters. *Sensors*, *14*(10), 19639–19659. https://doi.org/10.3390/s141019639

Boman, B. (1989). Distribution Patterns of Microirrigation Spinner and Spray Emitters. *American Society of Agricultural Engineers*, *5*(1), 50–56.

Bordoloi, R., Das, B., Yam, G., Pandey, P. K., & Tripathi, O. P. (2019). Modeling of Water Holding Capacity Using Readily Available Soil Characteristics. *Agricultural Research*, *8*(3), 347–355. https://doi.org/10.1007/s40003-018-0376-9

Bralts, V. F., & Kesner, C. D. (1983). Drip Irrigation Field Uniformity Estimation. *Transactions of the American Society of Agricultural Engineers*, *26*(5), 1369–1374. https://doi.org/10.13031/2013.34134

Brennan, D. (2008). Factors affecting the economic benefits of sprinkler uniformity and their implications for irrigation water use. *Irrigation Science*, *26*(2), 109–119. https://doi.org/10.1007/s00271-007-0077-9

Briggs, L. J., & Homer, L. S. (1912). *The Wilting Coefficient for Different Plants: And Its Indirect Determination* (J. E. Rockwell (ed.); 230th ed.). USDA.

Brouwer, C., Prins, K., Kay, M., & Heibloem, M. (1985). *Irrigation Water Management: Training Manual No 5, Irrigation Methods*. FAO Land and Water Development Division.

Brouwer, J., & Anderson, H. (2000). Water Holding Capacity of Ironstone Gravel in a Typic Plinthoxeralf in Southeast Australia. *Soil Science Society of America Journal*, *64*(5), 1603–1608. https://doi.org/10.2136/sssaj2000.6451603x

Burt, C. M. (1999). *Irrigation Water Balance Fundamentals*. *93407*, 1–13.

Burt, C. M. (2004). Rapid field evaluation of drip and microspray distribution uniformity. *Irrigation and Drainage Systems*, *18*(4), 275–297. https://doi.org/10.1007/s10795-004-2751-x

Caliman, J. P. (1992). Palmier à huile et déficit hydrique, production, techniques culturales adaptées. *Oléagineux*, *47*(5), 205–216.

Caliman, J. P., Olivin, J., & Dufour, O. (1987). Degradation of sandy ferralitic soils in oil palm cultivation through acidification and compaction – correction methods. In A. H. H. et Al. (Ed.), *Int. Oil Palm Conf. Progress and prospects* (p. 287-293). Palm Oil Research Institute of Malaysia.

Caliman, J. P., & Southworth, A. (1998). Effect of drought and haze on the performance of oil palm. *International Oil Palm Conference*, *I*. http://agritrop.cirad.fr/401034/1/ID401034.pdf

Cambardella, C. A., Moorman, T. B., Novak, J. M., Parkin, T. B., Karlen, D. L., Turco, R. F., & Konopka, A. E. (1994). Field-scale variability of soil properties in central Iowa soils. *Soil Science Society of America Journal*, *58*(5), 1501–1511. https://doi.org/10.2136/sssaj1994.03615995005800050033x

Carr, M. K. V. (2011). The Water Relations and Irrigation Requirements of Oil Palm (Elaeis guineensis): A Review. *Experimental Agriculture*, *47*(04), 629–625. https://doi.org/10.1017/S0014479713000288

Chakraborty, K., & Biswaranjan, M. (2015). Importance of Soil Texture in Sustenance of Agriculture : A Study in Burdwan-I Importance of Soil Texture in Sustenance of Agriculture : A Study in Burdwan-I C . D . Block , Burdwan , West Bengal. *Eastern Geographer*, *21*(1), 475–482.

Chan, K. W. (1977). A rapid method for studying the root distribution of oil palm and its application. In D. A. Earp & W. Newall (Eds.), *International developments in oil palm* (pp. 131–151). Incorporated Society of Planters.

Chan, K. W. (1979). Irrigation of oil palm in Malaysia. In E. Pushparajah (Ed.), *Symp. Water in Malaysian Agriculture* (pp. 103–116). Malaysian Society of Soil Science.

Chaya, L. A., & Hills, D. J. (1991). Droplet size and drift potential from micro-sprayer irrigation emitters. *Transactions of the ASAE, 34*(6), 2453–2459.

Cheng Xu, S., Hong Xing, C., Hong Bo, S., Xin Tao, L., & Yong, X. (2011). Growth and physiological responses to water and nutrient stress in oil palm. *African Journal of Biotechnology*, *10*(51), 10465–10471. https://doi.org/10.5897/AJB11.463

Chirgwin, G. A., & Sutton, B. (2019). A low-cost, high-precision drip emitter suitable for low-pressure micro-irrigation systems. *Irrigation Science*, *37*(6), 725–735. https://doi.org/10.1007/s00271-019-00641-7

Chong, S. Y., Teh, C. B. S., Ainuddin, A. N., & Philip, E. (2018). Simple net rainfall partitioning equations for nearly closed to fully closed canopy stands. *Pertanika Journal of Tropical Agricultural Science*, *41*(1), 81–100.

Clark, G. A., & Haman, D. Z. (2017). Water hammer in irrigation systems. *UF/IFAS Extension*, *CIR828*, 1–6. https://doi.org/10.14256/jce.2064.2017

Clemmens, A. J., & Molden, D. J. (2007). Water uses and productivity of irrigation systems. *Irrigation Science*, *25*(3), 247–261. https://doi.org/10.1007/s00271-007-0067-y

Cleophas, F., Isidore, F., Musta, B., Ali, B. N. M., Mahali, M., Zahari, N. Z., & Bidin, K. (2021). Effect of soil physical properties on soil infiltration rates. *Journal of Physics*, *2314*(Conference Series), 1–6. https://doi.org/10.1088/1742-6596/2314/1/012020

Corley, R. H. V., Hardon, J. J., & Tan, G. Y. (1971). Analysis of growth of the oil palm (Elaeis guineensis Jacq.) I. Estimation of growth parameters and application in breeding. *Euphytica*, *20*(2), 307–315. https://doi.org/10.1007/BF00056093

Corley, R. H. V., & Hong, T. K. (1982). Irrigation of oil palms in Malaysia. In E. Pushparajah & P. S. Chew (Eds.), *The Oil Palm in Agriculture in the Eighties – Volume II* (pp. 343–356). Incorporated Society of Planter. https://agris.fao.org/agris-search/search.do?recordID=XB8305208

Corley, R. H. V., Ng, M., & Donough, C. R. (1995). Effects of Defoliation on Sex Differentiation in Oil Palm Clones. *Experimental Agriculture*, *31*, 177–190. https://doi.org/10.1017/S0014479700025266

Corley, R. H. V., & Tinker, P. B. (2016). *The Oil Palm* (Fifth). Wiley Blackwell. https://doi.org/10.1002/9781118953297

Cornaire, B., Daniel, C., Lamade, E., & Fodil, Z. (1994). Comportamiento de la palma de aceite bajo estrés hídrico. *Palmas*, *15*(1), 61–70.

Da Silva, A. P., Kay, B. D., & Perfect, E. (1994). Characterization of the Least Limiting Water Range of Soils. *Soil Science Society of America Journal*, *58*(6), 1775. https://doi.org/10.2136/sssaj1994.03615995005800060028x

Daccache, A., Knox, J. W., Weatherhead, E. K., Daneshkhah, A., & Hess, T. M. (2015). Implementing precision irrigation in a humid climate - Recent experiences and on-going challenges. *Agricultural Water Management*, *147*, 135–143. https://doi.org/10.1016/j.agwat.2014.05.018

Dastane, N. G. (1976). Effective rainfall in irrigated agriculture. *FAO Irrigation and Drainage Paper*, *25*.

Dawson, A., & Knowles, O. (2018). To Grid or not to Grid -A Review of Soil Sampling Strategies. In L. D. Currie & C. L. Christensen (Eds.), *Farm environmental planning – Science, policy and practice* (Occasional, pp. 1–10). Fertilizer and Lime Research Centre, Massey University.

De Andrade, C. D. L. T., Allen, R. G., & Wells, R. D. (1999). SPRINKMOD - Pressure and discharge simulation model for pressurized irrigation systems. 3. Sensitivity to lateral hydraulic parameters and leakage. *Irrigation Science*, *18*(3), 157–161. https://doi.org/10.1007/s002710050057

Debnath, P., Deb, D., Sen, S. K., Pattannaik, S. K., Sah, D., & Ghosh, S. K. (2012). Physico-chemical properties and its relationship with water holding capacity of cultivated soils along altitudinal gradient in Sikkim. *Intl. J. Agric. Env. Biotech*, *5*(1), 99–102.

Dettmann, U., & Bechtold, M. (2018). Evaluating Commercial Moisture Probes in Reference Solutions Covering Mineral to Peat Soil Conditions. *Vadose Zone Journal*, *17*(1), 170208. https://doi.org/10.2136/vzj2017.12.0208

Di Dio, P., Provenzano, G., Provenzano, C., & Savona, P. (2008). Irripro: A Powerful Software to Graphic and Hydraulic Design of Irrigation Plants. *International Conference on Agricultural and Biosystems Engineering for Sustainable World*, *1*(23-25 June 2008), 1–14.

Diakhate, D. (2014). Net Irrigation Requirements for Maize and Sorgum In Isra-Nioro, Province of Kaolock (Senegal). *International Journal of Humanities and Social Science*, *4*(6), 267–281.

Dipak, S. K., Ganesh, S. G., & Patil, V. P. (2019). Performance Evaluation of Micro-Sprinklers System Under Varying Spacing and Operating Pressure. *Journal in Science, Agriculture & Engineering*, *8*(28), 157–162.

Divya, Y. A. (2019). Smart Water Monitoring System using Cloud Service. *International Journal of Trend in Scientific Research and Development (IJTSRD)*, *3*(2), 406–408. https://doi.org/10.31142/ijtsrd21379

Dufrene, E., Dubos, B., Rey, H., Quencez, P., & Saugier, B. (1992). Changes in evapotranspiration from an oil palm stand (Elaeis guineensis Jacq.) exposed to seasonal soil water deficits. *Acta Oecologica*, *13*(3), 299–314.

Dukes, M. D., & Scholberg, J. M. (2005). Soil moisture controlled subsurface drip irrigation on sandy soils. *Applied Engineering in Agriculture*, *21*(1), 89–101.

Ella, V. B., Reyes, M. R., & Yoder, R. (2008). Effect of hydraulic head and slope on water distribution uniformity of a low-cost drip irrigation system. *American Society of Agricultural and Biological Engineers Annual International Meeting 2008, ASABE 2008*, *3*(May 2009), 1551–1567. https://doi.org/10.13031/2013.26885

Evans, R. G., Kim, Y., & Iverson, W. (2007). Evaluation of Closed-loop Irrigation Control with Wireless Sensor Network. In *ASABE Annual International Meeting* (No. 072248).

FAO. (2014). *World reference base for soil resources 2014. International soil classification system* (106th ed.). FAO.

FGVAS. (2019). *Panduan 1*.

Folorunso, O., & Aribisala, J. (2018). Effect of Soil Texture on Soil Infiltration Rate. *Archives of Current Research International*, *14*(3), 1–8. https://doi.org/10.9734/acri/2018/41974

Foster, H. L. (1984). Available Water Holding Capacity for Oil Palm Soils in Malaysia. *PORIM Bulletin*, *8*.

Frank, G. Viets, J. (1972). Water Deficits and Nutrient Availability. In T. T. Kozlowski (Ed.), *Water deficit and Plant Growth* (Volume 3, p. 217). Academic Press.

García, I. F., Lecina, S., Ruiz-Sánchez, M. C., Vera, J., Conejero, W., Conesa, M. R., Domínguez, A., Pardo, J. J., Léllis, B. C., & Montesinos, P. (2020). Trends and challenges in irrigation scheduling in the semi-arid area of Spain. *Water (Switzerland)*, *12*(3), 1–26. https://doi.org/10.3390/w12030785

Ghazalli, M. Z., & Nieuwolt, S. (1982). The use of an agricultural rainfall index in Malaysia. *International Journal of Biometeorology*, *26*(4), 277–283. https://doi.org/10.1007/BF02219494

Goh, K. J., Chew, P. S., & Teo, C. B. (1994). Maximising and maintaining oil palm yields on commercial scale in Malaysia. *International Planters Conference*, *January*, 121–141.

González, O., Montaña, A., López, E., Sánchez, S., Zambrano, D., Macias, L., & Herrera, M. (2020). Irrigation water productivity in selected crops from central region of Cuba. *Revista Ciencias Técnicas Agropecuarias*, *29*(1), 56–63.

Goyal, M. R. (2015). *Sustainable Micro Irrigation Sustainable Micro Irrigation Sustainable Micro Irrigation*.

Gyasi-Agyei, Y. (2020). Identification of the optimum rain gauge network density for hydrological modelling based on radar rainfall analysis. *Water (Switzerland)*, *12*(7). https://doi.org/10.3390/w12071906

Haniff, M. H., Zuraidah, Y., & Roslan, M. M. N. (2014). Oil Palm Root Study at a Northern Region in Peninsula Malaysia. *International Journal of Agriculture Innovations and Research*, *3*(3), 797–801.

Hardon, J. J., Williams, C. N., & Watson, I. (1969). Leaf area and yield in the oil palm in malaya. *Experimental Agriculture*, *5*(1), 25–32. https://doi.org/10.1017/S0014479700009935

Hartley, C. W. S. (1988). *The Oil Palm* (3rd Editio). Longman.

Haruna, S. N., & M. Hanafiah, M. (2017). Consumptive Use of Water By Selected Cash Crops in Malaysia. *Malaysian Journal of Sustainable Agriculture*, *1*(2), 06–08. https://doi.org/10.26480/mjsa.02.2017.06.08

Hasan, M., Chowdhury, T., Drabo, M., Kassu, A., & Glenn, C. (2015). Modeling of Infiltration Characteristics by Modified Kostiakov Method. *Journal of Water Resource and Protection*, *7*(November), 1309–1317.

Hashim, Z., Muhamad, H., Subramaniam, V., & May, C. Y. (2014). Water footprint : Part 2 - FFB production for oil palm planted In Malaysia. *Journal of Oil Palm Research*, *26*(4), 282–291.

Hebbar, S., & Prasad, G. V. (2017). Automatic water supply system for plants by using wireless sensor network. *Proceedings of the International Conference on IoT in Social, Mobile, Analytics and Cloud, I-SMAC 2017*, 742–745. https://doi.org/10.1109/I-SMAC.2017.8058277

Henson, I. E., & Dolmat, M. T. (2003). Physiological analysis of an oil palm density trial on a peat soil. *Journal of Oil Palm Research*, *15*(2), 1–27.

Henson, I.E. (1999). Notes on oil palm productivity. IV. carbon dioxide gradients and fluxes and evapotranspiration, above and below the canopy. *Journal of Oil Palm Research*, *11*(1), 33–40.

Henson, I.E. (1995). Carbon assimilation, water use and energy balance ofan oil palm plantation assessed using micrometeorological techniques. In B.S. Jalani et al. (Ed.), *PORIM Int. Palm Oil Congr. – Agriculture* (pp. 137–158). Palm Oil Research institution Malaysia.

Henson, I.E. (1991). Use of leaf temperature measurements for detection of stress conditions in oil palm. *Trans. Malays. Soc. Plant Physiology*, *2*, 51–57.

Henson, I.E., & Harun, M. H. (2005). The Influence of Climatic Conditions on Gas and Energy Exchanges Above a Young Palm Stand in North Kedah, Malaysia. *Journal Od Oil Palm Research*, *17*(December), 73–91.

Henson, I.E, Mohd Roslan, M. N., Mohd Haniff, H., Zuraidah, Y., & Siti, N. A. M. (2005). Stress development and its detection in young oil palms in north kedah, malaysia. *Journal of Oil Palm Research*, *17*(June), 11–26.

Henson, I E. (1998). Notes on oil palm productivity. I. Productivity at two contrasting sites. *Journal of Oil Palm Research*, *10*(1), 57–67.

Henson, Ian E., & Chang, K. C. (2000). Oil palm productivity and its component processes. In Y. Basiron, B. S. Jalani, & K. . Chan (Eds.), *Advances in oil palm research* (Volume 1, pp. 97–145). Malaysian Palm Oil Board. https://agris.fao.org/agris-search/search.do?recordID=MY2011050060

Hezarjaribi, A., Dehghani, A. ., Helghi, M. M., & Kiani, A. (2008). Hydraulic Performances of Various Trickle Irrigation Emitters. *Journal of Agronomy*, *7*(3), 265–271.

Hillel, D. (2004). *Introduction to Environmental Soil Physics* (D. Hillel (ed.)). Elsevier Academic Press.

Hoekstra, A. Y., & Chapagain, A. K. (2008). *Globalization ofWater Sharing the Planet's Freshwater Resources* (A. Y. Hoekstra & A. K. Chapagain (eds.); 1st ed.). Blackwell Publishing.

Hong, L. A. (1979). Some Lysimetric Measurements of Evapotranspiration of Oil Palm in Central Peninsular Malaysia. In E. Pushparajah (Ed.), *Proceedings Symposium Water in Agriculture in Malaysia* (pp. 89–101). Malaysian Society of Soil Science.

IAEA. (2008). Field estimation of soil water content: A practical guide to methods, instrumentation and sensor technology. In *Training Course Series 30*. International Atomic Energy Agency. https://doi.org/10.2489/jswc.64.4.116A

Irmak, S., & Haman, D. Z. (2017). Evapotranspiration : Potential or Reference? In *IFAS Extension ABE 343*.

Irmak, S., Odhiambo, L. O., Kranz, W. L., & Eisenhauer, D. E. (2011). Irrigation Efficiency and Uniformity, and Crop Water Use Efficiency. *Publications of University of Nebraska-Lincoln Extension, Lincoln*, *EC732*. https://digitalcommons.unl.edu/biosysengfacpub

Irmak, S., & Rathje, W. R. (2008). Plant Growth and Yield as Affected by Wet Soil Conditions Due to Flooding or Over-Irrigation. *Publications of University of Nebraska-Lincoln Extension*, *G1904*. http://www.ianrpubs.unl.edu/epublic/live/g1904/build/

Irriworks. (2022). *The hydraulic calculation*. https://www.irriworks.com/design-services/the-hydraulic-calculation

Irrometer. (2020). *Conversion from HEX to kPa*. Personal communication.

Isa, I., Orewole, O.M., & Abayomi, T. A. (2016). Geospatial Assessment of Crop Water Requirement for Yield Optimization of Oil Palm in South West Nigeria. *Greener Journal of Agricultural Sciences*, *6*(7), 226–233. https://doi.org/10.15580/gjas.2016.8.071316118

Işik, M. F., Sönmez, Y., Yilmaz, C., Özdemir, V., & Yilmaz, E. N. (2017). Precision Irrigation System (PIS) using sensor network technology integrated with IOS/Android Application. *Applied Sciences (Switzerland)*, *7*(9). https://doi.org/10.3390/app7090891

Izwanizam, A., Hanafi, M. M., Roslan, I., Mohd Umar, U., Yahya, A. K., & Hamzah, S. (2022). Responses of irrigated oil palm to nitrogen, phosphorus and potassium fertilizers on clayey soil. *Agricultural Water Management*, *274*(107922), 1–11. https://doi.org/10.1016/j.agwat.2022.107922

Jazayeri, S. M., Rivera, Y. D., Camperos-Reyes, J. E., & Romero, H. M. (2015). Physiological effects of water deficit on two oil palm (Elaeis guineensis Jacq.) genotypes. *Agronomía Colombiana*, *33*(2), 164–173. https://doi.org/10.15446/agron.colomb.v33n2.49846

Jeon, S., Hwang, S., Sonn, Y., Hyun, B., Go, W., Yun, S., & Han, K. (2018). Micro-sprinkler Irrigation Uniformity as Affected by Different Water Pressure and Outlet Intervals. *Korean Journal of Soil Science and Fertilizer*, *51*(4), 327–338.

Jeranyama, P., Demoranville, C. J., & Kennedy, C. D. (2017). Evaluating tensiometers and moisture sensors for cranberry irrigation. *Acta Horticulturae*, *1180*(November 2017), 369–372. https://doi.org/10.17660/ActaHortic.2017.1180.50

Jha, S. K., Ramatshaba, T. S., Wang, G., Liang, Y., Liu, H., Gao, Y., & Duan, A. (2019). Response of growth, yield and water use efficiency of winter wheat to different irrigation methods and scheduling in North China Plain. *Agricultural Water Management*, *217*(380), 292–302. https://doi.org/10.1016/j.agwat.2019.03.011

JMG. (2024). *Drilling*. https://www.jmg.gov.my/en/perkhidmatan-kami/penggerudian

Jobbágy, J., Simoník, J., & Findura, P. (2011). Evaluation of Efficiency of Precision Irrigation for Potatoes. *Research in Agricultural Engineering*, *57*(Special Issue), S14–S23.

Journel, A. G., & Huijbregts, C. J. (1978). *Mining Geostatistics*. Academic Press. https://www.osti.gov/etdeweb/biblio/5214736

Kato, Y., Okami, M., & Katsura, K. (2009). Yield potential and water use efficiency of aerobic rice (Oryza sativa L.) in Japan. *Field Crops Research*, *113*(3), 328–334. https://doi.org/10.1016/j.fcr.2009.06.010

Kee, K. K., Goh, K. J., & Chew, P. S. (2000). Water cycling and balance in a mature oil palm agroecosystem in Malaysia. *International Planters Conference*, 153–169.

Keller, J., & Karmeli, D. (1974). Trickle Irrigation Design Parameters. *Transactions of the ASAE*, *73*(234), 678–684.

King, B. A., Stark, J. C., & Wall, R. W. (2006). Comparison of Site-Specific and Conventional Uniform Irrigation Management for Potatoes. *Applied Engineering in Agriculture*, *22*(5), 677–688. https://doi.org/10.13031/2013.22000

Kirkham, M. B. (2014). Principles of soil and plant water relations, 2nd Edition. In *Principles of Soil and Plant Water Relations, 2nd Edition*. https://doi.org/10.1016/C2013-0-12871-1

Klein, V. A., Reichert, J. M., & Reinert, D. J. (2006). Available water in a clayey Oxisol and physiological wilting of crops. *Revista Brasileira de Engenharia Agricola e Ambiental*, *10*(3), 646–650. https://doi.org/10.1590/S1415-43662006000300016

KMB. (2024). *Windmill Spray Jet WM206*. https://kmb.net.my/product/spray-jet-wm206/

Korom, A., Phua, M. H., & Matsuura, T. (2016). Relationships between crown size and aboveground biomass of oil palms: An evaluation of allometric models. *Sains Malaysiana*, *45*(4), 523–533.

Krishna, K. L. (2017). Internet of Things Application for Implementation of Samrt Agriculture System. *International Conference on I-SMAC (IoT in Social, Mobile, Analytics and Cloud)*, 54–59.

Kumar, A., Surendra, A., Mohan, H., Muthu Valliappan, K., & Kirthika, N. (2017). Internet of things based smart irrigation using regression algorithm. *International Conference on Intelligent Computing, Instrumentation and Control Technologies, ICICICT*, 1652–1657. https://doi.org/10.1109/ICICICT1.2017.8342819

Kushairi, A., & Amiruddin, M. D. (2020). Development of New Oil Palm Cultivars in Malaysia. *Journal of Oil Palm Research*, *32*(September), 420–426.

Lamm, F. R., Storlie, C. A., & Pitts, D. J. (1997). Field Evaluation of Microirrigation Systems. In *ASAE Meeting Presentation: Vol. Revision o*.

Lee, C. T., & Izwanizam, A. (2013). Lysimeter Studies and Irrigation of Oil Palm in Some Inland Soils of Peninsular Malaysia - Felda's Experience. *The Planter*, *89*(1042), 15–29.

Lee, C. T., Zaharah, A. R., Hanafi, M. M., Ishak, C. F., Shahkhirat, M. N., Tan, C. C., & Salihuddin, M. M. Y. (2014). Rachis Nutrient Concentrations of Different Oil Palm Genotypes as Affected by Irrigation and Terrain. *Journal of Oil Palm Research*, *26*(2), 146–153.

Li, J. (2009). *Assessing Emitter Clogging In Drip Irrigation Systems With Sewage Effluent* (No. 095827; Issue June). https://doi.org/10.13031/2013.26970

Liakos, V., Vellidis, G., Lacerda, L., Tucker, M., Porter, W., & Cox, C. (2018). Management Zone Delineation for Irrigation Based on Sentinel-2 Satellite Images and Field Properties. *14th International Conference on Precision Agriculture*, 1–11.

Liang, S., & Wang, J. (2020). *Advanced Remote Sensing: Terrestrial Information Extraction and Applications* (Second). Academic Press. https://doi.org/10.1016/C2017-0-03489-4

Liang, X., Liakos, V., Wendroth, O., & Vellidis, G. (2016). Scheduling irrigation using an approach based on the van Genuchten model. *Agricultural Water Management*, *176*, 170–179. https://doi.org/10.1016/j.agwat.2016.05.030

Lim, K. (1988). Drip irrigation and fertigation of mature oil palms: equipment, layout, operations and costs. In *MPOGC-ARC Workshop on Mechanization in the Oil Palm Estates*.

Lopes, A. R., Boas, M. A. V., Pazuch, F. A., Corte, L. D., Ostroski, D. A., Remor, M. B., Mohr, F. B. M., Dotto, M., Zanella, A. P., Carvalho, A. F. G., Freddo, A. R., Bertoldo, I. C., Pirola, K., & Giarola, C. M. (2019). Statistical Quality Control in Uniformity of Drip Irrigation With Different Slopes. *Journal of Agricultural Science*, *11*(16), 195. https://doi.org/10.5539/jas.v11n16p195

Mahadani M.L., & Foster, H. . (2007). Effect of Minimal Irrigation of Oil Palm in North Sumatra on Nutrient Uptake and Yield. *International Palm Oi Congress*, 670–679.

Maillard, G., Daniel, C., & Ochs, R. (1974). Analysis of the effects of drought on the oil palm. *Oleagineux*, *29*(8/9), 397–404.

Malaysian Meteorological Department. (2016). Annual Report 2016. In *Annual Report 2016*.

Mando, A., Stroosnijder, L., & Brussard, L. (1996). Effects of termites on infiltration into crusted soil. *Geoderma*, *74*, 107–113.

Mangrio, A. G., Asif, M., Ahmed, E., Sabir, M. W., Khan, T., Jahangir, I., Change, C., Energy, A., & Agricultural, N. (2013). *Hydraulic Performance Evaluation of*

Pressure Compensating (Pc) Emitters and Micro-Tubing for Drip Irrigation System. *32*(4), 290–298.

Maroufpoor, E., Faryabi, A., Ghamarnia, H., & Moshrefi, G. Y. (2010). *Evaluation of Uniformity Coefficients for Sprinkler Irrigation Systems under Different Field Conditions in Kurdistan Province (Northwest of Iran)*. *2010*(4), 139–145.

Martin, E. C. (2011). Determining the amount of irrigation water applied to a field. *Arizona Water Series No. 29*. https://doi.org/DOI:29

Marwa, M. A. E. B., Abdelraouf, R. E., Wahba, S. A., El-Bagouri, K. F., & El-Gindy, A. G. (2017). Scheduling Irrigation using automatic tensiometers for pea crop. *Agricultural Engineering International: CIGR Journal*, *2017*, 174–183.

Mbagwu, J. S. C. (1994). Soil Physical Properties Influencing The Fitting Parameters in Philip and Kostiakov Infiltration Models. In *International Centre for Theoretical Physics* (Issue Internal Report IC/94/97).

McCarty, L. B., Hubbard Jr., L. R., & Quisenberry, V. (2016). *Applied Soil Physical Properties, Drainage, and Irrigation Strategies*. https://doi.org/10.1007/978-3-319-24226-2_1

McCready, M. S., & Dukes, M. D. (2011). Landscape irrigation scheduling efficiency and adequacy by various control technologies. *Agricultural Water Management*, *98*(4), 697–704. https://doi.org/10.1016/j.agwat.2010.11.007

Mello, C. R., Oliveira, G. C., Siqueira, D. V., Lima, J. M., & Dias Jr, M. S. (2002). Esmativa da capacidade de campo baseada no ponto de inflexao da curva caracteristica. *Ciênc. Agrotec*, *26*(4), 836–841.

Merriam, J. L., & Keller, J. (1978). *Farm irrigation system evaluation: A guide for management*. *211*(d), 271.

Meterology Department Malaysia. (2017). Annual Report 2017. In *Annual Report*. www.met.gov.my

Minasny, B., & McBratney, A. B. (2018). Limited effect of organic matter on soil available water capacity. *European Journal of Soil Science*, *69*(1), 39–47. https://doi.org/10.1111/ejss.12475

Mishra, A. K. (2013). Effect of rain gauge density over the accuracy of rainfall: A case study over Bangalore, India. *SpringerPlus*, *2*(1), 1–7. https://doi.org/10.1186/2193-1801-2-311

Mohammed, T. A., & Ghazali, A. H. (2009). Evaluation of Yield and Groundwater Quality for Selected Wells in Malaysia. *Pertanika J. Sci. & Technol*, *17*(1), 33–42.

Mohan, S., Simhadrirao, B., & Arumugam, N. (1996). Comparative study of effective rainfall estimation methods for lowland rice. *Water Resources Management*, *10*(1), 35–44. https://doi.org/10.1007/BF00698810

MPOB. (2020). *Overview of The Malaysia Oil Palm Industry 2020*. https://bepi.mpob.gov.my/images/overview/Overview_of_Industry_2020.pdf

MPOB. (2022). *Overview of The Malaysia Oil Palm Industry 2022*. https://bepi.mpob.gov.my/images/overview/Overview2022.pdf

Mungkalasiri, J., Wisansuwannakorn, R., & Paengjuntuek, W. (2015). Water Footprint Evaluation of Oil Palm Fresh Fruit Bunches in Pathumthani and Chonburi (Thailand). *International Journal of Environmental Science and Development*, *6*(6), 455–459. https://doi.org/10.7763/IJESD.2015.V6.636

Mustafa, O. S., Arshad, M., Sattar, I., & Ali, S. (2003). Adoption of Kostiakov Model to Determine the Soil Infiltration for Surface Irrigation Methods under Local Conditions. *International Journal of Agriculture and Biology*, *5*(1), 40–42.

Nageswara, R. R., & Sridhar, B. (2018). IoT based smart crop-field monitoring and automation irrigation system. *Proceedings of the 2nd International Conference on Inventive Systems and Control, ICISC*, 478–483. https://doi.org/10.1109/ICISC.2018.8399118

Nakayama, F. S., Bucks, D. A., & Clemmens, A. J. (1979). Assessing Trickle Emitter Application Uniformity. *Transactions of the ASAE*, 816–821.

Nelson, P. N., Banabas, M., Scotter, D. R., & Webb, M. J. (2006). Using soil water depletion to measure spatial distribution of root activity in oil palm (Elaeis guineensis Jacq.) plantations. *Plant and Soil*, *286*(1–2), 109–121. https://doi.org/10.1007/s11104-006-9030-6

Norhajijah, D. K., Mohiddin, A. K., & Darius, E. P. (2021). Exploring Mechanization Degree and Capacity in Malaysia's Oil Paplm Plantations. *CIGR Journal*, *23*(2), 220–228.

Ochs, R., & Daniel, C. (1976). Research on techniques adapted to dry regions. In R. H. V. Corley, J. J. Wood, & H. B.J. (Eds.), *Oil Palm Research* (p. 315-330). Elsevier Scientific.

Oelofse, H. (2018). *Lightning and surge protection of SSEG installations*.

Oldoni, H., & Bassoi, L. H. (2016). Delineation of irrigation management zones in a Quartzipsamment of the Brazilian semiarid region. *Pesquisa Agropecuaria Brasileira*, *51*(9), 1283–1294. https://doi.org/10.1590/S0100-204X2016000900028

Olivin, J. (1968). Etude pour la localisation d'un bloc industriel de palmiers à huile. *Oléagineux*.

Pachepsky, Y., & Timlin, D. (2001). Soil Water Retention as Related to Topographic Variables. *Soil Sci. Soc. Am. J.*, *65*(November-December), 1787–1795. https://doi.org/10.2136/sssaj2001.1787

Pala, G. K., Pathivada, A. P., Jyothishma, S., Velugoti, H., Yerramsetti, C., & Veeranki, S. (2021). Materials Today : Proceedings Rainwater harvesting - A review on conservation , creation & cost-effectiveness. *Materials Today: Proceedings*, *45*, 6567–6571. https://doi.org/10.1016/j.matpr.2020.11.593

Palat, T., Chayawat, N., Clendon, J. H., & Corley, R. H. V. (2008). A review of 15 years of oil palm irrigation. *Indian National Conference on Oil Palm*, w537–w545.

Palat, T., Smith, B. G., & Corley, R. H. V. (2000). Irrigation of oil palms in Southern Thailand. In E. Pushparajah (Ed.), *Proceedings of the International Planters Conference* (pp. 303–315). Incorporated Society of Planters, Kuala Lumpur.

Paramananthan, S. (2013). Journal of Oil Palm & The Environment An official publication of the Malaysian Palm Oil Council (MPOC) Managing Marginal Soils for Sustainable Growth of Oil Palms. *Journal of Oil Palm and the Environment*, *4*, 1–16. https://doi.org/10.5366/jope.2013.1

Paramananthan, S. (2015). *Report on Soil Mapping for FGVAS Sdn Bhd*.

Paramananthan, S. (2020). *Malaysia Soil Taxonomy* (S. Paramananthan (ed.); Revised Th). Agricultural Crop Trust (ACT) and Param Agricultural Soil Survey (M) Sdn Bhd.

Patle, G. T., Sikar, T. T., Rawat, K. S., & Singh, S. K. (2018). Estimation of infiltration rate from soil properties using regression model for cultivated land. *Geology, Ecology, and Landscapes*, *00*(00), 1–13. https://doi.org/10.1080/24749508.2018.1481633

Payero, J. O., Yonts, C. D., Irmak, S., & Tarkalson, D. (2005). Advantages and Disadvantages of Subsurface Drip Irrigation. *Publications of University of Nebraska-Lincoln Extension*, *EC776*.

Perrier, E. R., & Salkini, A. B. (1991). Supplemental Irrigation in the Near East and North Africa. In E. R. Perrier & A. B. Salkini (Eds.), *Supplemental Irrigation in the Near East and North Africa*. Springer Science+ Business Media, B.V. https://doi.org/10.1007/978-94-011-3766-9

Peters, T., Desta, K., & Nelson, L. (2013). Practical Use of Soil Moisture Sensors and Their Data for Iirrigation Scheduling. *Washington State University Extention*, *FS083E*.

Post, S. E. C., Peck, D. E., Brendler, R. A., Sakovich, N. J., & Waddle, L. (1986). Evaluation of Low-Flow Sprinklers. *California Agriculture*, *July-August*, 27–29.

Postel, S., Polak, P., Gonzales, F., & Keller, J. (2001). Drip irrigation for small farmers: A new initiative to alleviate hunger and poverty. *Water International*, *26*(1), 3–13. https://doi.org/10.1080/02508060108686882

Prabowo, N. E., Tandiono, J., & Foster, H. L. (2010). Identification and Evaluation of Problem Fields: An Implementation of a Yield Prediction Tool Based on Palm Data. *International Oil Palm Conference*, *June*.

Pradeep, S. A. (2021). Performance Evaluation of Micro Sprinkler System. *International Journal of Current Microbiology and Applied Sciences*, *10*(01), 1630–1635. https://doi.org/10.20546/ijcmas.2021.1001.190

Provenzano, G., & Pumo, D. (2004). Experimental Analysis of Local Pressure Losses for Microirrigation Laterals. *Journal of Irrigation and Drainage Engineering*, *130*(4), 318–324. https://doi.org/10.1061/(asce)0733-9437(2004)130:4(318)

Provenzano, G., Pumo, D., & Dio, P. Di. (2005). Simplified Procedure to Evaluate Head Losses in Drip Irrigation Laterals. *Journal of Irrigation and Drainage Engineering*, *131*(6), 525–532. https://doi.org/10.1061/(ASCE)0733-9437(2005)131:6(525)

Puig-Bargués, J., & Lamm, F. R. (2013). Effect of flushing velocity and flushing duration on sediment transport in microirrigation driplines. *Transactions of the ASABE*, *56*(5), 1821–1828. https://doi.org/10.13031/trans.56.10293

Rafii, M. Y., Isa, Z. A., Kushairi, A., Saleh, G. B., & Latif, M. A. (2013). Variation in yield components and vegetative traits in Malaysian oil palm (Elaeis guineensis jacq.) dura×pisifera hybrids under various planting densities. *Industrial Crops and Products*, *46*, 147–157. https://doi.org/10.1016/j.indcrop.2012.12.054

Rahimi, J., Bazrafshan, J., & Khalili, A. (2013). A Comparative Study on Empirical Methods for Estimating Effective Rainfall for Rainfed Wheat Crop in Different Climates of Iran. *Physical Geography Research Quarterly*, *3*(3), 31–46. https://doi.org/10.22059/JPHGR.2013.35833

Rain bird Corporation. (2023). *Micro-Quick ™ Sprays*. https://www.rainbird.com/sites/default/files/media/documents/2021-03/bro_microquick.pdf

Raine, S. R., Meyer, W. S., Rassam, D. W., Hutson, J. L., & Cook, F. J. (2007). Soil-water and solute movement under precision irrigation: Knowledge gaps for managing sustainable root zones. *Irrigation Science*, *26*(1), 91–100. https://doi.org/10.1007/s00271-007-0075-y

Rashidi, M., Ahmadbeyki, A., & Hajiaghaei, A. (2014). *Prediction of Soil Infiltration Rate Based on Some Physical Properties of Soil*. *14*(12), 1359–1367. https://doi.org/10.5829/idosi.aejaes.2014.14.12.12461

Ravi Kishore, V. K. Gahlot, & C. K. Saxena. (2016). Pressure Compensated Micro Sprinklers: A Review. *International Journal of Engineering Research And*, *V5*(01), 237–242. https://doi.org/10.17577/ijertv5is010184

Reichardt, K. (1988). K. Capacidade de campo. *R. Bras. Ci. Solo*, *12*, 211–216.

Reimar Carlesso. (1995). Water Absorption by Plants: Available Versus Extractable Soil Water and Crop Production. *Cienc. Rural*, *25*(1). https://doi.org/https://doi.org/10.1590/S0103-84781995000100035

Rey, H., Quencez, P., Dufrêne, E., & Dubos, B. (1998). Profils hydriques et alimentation en eau du palmier à huile en Côte d'Ivoire. *Plantations, Recherche, Developpement*, *5*(1), 47–53.

Rhebergen, T., Fairhurst, T., Giller, K. E., & Zingore, S. (2019). The influence of water and nutrient management on oil palm yield trends on a large-scale plantation in Ghana. *Agricultural Water Management*, *221*(May), 377–387. https://doi.org/10.1016/j.agwat.2019.05.003

Richards, L. A. (1952). *Report of the Subcommittee on Permeability and Infiltration, Committee on Terminology, Soil Science Society of America 1. 1*, 85–88. https://doi.org/10.2136/sssaj1952.03615995001600010025x

Rogers, D., Lamm, F., Alam, M., Trooien, T., Barnes, P. L., & Mankin, K. (1997). *Efficiencies and water losses of irrigation systems*. Irrigation Management Series. https://bookstore.ksre.ksu.edu/pubs/MF2243.pdf

Romano, N., & Santini, A. (2002). Water Retention and Storage: Field. In J. H. Dane & G. C. Topp (Eds.), *Methods of Soil Analysis, Part 4, Physical Methods* (SSSA Book, pp. 739–758). Soil Science Society of America.

Roslan, M. M. N., & Haniff, M. H. (2004). Water deficit and irrigation in oil palm : A review of recent studies and findings. *Oil Palm Bulletin*, *49*(November), 1–6.

Rovelo, C. O. R., Ruiz, N. Z., Tolosa, J. B., Félix, J. R. F., & Latorre, B. (2019). Characterization and simulation of a low-pressure rotator spray plate sprinkler used in center pivot irrigation systems. *Water (Switzerland)*, *11*(8). https://doi.org/10.3390/w11081684

Ruer, P. (1967). Répartition en surface du système radiculaire du palmier à huilele. *Oléagineux*, *22*, 535–537.

Ruer, P. (1969). Système racinaire du palmier à huile et alimentation hydrique. *Oléagineux*, *24*, 327–330.

Sadeghi, H., Chiu, A. C. F., Ng, C. W. W., & Jafarzadeh, F. (2018). A vacuum-refilled tensiometer for deep monitoring of in-situ pore water pressure. *Scientia Iranica*, *0*(0), 0–0. https://doi.org/10.24200/sci.2018.5052.1063

Sadler, E. J., Evans, R. G., Stone, K. C., & Camp, C. R. (2005). *Opportunities for conservation with precision irrigation*. *60*(6), 371–379.

Safitri, L., Hermantoro, H., Purboseno, S., Kautsar, V., Saptomo, S. K., & Kurniawan, A. (2018). Water footprint and crop water usage of oil palm (Eleasis guineensis) in Central Kalimantan: Environmental sustainability indicators for different crop age and soil conditions. *Water (Switzerland)*, *11*(1), 1–16. https://doi.org/10.3390/w11010035

Salvi, S., Pramod, J. S. A., Sanjay, H. A., Harshita, T. K., Farhana, M., Jain, N., & Suhas, M. V. (2020). Smart Irrigation System Using IoT. *2020 6th International Conference on Advanced Computing and Communication Systems, ICACCS 2020*, 1292–1295. https://doi.org/10.1109/ICACCS48705.2020.9074201

Saxton, K E, & Rawls, W. J. (2006). *Soil Water Characteristic Estimates by Texture and Organic Matter for Hydrologic Solutions*. *1578*, 1569–1578. https://doi.org/10.2136/sssaj2005.0117

Saxton, Keith E. (2009). *SPAW: Soil -Plant-Air -Water, Field and Pond Hydrology*. Soil Water Characteristic: Hydraulic Properties Calculator.

Shaari, N. A., Khan, M. M. A., Bahar, A. M. A., & Nazaruddin, D. A. (2017). Estimation of Infiltration Rate in Major Soil Types of Kota Bharu, Kelantan, Malaysia. *Bulletin of the Geological Society of Malaysia*, *62*(December 2016), 7–11. https://doi.org/10.7186/bgsm62201602

Sharma, B., Molden, D., & Cook, S. (2006). Water use efficiency in agriculture: Measurement, current situation and trends. In *AgEcon Search* (Vol. 1, Issue 3, p. 11).

Sharma, M. (2013). Journal of Oil Palm & The Environment An official publication of the Malaysian Palm Oil Council (MPOC) Sustainability in the Cultivation of Oil Palm – Issues & Prospects for. *Journal of Oil Palm & The Environment*, *April*, 47–68. https://doi.org/10.5366/jope.2013.06

Shigeta, R., Kawahara, Y., Goud, G. D., & Naik, B. B. (2018). Capacitive-Touch-Based Soil Monitoring Device with Exchangeable Sensor Probe. *2018 IEEE SENSORS*, 1–4. https://doi.org/10.1109/ICSENS.2018.8589698

Silva, B. M., Silva, É. A. da, Oliveira, G. C. de, Ferreira, M. M., & Serafim, M. E. (2014). Plant-available soil water capacity: estimation methods and implications. *Revista Brasileira de Ciência Do Solo*, *38*(2), 464–475. https://doi.org/10.1590/s0100-06832014000200011

Silva, H. P. (1985). Sistemas de riego en palma africana : eficiencia y costos. *Revista Palmas*, *6*(1), 38–40.

Singh, A. K., Arora, S., Singh, Y. P., Verma, C. L., Srivastava, A., & Sharma, N. (2017). Enhancing irrigation water productivity in paddy grown under sodic environment. *Journal of Soil and Water Conservation*, *16*(1), 67. https://doi.org/10.5958/2455-7145.2017.00008.x

Singh, V. P., & Yu, F. X. (1990). Derivation of Infiltration Equation Using Systems Approach. *J. Irrig. Drain Eng*, *116*(6), 837–858.

Smith, J. B., & Kean, J. W. (2018). Long-Term Soil-Water Tension Measurements in Semiarid Environments: A Method for Automated Tensiometer Refilling. *Vadose Zone Journal*, *17*(1), 180070. https://doi.org/10.2136/vzj2018.04.0070

Smith, M. (1992). CROPWAT : A Computer Program for Irrigation Planning and Management. *FAO Irrigation and Drainage Paper*, *46*.

Smith, R. J., Baillie, J. ., McCarthy, A. C., Raine, S. R., & Baillie, C. P. (2010). Review of Precision Irrigation Technologies and Their Application. In *A Report for National Program for Sustainable Irrigation* (Issue November).

Smith, R. J., & Baillie, J. N. (2009). Defining precision irrigation: A new approach to irrigation management. *Irrigation and Drainage Conference*, 1–6.

Sobowale, A., Omotayo, A., Olobashola, J., Abdulsalaam-sagir, P., Elemo, K., Badu-apraku, B., Oladapo, M., & Omonayajo, L. (2015). Low Cost Constant – Head Drip Irrigation Emitter for Climate Change Adaptation in Nigeria: Engineering Design and Calibration. *Nigerian Journal of Technology*, *34*(4), 898. https://doi.org/10.4314/njt.v34i4.32

Solomon, K. (1979). Manufacturing Variation of Trickle Emitters. *Transactions of the American Society of Agricultural Engineers*, *22*(5). https://doi.org/10.13031/2013.35150

Souza, A. S., & Neiva Rodrigues, L. (2022). Irrigation management zone strategies impact assessment on potential crop yield, water and energy savings. *Computers and Electronics in Agriculture*, *201*(February). https://doi.org/10.1016/j.compag.2022.107349

Sparnaaij, L. D. (1969). Oil Palm (Elaeis guineensis Jacquin). In F. P. Ferwerda & F. Wit (Eds.), *Outlines of Perennial Crop Breeding* (Papers 4, pp. 339–387). Landbouwhogeschool.

Stone, K. C., Bauer, P. J., & Sigua, G. C. (2016). Irrigation management using an expert system, soil water potentials, and vegetative indices for spatial applications. *Transactions of the ASABE*, *59*(3), 941–948. https://doi.org/10.13031/trans.59.11550

Studer, C., & Spoehel, S. (2019). Potential and actual water savings through improved irrigation scheduling in small-scale vegetable production. *Agronomy*, *9*(12). https://doi.org/10.3390/agronomy9120888

Sui, R. (2017). Irrigation Scheduling Using Soil Moisture Sensors. *Journal of Agricultural Science*, *10*(1), 1. https://doi.org/10.5539/jas.v10n1p1

Surendran, U., Sushanth, C. M., Mammen, G., & Joseph, E. J. (2017). FAO-CROPWAT Model-Based Estimation of Crop Water Need and Appraisal of Water Resources for Sustainable Water Resource Management:Pilot Study for Kollam District - Humid Tropical Region of Kerala, India. *Current Science*, *112*(1), 76–86. https://doi.org/10.18520/cs/v112/i01/76-86

Surre, C. (1968). Les besoins en eau du palmier huile. *Oléagineux (Paris)*, 10–12. https://agritrop.cirad.fr/440528/

Syakura, A. R., Ab Kadir, M. Z. A., Gomes, C., Elistina, A. B., & Cooper, M. A. (2018). Comparative study on lightning fatality rate in Malaysia between 2008 and 2017. *34th International Conference on Lightning Protection, ICLP 2018*. https://doi.org/10.1109/ICLP.2018.8503420

Tailliez, B. (1971). Le système racinaire du palmier à huile sur la plantation de San Alberto (Colombie). *Oléagineux*.

Temizel, K. E. (2016). Mapping of some soil properties due to precision irrigation in agriculture. *Agronomy Research*, *14*(3), 959–966.

Thalheimer, M. (2013). A low-cost electronic tensiometer system for continuous monitoring of soil water potential. *Journal of Agricultural Engineering*, *44*(3), 114–119. https://doi.org/10.4081/jae.2013.e16

Tinker, P. B. (1976). Soil requirements of the oil palmle. In R. H. V. Corley, J. J. Hardon, & B.J. Wood (Eds.), *Oil palm research* (pp. 165–181). Elsevier.

Toll, D. G., Asquith, J. D., Fraser, A., Hassan, A. A., Liu, G., Lourenço, S. D. N., Mendes, J., Noguchi, T., Osinski, P., & Stirling, R. (2016). Tensiometer techniques for determining soil water retention curves. *Unsaturated Soil Mechanics from Theory to Practice - Proceedings of the 6th Asia-Pacific Conference on Unsaturated Soils, October*, 15–22. https://doi.org/10.1201/b19248-4

USDA. (1998). Inherent Factors Affecting Bulk Density and Available Water Capacity. *Soil Quality Kit-Guides for Educators*.

Valdivia-Cea, W., Holzapfel, E., Rivera, D., & Paredes, J. (2017). Assessment of methods to determine soil characteristics for management and design of irrigation systems. *Journal of Soil Science and Plant Nutrition*, *17*(3), 735–750. https://doi.org/10.4067/S0718-95162017000300014

Van der Vossen, H. A. M. (1974). Towards More Efficient Selection for Oil Yield in the Oil Palm. In *Centre for Agricultural Publishing and Documentation*. Landbouwhogeschool te Wageningen.

Van Lier, Q. de J. (2000). Índice da disponibilidade de água para as plantas. In *Tópicos em ciência do solo.* (pp. 95–106).

Vaz, C. M. P., Jones, S., Meding, M., & Tuller, M. (2013). Evaluation of Standard Calibration Functions for Eight Electromagnetic Soil Moisture Sensors. *Vadose Zone Journal*, *12*(2), vzj2012.0160. https://doi.org/10.2136/vzj2012.0160

Veihmeyer, F. J., & Hendrickson, A. H. (1949). Methods of Measuring Field Capacity and Permanent Wilting Percentage of Soils. *Soil Science*, *68*(1), 75–94.

Villalobos, E., C. H Umana, & Chinchila, C. (1992). Oil palm water status in response to drought in Costa Rica. *Oléagineux, 47*(1), 1–7.

Woittiez, L. S., van Wijk, M. T., Slingerland, M., van Noordwijk, M., & Giller, K. E. (2017). Yield gaps in oil palm: A quantitative review of contributing factors. *European Journal of Agronomy*, *83*, 57–77. https://doi.org/10.1016/j.eja.2016.11.002

Xu, H., Xu, C. Y., Chen, H., Zhang, Z., & Li, L. (2013). Assessing the influence of rain gauge density and distribution on hydrological model performance in a humid region of China. *Journal of Hydrology*, *505*, 1–12. https://doi.org/10.1016/j.jhydrol.2013.09.004

Yahya, Z., Husin, A., Talib, J., Othman, J., Ahmed, O. H., & Jalloh, M. B. (2010). Soil compaction and oil palm (Elaeis guineensis) yield in a clay textured soil. *American Journal of Agricultural and Biological Science*, *5*(1), 15–19.

Yashaswini, L. S., Vani, H. U., Sinchana, H. N., & Kumar, N. (2018). Smart automated irrigation system with disease prediction. *IEEE International Conference on Power, Control, Signals and Instrumentation Engineering, ICPCSI 2017*, *September 2017*, 422–427. https://doi.org/10.1109/ICPCSI.2017.8392329

Zaghluol, K. F., ELNaggar, A. M., & Salih, M. A. (2014). Clogging Evaluation of Six Emitters As Affected By Suspended Sand Particles in Irrigation Water. *Journal of Soil Sciences and Agricultural Engineering*, *5*(5), 645–657. https://doi.org/10.21608/jssae.2014.49376

Zaharah, A. R., Sharifuddin, H. A. ., Ahmad Sahali, M., & M.H.S., H. (1989). Fertilizer placement studies in mature oil palm using isotope technique. *Planter*, *65*, 384–388.

Zebarth, B. J., Neilsen, G. H., Hogue, E., & Neilsen, D. (1999). Influence of organic waste amendments on selected soil physical and chemical properties. *Canadian Journal of Soil Science*, *79*(3), 501–504. https://doi.org/10.4141/S98-074

Zhang, L., Fu, B., Hui, X., & Ren, N. (2018). Simplified method for estimating throw radius of rotating sprinklers on sloping land. *Irrigation Science*, *36*(6), 329–337. https://doi.org/10.1007/s00271-018-0594-8

Zhao, W. X., Li, J., Yang, R. M., & Li, Y. F. (2017). Crop yield and water productivity responses in management zones for variable-rate irrigation based on soil water holding capacity. *Transactions of the ASABE*, *60*(5), 1659–1667.

Zotarelli, L., Dukes, M. D., & Morgan, K. T. (2010). Interpretation of Soil Moisture Content to Determine Soil Field Capacity and Avoid Over-Irrigating Sandy Soils Using Soil Moisture Sensors. *University of Florida Cooperation Extension Services, AE 460. Http://Edis.Ifas.Ufl.Edu/Ae460.*, 1–4.

APPENDICES

This section contains any figures or tables related to work activities carried on during this study.

A. Soil physical analysis

Figure A.1: Preparation of sample for reaction with Sodium Peroxide

Figure A.2: Apparatus used to stir the solution

Figure A.3: Solution was left at room temperature overnight

Figure A.4: Dried sample for porcelain A and B

Figure A.5: Water was added to the supernatant until the colour of the solution became clear

Figure A.6: Fraction of coarse and fine sand

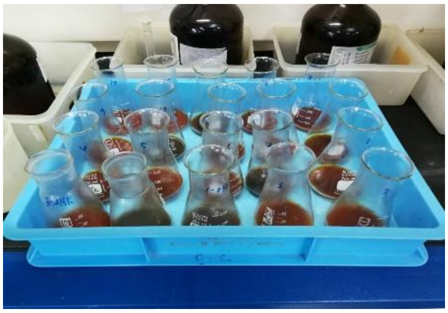

Figure A.7: Preparation of sample for titration process

Figure A.8: Titration process setup

Figure A.9: Preparation of the sample before transfer to the muffle furnace

Figure A.10: Sample was left inside the muffle furnace

Table A.1: Matric correlation between all soil properties variables

	Depth	BD	AWHC	Clay	Silt	Csand	Fsand	Tsand	OM	OC
Depth	1									
p-value	0									
BD	-0.053	1								
	0.644	0								
AWHC	0.554	0.072	1							
	**	0.527	0							
Clay	0.530	-0.301	0.137	1						
	**	**	0.225	0						
Silt	-0.048	-0.162	-0.280	0.278	1					
	0.672	0.152	*	*	0					
Csand	-0.117	0.241	-0.156	-0.438	-0.193	1				
	0.302	*	0.168	**	0.087	0				
Fsand	-0.402	0.252	0.078	-0.814	-0.650	0.087	1			
	**	*	0.490	**	**	0.442	0			
Tsand	-0.403	0.316	0.011	-0.893	-0.653	0.457	0.930	1		
	**	**	0.924	**	**	**	**	0		
OM	-0.529	-0.165	-0.291	-0.246	0.023	-0.090	0.243	0.183	1	
	**	0.144	**	*	0.839	0.430	*	0.104	0	
OC	-0.531	-0.164	-0.292	-0.247	0.024	-0.089	0.243	0.183	1.000	1
	**	0.145	**	*	0.834	0.431	*	0.104	**	0

Note: * is for P value < 0.05, ** is for P value <0.01

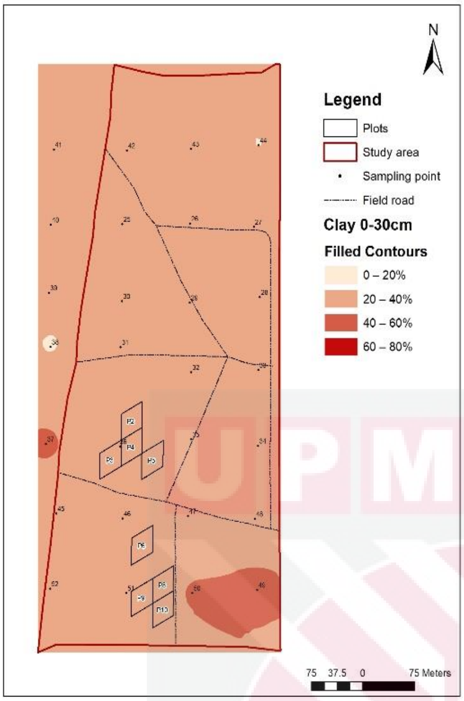

Figure A.11: Interpolation map for Clay 0-30 cm

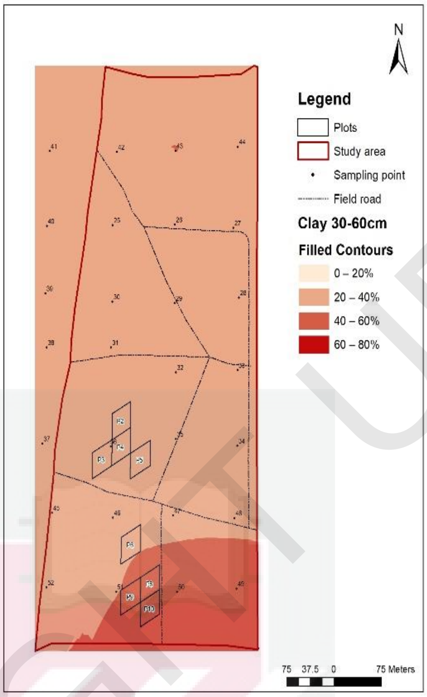

Figure A.12: Interpolation map for Clay 30-60 cm

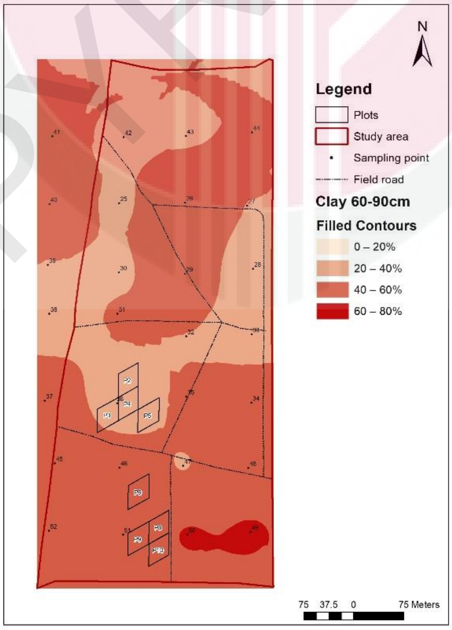

Figure A.13: Interpolation map for Clay 60-90 cm

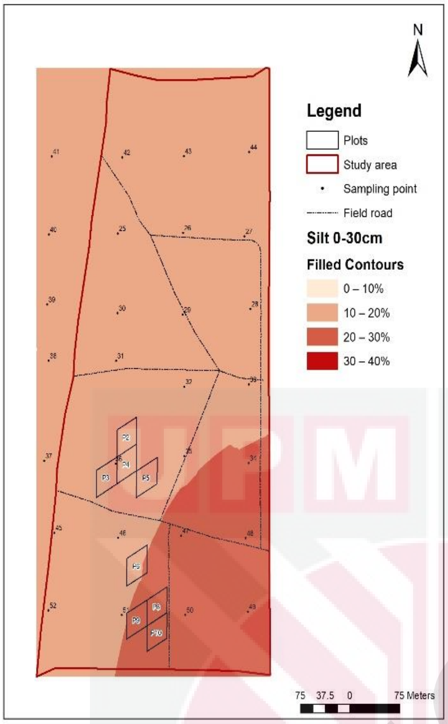

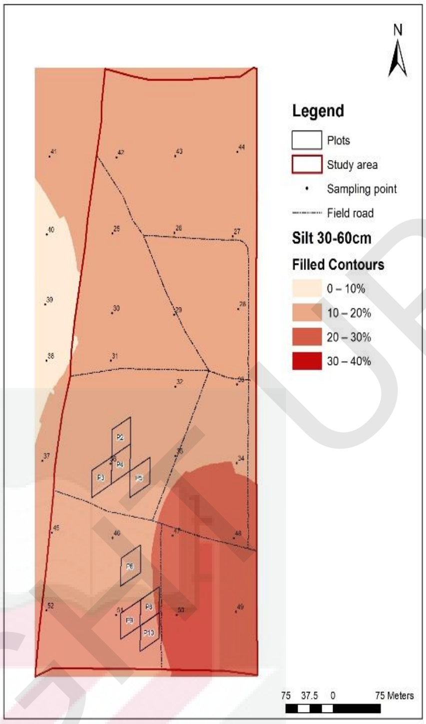

Figure A.14: Interpolation map for Silt 0-30 cm

Figure A.15: Interpolation map for Silt 30-60 cm

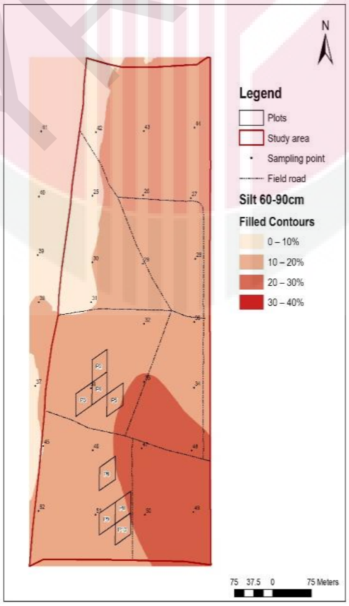

Figure A.16: Interpolation map for Silt 60-90 cm

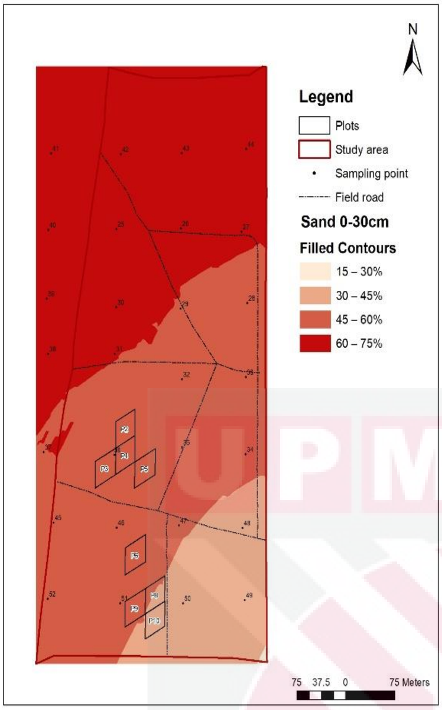

Figure A.17: Interpolation map for Sand 0-30 cm

Figure A.18: Interpolation map for Sand 30-60 cm

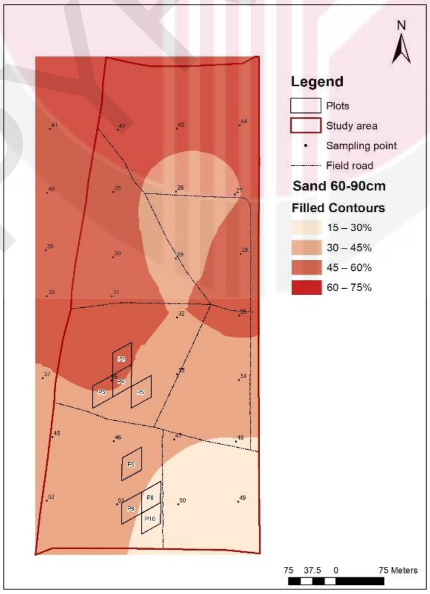

Figure A.19: Interpolation map for Sand 60-90 cm

B. Emitter experiments

Figure B.1: Emitter use in this experiment

Figure B.2: Special cone for water collection below the emitter

Figure B.3: Arrangement of the container to observed on spraying pattern of the emitter

C. IrriPro software user interface

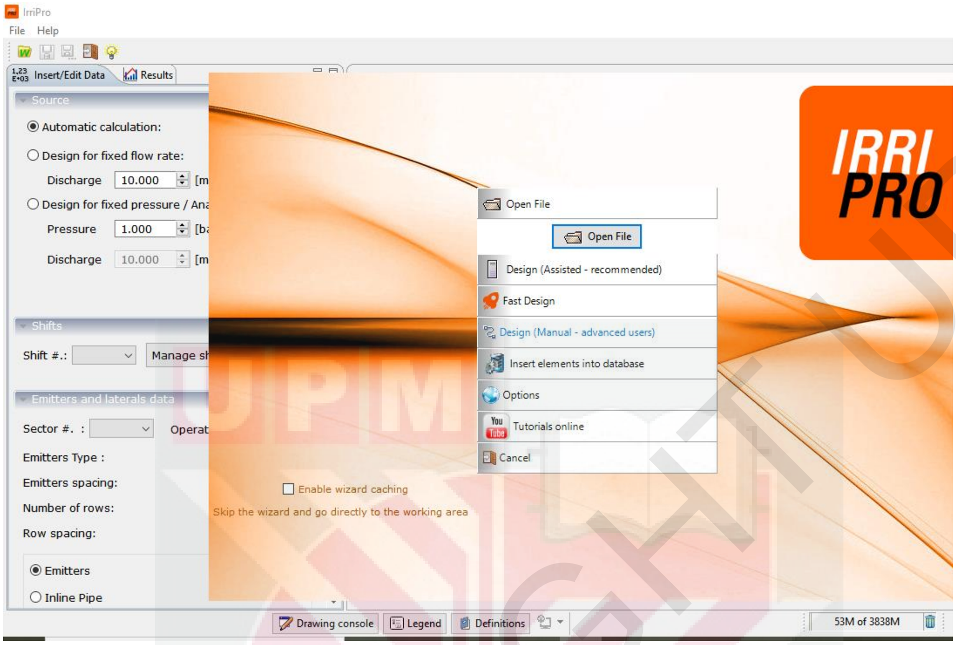

Figure C.1: The main interface of IrriPro software

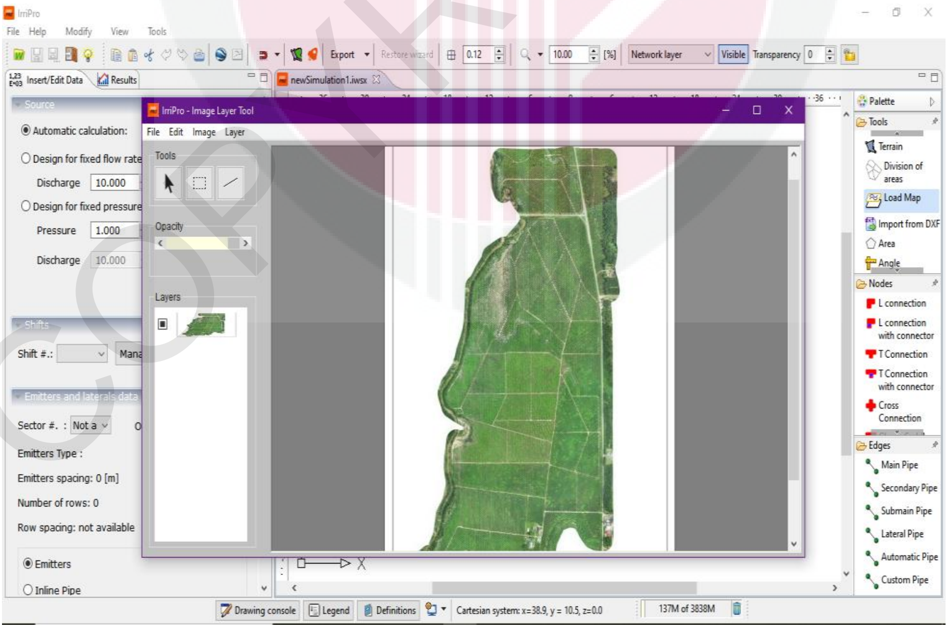

Figure C.2: The drone image has been used as a background layer for drawing

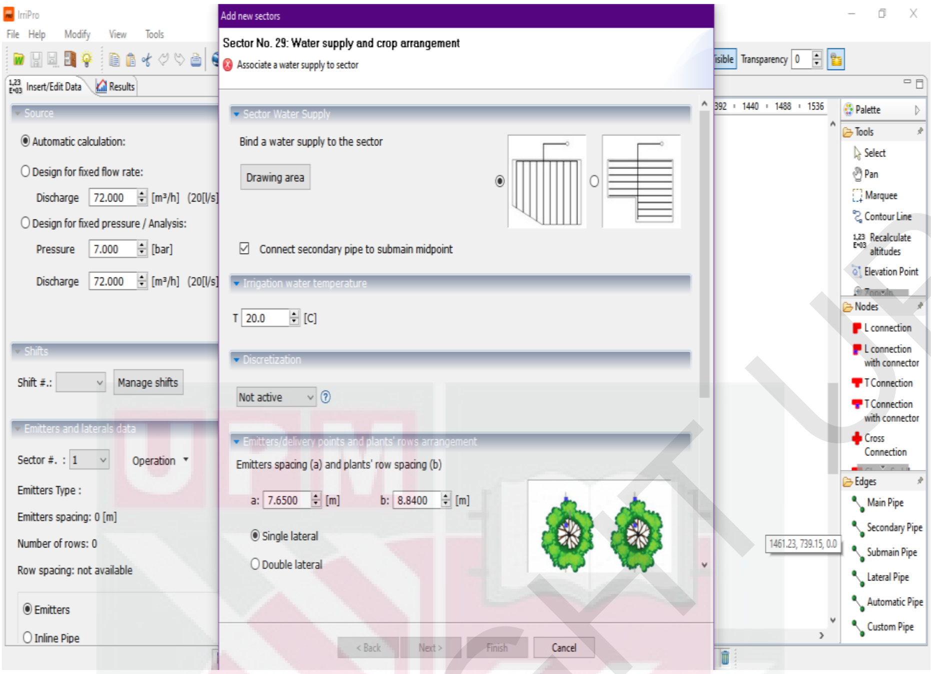

Figure C.3: Associating the water supply process to the intended sector

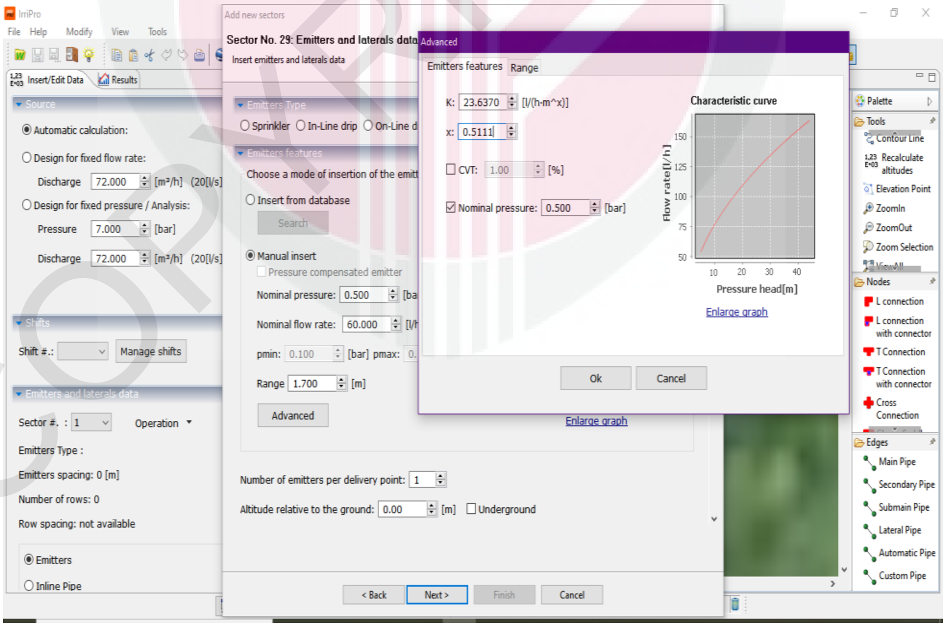

Figure C.4: Insertion of emitter properties into the system

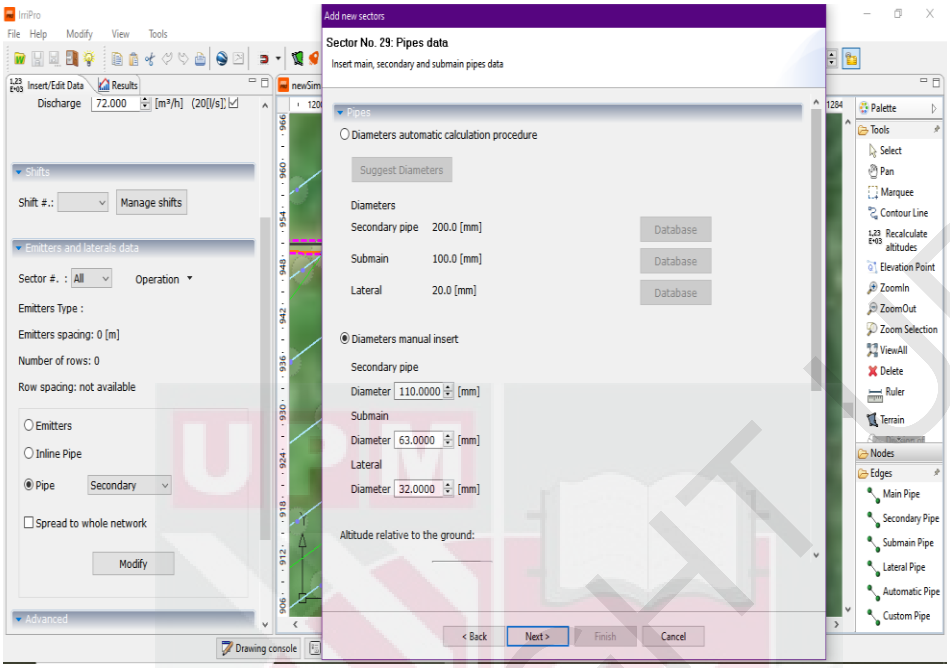

Figure C.5: Determination of piping size for the sector

D. Installation of SBI network

Table D.1: Kinematic viscosity (v) value of water at a specific temperature

Temperature	Dynamic Viscosity	Kinematic Viscosity
	μ	**v**
˚C	(N s m-2) x 10^{-3}	(m^2 s^{-1}) x 10^{-6}
0	1.767	1.787
5	1.519	1.519
10	1.307	1.307
20	1.002	1.004
30	0.798	0.801
40	0.653	0.658
50	0.547	0.553
60	0.467	0.475
70	0.404	0.413
80	0.355	0.365
90	0.315	0.326
100	0.282	0.294

Table D.2: Value of absolute roughness according to commercial pipe

Surface	Absolute Roughness Coefficient
	(m) 10^{-3}
Copper, Lead, Brass, Aluminium	0.001 - 0.002
PVC and plastic pipes	0.0015 - 0.007
Stainless steel	0.015
Steel commercial pipe	0.045 - 0.09
Stretched steel	0.015
Weld steel	0.045
Galvanised steel	0.15
Rusted steel (corrosion)	0.15 - 4.00
New cast iron	0.25 - 0.80
Worn cast iron	0.80 - 1.50
Rusty cast iron	1.50 - 2.50
Sheet or asphalted cast iron	0.01 - 0.015
Smoothed cement	0.30
Ordinary cement	0.30 - 1.00
Coarse concrete	0.30 - 5.00
Well planed wood	0.18 - 0.90
Ordinary wood	5.00

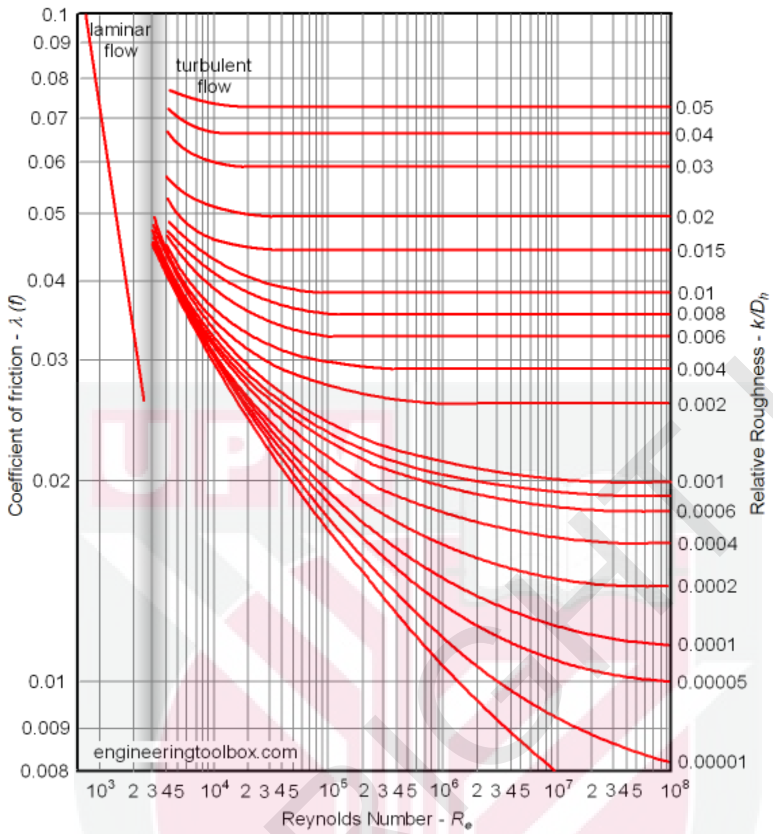

Figure D.1: Moody diagram

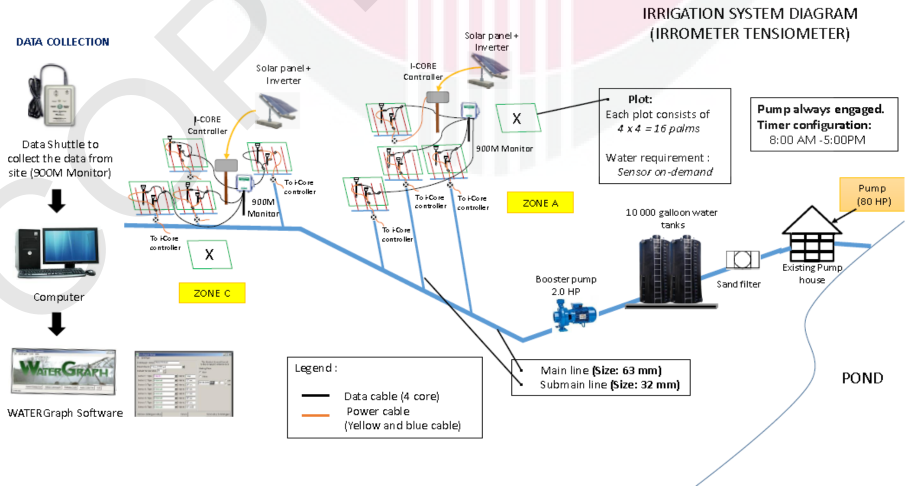

Figure D.2: General schematic drawing for all segmentation of SBI setup

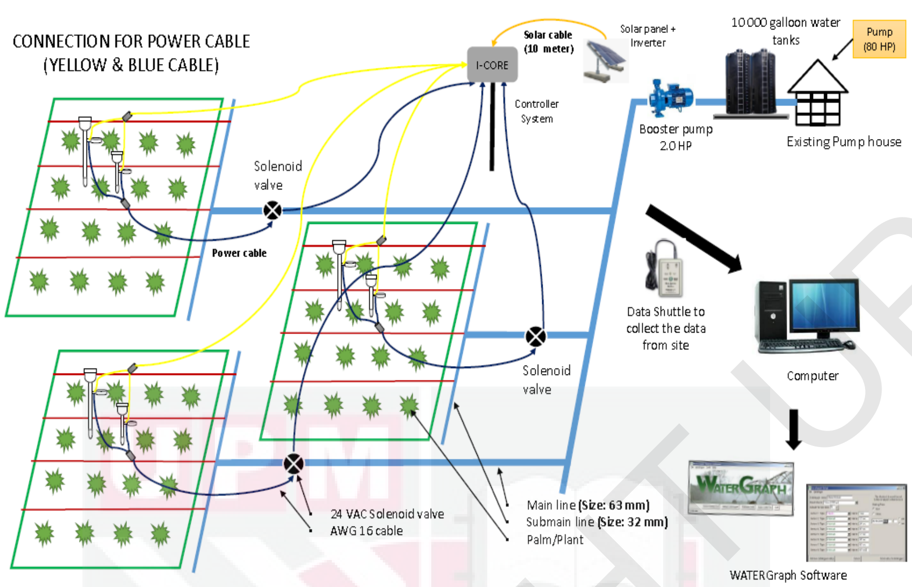

Figure D.3: Diagram of power wired connection between devices

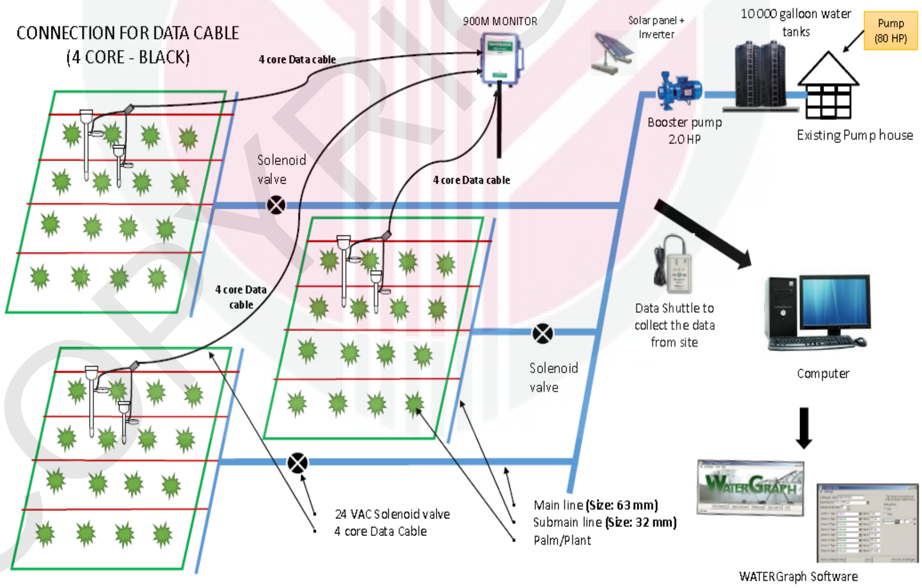

Figure D.4: Diagram of data wired connection between devices

Table D.3: Details on power and data cable for connection between tensiometer, iCORE, and solenoid valves

Connection type	Tensiometer	Hunter iCORE	Remark
Power	Red	Yellow	Direct
	Black	Blue	to Solenoid valve first
	Tensiometer	Watermark 900M	Remark
	Red	Red-Green	Power supply
Data	Black	Yellow-Blue	Power supply
	White (12”)	Yellow-Green	Data
	White (24”)	Yellow-Dark Green	Data

Figure D.5: Some part of the main pipe was buried in the soil for safety purposes

Figure D.6: Several parts for monitoring purposes were installed on this segmentation

Figure D.7: Electrical pump unit to draw water from the tank

Figure D.8: One emitter was placed for each palm

Figure D.9: Actual picture of the power connection

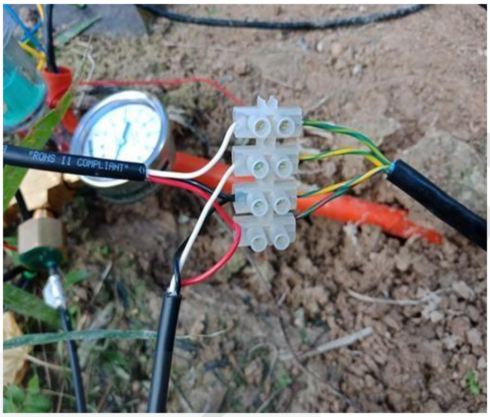

Figure D.10: Actual picture of data connection

Figure D.11: A photovoltaic panel was installed at the roof of this structure

Figure D.12: Inverter used in the controller system

Figure D.13: Hunter iCORE used as a centre of the system

Figure D.14: Deep cycle battery used to store to energy

Figure D.15: Arrangement of the control system inside the bunker

Figure D.16: Tensiometer auger set

Figure D.17: Slurry made by in situ soil

Figure D.18: Air bleed was used to release air compression inside the tensiometer

Figure D.19: Special cage used to protect tensiometer

Figure D.20: Small screw to manually adjust the trigger point

Figure D.21: Solenoid valve installed at sub main pipe

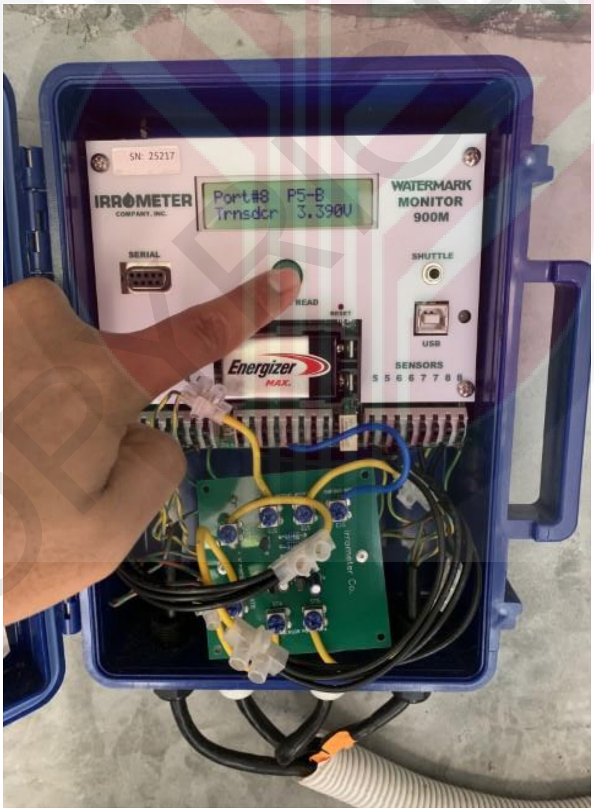

Figure D.22: LCD display shows the value of the data

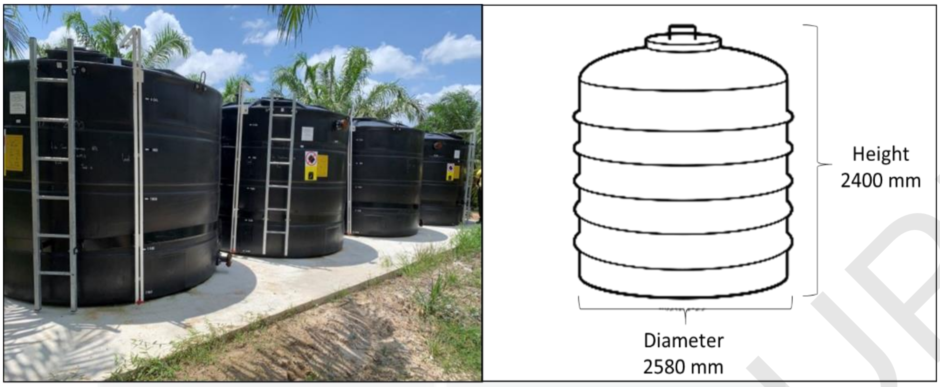

Figure D.23: Diagram and size of the polywater tank

E. Activities to evaluate SBI

Figure E.1: The process of bunch harvesting

Figure E.2: Weighing activities by using 50 kg scale

Figure E.3: Rudimentary leaf either at the right or left side of frond

Figure E.4: Technique to measure leaf width

Figure E.5: Technique to measure rachis width

Figure E.6: Technique to measure palm height

Figure E.7: Technique to measure palm trunk diameter

Figure E.8: Fresh weight of whole frond number 17

Figure E.9: Drying process of the frond by using oven

Figure E.10: Custom plastic protective case for water measurement

F. Cost analysis table

Table F.1: Calculation for cost analysis for SBI project from 2019 – 2028

Irrigation (ha)	20.30
Budget Capex (RM)	317,732.00
Budget Capex (RM/Ha)	15,651.82
Discount rate	0.1

Year	**2019**	**2020**	**2021**	**2022**	**2023**	**2024**	**2025**	**2026**	**2027**	**2028**
Irrigation Year	**0**	**1**	**2**	**3**	**4**	**5**	**6**	**7**	**8**	**9**
Palm Age	**5**	**6**	**7**	**8**	**9**	**10**	**11**	**12**	**13**	**14**
Harvesting Year	**2**	**3**	**4**	**5**	**6**	**7**	**8**	**9**	**10**	**11**

Cost	**2019**	**2020**	**2021**	**2022**	**2023**	**2024**	**2025**	**2026**	**2027**	**2028**
Capital (RM)/Ha	15,652									
Maintenance (RM/ha)			1,478		1,552		1,629		1,711	
Operation (RM)/Ha		1084	1084	1084	1084	1084	1084	1084	1084	1084
Extra Cost for harvesting (RM/ha)		549	639	69	480	480	480	480	480	480
Total (RM/ha)		**1,633**	**3,201**	**1,153**	**3,115**	**1,564**	**3,193**	**1,564**	**3,275**	**1,564**

Revenue	**2019**	**2020**	**2021**	**2022**	**2023**	**2024**	**2025**	**2026**	**2027**	**2028**
Extra Yield (t/ha)		9	11	1	8	8	8	8	8	8
FFB Price (RM/ha)		561	955	1,087	750	750	750	750	750	750
Total(RM/ha)		5,133	10,171	1,250	6000	6000	6000	6000	6000	6000

Profit (RM)		3,500	6,970	97	2,885	4,436	2,807	4,436	2,725	4,436
Cumulative profit (RM)	**(15,652)**	**(12,151)**	**(5,181)**	**(5,084)**	**(2,199)**	**2,237**	**5,044**	**9,480**	**12,206**	**16,642**

Year		1	2	3	4	5	6	7	8	9
Investment Cost		15,652								
Net Cash inFlow (RM/ha)		3,500	6,970	97	2,885	4,436	2,807	4,436	2,725	4,436
Discounted factor 10%		0.909	0.826	0.751	0.683	0.621	0.564	0.513	0.467	0.424
PV of net cashflow		3,182	5,760	170	1,970	2,755	1,584	2,277	1,271	1,881

Note: Red letter referred to estimation value

Table F.2: Calculation for cost analysis for SBI project from 2029 – 2039

Irrigation (ha)	20.30
Budget Capex (RM)	317,732.00
Budget Capex (RM/Ha)	15,651.82
Discount rate	0.1

Year	**2029**	**2030**	**2031**	**2032**	**2033**	**2034**	**2035**	**2036**	**2037**	**2038**	**2039**
Irrigation Year	**10**	**11**	**12**	**13**	**14**	**15**	**16**	**17**	**18**	**19**	**20**
Palm Age	**15**	**16**	**17**	**18**	**19**	**20**	**21**	**22**	**23**	**24**	**25**
Harvesting Year	**12**	**13**	**14**	**15**	**16**	**17**	**18**	**19**	**20**	**21**	**22**

Cost	**2029**	**2030**	**2031**	**2032**	**2033**	**2034**	**2035**	**2036**	**2037**	**2038**	**2039**
Capital (RM)/Ha											
Maintenance (RM/ha)	1,796		1,886		1,980		2,079		2,183		2,293
Operation (RM)/Ha	1084	1084	1084	1084	1084	1084	1084	1084	1084	1084	1084
Extra Cost for harvesting (RM/ha)	480	480	480	480	480	480	480	480	480	480	480
Total (RM/ha)	**3,360**	**1,564**	**3,450**	**1,564**	**3,544**	**1,564**	**3,643**	**1,564**	**3,747**	**1,564**	**3,856**

Revenue	**2029**	**2030**	**2031**	**2032**	**2033**	**2034**	**2035**	**2036**	**2037**	**2038**	**2039**
Extra Yield (t/ha)	8	8	8	8	8	8	8	8	8	8	8
FFB Price (RM/ha)	750	750	750	750	750	750	750	750	750	750	750
Total(RM/ha)	6000	6000	6000	6000	6000	6000	6000	6000	6000	6000	6000

Profit (RM)	2,640	4,436	2,550	4,436	2,456	4,436	2,357	4,436	2,253	4,436	2,144
Cumulative profit (RM)	**19,282**	**23,718**	**26,268**	**30,704**	**33,160**	**37,596**	**39,953**	**44,389**	**46,642**	**51,079**	**53,222**

Year	10	11	12	13	14	15	16	17	18	19	20
Investment Cost											
Net Cash inFlow (RM/ha)	2,640	4,436	2,550	4,436	2,456	4,436	2,357	4,436	2,253	4,436	2,144
Discounted factor 10%	0.386	0.350	0.319	0.290	0.263	0.239	0.218	0.198	0.180	0.164	0.149
PV of net cashflow	1,018	1,555	813	1,285	647	1,062	513	878	405	725	319

Note: Red letter referred to estimation value

LIST OF PUBLICATIONS

Norizan, M. S., Wayayok, A., Abd Karim, Y., Abdullah, A. F., & Mahadi, M. R. (2021). Quantitative approach for irrigation requirement of oil palm: Case study in Chuping, Northern Malaysia. *Journal of Oil Palm Research*, *33*, 278-288.

Norizan, M. S., Wayayok, A., Abdullah, A. F., Mahadi, M. R., & Abd Karim, Y. (2021). Spatial Variations in Water-Holding Capacity as Evidence of the Need for Precision Irrigation. *Water*, *13*(16), 2208.